

**GREEN CATALYTIC PROCESSES FOR SELECTIVE
OXYFUNCTIONALIZATION OF HYDROCARBONS
AND BIOMASS DERIVED FEEDSTOCKS**

THESIS

SUBMITTED TO THE

SAVITRIBAI PHULE PUNE UNIVERSITY

FOR THE DEGREE OF

DOCTOR OF PHILOSOPHY

IN

CHEMISTRY

BY

NARASIMHARAO KANNA

RESEARCH SUPERVISOR

Dr. C.V.V. SATYANARAYANA

CATALYSIS DIVISION

CSIR - NATIONAL CHEMICAL LABORATORY

PUNE-411008, INDIA

SEPTEMBER 2014

CERTIFICATE

This is to certify that the work incorporated in the thesis entitled “**Green catalytic processes for selective oxyfunctionalization of hydrocarbons and biomass derived feedstocks**” submitted by **Mr. Narasimharao Kanna**, to the Savitribai Phule Pune University, for the degree of **Doctor of Philosophy** in Chemistry, was carried out by the candidate under my supervision at the Catalysis Division, CSIR-National Chemical Laboratory, Pune –411 008, India. Such material as has been obtained from other sources has been duly acknowledged in the thesis. To the best of my knowledge, the present work or any part thereof has not been submitted to any other university for the award of any other degree or diploma.

Date:
Place: Pune

Dr. C.V.V. SATYANARAYANA
(Research Supervisor)
CSIR- National Chemical Laboratory,
Pune-411008, India.

DECLARATION BY RESEARCH SCHOLAR

I hereby declare that the thesis entitled **“Green catalytic processes for selective oxyfunctionalization of hydrocarbons and biomass derived feedstocks”** submitted for the Degree of **Doctor of Philosophy** in chemistry to the Savitribai Phule Pune University, has been carried out by me at the Catalysis and Inorganic Chemistry Division, National Chemical Laboratory, Pune – 411 008, India, under the supervision of **Dr. C. V. V. Satyanarayana**. Such material as has been obtained from other sources has been duly acknowledged in this thesis. The work is original and has not been submitted in part or full by me for any other degree or diploma to this or any other University.

Date:
Place: Pune

NARASIMHARAO KANNA
(Research Scholar)
CSIR- National Chemical Laboratory,
Pune-411008
India

*.....dedicated to my
beloved parents and
nation*



If we can really understand the problem, the answer will come out of it, because the answer is not separate from the problem

Jiddu Krishnamurti

ACKNOWLEDGEMENTS...

This thesis has been seen through to completion with the support and encouragement of numerous people including my well wishers, friends and colleagues. At this point of accomplishment I like to thank all those people who made this possible, which is an unforgettable experience for me.

First and foremost, I would like to express my heartfelt and sincere gratitude to my research supervisor Dr. Satyanarayana Chilukuri who introduced me to a fascinating realm of chemistry. I am deeply indebted to him for his invaluable guidance and unconditional support. His constant inspiration and constructive criticism helped me a lot to focus my views in proper perspective. His tireless attitude has been an impetus for me throughout the course of study. He gave me the freedom to think, experiment and accomplish. I shall cherish my learning experience under his guidance. I take this opportunity to express my deepest sense of gratitude and reverence towards him for guiding me in the right direction throughout the course of this work.

Words fail me when I intend to express my thanks and gratitude to Dr. Gopinath Chinnakonda for his professional and personal support. I believe the better way of thanking him would be through my future contribution to scientific community.

I extend my sincere thanks to the Director of CSIR-NCL Dr. Sourav Pal, Dr. Sivaram (former director) and Dr. A.P. Singh (Head, Catalysis division) for providing me the opportunity to carry out my research work in this prestigious and well-equipped laboratory. My heartfelt thanks are due to Dr. T. Raja, Dr. Nandini Devi, Dr. D. Srinivas, Dr. Paresh Dhepe, Dr. C.P. Vinod, Dr. Umbarkar and Ms. Violet Samuel. I also like to thank Mr. Madhu, Mr. Jha, Mr. Purushothaman and all other scientific and non-scientific staff for their help and support during my tenure as a research student.

My deepest gratitude to my teachers Prof. Vinod K Tiwari, Prof. D.S. Pandey, Prof. T.R. Rao, Prof. Bachcha Singh, Mr. Ramakrishna, Mr. Naveen, Mr. P. Sambhasivarao, Mrs. Anitha, Miss. C.P. Denis and Mr. Narayanacharyulu for their inspirational teaching, guidance and blessings.

I extend my sincere thanks to Student Academic Office and catalysis division at CSIR-NCL for their help and support at crucial times. I am also thankful to the University of Pune for the smooth documentation process during my doctoral study. I am grateful to UGC, New Delhi, for awarding the research fellowship and Director, CSIR-National Chemical Laboratory for extending all infrastructural facilities.

I have high regard to my seniors Dr. Satyanarayana Reddy, Dr. Ganesh, Dr. Sachin, Mr. Koteswararao and Mr. Reji for their unconditional support and help during my Ph D. Course. I am indebted to my labmates Hanmant, Nishita, Richa, Lakshmi, Atul, Srikanth, Pranjali and my previous labmates Kalpana, Lakshman, Aditya, Jay, Mangesh, Srinivasarao, Lalit, Gajanan, Santosh, Amlan and Chandan for their love and encouragement.

I sincerely thank all my divisional friends especially Rajesh, Edwin, Devadutta, Ashok, Jijil, Anupam, Joby, Vysaksh, Sunil and my senior colleagues and friends Dr. Rajender, Dr. Sridhar, Dr. Swaroop, Dr. Yadagiri, Dr. Sudhakar, Suneel, Innaiah, Bala, Manoj, Suresh, Chandrababu, Rami, Bhaskar, Rambabu, Chaitanya Krishna, Janaki ram, Durga, Siva, Nagendra, Narendra, Srinivas, Tarun, Eswar, Satish, Shanthi, Hanuman, Kumar Raja, Chandan, Saikat, Eldho, Pravat, Vasu, Bhausahab, Tamboli. I extend huge thanks to my friends during school, College and Master's days.

Need to invent a new word in English for expressing highest gratitude to the people whom I came across and made substantial impact on my life Dr. Srinivasarao, Dr. Ramesh, Mallikarjuna Reddy (for guiding me as elder brothers), Dr. Venu babu, Dr. Chaitanya Kiran, Bhogesh and Trinadh (for making me to realize the value of friendship), Dr. Ramanujam (for his devotional preachings) Sudhakar Narra, Chandra Prakash (for mentoring me to how to live a life for others) and last but not least Mr. Kalesha Vali for being my role model, best pal and teaching me to how to lead the life with clean heart and soul.

I would like to pay high regards to my parents, Shri Kanakaiah Naidu and Smt. Syamala Devi and my sister Sathvika for their unconditional love and affection. It gives me great pleasure to thank them for their love, sacrifice, moral support, blessings, care and constant encouragement that they have shown to me. Special thanks and wishes to my cousins Subhash, Sundeep, Charan, Prasanth, Narendra, Surendra and uncles Late Bhaskar rao, Venkata Krishna, Srinivasa rao. B and my aunts Vijayamma, Lakshmi, Sarada for their constant love, support and encouragement. I am very much indebted to all my family members.

Above all, I owe it all to Almighty God for giving me the wisdom, health and belief to undertake research work of my thesis and enabling me to its completion.

Narasimharao Kanna

Table of Contents

Contents	vii
Abbreviations	xiii

Chapter 1: Introduction	1
1.1 Introduction of Catalysis	2
1.2. Green Chemistry	3
1.3. Dioxygen	4
1.3.1. Chemical History	4
1.3.2. Activity and reactivity of dioxygen species	5
1.3.3. Reactivity of Oxygen	6
1.3.4. Chemical activation of oxygen	8
1.4. Selective oxidations	9
1.4.1. Single Step Oxidation of cyclohexane to Adipic acid	13
1.4.1.1. Production of AA	14
1.4.1.2. Possible pathways in the production of adipic acid	14
1.4.1.3. Current industrial process	15
1.5. Biomass valorization	15
1.5.1. Incentives and scope	15
1.5.2. Composition of biomass	16
1.5.3. Direct and indirect green substitution	17
1.5.4. 5-Hydroxymethyl furfural as a platform chemical	18
1.5.5. Selective oxidation of 5-HMF to 2,5-Furandicarboxylic acid	20
1.6. Introduction to porous manganese oxides	20
1.6.1. Manganese	20
1.6.2. Manganese oxide minerals	21
1.6.3. Manganese oxide mineral with tunnel structures	22
1.6.3.1. Todorokite	22
1.6.3.2. Hollandite group	23
1.7. Carbon nitrides	25
1.7.1. Introduction	25
1.7.2. A brief history of carbon nitride	26

1.8. Scope and objective of the present thesis	30
1.9. Organization of the thesis	31
1.10 References	34
<hr/>	
Chapter 2: Experimental Methods and Characterization Techniques	40
<hr/>	
2.1. Introduction	41
2.2. Catalyst preparation	41
2.2.1. Preparation of K-OMS-2 and Co substituted K-OMS-2	41
2.2.2. Preparation of Ru exchanged Mg-OMS-1	42
2.2.2.1. Preparation of Mg-OMS-1	42
2.2.2.2. Synthesis of Ru exchanged Mg-OMS-1	43
2.2.2.3. Preparation of other precious metal (Au, Pd, Pt) exchanged Mg-OMS-1	43
2.2.3. Preparation of Ru exchanged Mg-OMS-2	43
2.2.4. Preparation of carbon nitride nano tubes	43
2.3. Characterization of catalysts	44
2.3.1. Powder X-ray diffraction	44
2.3.2. N ₂ Physisorption and CO chemisorption	45
2.3.3. Electron microscopy	47
2.3.3.1. Transmission electron microscopy	47
2.3.3.2 Scanning electron microscopy	48
2.3.4. X-ray Photoelectron Spectroscopy	49
2.3.5. Inductively coupled plasma-optical emission spectroscopy	50
2.3.6. Infrared Spectroscopy	52
2.3.7. Thermal analysis	53
2.3.8. Cyclic Voltammetry Studies	53
2.4. References	55
<hr/>	
Chapter 3: Selective oxidation of cyclohexane with Co-K-OMS-2 catalysts	57
<hr/>	
3.1 Introduction	58
3.2. Current industrial processes for the production of AA	59
3.2.1. First step: Oxidation of cyclohexane with air	59

3.2.2. Second step: Oxidation of KA oil with nitric acid	60
3.2.3. Environmental impact of the second step	61
3.3. Alternate pathways for AA production	62
3.3.1. Oxidation of cyclohexene	62
3.3.2. Butadiene as starting material	63
3.3.3. n-Hexane as starting material	63
3.3.4. D-Glucose as starting material	63
3.4. Literature overview of one step oxidation of cyclohexane	64
3.4.1. Homogeneous catalysts	64
3.4.2. Heterogeneous catalysts	65
3.5. Experimental procedures	66
3.5.1. Materials	66
3.5.2. Initiator Preparation	66
3.5.3. Experimental Setup	67
3.6. Analytical Procedure	67
3.6.1. Esterification procedure of Diacids	67
3.7. Textural Characterization of Catalysts	67
3.7.1. Powder X-ray diffraction	67
3.7.2. N ₂ physisorption	68
3.7.3. Raman Spectroscopy	69
3.7.4. Fourier-Transform infrared Spectroscopy	71
3.7.5. Thermo gravimetric analysis	72
3.7.6. Scanning Electron Microscopy	73
3.7.7. Transmission Electron Microscopy	74
3.7.8. H ₂ -Temperature programmed reduction	75
3.7.9. X-ray photoelectron spectroscopy	76
3.7.9.1. Mn 2p spectra	77
3.7.9.2. O 1s spectra	78
3.7.9.3. Co 2p spectra	70
3.8. Catalytic Activity- Single step selective oxidation of cyclohexane to adipic acid	80
3.8.1. Effect of temp on Adipic acid yield	81
3.8.2. Effect of time on AA yield	81

3.8.3. Effect of Catalyst content on AA yield	82
3.8.4. Effect of initiator amount on the yield of AA	83
3.8.5. Effect of Co content of the catalyst on the yield of AA	84
3.8.6. Recycle study of the Catalyst	85
3.9. Proposed reaction mechanism	86
3.10. Conclusions	88
3.11. References	90
<hr/>	
Chapter 4: Metal free carbon nitride nano tubes as catalysts for hydrocarbon Oxidation.	94
<hr/>	
4.1 Introduction	95
4.1.1 Elemental sustainability	95
4.2 Experimental Procedures	99
4.2.1 Materials	99
4.2.2 Experimental setup for selective oxidation	99
4.3 Textural characterization of catalyst	99
4.3.1. X-ray diffraction	99
4.3.2. IR spectra of as synthesized materials	101
4.3.3. UV visible spectra of carbon nitride nano tubes	102
4.3.4. Scanning electron microscopy	103
4.3.5. Transmission Electron Microscopy	103
4.3.6. X-ray photoelectron spectroscopy	104
4.3.7. Cyclic voltammetry	104
4.4 Selective oxidation of cyclohexane to adipic acid in single step	106
4.4.1. Effect of temperature	106
4.4.2. Effect of reaction time	107
4.4.3. Effect of catalysts content	108
4.4.4. Effect of oxygen pressure	109
4.4.5. Recyclability of catalyst	109
4.5. Solvent free oxidation of cyclohexane	110
4.5.1. Effect of temperature	110
4.5.2. Effect of time	111

4.6. Comparison of various catalysts in the selective oxidation of cyclohexane	112
4.7. Proposed reaction mechanism	113
4.8. Carbon nitride nanotube as catalyst for other selective oxidation processes	114
4.8.1. Oxidation of cyclohexanone to adipic acid	115
4.8.1.1. Effect of temperature	115
4.8.1.2. Effect of reaction time	116
4.8.2. Selective oxidation of ethyl benzene to acetophenone	116
4.8.2.1. Effect of reaction temperature	117
4.8.2.2. Effect of time	118
4.8.2.3. Effect of catalyst content	119
4.8.3. Bayer-Villiger oxidation of cyclohexanone to Caprolactone	120
4.9. Conclusions	121
4.10. References	123

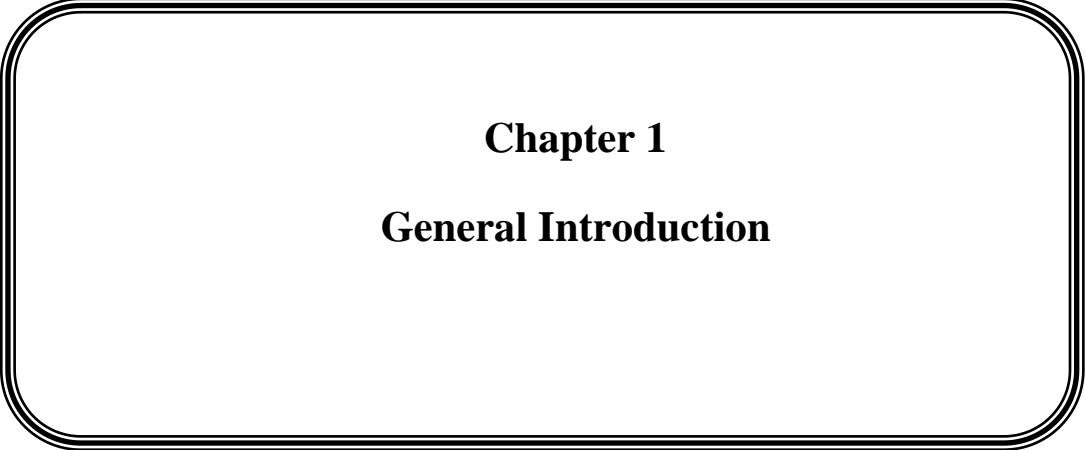
Chapter 5: Base free oxidation of biomass derived compounds to their corresponding acids 126

5.1. Introduction	127
5.2. 5-HMF – A precursor for commercial chemicals	127
5.3. 2,5- FDCA- a polymer building block	129
5.4. Literature overview on HMF oxidation to 2,5-FDCA.	130
5.5 Experimental Procedures	134
5.5.1 Materials	134
5.5.2 Standard procedure for HMF selective oxidation	134
5.6. Textural Characterization of catalysts	134
5.6.1. X-ray diffraction	134
5.6.2. N ₂ physisorption	136
5.6.3. H ₂ Chemisorption of 2wt% Ru-Mg-OMS-1	137
5.6.4. Chemical analysis of the prepared materials	137
5.6.5. Thermo gravimetric analysis	137
5.6.6. Scanning Electron Microscopy	139
5.6.7. Transmission Electron Microscopy	140
5.6.8. Temperature programmed desorption of CO ₂	140

5.6.9. X-ray photoelectron spectroscopy	141
5.7. Base free oxidation of 5-HMF to 2,5-FDCA with 2Wt% Ru-Mg-OMS-1	143
5.7.1. Effect of temperature and reactiontime on the yield	144
5.7.2. Effect of HMF/Ru mole ratio on the yield	145
5.7.3. Effect of oxygen pressure on the yield	146
5.7.4. Effect of OMS structure on FDCA yield	146
5.7.5. Effect of noble metals on the yield of FDCA	148
5.7.6. Recyclability of catalyst	148
5.7.7. Possible Mechanism of HMF selective oxidation to FDCA	149
5.8. Introduction to base free Oxidation of furfural to furoic acid	152
5.8.1. Applications and literature overview of 2-furoic Acid	152
5.9. Standard operating procedure for furfural selective oxidation reaction	153
5.10. Catalytic activity of 2% Ru-Mg-OMS-1 for selective oxidation of furfural	153
5.10.1. Effect of temperature and time	153
5.10.2. Effect of substrate to metal mole ratio	154
5.10.3. Variation of precious metals on selective oxidation of 2-furfural	155
5.10.4. Role of support on selective oxidation of 2-furfural	156
5.11. Possible Mechanism for the oxidation of 2-furfural to 2-furoic acid	157
5.12. Conclusions	158
5.13. References	159
<hr/>	
Chapter 6: Summary and Conclusions	162
<hr/>	
6.1 Summary and Conclusions	163
6.2 Suggestions for future research	166

LIST OF ABBREVIATIONS

KOMS-2	Potassium octahedral molecular sieves-2 (Cryptomelane)
BE	Binding energy
BET	Brunauer-Emmett-Teller
GC	Gas chromatography
HPLC	High-Performance liquid chromatography
FID	Flame Ionization detector
FTIR	Fourier Transform Infra-red
ICP-AES	Inductively coupled plasma atomic emission spectroscopy
PXRD	Powder X-ray diffraction
SEM	Scanning electron microscopy
HRTEM	High Resolution Transmission electron microscopy
TGA	Thermogravimetric analysis
XPS	X-ray photoelectron spectroscopy
CV	Cyclic Voltammetry
NHPI	N-hydroxy phthalimide
NAPI	N-acetoxy phthalimide
C-C	Carbon - Carbon



Chapter 1
General Introduction

1.1. Introduction of Catalysis

Catalysis is part of our everyday life and contributes substantially to societal wellbeing. Catalysis research and development of chemical industry go hand in hand. It is therefore not surprising that many basic chemical processes e.g. hydrogenations, oxidations etc., which are of utmost interest to both academia and industry bring forth more and more effective catalysts, new technologies and in-depth understanding of fundamental catalytic principles. Catalysis is important to the development of environmentally benign and sustainable processes and a corner stone to the concept of “Green Chemistry” [1-3]. Heterogeneous catalysis takes place at the interface between two phases; hence it requires great skills to study it. As a result of intensive research, better knowledge is available on important gas-phase reactions like ammonia synthesis and CO oxidation [4].

The term catalysis was first coined by Swedish chemist Berzelius in 1836. According to him, besides “Affinity” a new force is operative, that is “catalytic force” [5-7]. Reaction occurs by catalytic contact. The word 'catalysis' stems from the Greek: it has the sense of “down” and “loosen”. At the end of the 18th and the beginning of the 19th century, the influence of metals and metal oxides on the decomposition of several substances was studied by many scientists. The principle features of catalysis were first presented by Fulhame [8] in 1794, when she suggested that the presence of small quantities of water was required for the oxidation of carbon monoxide and that the water was unaffected by the chemical reaction. Similar observations were made by Kirchhoff who hydrolyzed starch to sugars by using dilute acids in 1812 [9]. Sir Humphry Davy in 1817 suggested that combustible gases, when mixed with oxygen, could explode if they were exposed to heated platinum at temperatures below the ignition temperature [10]. In 1834, Faraday proposed that the reactants have to be adsorbed simultaneously on the surface. Lemoine in 1877 explained for the first time that a catalyst cannot influence the position of the equilibrium; it can only alter the rate at which it can be reached [12]. This view was modified by Ostwald who claimed that a catalyst cannot initiate a chemical change; it can only accelerate or retard [13].

1.2. Green Chemistry

These days, there is a growing concern about environment, thus development of environmentally benign and sustainable processes for the chemical industry has gained importance. These developments drive a paradigm shift from orthodox concept of process efficiency that focuses largely on chemical yield, to one that provides economic value to eliminating waste at source and avoid the use of toxic and/or hazardous substances. This concept is called Green chemistry [14] by P. Anastas

Green chemistry efficiently utilizes renewable raw materials, eliminates waste and avoids use of toxic and/or hazardous reagents and solvents in the manufacture and application of chemical products

This concept is embodied in the 12 principles of 'Green Chemistry' which can be paraphrased as

1. Waste prevention instead of remediation
2. Energy efficient by design
3. Shorter synthesis (avoid derivatization)
4. Less hazardous/toxic chemicals
5. Design products for degradation
6. Energy efficient by design
7. Safer products by design
8. Catalytic, rather than use of stoichiometric reagents
9. Innocuous solvents and auxiliaries
10. Atom efficiency
11. Renewable raw materials preferably
12. Analytical methodologies for pollution control

The ideology of green chemistry calls for the development of innovative processes and catalysts that can potentially benefit chemical synthesis in terms of resource utilization, energy efficiency, product selectivity, operational simplicity, health and environmental safety.

An alternative term, which is currently favored by the chemical industry, is sustainable technologies. Sustainable development has been defined as “Meeting the needs of the present generation without compromising the ability of future generations to meet their own needs” [15]. One could say that sustainability is the goal and green chemistry is the means to achieve it.

Most of the polluting agents are synthetic and are discharged into the environment by the chemical industry, through fluid leakage, as waste materials into the natural aquifers. Currently production of bulk chemicals is carried out largely based on environmental hazardous catalysts like homogeneous metal salts, acids and toxic solvents. The present thesis mainly focuses on the development of green processes for the oxidation of hydrocarbons and biomass derived chemicals.

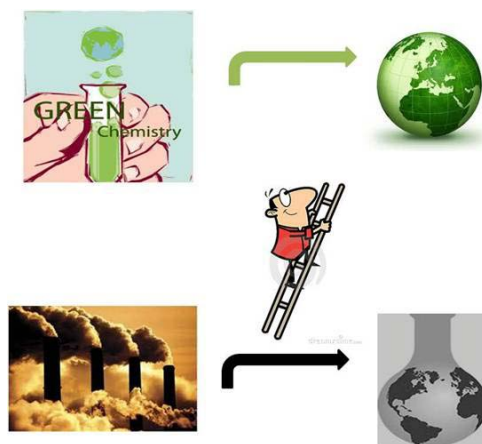


Fig. 1.1. A ladder towards the green process from the traditional process.

1.3. Dioxygen

1.3.1. Chemical History

In 1777, Antoine L. Lavoisier identified dioxygen as a component of air, and named it oxygen on the basis that it reacts with other elements generating oxyacids [14]. He established that dioxygen is the oxidant of fuels in combustion, and it is the essential oxidant for biological respiration. The dioxygen comprises about 21 % (by volume) of the Earth's atmosphere, which is essential for aerobic life and toxic to plant life at higher concentrations. It is an essential oxidant for the combustion of organic molecules (fuels). Joseph Priestley also noted that nitric oxide reacts with O_2

to produce NO_2 and N_2O_4 , which react with water to form $\text{HON}(\text{O})$ and $\text{HON}(\text{O})_2$ (nitrous acid and nitric acid).

1.3.2. Activity and reactivity of dioxygen species (O_2^\bullet , HO^\bullet , $\text{O}_2^{\bullet-}$, HOOH)

Reactive oxygen species are (i) molecules like hydrogen peroxide, (ii) ions like hypochlorite, (iii) radicals like hydroxyl radical (the most reactive of all) and (ii) Superoxide anion which is both ion and a radical.

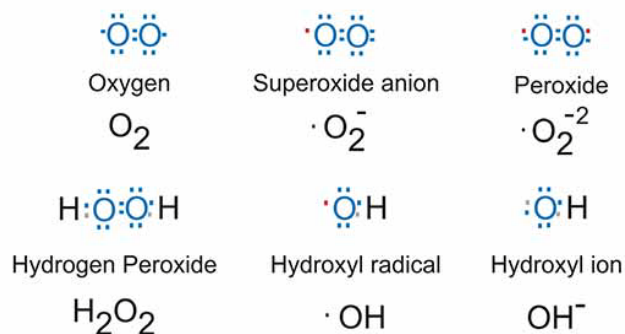


Fig. 1.2. Various reactive oxygen species.

A great emphasis, these days is on the use of environment friendly oxidants (“green” oxidants) that generate minimum amount of waste. Table 1.1 lists the most commonly used oxidants. They are classified as per their active oxygen content, which is the ratio between the weight of the oxygen atoms to be transferred to the substrate and the weight of the oxidant itself. By-products, formed during the oxidation reaction, are also reported.

An oxidative process of interest from a sustainable point of view, should address economical benefits as well as green chemistry concerns by (i) providing the highest percentage of active oxygen, leading to greater atom economy [15]; (ii) avoid the formation of toxic and difficult to eliminate by-products; (iii) using an oxidant abundantly available at low cost.

Based on the above considerations, it is obvious that the most attractive oxidant is molecular dioxygen - (O_2) [16] because of (i) its high active oxygen content (depending on the reaction, it can reach 50% or 100%, when one or two oxygen atoms

are respectively introduced in the substrate (ii) it does not give any oxidation by-products (iii) it is cheap and abundant, in the atmosphere. Hydrogen peroxide is also of great interest, though its costs are still high.

Table 1.1 Classification of oxidants on the basis of the active oxygen percentage and the by-products formed.

Oxidant (OD)	% of Active Oxygen	By-Product (D)
O ₂	100	none
H ₂ O ₂	47	H ₂ O
N ₂ O	36.4	N ₂
O ₃	33.3	O ₂
ClO ⁻	21.6	Cl ⁻
(CH ₃) ₃ COOH (TBHP)	17.8	(CH ₃) ₃ COH
HSO ₅ ⁻	10.5	HSO ₄ ⁻
ClC ₆ H ₄ COOOH (m-CPBA)	10.2	ClC ₆ H ₄ COOH
IO ₄ ⁻	7.5	IO ₃ ⁻
C ₆ H ₅ IO (PhIO)	7.3	C ₆ H ₅ I

1.3.3. Reactivity of oxygen

The importance and reactivity of molecular oxygen in oxidation was realized in 18th century. Later observations suggested that the deterioration of many organic materials (such as rubber and natural oils) results from oxygen adsorption. Further studies led to the recognition that organic peroxides were the primary products of these oxidative processes. As a result, free-radical chain theory of autoxidation was established in 1940's [17]. The liquid-phase autoxidation of hydrocarbons has been studied extensively and is well-established now.

Autoxidation reactions are recognized for long induction periods, because of the thermodynamically unfavorable C-H bond cleavage in the first step. Molecular oxygen is in triplet state, whereas the substrate is in a singlet state. The spin-

conservation rule forbids the interaction of the two species in the ground state. Thus, despite favorable thermodynamics for reaction between dioxygen and the organic molecules, an activation step for the substrate, dioxygen or both of them is required. Rate of oxidation mostly depends on different parameters like catalyst, substrate and reaction time. Examples of various oxidation rates are given in Table 1.2.

Table 1.2 Various oxidation reactions and their rate of conversion.

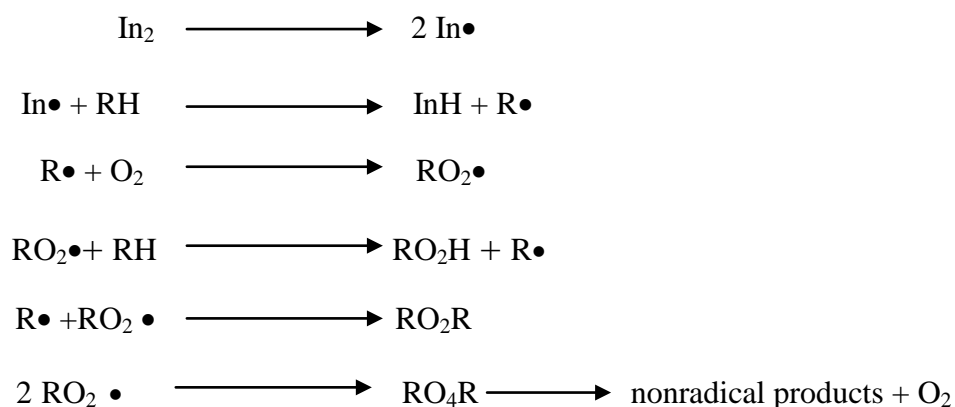
<i>Rate of reaction^a (molecules $\text{cm}^{-3} \text{s}^{-1}$)</i>	<i>Time required for complete conversion^b</i>	Examples of reaction
$10^3 - 10^{10}$	$10^{10} - 10^3 \text{ yr}$	Initial rate of uncatalyzed hydrocarbon oxidations
$10^{13} - 10^{14}$	2 yr- 10 weeks	Degradation of unstabilized plastics under irradiation
10^{16}	ca. 20h	Industrial radical reactions (e.g., liquid-phase oxidation and polymerization)
10^{18}	ca. 10min	Heterolytic reactions (e.g., epoxidation with ROOH/Mo complex)
10^{20}	ca. 6s	Heterolytic reactions heterogeneously catalyzed hydrocarbon oxidations
10^{22}	ca. 10^{-2} s	Heterogeneously catalyzed hydrocarbon oxidations
10^{24}	ca. 10^{-4} s	Explosions; ion reactions

^a pure hydrocarbons contain ca. 6×10^{21} molecules per cubic centimeter.

^b 1 year \approx 8760h \approx $3.15 \times 10^7 \text{ s}$.

Use of molecular oxygen as a terminal oxidant in metal catalyzed oxidation of hydrocarbons has been an area of vigorous and intense research mainly because of the environmental and economic advantages of using dioxygen in place of peroxides, per acids or iodoarenes. The various mechanisms by which metals catalyze oxidation of hydrocarbons can be separated into three broad categories: (i) Metal catalyzed decomposition of intermediate peroxide, (ii) Direct attack on the substrate by the metal complex, (iii) Direct activation of molecular oxygen by the metal complex [18].

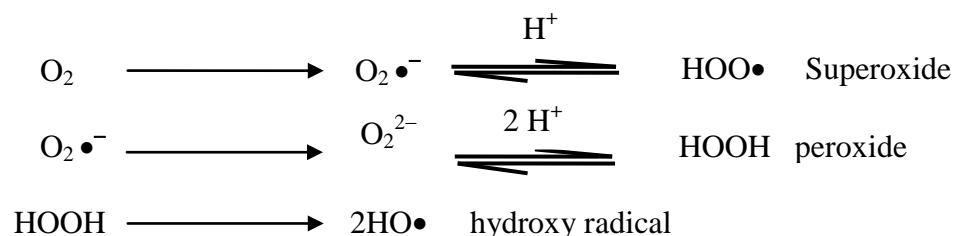
The substrate activation is generally obtained by homolytic reactions in which a radical initiator provides organic radicals which are able to react with dioxygen, affording oxidized species. Such mechanism, reported in Scheme 1.1 foresees the presence of radical species in the initiation steps, as well as in the propagation and termination steps [19].



Scheme 1.1 Reaction mechanisms in auto oxidation reactions.

These are known as auto oxidation reactions [20]. Though, not very selective, they are still used for the production of many important industrial chemicals [21].

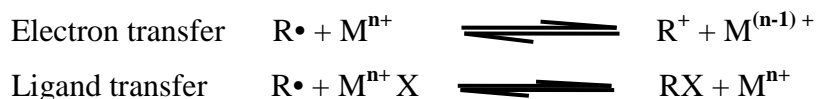
1.3.4. Chemical activation of oxygen



Scheme 1.2- Reaction mechanisms in auto oxidation reactions.

The activation of the molecular oxygen can be achieved by means of chemical processes (scheme 1.2).

The reactions of free radicals with metal complexes (MX) can be classified as either electron transfer or ligand transfer processes. Competition between electron transfer and ligand transfer depends to a large extent on the nature of the ligand X. Hard ligands, such as acetate tend to favor electron transfer processes, whereas soft ligands, such as bromide, favor ligand transfer.



The reactions of organic compounds with oxygen have received considerable attention, particularly with reference to metal catalysis, because of their utility as oxygen “carriers” and from the standpoint of oxygen “activation”. The oxidation of hydrocarbons by dioxygen catalyzed by metal complexes is normally a radical chain reaction. Usual product of the radical chain is an alkyl hydroperoxide, ROOH. These hydroperoxides are unstable under reaction conditions and decompose to give alcohols, ketones, aldehydes, carboxylic acids and esters. The major function of a metal complex in many oxidation processes is the catalytic decomposition of hydroperoxides. In this way the metal enhances the formation of desirable products and stimulates the production of free radical species that initiate the radical chain reaction between the hydrocarbon and dioxygen. These two effects give substantial control over the yield and the rate of the overall oxidation process.

1.4. Selective oxidations

Selective oxidation of hydrocarbons is of crucial importance in activating hydrocarbons to form intermediates and final products for applications in chemical and pharmaceutical sectors [23]. Around the world, about one quarter of all the organic compounds produced are synthesized via selective oxidation of the hydrocarbons [24]. During the last two decades, a significant progress has been made within the area of catalytic oxidations, which has led to a range of selective and mild processes from both industrial and synthetic point of view. These reactions may be based on organocatalysis, metal catalysis or biocatalysis. Some of the large scale industrial catalytic oxidation processes include: oxidation of (a) p-Xylene to

terephthalic acid (oxidant–oxygen, liquid phase process), (b) cyclohexane to adipic acid (oxygen, liquid phase), (c) cumene to cumyl hydroperoxide (oxygen, liquid phase), (d) n-butane to maleic anhydride (oxygen, gas phase) etc. In all these processes, reactions are conducted at high temperatures and high O₂ pressures.

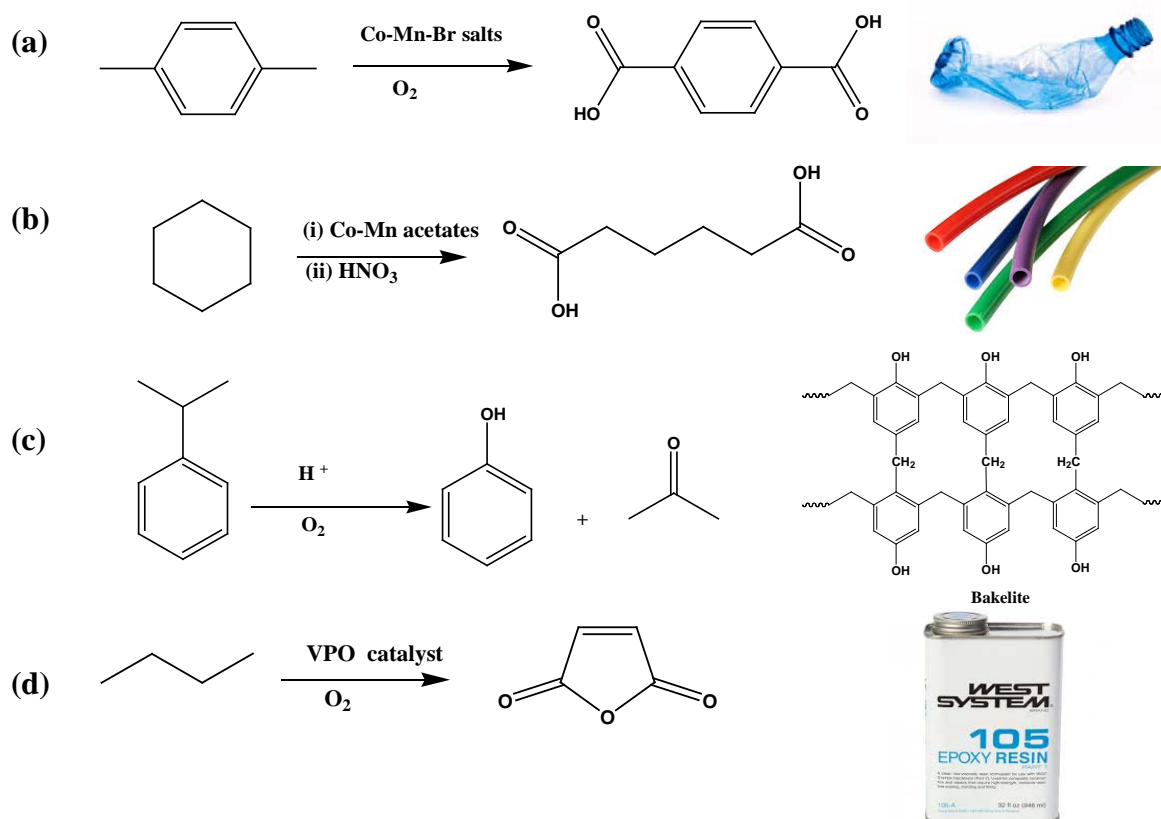


Fig. 1.3. Catalytic oxidation reactions.

In this context, oxidation catalysis has been playing and will be playing a leading role [25]. The reason for this is that oxidation is the tool for the production of huge quantities of intermediates and monomers for the polymer industry (Table 1.3).

The impact of these manufacture on the environment might have been much greater, if considerable efforts are not gone into continuous improvement of the technologies used for the production of these chemicals, including the replacement of toxic and dangerous reactants, better heat recovery and energy integration in the plant, recovery of waste streams and abatement of tail emissions, and downstream use of by-products. In the chemical industry, oxidation is one of the technologies that have great potential for improvement, and this has led to a series of better processes in recent years.

Table 1.3. Organic chemical intermediates produced by means of selective oxidation

Chemical	Capacity [Mta ⁻¹]	oxidant
Terephthalic acid	44	air
Formaldehyde	19	air
Ethylene Oxide	18	O ₂
Propylene Oxide	8	Cl ₂ , ROOH, H ₂ O ₂
Acrylonitrile	6	air
Styrene	5	air, O ₂
Phenol	5	air
Adipic acid	3	HNO ₃
Maleic anhydride	2	air

Mta⁻¹ : Million tonnes per annum

Improvements to catalysts, reaction and process technologies have moved in the direction of an improved sustainability and have been widely documented in the books and research publications in recent years [26]. Although the developments were driven by economics, it also led to more sustainable processes (Table 1.4.). However, some processes still co-produce large amounts of waste or operate under conditions leading to non-optimal selectivity to the desired compound.

Table 1.4 Some industrial selective oxidation processes: improvements achieved and targets for a better process economics and sustainability [27].

Industrial Oxidation Process	Oxi-dant	Conversion, Selectivity [%]	Achievements	Targets
Methanol to Formaldehyde	air	99, 94-95	Better heat integration, Higher productivity.	More efficient reactors for larger scale productions.
Cyclohexane to Cyclohexanol/-one	O ₂	10-15, 90	Technological improvements adopted. Use of O ₂ in place of air.	Increase per-mass conversion and selectivity.

Cyclohexanol/-one to adipic acid	HNO ₃	100, 95	Several technological improvements adopted. Catalytic or thermal abatement of by-product N ₂ O. Recycle of NO and NO ₂ .	Direct oxidation of cyclohexane to adipic acid: performance to be improved; avoid acetic acid as solvent.
Cyclohexanone + NH ₃ to Cyclohexanone oxime	H ₂ O ₂	100, 96-98	Several improvements to the classical process. New H ₂ O ₂ -based process: no by-product in oxime formation.	Alternative, non-oxidation technology available (hydrogenation of adiponitrile to 6-aminocapronitrile and subsequent cyclization or direct polymerization).
para-Xylene to Terephthalic acid	air	98-99, 93-97	Technological improvements adopted (energy integration, safety, overall performance).	Avoid use of corrosive medium (acetic acid), bromide salt. Avoid undesired by-product impurities.
n-butane to maleic anhydride	air	75-85, 65-73	Replacement of the earlier process that used benzene.	Better replacement.
Acetaldehyde to Acetic acid	O ₂ air	96-98, 97-99 91-92, 93-94	Replaced by methanol carbonylation.	Direct oxidation of ethane to acetic acid.
Two-step propene to acrylic acid (via acrolein)	air	92-95, 84-89	Technology improved over the years: energy integration, overall performance.	One-step process from propane. The direct oxidation of propane, a cheaper reactant than propene, would also allow lower investment costs

A sustainable catalytic oxidation should present the following fundamental features

(i) capability to activate O_2 and H_2O_2 , in aqueous phase, with solvent-free protocols, or by using environmental friendly solvents, including per fluorinated environment, ionic liquids and carbon dioxide, (ii) high selectivity, (iii) oxidative, hydrolytic and thermal stability in the reaction conditions.

The contemporary presence of these features could provide the “ideal oxidation catalyst” (Fig. 1.4).

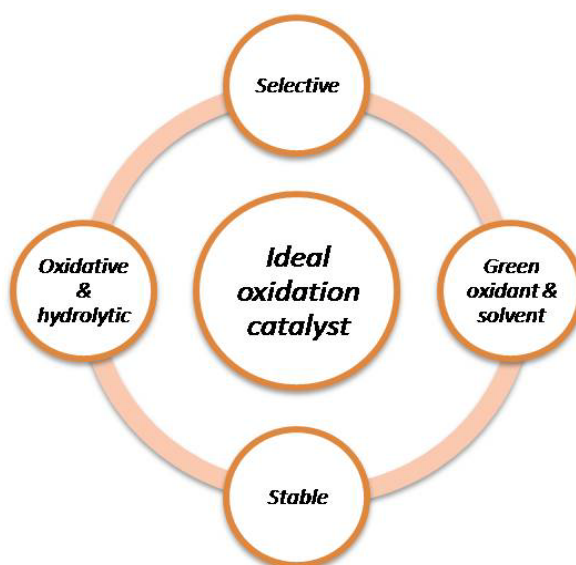


Fig. 1.4 Schematization of the features of an “ideal” oxidation catalyst.

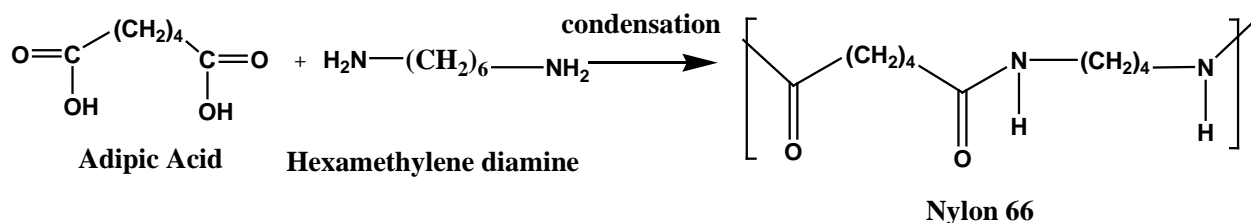
1.4.1. Single step oxidation of cyclohexane to adipic acid

Adipic acid (AA) is one of the most important aliphatic acids with the chemical formula: $COOH-(CH_2)_4-COOH$. Little of adipic acid occurs naturally, but it is produced on large scale around the world.

Adipic acid is an important chemical intermediate; the main use of AA is for the manufacture of Nylon 6,6. This polymer was first synthesized by Wallace Hume Carothers in 1935 in the laboratories of DuPont and after three years DuPont patented the process. Scheme 1.3 shows the reaction for production of Nylon 6,6 [28], which is mainly used for production of fibers (fishing lines, tyres, carpets, home furnishing, and in tough fabrics for backpacks, parachutes, luggage and business cases) and of

resins. Nylon resins are used in electrical connectors, auto parts, and items such as self-lubricating bearings, gears and cams [29].

Though the main use of adipic acid is as given above, there are more ways of using adipic acid which is evident from Fig. 1.5.



Scheme 1.3. Production of Nylon 6,6 from adipic acid and hexamethylene diamine.

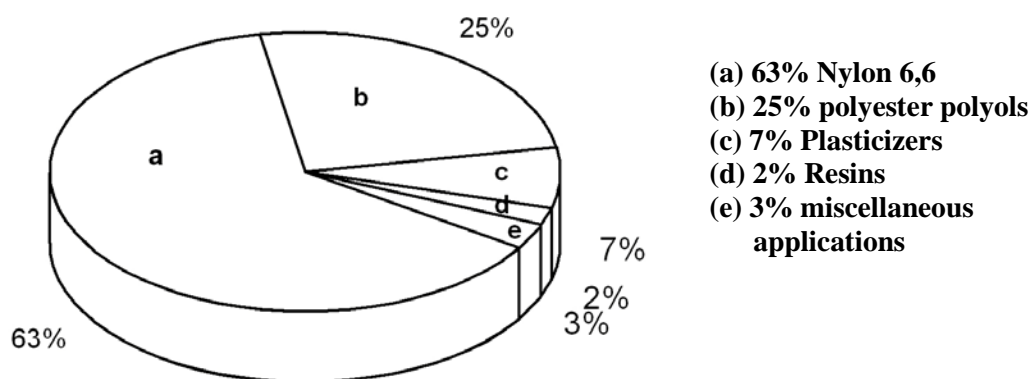


Fig. 1.5. Applications of Adipic acid.

1.4.1.1. Production of AA

The global AA capacity in the year 2010 was around 2.9 million metric tons per annum. The overall growth for AA is about 3% per year and expected to grow much faster in near future. The most rapidly growing sector is the nylon one, where during the past decade it was between 8-10% per year [30].

1.4.1.2. Possible pathways for the production of adipic acid

Fig. 1.6 summarizes the possible routes for the synthesis of adipic acid. Some of them are “green”, but only a few of them can be considered truly sustainable, from both an environmental and an economic standpoint, if the cost of reactants and the complexity of the operation are taken into consideration.

difference in cost between fossil and biomass resources is now narrowing. Moreover, the tipping economic balance is accompanied by an increased environmental awareness of the public and renewed political concerns about global warming. As a result, utilization of biomass has once again become priority. Biomass utilization offers at least a supplementary source of energy and chemicals, thus relieving the import of fossil resources. One of the advantages of using biomass is that this vast resource is not solely located in specific regions of the world and the implementation strategies can vary depending on local conditions such as weather, demand, wages, soil quality, soil availability as well as local human expertise.

Biomass is currently the only viable non-fossil source for liquid hydrocarbons that can be used as additives to conventional liquid transportation fuels [33]. One such additive produced in large scale is bioethanol which can be obtained through fermentation. The potential for biomass utilization is very high, however the practical implementation is technically complex and politically sensitive due to a number of reasons. The most obvious complication is the potential competition between biofuel production and the food production, protection of biodiversity, soil degradation issues for the fluctuating price of fossil fuels as well as the willingness and determination for the abatement of CO₂ emissions [34]. The US DOE (Department of Energy) and Department of Agriculture have made an estimate which concludes that more than 1 billion tons/year of lignocellulosic material could be sustainably produced within the US before the middle of this century. This, however, is not enough to meet the fuel requirement and only covers perhaps around 1/3 of the need but it could theoretically suffice to replace the fossil compounds used in the production of chemicals [35,36].

1.5.2. Composition of biomass

The most abundant biomass is lignocellulosic material such as wood or straw. Figure. 1.7 shows the structure of cellulose, hemicellulose and lignin which are the major components of lignocellulose. Cellulose is a linear polysaccharide of D-glucose. The percentage of cellulose differs from source to source, for example in wood it is around 40%, while hemicelluloses content is approximately 30% of the

matter. Hemicellulose is a branched amorphous polysaccharide made up of several different sugar monomers mainly the hexoses such as glucose, galactose and mannose; and the pentoses xylose and arabinose. Whereas, the lignin content in biomass is around 25% [37]. Lignin is a polymer that consists of branched phenyl propane units predominantly linked by ether bonds. Additionally, minor amounts of extractable organics and inorganic salts are present in lignocellulose [31].

Through mechanical and/or chemical treatment it is possible to roughly separate the individual three major components based on differences in the rate of hydrolysis by steam explosion, base stability etc. thus allowing for the very different components to be utilized through separate dedicated processes [38, 39].

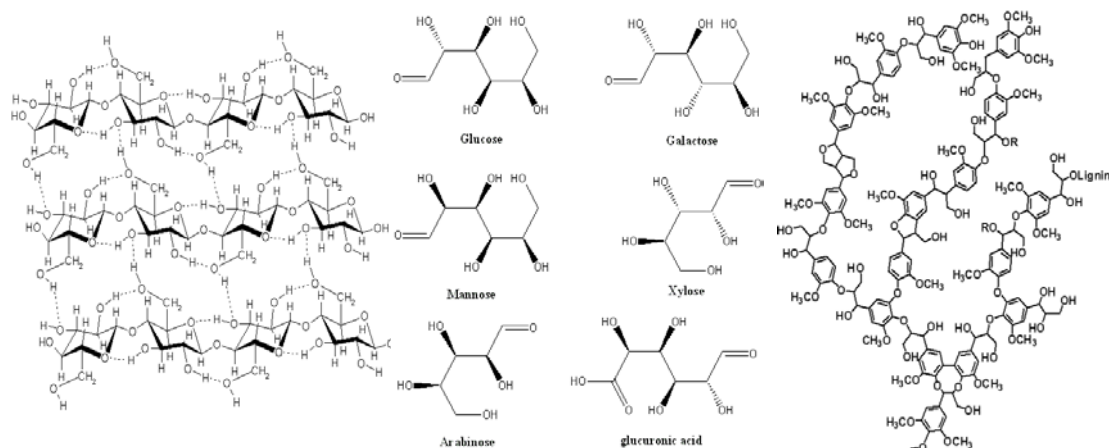


Fig. 1.7. Cellulose polysaccharide (left), monomers present in hemicellulose (middle) and lignin (right).

1.5.3. Direct and indirect “green” substitution

The majority of chemicals, which are used in producing the huge amount of wrappings, tools etc. derive from fossil sources. Fascinatingly, only few molecular building blocks including syngas (CO and H_2), ethylene, propylene, methanol, benzene, toluene and xylene make up the usual starting materials in the complex value chain [40]. If biomass aims to vary the use of fossil resources a key difference will therefore be whether it is transformed into one of the present basic building blocks or whether new chemicals are targeted [41]. Due to the high functionality, biomass

derived compounds carry little similarity to the classical fossil building blocks. It is thus important to differentiate between direct and indirect substitution strategies. In a direct strategy, similar chemicals that can replace fossil chemicals are produced from biomass, whereas an indirect substitution would produce a different chemical which could fulfill the identical function as the conventionally fossil derived product. It is obvious that both advantages and disadvantages exist when targeting an “old” or otherwise a new platform molecule. For example, if biomass can be converted selectively to xylene, a known market already exists including a unit price and therefore the economical potential of the process could be evaluated. It would however also make the production highly vulnerable to price fluctuations of the specific chemical.

1.5.4. 5-Hydroxymethyl furfural as a “platform chemical”

The word “platform chemical” is used to describe a compound which has a suitable chemistry to allow multiple transformations into various value added products. Through a variety of chemical techniques, hexoses can be converted to furanics, which are heterocyclic compounds with an aromatic ring comprised of four carbon atoms and oxygen. One such furanic that is becoming increasingly significant is 5-(Hydroxymethyl) furfural (HMF). It constitutes a furan ring system with an aldehyde and a hydroxymethyl group at the 2 and 5 positions respectively. It can be prepared from the furanose forms of hexose sugars by dehydration reaction (Fig. 1.8.) [42]. HMF has been shown to form when sugars are heated, typically under acidic conditions [43]. Additionally, HMF has been detected in foods such as dried fruits [44] and baking products [45], and it is found that the daily intake of HMF is 30–150 mg per person [46]. HMF can be toxic to humans when ingested at concentrations of 75 mg per kg of body weight or greater.

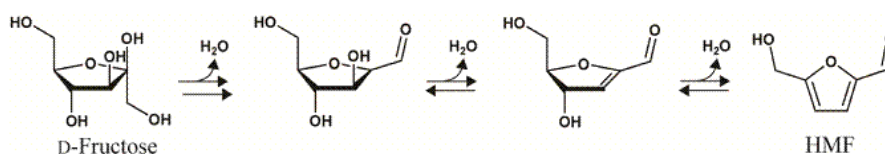


Fig. 1.8. Dehydration of D-fructose to HMF.

The true value of HMF lies in its capacity to transform into a number of useful compounds (Fig. 1.9.) [47]. Rehydration of HMF leads to its decomposition into levulinic acid and formic acid [48], both valuable commodity chemicals. Levulinic acid is a precursor to the liquid fuel γ -valerolactone [49]. Oxidation of hydroxymethyl group of HMF leads to 2,5-diformylfuran and subsequently to furan-2,5-dicarboxylic acid (FDCA). This is of particular interest as it can be used as a polymeric substitute for terephthalic and isophthalic acids which are used to form polyamides, polyesters and polyurethanes [50]. Hydrogenation of HMF leads to the formation of 2,5-bis(hydroxymethyl) tetrahydrofuran and 2,5-diformyl-tetrahydrofuran. These products can undergo condensation to generate polymers that can ultimately become liquid alkanes [51]. Hydrogenolysis of HMF can give 1,6-hexane diol, a precursor for adipic acid production [52]. HMF can also undergo undesirable degradation and polymerization to form insoluble polymers known as humins by reaction with itself and other monosaccharides [53]. Finally, hydrogenolysis can lead to 2,5-dimethylfuran (DMF), 2,5-dimethyltetrahydrofuran and 2-methyltetrahydrofuran. DMF is of great interest as a biofuel with its high energy density, low volatility and immiscibility with water [54].

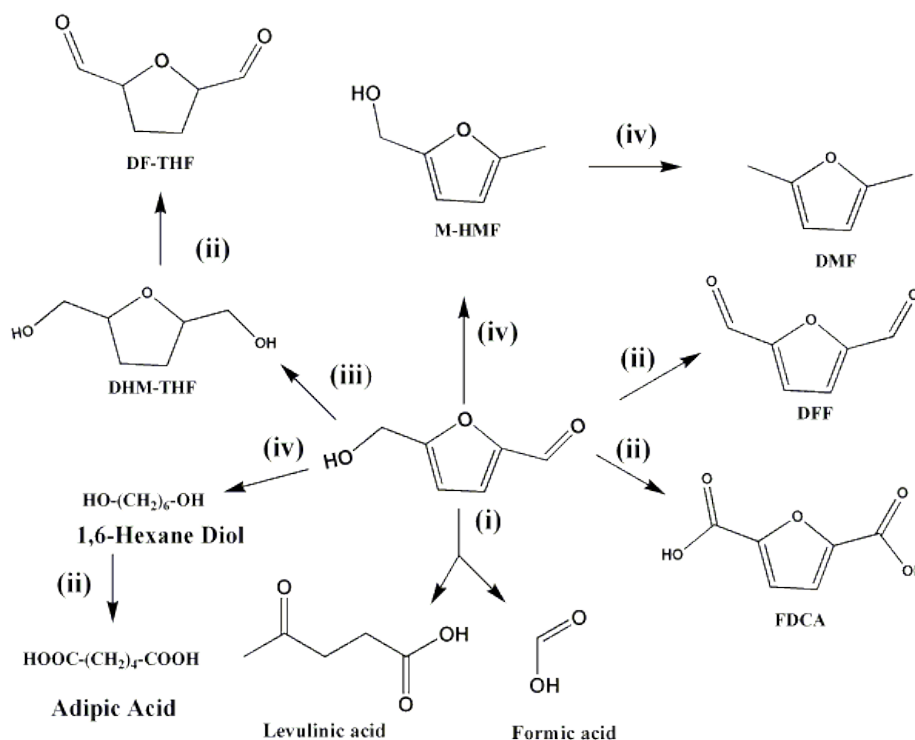


Fig. 1.9. Synthetic routes from HMF by (i) rehydration, (ii) oxidation, (iii) reduction, (iv) hydrogenolysis.

1.5.5. Selective oxidation of 5-HMF to 2,5-Furandicarboxylic acid (FDCA)

Selective hydrolysis of hexoses gives a potential platform chemical called 5-hydroxymethylfurfural [55]. Under suitable reaction conditions, HMF can be oxidized to FDCA [56]. US DOE biomass program has identified FDCA as one of the 12 important chemicals derived from biomass that can be used as a chemical building blocks in future. It is a potential replacement for terephthalic acid; the monomer currently used for the production of polyethylene terephthalate (PET), which is derived from petroleum based hydrocarbons. To overcome the reported shortcomings of the selective HMF oxidation process, we have developed alternative, cost-effective and recyclable catalyst. This catalyst comprises of a precious metal, supported on a alkali or alkaline earth exchanged octahedral molecular sieve; thus has both redox centers and basic sites. The detailed results of this green process, developed in our research group will be discussed as one of the chapters in this thesis.

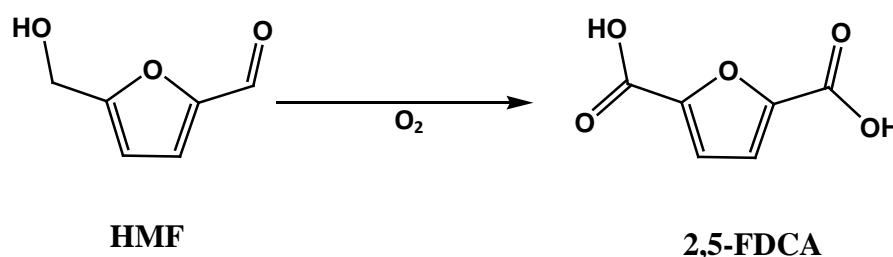


Fig. 1.10. Selective oxidation of HMF to 2,5-FDCA.

1.6. Introduction to porous manganese oxides

1.6.1. Manganese

Manganese (Mn) is the 10th most abundant element in the Earth's crust and second only to iron as the most common heavy metal; on average crustal rocks contain about 0.1% Mn [57]. Near the Earth's surface, Mn is easily oxidized, giving rise to more than 30 known Mn oxide/hydroxide minerals[58]. These oxides are the major players in the story of the mineralogy and geochemistry of Mn in the upper crust and the major sources of industrial Mn. As ores, Mn oxides have been exploited since ancient times. In particular, pyrolusite (MnO₂) was used as a pigment for its ability to remove the green tint imparted by iron to glass [59]. By the mid 19th century

Mn was an essential component in steel making, as a deoxidizer and desulfurizer and for making hard-steel alloys [60, 61].

1.6.2 Manganese oxide minerals

Generally in normal systems manganese exists in three different oxidation states (+2, +3, +4), giving rise to a range of multivalent phases. Most Mn oxide minerals are brown-black and classically occur as intimately intermixed, poorly crystalline masses or coatings. Naturally, identifying the particular mineral(s) in a Mn oxide specimen can be a challenge. Hence many researchers report simply “Mn oxide” rather than a specific mineral phase. Even, classification of the minerals in many Mn oxide samples is not straightforward. In general, powder X-ray diffraction is a good diagnostic tool for monophasic, well-crystallized samples. Unfortunately, the crystal structures and accordingly, the powder diffraction patterns are similar for many of the Mn oxide minerals.

The basic building block of most of the Mn oxide structures is the MnO_6 octahedron. These octahedra can be constructed by sharing edges and/or corners into a large variety of different structural arrangements, most of which fall into one of two major groups: (i) layer structures and (ii) chain, or tunnel structures. The layer Mn oxides, occasionally referred to as phyllo-manganates, consist of stacks of sheets, or layers, of edge-sharing MnO_6 octahedra. The interlayer regions can host water molecules and a wide range of cations. The tunnel Mn oxides are constructed of single, double, or triple chains of edge-sharing MnO_6 octahedra, and the chains share corners with each other to produce frameworks that have tunnels with square or rectangular cross sections. These wide tunnels are partially filled with water molecules and/or cations [62]. The major complexity of Mn oxide crystal chemistry is the multiple valence states exhibited by Mn, commonly even in a single mineral. It is practically simple to measure the average Mn oxidation state for a mineral, but it is considerably more difficult to determine the proportions of Mn (IV), Mn (III), and /or Mn (II).

Summarized below are descriptions of some of the most important Mn oxide minerals. The minerals and their chemical formulae are listed in Table 1.5.

Table 1.5 Various minerals of Mn and their chemical formulae

Mineral	Chemical Formula	Ref
Pyrolusite	MnO ₂	63
Ramsdellite	MnO ₂	64
Nsutite	Mn(OOH) ₂	65
Hollandite	Ba _x (Mn ⁴⁺ , Mn ³⁺) ₈ O ₁₆	66
Cryptomelane	K _x (Mn ⁴⁺ , Mn ³⁺) ₈ O ₁₆	66
Manjiroite	Na _x (Mn ⁴⁺ , Mn ³⁺) ₈ O ₁₆	67
Coronadite	Pb _x (Mn ⁴⁺ , Mn ³⁺) ₈ O ₁₆	68
Romanechite	Ba _{0.66} (Mn ⁴⁺ , Mn ³⁺) ₅ O ₁₀ 1.34H ₂ O	69
Todorokite	(Ca,Na,K) _x (Mn ⁴⁺ , Mn ³⁺) ₆ O ₁₂ 3.5H ₂ O	70
Lithiophorite	LiAl ₂ (Mn ₂ ⁴⁺ Mn ³⁺)O ₆ (OH) ₆	71
Birnessite	(Na,Ca)Mn ₇ O ₁₄ 2.8H ₂ O	72
Manganite	MnOOH	73
Feitknechtite	MnOOH	74
Hausmannite	Mn ²⁺ Mn ₂ ³⁺ O ₄	75
Bixbyite	Mn ₂ O ₃	76
Manganosite	MnO	77

1.6.3. Mn oxide minerals with tunnel structures

There are many Mn oxide minerals which exist with tunnel structure. These are described below.

1.6.3.1 Todorokite (Ca, Na, K)₃₋₅[Mn(IV), Mn(III), Mg]₆O₁₂ 0.3–4.5H₂O

Todorokite (OMS-1) is one of the main Mn minerals deposited in ocean Mn nodules (10 Å manganate), and it is likely the host phase for transition metals such as Ni, Co, etc. Todorokite occurs with apparent plate type or fibrous morphologies, that supports a tunnel or layer-type structure and it is extracted as major mineral from many terrestrial Mn deposits[78]. For many years the crystal structure of todorokite was a subject of considerable conjecture and controversy. The tunnel structure of todorokite was confirmed by high resolution TEM images, which illustrates that

tunnels are constructed of triple chains of MnO_6 octahedra. The triple chains share corners with each other to form large tunnels with square cross sections that measure three octahedra on a side [79]. It has a tunnel size of $6.9 \times 6.9 \text{ \AA}$.

The water and cation positions in the tunnels of todorokite were predicted by Rietveld method using powder X-ray diffraction data recently [70]. Lower valence cations such as Mn (III), Ni (II), and Mg (II), which substitute for Mn (IV) to offset charges on the tunnel cations, appear to be concentrated into the sites at the edges of the triple chains, as in romanechite. Chemical analyses of todorokite show considerable variation in tunnel cation composition [80], while samples from ocean nodules have up to several weight% Ni, Co, and Cu [81]. Because of todorokite's large zeolite-like tunnels, there has been considerable interest in recent years in producing synthetic analogues for possible use as catalysts or molecular sieves [82].

Todorokite typically occurs in Mn deposits as an alteration product of primary ores such as braunite. It is an important phase in many Mn coatings, dendrites and varnishes [83]. In the case of ocean nodules, the mechanism of todorokite formation is not well understood, but some experiments suggest that biological processes might play an important role. It has been speculated that nodular todorokite alters from a precursor busserite-like phase [70]. Recent studies have shown that todorokite can be synthesized starting with Mg-rich birnessite-like phase [84].

1.6.3.2. Hollandite group $\text{R}_{0.8-1.5}[\text{Mn (IV), Mn (III)}]_8\text{O}_{16}$ R=Ba, Pb, K or Na.

The hollandite structure is constructed of double chains of edge-sharing MnO_6 octahedra, which are linked in such a way as to form tunnels with square cross sections, measuring two octahedra on a side (Fig. 1.11.). The tunnels are partially filled with large uni- or di-valent cations and in some cases, water molecules. The charges on the tunnel cations are balanced by substitution of lower valence cations [e.g., Mn (III), Fe (III), Al (III), etc.] for some of the Mn (IV). Hollandite minerals can be major phases in the oxidized zones of Mn deposits and important ores. The different minerals in the hollandite group are defined on the basis of the predominant

tunnel cation: hollandite (Ba), cryptomelane or OMS-2 (K), coronadite (Pb), and manjiroite (Na). Natural specimens having end-member compositions are unusual, and chemical analyses show a wide range of tunnel cation compositions. Consistent with their chain structure, they typically are found as fibrous crystals, usually in compact botryoidal masses. Cryptomelane has a tunnel size of 4.6 X 4.6 Å.

In recent years there has been great interest in the hollandite minerals and in the hollandite structure-type in general, both for potential applications as solid ionic conductors and for immobilizing certain radioactive cations as part of a waste storage system [85]. Mixed valency of OMS type manganese makes them good semiconductors and oxidation catalysts. The average manganese oxidation state has been reported from 3.4 to 3.9 due to the presence of a mixture of Mn^{4+} , Mn^{3+} and Mn^{+2} ions. Manganese oxides of OMS-type are easy and inexpensive to prepare. Various synthetic routes have been explored, such as reflux [86], thermal or hydrothermal treatment of birnessite [87] and sol-gel route [88].

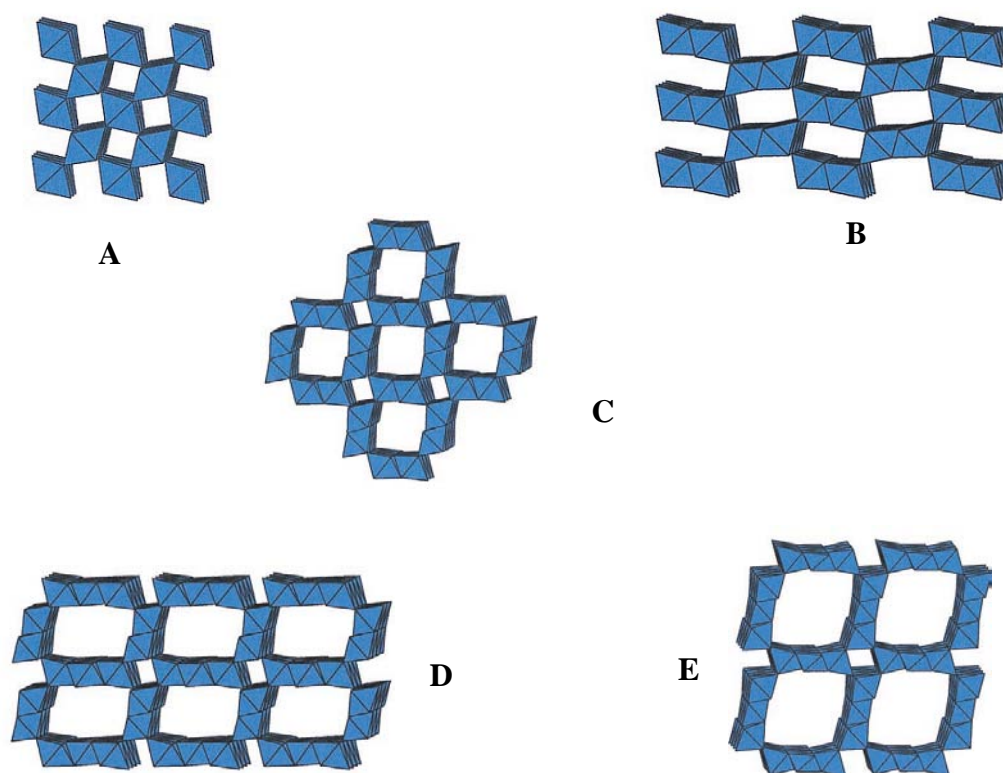


Fig. 1.11. Polyhedral representations of the crystal structures of (A) pyrolusite, (B) ramsdellite, (C) hollandite, (D) romanechite, and (E) todorokite, looking approximately parallel to the Mn octahedral chains.

1.7. Carbon nitrides

1.7.1. Introduction

If one looks at our surroundings, it is realized that a greater part of the material is based on carbon. Amorphous carbon, tetrahedral carbon, diamond-like carbon, fullerenes, CN_x, graphene, carbon nanotubes; the list of new or different structures based on carbon grows each year due to the extensive research and discovery of new carbon based materials.

Carbon nitrides are compounds of carbon and nitrogen as the backbone forming elements. Carbon nitride in the strict sense however refers to the binary carbon nitride with the formula C₃N₄, which still is an elusive monomer compound. Five different crystalline modifications of the binary carbon nitride, which were described in an earlier article by Teter and Hemely are shown in Fig1.12. Carbon nitride materials are in the focus of this thesis. Graphitic carbon nitrides, derived from the parent binary compound g-C₃N₄, are a family of largely planar structures with a composition close to “C₃N₄”, which are based on either triazine or heptazine units. These exhibit different degrees of condensation, physical and chemical properties and reactivities.

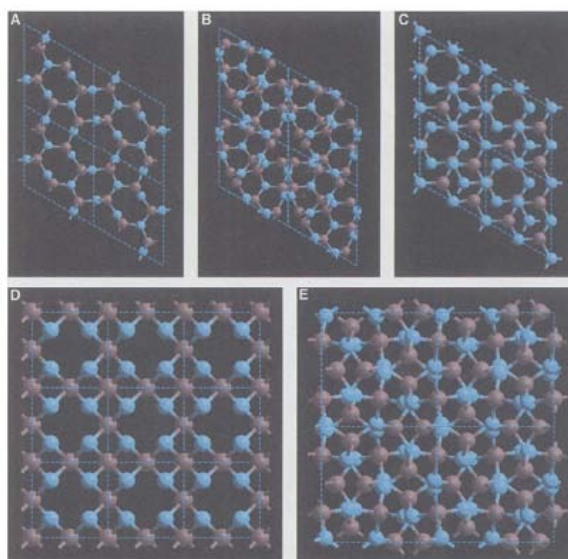


Fig. 1.12. Representation of (A) β -C₃N₄, (B) α -C₃N₄, (C) graphitic-C₃N₄, (D) pseudo-cubic-C₃N₄ and (E) cubic-C₃N₄ modifications, viewed down the [001] axis. The ‘C’ and ‘N’ atoms are depicted as gray and blue spheres, respectively.

In the beginning of the “carbon nitride era”, numerous papers were published on β - C_3N_4 , the hypothetical compound predicted by Liu and Cohen [89] to have a bulk modulus of 427 GPa, which is a value close to that of diamond (443 GPa). In addition, four other structures of crystalline CN have been predicted, e.g. α - C_3N_4 , this is an iso-structural phase to the more well-known α - Si_3N_4 . While the evidence for the existence of the C_3N_4 compounds remains to be proven, CN_x has been deposited in different structures and compositions, as e.g. amorphous, graphitic, turbostratic and “fullerene-like”, using a variety of deposition techniques and the mechanical, electrical and optical properties, as well as detailed structures of these materials have been examined by many groups.

The effect of introducing nitrogen into the amorphous or graphite-like carbon matrix is that it induces curvature into the structure, with bent and intersecting basal graphite planes as a result. The fullerene-like microstructure has been of interest, because of the elastic behavior in combination with a high hardness which is of great importance in certain applications. Hardness values for carbon nitride (CN_x) have been reported in the range 10-40 GPa depending on microstructure and deposition technique [90].

1.7.2. A brief history of carbon nitride

The first work of carbon nitride appeared in the early 19th century. Jöns Jakob Berzelius, considered the father of modern chemistry, who famously coined the word “polymer”, first synthesized a carbon nitride material through heating of $Hg(SCN)_2$. In 1834, Justus von Liebig discovered a material which has a formula $C_6N_9H_3$, same as that of earlier product [91]. He identified several triazine and heptazine-based molecular compounds such as melamine, melam, melem, ammeline, ammelide, and melon. He obtained a yellow, amorphous and insoluble product which was named melon which was obtained by the pyrolysis of ammonium chloride with potassium thiocyanate. As his products were of high purity, the first reliable characterizations of several carbon nitride compounds by elemental analysis were recorded. However, not all of his products could be well synthesized and characterized. By elemental analysis of melon, he could not ascertain a clearly reproducible formula. In 1835, another important discovery was potassium hydromelonate, $K_3C_6N_7$ (NCN), by Leopold

Gmelin [92]. The synthesis was conducted using potassium ferricyanide and sulfur, which were heated in a crucible. When the potassium hydromelonate was acidified, hydromelonic acid was formed. In 1855, Hennenberg discovered cyameluric acid ($\text{H}_3\text{C}_6\text{N}_7\text{O}_3$) by hydrolyzing hydromelonate salts.

The structure of these above mentioned compounds remained vague due to the lack of suitable analytical methods at that time. In 1922, Edward C. Franklin published a detailed review of the carbon-nitrogen family of compounds which also included the well-known guanidine, biguanidine, cyanamide, dicyandiamide and melamine [93]. He found that the empirical composition of melon derivatives derived from mercuric thiocyanate varied with the method of preparation and the hydrogen content varied from 1.1 to 2.0 wt%. This brought these compounds into consideration once more. In 1933, Franklin gave Linus Pauling some crystals with the formula $\text{C}_6\text{N}_7\text{O}_3\text{Na}_3 \cdot 3\text{H}_2\text{O}$ to perform an X-ray study. After studying this material and some related materials, the assertion was that the most likely structure would be a coplanar arrangement of three fused rings [94]. Therefore, Pauling proposed the cyameluric nucleus, C_6N_7 , which is shown in Fig. 1.13.

Later, Redemann and Lucas predicted that there is a similarity between melon and graphite in that the molecules are infinitely large and planar. They indicated that the Franklin's carbon nitride closed to a compact condensation product with 21 molecules of 2,5,8-triamino-tris-s-triazine, $\text{C}_{126}\text{H}_{21}\text{N}_{175}$ [95]. Based on these findings it was stated that one single structure should probably not be assigned to melon as it is more likely a mixture of polymers of different size and architecture.

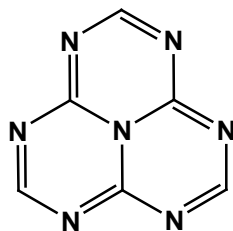
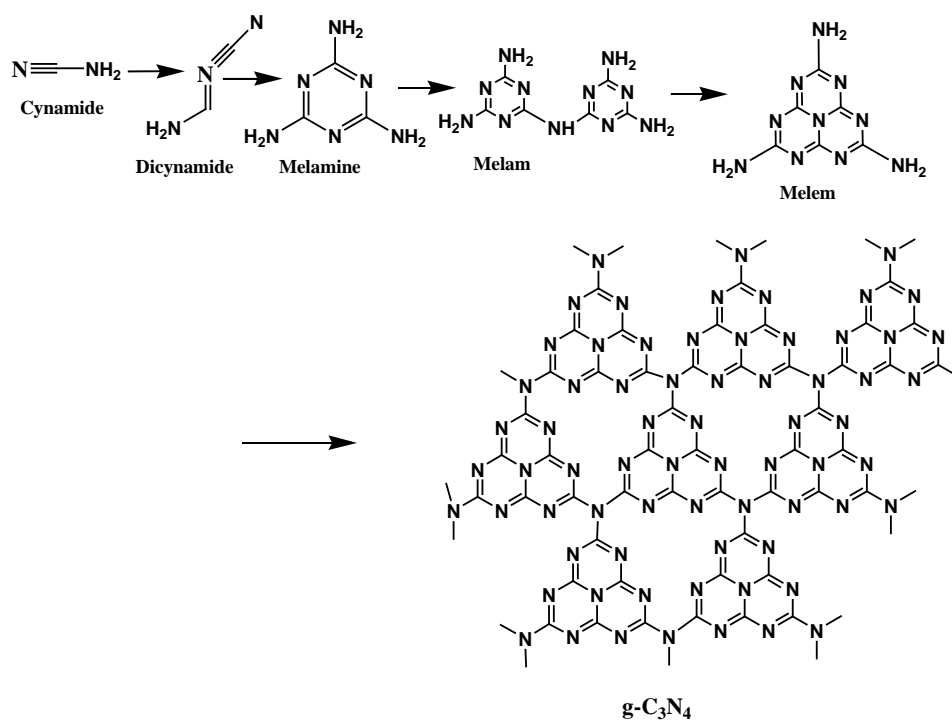


Fig. 1.13. Pauling's proposed structure for the cyameluric nucleus.

In the second half of the 20th century, the Russian chemist Finkel'shtein examined the spectroscopic properties of these known cyameluric molecules by IR and UV-Vis spectroscopy [96]. In 1961, the compound 2-oxo-6,10-diamino-s-heptazine, which was synthesized by a careful partial alkaline hydrolysis of melon, was reported by Finkel'shtein [97]. Until now, there have been no further reports about this compound. In 1982, Leonard and coworkers reported the first crystal structure of a cyameluric derivative, after successfully synthesizing the unsubstituted cyameluric nucleus, C₆N₇H₃, by a bottom-up assembly starting from 2,4-diamino-1,3,5-triazine and methyl N-cyanomethanimidate [98]. The crystal structure showed a coplanar arrangement of three fused triazine units, which proved the structure proposed by Pauling earlier.

The interest in these carbon nitride compounds blossomed by the theoretical prediction that dense sp³-bonded C₃N₄ phase (β -C₃N₄) could have extremely high bulk modulus and hardness values comparable with or exceeding that of diamond [99]. These results motivated further experimental efforts to synthesize and characterize β -C₃N₄ [100]. Further theoretical work indicated g-C₃N₄ to be the most stable allotrope at ambient conditions [101]. The synthesis and characterization of g-C₃N₄ is a challenging task by itself, and to date a large number of different experimental attempts have been made.

Due to the lack of experimental data, there is a predominant discussion about the actual existence of a graphitic material with composition of C₃N₄ and possible structure models for g-C₃N₄. Inspired by the structure of graphite, triazine (C₃N₃) had been put forward as elementary building blocks of g-C₃N₄ (Scheme 1.4) [102]. However, another possible building block, tri-s-triazine (heptazine) rings, which are structurally related to the hypothetical polymer melon [103], has recently been shown to be energetically favored with respect to the triazine-based modification [104]. The tri-s-triazine rings are cross-linked by trigonal nitrogen atoms. Recent work has shown that the pyrolysis of cyanamide, dicyandiamide, or melamine yields a melon polymer built up from melem units [105], confirming that this tecton is the most stable local connection pattern.



Scheme 1.4. Reaction path for the formation of graphitic C₃N₄ starting from cyanamide.

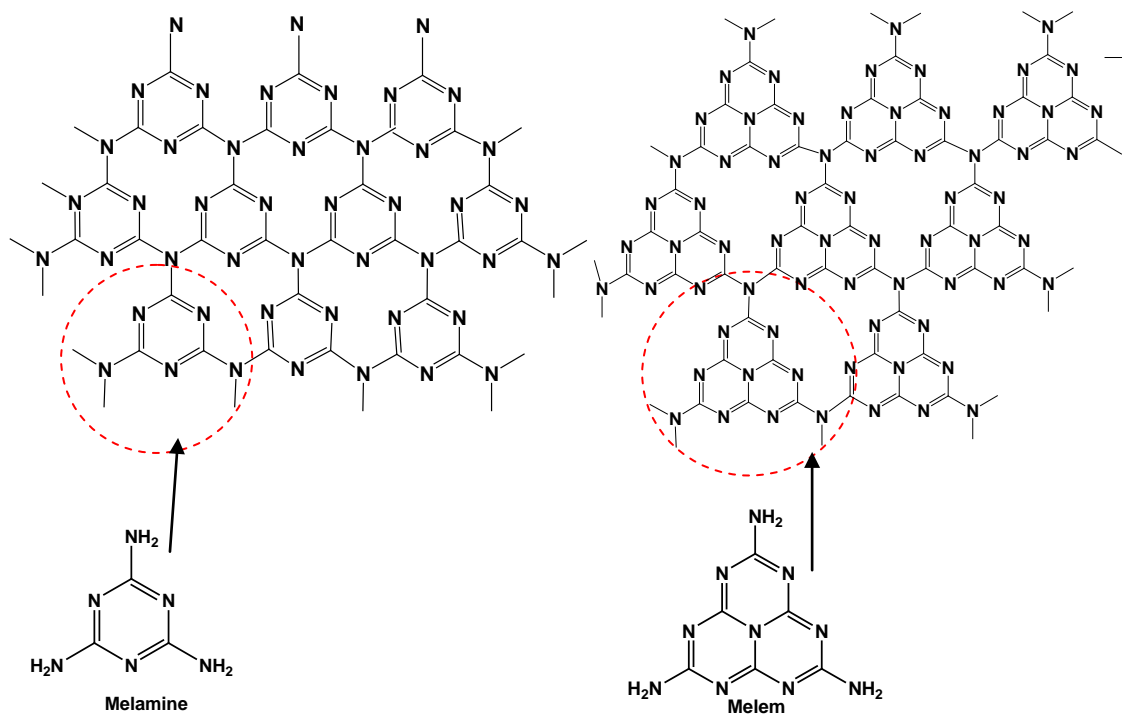


Fig. 1.14. Triazine- (left) and tri-s-triazine-based connection patterns (right) of potential g-C₃N₄ allotrope.

The calculated energy diagram for the synthesis of carbon nitrides is outlined in Fig. 1.15. [106]. The starting precursor cyanamide condenses into melamine. Further condensation can then proceed via the triazine route (dash-dot line) to C_3N_4 , or melamine can form melem and then follow the tri-s-triazine route (dashed line) to form C_6N_8 . The energies are presented per atom. The material intermediate in condensation degree between melem and melon is called dimelem, which also belongs to the incompletely condensed melon group of materials. Because of the expected larger band gap, these kinds of carbon nitride materials have not been considered as photo catalysts as yet. However, recently, Zou and coworkers reported on effectively narrowing the band gap of carbon nitride photo catalysts by coupling with a narrow gap molecule [107].

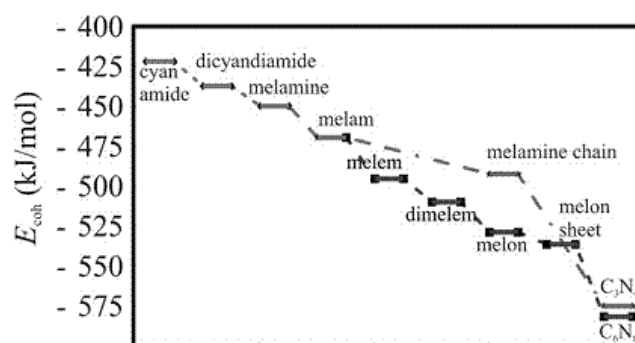


Fig. 1.15. Calculated energy diagram for the synthesis of carbon nitride.

1.8. Scope and objective of the present Thesis

Development of highly active and stable heterogeneous catalysts for the selective oxyfunctionalization of hydrocarbons is a challenging task in catalysis. In pursuit of this, the scope and objectives of this thesis are (i) to prepare Co substituted manganese containing octahedral molecular sieves by direct reflux synthesis method; (ii) to characterize them by various physico-chemical techniques and (iii) to investigate their catalytic properties in selective oxidation of cyclohexane to adipic acid. Accordingly, Co-K-OMS-2 catalysts with varying Co/Mn molar ratio were synthesized. The present thesis also focuses on the design of green process for the selective oxidation of hydrocarbons. In order to achieve it, we have conducted these selective oxidations with metal free carbon nitride catalysts.

Conversion of renewable biomass into value-added chemicals and fuels is an area of considerable current interest. In the quest for designing base free selective oxidation catalysts to obtain biomass derived compounds, we have synthesized Ru exchanged Mg & Mn containing octahedral molecular sieves (Ru-Mg-OMS-1). The prepared catalysts were tested for the oxidation of 5-hydroxymethylfurfural and 2-furfural to their corresponding acids. Factors influencing the activity of these catalysts are investigated.

1.9. Organization of the Thesis

The thesis is divided into six chapters. A brief description of the contents of each chapter is given below.

Chapter 1: Introduction

Chapter 1 gives a general introduction to heterogeneous catalysis, which includes a brief description of various methods used for the preparation of catalysts reported in the thesis. This chapter presents an introduction to selective oxidation of hydrocarbons and its importance in the synthesis of industrially important organic chemicals and intermediates. It also describes about the manganese containing octahedral molecular sieves, types of nitrogen doped carbons and their electronic and catalytic properties. Utilization of biomass based feedstocks to renewable chemicals, particularly through selective oxidation also forms part of this chapter. Finally, the aim of the thesis is outlined briefly.

Chapter 2: Catalyst preparation and experimental techniques for characterization

Chapter 2 describes different methods of catalyst synthesis used for various catalysts and experimental techniques employed for their characterization. The catalysts synthesized were Co substituted K-OMS-2, Ru exchanged Mg-OMS-1, carbon nitride nano tubes (CNNT). They were characterized by various physico-chemical techniques. Theory and experimental procedures of each of these techniques have been described in this chapter.

Chapter 3: Co-K-OMS-2 catalysts for oxidation reactions

Chapter 3 provides detailed introduction to selective hydrocarbon oxidation reactions. It deals with the investigations pertaining to Co and Mn containing octahedral molecular sieves as catalysts for single step selective oxidation of cyclohexane to adipic acid (AA) in presence of an initiator. This chapter is divided into two parts. Part-A presents the characterization results of Co-K-OMS-2 catalysts Part-B presents the activity of catalysts in the oxidation of cyclohexane to AA, which is an industrially important organic transformation.

Our investigations on Co-K-OMS-2 catalysts show that Co doping enhances the rate of reaction. The AA selectivity was found to decrease at higher reaction temperatures, contact time and at high Co concentrations. The rate of the decarboxylation of AA to succinic and glutaric acids was found to increase with increasing Co content. Addition of initiator enhances the rate of reaction. The catalyst was successfully recycled 5 times. Conclusions were drawn based on the catalytic studies and their correlation with the characterization results, which were given at the end of this section.

Chapter 4: Metal free carbon nitride catalysts for hydrocarbon oxidations

Chapter 4 gives detailed introduction to nitrogen doped carbons and industrially important selective hydrocarbon oxidation reactions. This chapter is divided into two parts. Part-A describes the synthesis and characterization of carbon nitride nanotube (CNNT) catalysts. Part-B describes catalytic activity of these catalysts for industrially important hydrocarbon oxidations, particularly cyclohexane to adipic acid.

Carbon nitride nanotube catalysts show superior activity in the selective hydrocarbon oxidation using O₂ as oxidant. In cyclohexane oxidation, reaction temperature, time, oxygen pressure plays vital role in conversion of cyclohexane and AA selectivity. An important finding was that the reaction can be conducted even in the absence of solvent, except that it offers somewhat inferior performance. Nitrogen

content plays an important role. The characterization results were correlated with the catalytic activity at the end of the chapter.

Chapter 5: Base free process for the oxidation of biomass derived feedstocks to corresponding acids

Chapter 5 deals with biomass utilization, particularly selective oxidation of biomass derived compounds. This chapter is also divided into two parts. Part-A describes the synthesis and characterization of Ru-Mg-OMS catalysts. Part-B describes the catalytic activity of these catalysts in the selective oxidation of biomass components to obtain important renewable chemical feedstocks.

The role of Ru exchanged Mg-OMS-1 catalyst was investigated for oxidation of HMF and furfural to their respective acids. The oxidation was performed without addition of an external base. Effect of reaction conditions like temperature, catalyst weight, Ru content, O₂ pressure and duration of the reaction were studied. Catalyst recyclability was also demonstrated. The possible causes for the high catalytic oxidation activity of these catalysts was examined.

Chapter 6: Summary and conclusions

This chapter discusses various conclusions drawn upon the investigations conducted with regard to various catalysts in the selective oxidation of hydrocarbons as well as biomass components. Since, it is mandatory to summarize the work for the benefit of the reader; this chapter compares the present work with the reported results as a summary. Further, at the end of this chapter, it offers suggestions for further research in these areas.

By and large, the work presented in this thesis reports the synthesis, characterization and catalytic applications of Co and Ru exchanged manganese containing octahedral molecular sieves and carbon nitride nano tubes. These catalysts were found to be superior in activity in comparison with the reported catalysts for their respective reactions. The catalysts used in these investigations were recyclable.

In general, the work presented in this dissertation contributes to the area of new materials and sustainable catalytic processes.

1.10. References

- 1 J.H. Clark, *Green Chem.* **1** (1999) 1.
- 2 P.T. Anastas, M.M. Kirchhoff, *Acc. Chem. Res.* **35** (2002) 686.
- 3 C.H. Christensen, J. Rass-Hansen, C.C. Marsden, E. Taarning, K. Egeblad, *ChemSusChem* **1** (2008) 283.
- 4 G. Ertl, *Angew. Chem. Int. Ed.* **120** (2008) 3578.
- 5 S. Green, *Industrial Catalysis*, Macmillan Company, New York, 1928.
- 6 J. J. Berzelius, *Årsberättelsen om framsteg i fysik och kemi*, Royal Swedish Academy of Sciences, 1835.
- 7 J. J. Berzelius, *Reseanteckningar*, P. A. Norstedt & Söner, Stockholm, 1903.
- 8 J. Mellor, *J. Phys. Chem.* **7** (1903) 557.
- 9 G. M. Kirchhoff, *Schweigger's J.* **4** (1812) 108.
- 10 H. Davy, *Phil. Trans.* **107** (1817) 77.
- 11 M. Faraday, *Phil. Trans.* **124** (1834) 55.
- 12 G. Lemoine, *Ann. Chim. Phys.* **12** (1877) 145.
- 13 B.H. Davis, in G. Ertl, H. Knözinger and J. Weitkamp (Eds.), *Handbook of Heterogeneous Catalysis*, Vol. **1**, VCH, Weinheim, 1997.
- 14 (a) P.T. Anastas, J.C. Warner (Eds.), *Green Chemistry: Theory and Practice*, Oxford University Press, Oxford, 1998. (b) J.H. Clark, D.J. Macquarrie, *Handbook of Green Chemistry and Technology*, Blackwell, Abingdon, 2002. (c) M. Lancaster, *Green Chemistry: An Introductory Text*, Royal Society of Chemistry, Cambridge, 2002.
- 15 D.L. Gilbert, (ed.). *Oxygen and Living Processes. An Interdisciplinary Approach*. New York: SpringerVerlag, 1981, 1-43.
- 16 C.L. Hill, I.A. Weinstock, *Nature* **388** (1997) 332.
- 17 (a) H.L.J. Backstrom, *J. Am. Chem. Soc.* **49** (1927) 1460.
- 18 (a) R.A. Sheldon, J.K. Kochi, *Metal-Catalyzed Oxidations of Organic Compounds*, Academic Press: New York, 1981. (b) A.E. Shilov, G.B. Shul'pin, *Activation and Catalytic Reactions of Saturated Hydrocarbons in the Presence of Metal Complexes*; Kluwer Academic Publishers: Boston, 2000.
- 19 LY Margolis, *Adv. Catal*, 1963.

- 20 (a) J.L. Bolland, *Q. Rev.Chem. Soc.* **3** (1949) 1. (b) L. Bateman, *Q. Rev.Chem. Soc.* **8** (1954) 147.
- 21 A.K. Suresh, M.M. Sharma, T. Sridhar, *Ind. Eng. Chem. Res.* **39** (2000) 3958.
- 22 D.T. Sawyer, *Oxygen Chemistry*, Oxford University Press, 1991.
- 23 (a) R.A. Sheldon, Heterogeneous Catalytic oxidation and fine Chemicals, *Stud. Surf. Sci. Catal.* **66** (1991) 33. (b) R.A. Sheldon, I.W.C.E. Arends, H.E.B. Lempers, *Catal. Today* **41** (1998) 387. (c) R.A. Sheldon, *Chemtech* (1991) 566. (d) R.A. Sheldon, *J. Mol. Catal. A Chemical.* **107** (1996) 75. (e) P. Gallezot, Selective oxidation with air on metal catalysts, *Catal. Today.* **37** (1997) 405. (f) K. Shimizu, T. Kaneko, T. Fujishima, T. Kodama, H. Yoshida, Y. Kitayama, *Appl. Catal. A General.* **225** (2002) 185.
- 24 R.K. Graselli, *Catal. Today.* **49** (1999) 141.
- 25 (a) G. Centi, F. Cavani, F. Trifiro, *Selective oxidation by heterogeneous catalysis. Recent developments*, Plenum, New York, 2001. (b) P. Arpentinier, F. Cavani, F. Trifiro, *The Technology of Catalytic Oxidations*, Editions Technip, Paris, 2001. (c) A. Bielanski, J. Haber, *Oxygen in Catalysis*, Marcel Dekker, New York, 1991. (d) K. Hodnett, *Heterogeneous catalytic Oxidation*, Wiley-VCH, Weinheim, 2000. (e) R. K. Grasselli, *Catal. Today* **49** (1999) 141; (f) R. K. Grasselli, *Catal. Today* **99** (2005) 23. (g) T. Punniyamurthy, S. Velusamy, J. Iqbal, *Chem. Rev.* **105** (2005) 2329.
- 26 (a) G.I. Panov, *Cattech* **4** (2000) 18. (b) B.K. Min, C. Friend, *Chem. Rev.* **107**, (2007) 2709. (c) D. Lenoir, *Angew. Chem. Int. Ed.* **118** (2006). (d) A. Corma, H. Garcia, *Chem. Soc. Rev.* **37** (2008), 2096. (e) T. Ishida, M. Haruta, *Angew. Chem. Int. Ed.* **119** (2007) 7288. (f) M.G. Clerici, M. Ricci, G. Strukul in *Metal-catalysis in Industrial Organic Processes*, Royal Society of Chemistry, Cambridge, 2007, p. 23. (g) P. Ratnasamy, R. Raja, D. Srinivas, *Philos. Trans. R. Soc. London Ser. A* **363** (2005) 1001. (h) J. M. Thomas, R. Raja, *Catal. Today* **117** (2006) 22. (i) G.J. Ten Brink, I.W.C.E. Arends, R. A. Sheldon, *Science* **287** (2000) 1636.
- 27 F. Cavani and J. H. Teles, *ChemSusChem* **2** (2009) 508.
- 28 ULLMANN'S *Encyclopedia of Industrial Chemistry*, Wiley-VCH, 2nd edition (2002).
- 29 Cavani, *Sustainable Industrial Processes*, Wiley-VCH, 1st edition (2009).
- 30 A. Castellan, J.C.J. Bart, *Catal. Today.* **9** (1991) 237.
- 31 <http://tpmlivewire.talkingpointsmemo.com/2010/06/tpmtv-latest-videos-jon-stewart-8-presidents-said-wellget-off-foreign-oil----fool-me-8-times-am-i-a.php>.
- 32 E.S. Lipinsky, *Science* **212** (1981) 1465.

- 33 J.R. Regalbuto, *Science* **325** (2009) 822.
- 34 D.L. Klass, Biomass for Renewable Energy and Fuels, Encyclopedia of Energy, Volume 1. (2004) Elsevier Inc.
- 35 (a) *Biomass as Feedstock for a Bioenergy and Bioproducts Industry: The Technical Feasibility of a Billion-Ton Annual Supply* (feedstockreview.ornl.gov /pdf/billion _ton _vision.pdf). (b) D.R. Dodds, R.A. Gross, *Science*, **318** (2007), 1250.
- 36 T.Wiesenthal, A.Mourelatou, J.Petersen, P.Taylor, How much bioenergy can Europe produce without harming the environment? European Environmental Agency, Report No. 7/2006.
- 37 G.W. Huber, S. Iborra, A. Corma, *Chem. Rev.* **106** (2006) 4044.
- 38 K. Olofsson, M. Bertilsson, G. Lidèn, *Biotechnology for Bio fuels*, **1** (2008) 1.
- 39 R.H. Sims, A. Hastings, B. Schlamadinger, G. Taylors, P. Smith, *Glob. Change Biol.* **12** (2005) 2054.
- 40 J.H. Clark, F.E.I. Deswarte, *Introduction to Chemicals from Biomass*, Wiley, (2008).
- 41 C.H. Christensen, J. Rass-Hansen, C.C. Marsden, E. Taarning, K. Egeblad, *ChemSusChem*, **1** 2008, 283.
- 42 M.J. Antal, W.S.L. Mok, G.N. Richards, *Carbohydr. Res.* **199** (1990) 91.
- 43 A.A. Rosatella, S. P. Simeonov, R.F.M. Frade, C.A.M. Afonso, *Green Chem.***13** (2011) 754.
- 44 M. Murkovic, N. Pichler, *Mol. Nutr. Food Res.* **50** (2006) 842.
- 45 T. Husoy, M. Haugen, M. Murkovic, D. Jöbstl, H.Stolen, T. Bjellaas, C. Rønningborg, H.G.Alexander, *J. Food Chem. Toxicol.* **46** (2008) 3697.
- 46 C. Janzowski, V. Glaab, E. Samimi, J. Schlatter, J. Eisenbrand *Food Chem. Toxicol.* **38** (2000) 801.
- 47 S.P. Verevkin, V.N. Emel'yanenko, E.N. Stepurko, R.V. Ralys, D.H. Zaitsau, *Ind. Eng. Chem. Res.* **48** (2009) 10087.
- 48 (a) B. Girisuta, L.P.B.M. Janssen, H.J. Heeres, *Green Chem.* **8** (2006), 701. (b) B.Girisuta, B.Janssen, L. P. B. M.; Heeres, H. J. *Ind. Eng. Chem. Res.* **46** (2007) 1696.
- 49 (a) E.I. Gürbüz, D.M.Alonso, J.Q.Bond, J.A. Dumesic, *ChemSusChem* **4** (2011) 357. (b) M. Chia, J.A. Dumesic, *Chem. Commun.* **47** (2011) 12233.
- 50 S. Dutta, S. De, B. Saha, *ChemPlusChem* **77** (2012) 259.
- 51 D.M. Alonso, J.Q.Bond, J.A. Dumesic, *Green Chem.* **12** (2010) 1493.

- 52 J Tuteja, H. Choudhary, S. Nishimura, and K Ebitani, *ChemSusChem* **7** (2014), 96.
- 53 C. Sievers, I. Musin, T. Marzialetti, M.B.V. Olarte, P.K. Agrawal, C.W. Jones, *ChemSusChem* **2** (2009) 665.
- 54 Y. Román-Leshkov, C.J. Barrett, Z.Y. Liu, J.A. Dumesic, *Nature* 2007, **447**, 982.
- 55 T. Werpy, G. Petersen, Top Value Added Chemicals from Biomass Vol.1 2004, 26 – 28; available at: <http://www.osti.gov/bridge> (accessed May 2009).
- 56 J. Lewkowski, *Arkivoc* **1** (2001) 17.
- 57 K.K. Turekian, K.L. Wedepohl, *Geol. Soc. Am. Bull.* **72** (1961) 175.
- 58 D.A. Crerar, R.K. Cormick, & H.L. Barnes, *Geology and Geochemistry of Manganese*, eds. I.M. Varentsov, & Gy. Grasselly, (E. Schweizerbart'sche Verlagsbuchhandlung, Stuttgart), **1** (1980) 293.
- 59 I.M. Varentsov, *Manganese Ores of Supergene Zone: Geochemistry of Formation* (Kluwer, Boston) 1996.
- 60 D.A. Crerar, & H.L. Barnes, *Geochim. Cosmochim. Acta* **38** (1974) 279.
- 61 J. Murray, & A.F. Renard, Report on the Scientific Results of the Exploration Voyage of H.M.S. Challenger, 1981 (Neill and Co., Longon).
- 62 J.E. Post, & D.L. Bish, in *Modern Powder Diffraction*, eds. (Mineral. Soc. of Am., Washington, DC), Rev. in Mineralogy **20** (1989) 277.
- 63 W.H. Baur, *Acta Crystallogr. B* **32** (1976) 2200.
- 64 A.M. Bystro *Acta Chem. Scand.* **3** (1949) 163.
- 65 W.K. Zwicker, W.O.J.G. Meijer, H.W. Jaffe, *Am. Mineral.* **47** (1962) 246.
- 66 J.E. Post, R.B. Von Dreele, P.R. Buseck, *Acta Crystallogr. B* **38** (1982) 1056.
- 67 M. Nambu, K. Tanida, *J. Jpn. Assoc. Mineral. Petrol. Econ. Geol.* **58** (1967) 39.
- 68 J.E. Post, D.L. Bish, *Am. Mineral.* **74** (1989) 913.
- 69 S. Turner, J.E. Post, *Am. Mineral.* **73** (1988) 1155.
- 70 J.E. Post, D.L. Bish, *Am. Mineral.* **73** (1988) 861.
- 71 J.E. Post, D.E. Appleman, *Am. Mineral.* **79** (1994) 370.
- 72 J.E. Post, D.R. Veblen, *Am. Mineral.* **75** (1990) 477.
- 73 H. Dachs, *Zeit. Kristall.* **118** (1963) 303.
- 74 O. Bricker, *Am. Mineral.* **50** (1965) 1296.
- 75 K. Satomi, *J. Phys. Soc. Jpn.* **16** (1961) 258.

- 76 S. Geller, *Acta Crystallogr. B.* **27** (1971) 821.
- 77 S. Sasaki, K. Fujino, Y. Takeuchi, R. Sadanaga, *Acta Crystallogr. A* **36** (1980) 904.
- 78 R.G. Burns, & V.M. Burns, in *Marine Manganese Nodules*, ed. Glasby, G. P. (Elsevier, Amsterdam), 1977 pp.185.
- 79 S. Turner, P.R. Buseck, *Science* **212** (1981) 1024.
- 80 J. Ostwald, *Mineral. Mag.* **50** (1986) 336.
- 81 V.M. Burns, R.G. Burns, *Earth Planet. Sci Lett.* **39** (1978) 341.
- 82 Y.F. Shen, R.P. Zenger, R.N. Deguzman, S.L. Suib, L. Mccurdy, D.I. Potter, & C.L. O'Young, *Science* **260** (1993) 511.
- 83 R.M. Potter, G.R. Rossman, *Am. Mineral.* **64** (1979) 1219.
- 84 D.C. Golden, C.C. Chen, J.B. Dixon. *Science* **231** (1986) 717.
- 85 (a) A.E. Ringwood, S.E. Kesson, N.G. Ware, W. Hibberson, A. Major *Nature* (London) **278** (1979) 219. (b) A.E. Ringwood, A.F. Reid. *Acta Crystallogr.* **23**, (1967) 1093.
- 86 (a) R.N. De Guzman, Y.F. Shen, E.T. Neth. S. L. Suib, C.L. O Young, S. Levine, J.M. Newman, *Chem .Mater.* **6(6)** (1994) 815. (b) J. Luo, Q. Zhang. A. Huang, S.L. Suib, *Microporous Mesoporous Matter* **35-36** (2000) 209.
- 87 a) X.F. Shen, J.S. Ding, J. Liu, J. Cai, K. Laubernds, R.P. Zenger, A.Vasiliev, M. Aindow S.L. Suib, *Advanced Materials* **17(7)** (2005) 805. (b) J. Yuan, W. Li, S.Gomez, S.L. Suib, *JACS* , **127(41)** (2005) 14184.
- 88 (a) X. Hong, G. Zhang, Y. Zhu, H. Yang, *Materials Research Bulletin* **38(13)** (2003) 1695. (b) S. Ching, J.L. Roark, *Chem. Mater.* **9(3)** (1997) 750.
- 89 (a) A.Y. Liu, M.L. Cohen, *Science* **245** (1989) 841. (b) A.Y. Liu, M.L. Cohen, *Phys. Rev. B* **41** (1990) 10727.
- 90 (a) H. Sjöström, S. Stafström, M. Boman, J.-E. Sundgren, *Phys. Rev. Lett.* **75** (1995) 1336 (b) M. Kohzaki, A. Matsumuro, T. Hayashi, M. Muramatsu, K. Yamaguchi, *Thin Sol Films* **239** (1997) 308. (c) R. Gago, I. Jiménez, D. Cáceres, F. Agulló-Rueda, T. Sajavaara, J.M. Albella, A .Climent-Font, I. Vergara, J. Räisänen, E. Rauhala, *Chem. Mater.* **13** (2001) 129.
- 91 (a) J. V. Liebig, *Ann. Pharm.* **10** (1834) 10. (b) L. Gmelin, *Handbook of Chemistry* **9**, (1855) 378. (c) J. Liebig, *Annalen der Chemie und Pharmacie*, **53**, (1845) 330. (d) J. Liebig, *Annalen der Chemie und Pharmacie*, **95** (1855) 257.
- 92 (a) L. Gmelin, *Annalen der Pharmacie*, **15** (1835) 252. [b] W. Henneberg, *Annalen der Chemie und Pharmacie*, **73**, (1850) 228.
- 93 E. C. Franklin, *J. Am. Chem. Soc.* **44** (1922) 486.

- 94 L. Pauling, J. H. Sturdivant, *Proc. Natl. Acad. Sci. USA*. **23** (1937) 615.
- 95 C. E. Redemann, H. J. Lucas, *J. Am. Chem. Soc.* **62** (1940) 842 .
- 96 A. I. Boitsov, E. N. Finkel'shtein, *Zhurnal Obshchei Khimii*. **32** (1962) 321.
- 97 A.I. Spiridonova, N.V. Finkel'shtein, *Trudy po Khimii i Khimicheskoi Tekhnologii* (1967) 38.
- 98 N.J. Hosmane, R.S. Rossman, M.A. Leonard, *Journal of the American Chemical Society*, **104** (1982) 5497.
- 99 (a) M. L. Cohen, *Phys. Rev. B.* **32** (1985) 7988. (b) A.Y. Liu, M.L. Cohen, *Science* **245** (1989) 841. © M. L. Cohen, *Science*, **261** (1993) 307. (d) J.L. Corkill, M.L. Cohen, *Phys. Rev. B*, **48** (1993) 17622.
- 100 (a) L. Maya, D. R. Cole, E.W. Hagaman, *J. Am. Ceram. Soc.* **74** (1991) 1686. (b) C.M. Niu, Y.Z. Lu, C.M. Lieber, *Science* **261** (1993) 334. c) Rabalais, *Phys. Rev. Lett.* **73** (1994) 118.
- 101 (a) A.Y. Liu, R.M. Wentzcovitch, *Phys. Rev. B.* **50** (1994) 10362. (b) J. E. Lowther, *Phys. Rev. B.* **59** (1999) 11683. (c) J. Ortega, O.F. Sankey, *Phys. Rev. B.* **51** (1995) 2624.
- 102 (a) J. Kouvetakis, A. Bandari, M. Todd, B.Wilkens, N. Cave, *Chem. Mater.* **6**, (1994) 811. [b] C. Li, C.B. Cao, H.S. Zhu, *Mater. Lett.* **58** (2004) 1903. [c] B.V. Lotsch, W. Schnick, *Chem. Mater.* **18** (2006) 1891. [d] Y. Young-Gui, B.G. Pfrommer, F. Mauri, S. G. Louie, *Phys. Rev. Lett.* **80** (1999) 3388.
- 103 (a) E.C. Franklin, *J. Am. Chem. Soc.* **44** (1922) 486. (b) L. Gmelin, *Ann. Pharm.* **15** (1835) 252. [c] J. von Liebig, *Ann. Chem. Pharm.* **50** (1850) 337. [d] J. von Liebig, *Ann. Chem. Pharm.* **73** (1850) 257. [e] J. Sehnert, K. Baerwinkel, J. Senker, *J. Phys. Chem. B.* **111** (2007) 10671.
- 104 E. Kroke, M. Schwarz, E. Horath-Bordon, P. Kroll, B. Noll, A.D. Norman, *New J. Chem.* **26** (2002) 508.
- 105 (a) J. Sehnert, K. Baerwinkel, J. Senker, *J. Phys. Chem. B.* **111** (2007) 10671. (b) B.V. Lotsch, W. Schnick, *Chem. Eur. J.* **13** (2007) 4956. (c) T. Komatsu, *J. Mater. Chem.* **11** (2001) 799. (d) T. Komatsu, *J. Mater. Chem.* **11** (2001) 802.
- 106 A. Thomas, A. Fischer, F. Goettmann, M. Antonietti, J.-O. Müller, R. Schlögl, J. M. Carlsson, *Journal of Materials Chemistry* **18** (2008) 4893.
- 107 Y. Guo, J. Yang, S. Chu, F. Kong, L. Luo, Y. Wang, Z. Zou, *Chemical Physics Letters* **550** (2012) 175.

Chapter 2
Experimental Methods and Characterization Techniques

2.1. Introduction

This chapter describes the synthesis of various catalyst materials and experimental methods used for their characterization. Transition metal substituted manganese containing octahedral molecular sieves and carbon nitride nano tube catalysts were prepared for the present study. Detailed physicochemical characterization is essential to understand any material, particularly for catalyst materials. X-ray powder diffraction, various spectroscopic techniques, electron microscopy and methods based on adsorption and desorption are routinely used for characterization of catalytic materials. These investigations are expected to provide information about phase purity, crystallinity, crystallite size, surface structure, textural properties, nature of active sites, morphology, particle size, acidity and other relevant information. Photo electron spectra provide information about the nature and chemical state of dopant. Further, the structure-activity relationship is better understood by these techniques which in turn will help to improve the activity of the catalysts for various applications. The formation, structural integrity and textural properties of the prepared catalysts were investigated by various physicochemical techniques like X-ray diffraction analysis (XRD), FT-IR, surface area and pore volume, metal dispersion through chemisorption, thermo gravimetric analysis, transmission electron microscopy (TEM), X-ray photoelectron spectroscopy (XPS), inductively coupled plasma-optical emission spectroscopy, photoluminescence spectroscopy and cyclic voltammetry studies

2.2. Catalyst preparation

2.2.1. Preparation of K-OMS-2 and Co substituted K-OMS-2

A class of Mn containing oxide materials that have tunnel structures are called octahedral molecular sieves (OMS). K-OMS-2 is one such material that belongs to this class, which can be prepared by precipitation [1]. A solution of KMnO_4 (5.89 g in 100mL of water) was added drop-wise to a solution containing mixture of manganese sulfate (8.8 g in 30mL water) and 3mL of concentrated nitric acid which resulted in the formation of a black precipitate. This precipitate was stirred and refluxed at 373K for 24h, filtered and washed with distilled deionized water until the pH of the filtrate became neutral. Subsequently the material was dried for 12h at 383K and calcined at 623K for 3h to finally get K-OMS-2.

In case of Co-K-OMS-2 preparation, required amount of cobalt precursor (cobalt nitrate hexahydrate) was added prior to the addition of nitric acid following the above procedure. Similar procedure was adopted to prepare four catalysts with different cobalt contents (0.5 to 3 wt %), by varying the concentration of cobalt nitrate solution. These samples were designated based on the Co content as Co-OMS-I (0.58 %), Co-OMS-II (1.03 %), Co-OMS-III (2.26 %) and Co-OMS-IV (2.98 %). The cobalt content of the samples was estimated using ICP-OES (Spectro Arcos).

2.2.2. Preparation of Ru exchanged Mg-OMS-1

In addition to K-OMS-2 and Co substituted K-OMS-2, we have also prepared OMS-1 structure that has larger pore size compared to OMS-2.

2.2.2.1. Preparation of Mg-OMS-1

For the preparation of Mg-OMS-1, first we need to prepare Na-Buserite followed by Mg-Todorokite as given below.

Preparation of Na-Buserite

A solution of 0.1132 moles of Mn $(\text{CH}_3\text{COO})_2 \cdot 4\text{H}_2\text{O}$ and 0.0238 g of $\text{Mg}(\text{CH}_3\text{COO})_2 \cdot 4\text{H}_2\text{O}$ in 140 mL of distilled deionized water (DDW) was added slowly to a solution of 50 g of NaOH in 160 mL of DDW under vigorous stirring, that resulted in a white slurry of Mn and Mg hydroxides. A solution of 0.030 moles of KMnO_4 in 140 mL of DDW was added slowly to the slurry under vigorous stirring, producing a brownish black suspension. The suspension was aged without stirring at 313 K for 4 days. Well-crystallized product was filtered out and washed until the pH of the filtrate was below 9.5. The obtained product was further stabilized by aging at room temperature for 2 days.

Preparation of Mg-Todorokite

The above obtained buserite was ion exchanged to Mg-Buserite by stirring the mixture at room temperature for 12 h using a 200 mL solution of magnesium chloride (0.2M) and the solid part was separated and heated hydrothermally in an autoclave. The autoclave was heated without stirring at 423 K for 48 h to get Mg-Todorokite. (Mg-OMS-1) [2].

2.2.2.2. Synthesis of 2wt% Ru exchanged Mg-OMS-1

Ruthenium was exchanged into Mg-OMS-1 by using 4mL of RuCl₃ (1mL contains 5mg of Ru). This solution was added to 50mL of water and 1g of Mg-OMS-1 and stirred at 353 K for 3h. After cooling to room temperature, 200mg of NaBH₄ was added and stirred for 1h, filtered and washed.

2.2.2.3. Preparation of other precious metal (Au, Pd, Pt) exchanged Mg-OMS-1

In order to prepare Au, Pd and Pt metal exchanged Mg-OMS-1, required amount of respective metal salt (HAuCl₄, Pd(NH₃)₄NO₃, H₂PtCl₆) was added to 50 ml water. Parent Mg-OMS-1 was added to the above solution, stirred at 353K for 3h and cooled it to ambient temperature. The metal exchanged OMS-1 was further reduced using NaBH₄ (200mg) and obtained solid was further washed with ethanol and dried at room temperature.

2.2.3. Preparation of 2wt% Ru exchanged Mg-OMS-2

For the preparation of Ru exchanged Mg-OMS-2, we need to prepare Mg-OMS-2 initially. One gram of K-OMS-2 was added to 100mL 1M sol of Mg(NO₃)₂.6H₂O and this mixture was stirred for 3h at 353K. After reaching to room temperature, the transparent sol was decanted. The above procedure was repeated thrice to obtain Mg-OMS-2.

Ruthenium was exchanged into Mg-OMS-2 by using 4mL of RuCl₃ (1mL contains 5mg of Ru). This solution was added to 50mL of water and 1g of Mg-OMS-2 and stirred for 3h at 353K. After cooling to ambient temperature, NaBH₄ was added to and stirred for 1h to reduce Ru, followed by filtration and washing with ethanol.

2.2.4. Preparation of carbon nitride nano tubes

Required amount of melamine (0.9068 g) was dissolved in 40 mL of ethylene glycol to obtain saturated solution at ambient temperature. To this, aqueous nitric acid (120 mL of 0.12 M) was added drop wise to get white precipitate. This precipitate was washed with ethanol to remove residual nitric acid and ethylene glycol. Subsequently, the product was dried at 333 K for 6 h and calcined at 623 K for 3 h in air [3].

2.3. Characterization of catalysts

Characterization of the above synthesized materials would help to understand the properties of the catalysts in a better way, so that materials can be improved or it is possible to design new materials to meet the catalyst requirements. A brief account of the theory and principle of various characterization techniques used for the current study is given below, followed by the procedure used for each experimental technique to characterize the above materials.

2.3.1. Powder X-ray diffraction (XRD)

X-ray diffraction is one of the most essential and versatile techniques used in catalyst characterization. It is quite useful for determining the structure of materials that are characterized by long-range order. Crystalline phase(s) of the catalyst can be studied by means of lattice structural parameters and crystallinity [4]. The frequency of X-rays is intermediate between the ultra-violet (UV) and gamma radiations and their wavelength (λ) is in the range of 0.04 Å to 1000 Å. For diffraction applications, only short wavelength X-rays in the range of a few Å to 0.1 Å (1 keV -12 keV) are used. Since, this wavelength is comparable to the size of atoms, they are ideal for probing the structural arrangement of atoms in a wide range of materials.

The diffraction method involves the interaction between the incident monochromatized X-rays (like Cu K_{α} or Mo K_{α} source) with the atoms of a periodic lattice. X-rays scattered by atoms in an ordered lattice interfere constructively as per Bragg's law [5]:

$$n\lambda = 2d \sin\theta; n = 1, 2, 3, \dots \quad (2.1)$$

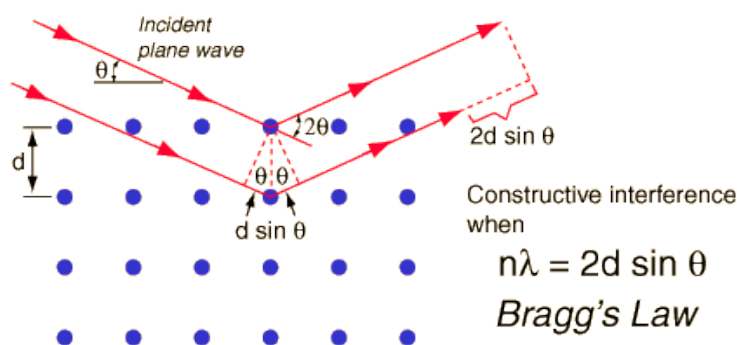


Fig. 2.1. Principle of Bragg's law.

where λ is the wavelength of X-rays, d is the distance between two lattice planes, θ is the angle between the incoming X-rays and the normal to the reflecting lattice plane and n is the integer called order of the reflection.

By measuring the angle 2θ , under which constructively interfering X-rays leave the crystal, the Bragg's equation gives the corresponding lattice spacing, which is characteristic for a particular compound. Width of the diffraction peaks signifies the dimension of the reflecting planes. It is known that the width of a diffraction peak increases when the crystallite size is reduced below a certain limit (<100 nm). Therefore, XRD patterns can be used to estimate the average crystallite size of small crystallites using XRD line broadening by applying the Scherrer formula [6];

$$t = 0.9\lambda / \beta \cos \theta \quad (2.2)$$

Where t is the thickness of the crystallites (\AA), λ is the wavelength of x-rays, θ is the diffraction angle and β is the full width at half maxima of the diffraction peak. X-ray diffraction pattern of all the catalysts reported in this thesis were collected using PANalytical X'pert Pro dual goniometer X-ray diffractometer. A proportional counter detector was used for low angle experiments. The data were collected with a step size of 0.02° at a scan rate of $0.5^\circ \text{ min}^{-1}$. The sample was rotated throughout the scan for better counting statistics. The incident radiation used was Cu - K_α (1.5418\AA) with Ni filter and the data collection was carried out using a flat holder in Bragg–Brentano geometry (0.2°).

2.3.2. N_2 Physisorption and CO chemisorption

The most accepted method of measuring surface area of catalytic materials is the one that is based on the theory developed by Brunauer, Emmett and Teller in 1938 considering the multilayer adsorption. Its assumptions are (i) adsorption energy remains constant from zero coverage to full coverage for the primary layer of the adsorbate and each of the layers above (ii) there is no inter molecular interaction, though they attract and retain molecules striking them from the gas phase (iii) enthalpy of adsorption is the same for any layer other than the first (iv) a new layer can be initiated before the one under formation is completed. The Brunauer-Emmett-Teller (BET) equation 2.3 is [7];

$$P/V(P_0-P) = 1/CV_m + [(C-1)/CV_m] (P/P_0) \quad (2.3)$$

Where P is adsorption equilibrium pressure, P_0 is saturation vapor pressure of the adsorbate at the experimental temperature, V is volume of gas adsorbed at pressure P , V_m is the volume of adsorbate required for monolayer coverage and C is a constant related to the heat of adsorption and liquefaction. A linear relationship between $P/V(P_0-P)$ and P/P_0 is required to obtain the quantity of nitrogen adsorbed. This linear portion of the curve is restricted to a limited portion of the isotherm, generally between 0.05-0.30. The monolayer volume, V_m is given by $1/(S+I)$, where S is the slope and is equal to $(C-1)/CV_m$ and I is the intercept and is equal to $1/CV_m$. The surface area of the catalyst (S_{BET}) is related to V_m , by the equation,

$$S_{BET} = (V_m/22414) N_a \sigma \quad (2.4)$$

Where N_a is Avogadro number and σ is mean cross sectional area covered by one adsorbate molecule. Nitrogen is the most widely used gas for surface area determinations since it exhibits intermediate values (50–250) for the C on most solid surfaces, precluding either localized adsorption or behavior as a two dimensional gas. Since it has been established that the C influences the value of the cross-sectional area of an adsorbate, the acceptable range of C for nitrogen makes it possible to calculate its cross-sectional area from its bulk liquid properties [8]. For the hexagonal close-packed nitrogen monolayer at 77 K, the cross-sectional area σ for nitrogen is 16.2 Å

In the case of supported metal (or metal oxide) catalysts, it is important to know what fraction of the active metal atoms are exposed. This is so because atoms located in the interior of the metal particles do not participate in surface reactions, hence not available for the purposes of catalytic processes. The metal dispersion, D , is defined as the fraction of metal atoms found on the surface of active metal particles; it is expressed as a percentage of all metal atoms present in the sample. The higher the dispersion, the more exposed is the metal surface and more efficient is the catalyst. The value of D is obtained from the equation

$$D = Nm S M/100L \quad (2.5)$$

Where M and L are the molecular weight and percent loading of the supported metal, S is adsorption stoichiometry, N_m is monolayer uptake of chemisorbed gas ($\mu\text{mol/g}$).

The N_2 physisorption and H_2 chemisorption experiments were conducted using Quantachrome autosorb IQ analyser. Nitrogen physisorption was carried out at 77K, after degassing the samples at 573 K. The isotherms were analyzed in a conventional manner in the relative pressure of region $P/P_0= 0.005$ to 1.0. The total pore volume of a sample was obtained at $P/P_0= 0.95$. Chemisorption (H_2) experiments were conducted at 313 K after reduction followed by evacuation at 573 K.

2.3.3. Electron microscopy

The electron microscopy has many variants. In this section, we deal only with scanning electron microscopy and transmission electron microscopy. The former is useful for the examination of physical features of the sample, like size and shape of crystals in the material. On the other hand TEM is much more useful to study the nano structure of the material alongwith metal dispersion.

2.3.3.1. Transmission electron microscopy (TEM)

The original form of electron microscopy, transmission electron microscopy (TEM) involves a high voltage electron beam emitted by a cathode and formed by magnetic lenses. The electron beam that has been partially transmitted through a very thin (and so semitransparent for electrons) specimen carries information about the structure of the specimen. The spatial variation in this information (the "image") is then magnified by a series of magnetic lenses until it is recorded by hitting a fluorescent screen, photographic plate or light sensitive sensor such as a CCD (charge-coupled device) camera. The image detected by the CCD may be displayed in real time on a monitor or computer.

The ability to determine the positions of atoms within materials has made the TEM an indispensable tool for nano-technologies research and development in many fields, including heterogeneous catalysis and the development of semiconductor devices for electronics and photonics.

Materials used in this study were analyzed using a high-resolution transmission electron microscope (HRTEM) Tecnai-T30 model at an accelerated voltage of 300 kV. Samples were prepared by placing a droplet of sample suspension in isopropyl alcohol on a carbon coated Cu grid for TEM measurements.

2.3.3.2. Scanning electron microscopy (SEM)

Unlike the TEM, where the electrons in the primary beam are transmitted through the sample, the scanning electron microscope (SEM) produces images by detecting secondary electrons which are emitted from the surface due to excitation by the primary electron beam. In SEM, the electron beam is scanned across the surface of the sample in a raster pattern, with detectors building up an image by mapping the detected signals with beam position.

The SEM micrographs of the samples were obtained on a Leo Leica Cambridge UK Model Stereoscan 440 scanning electron microscope. The samples were loaded on stubs and sputtered with thin gold film to prevent surface charging and also to protect from thermal damage due to electron beam [9]. The difference in the alignment of the above two microscopy is depicted in Fig. 2.2.

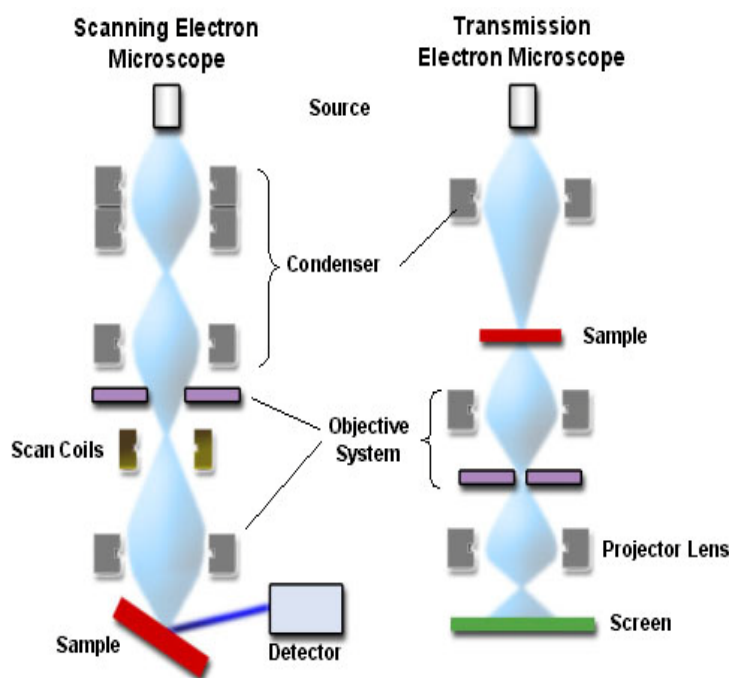


Fig. 2.2. Alignment of SEM and TEM.

2.3.4. X-Ray photoelectron spectroscopy (XPS)

X ray photoelectron spectroscopy has come into limelight as a result of the pioneering work by Kai Siegbahn (Nobel prize winner, 1981) and his colleagues at Uppsala university, Sweden. This technique is based on the photoelectric effect discovered by Heinrich Hertz and explained later by Albert Einstein [10], which involves the bombardment of a solid surface with X-rays and the measurement of the concomitant photo emitted electrons. It is a widely used technique for obtaining chemical information of various material surfaces. The low kinetic energy (≈ 1500 eV) of emitted photoelectrons limit the depth from which it can emerge, making XPS a very surface-sensitive technique and the sample depth is in the range of few nanometers. Photoelectrons are collected and analyzed by the instrument to produce a spectrum of emission intensity versus electron binding (or kinetic) energy.

XPS uses either monochromatic aluminum K_{α} or non-monochromatic magnesium K_{α} X-rays to eject a photoelectron from an atom at the sample's surface. An electron from a higher energy level then falls to fill the hole left behind and its emitted radiation energy is used to eject an Auger electron. Thus, XPS emits both photoelectrons and auger electrons which can be seen in the spectrum. The electrons ejected are analyzed with the help of XPS detector by measuring the kinetic energy of electrons which provides the information to determine the kind of elements present in the sample. Fig.2.3. illustrates the schematic representation of the X-ray photoelectron process.

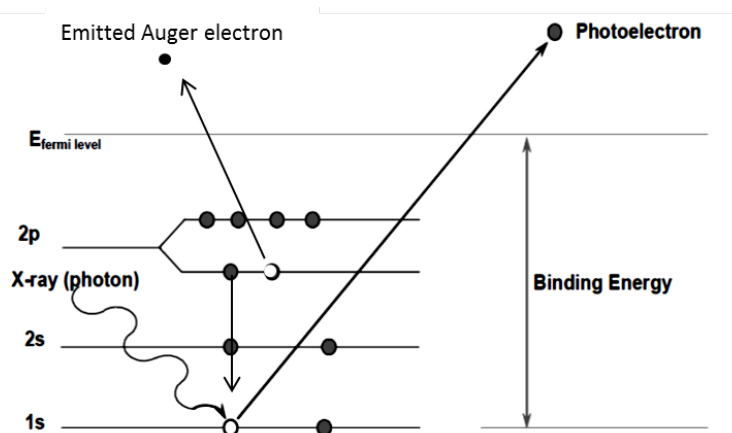


Fig. 2.3. Principle of photoelectron process.

The photoemitted electrons have discrete kinetic energy that is the characteristics of the emitting atoms and their bonding states. The kinetic energy, E_k of these photoelectrons is determined from the energy of the incident X-ray radiation ($h\nu$) and the electron binding energy (E_b) is given as

$$E_k = h\nu - E_b \quad (2.6)$$

The experimentally measured energies of the photoelectrons are given as

$$E_k = h\nu - E_b - E_w \quad (2.7)$$

Where E_w is the work function of the spectrometer.

Each element produces a characteristic set of XPS peaks at different binding energy values that directly identify each element present on the surface of the material being analyzed. These characteristic peaks correspond to the electronic configuration of the atoms, e.g., 1s, 2s, 2p, 3s, etc. To account for the multiplet splitting and satellites accompanying the photoemission peaks, the photoelectron spectra have to be interpreted in terms of many-electron states of the final ionized state of the sample, rather than the occupied one-electron states of the neutral species [11].

X-ray photoelectron spectroscopy analyses were performed on a VG Micro Tech ESCA 3000 instrument at a pressure of $\sim 1 \times 10^{-9}$ Torr (pass energy of 50 eV, electron take-off angle of 60° with overall resolution of ~ 0.1 eV) using a non monochromatized Mg K_α (1253.6 eV) or Al K_α radiation (1486.6 eV) operated at an accelerating voltage of 12.5 kV. The powder sample was pressed into thin discs and mounted on a sample rod to be placed in a pre-treatment chamber. After the pre-treatment, sample was transferred into the analysis chamber, where the spectra of required binding energy range was recorded. Charging effects were corrected by adjusting the binding energy of C1s peak to a known position of 285 eV.

2.3.5. Inductively coupled plasma-optical emission spectroscopy (ICP-OES)

ICP-OES is one of the most powerful and popular analytical tools for the determination of trace elements in a myriad of sample types. It was developed by Fassel at Iowa state university in US and by Greenfield at Albright & Wilson, in the UK Ltd in the mid 1960s [12]. The technique is based upon the spontaneous emission of photons from atoms and ions that have been excited in a RF discharge. Liquid and

gas samples may be injected directly into the instrument, while solid samples require extraction or acid digestion so that the analytes will be present in a solution.

The sample solution is converted into an aerosol and directed into the central channel of the plasma. At its core, the inductively coupled plasma (ICP) sustains a temperature of approximately 10,000 K, so the aerosol is quickly vaporized. Analyte elements are liberated as free atoms in the gaseous state. Further collisional excitation within the plasma imparts additional energy to the atoms, promoting them to the excited states. Sufficient energy is often available to convert the atoms to ions and subsequently promote the ions to excited states. Both the atomic and ionic excited state species may then relax to the ground state via the emission of a photon. These photons have characteristic energies that are determined by the quantized energy level structure for the atoms or ions. Thus the wavelength of the photons can be used to identify the elements from which they originated. The total number of photons is directly proportional to the concentration of the originating element in the sample. Sample introduction is depicted in Fig. 2.4.

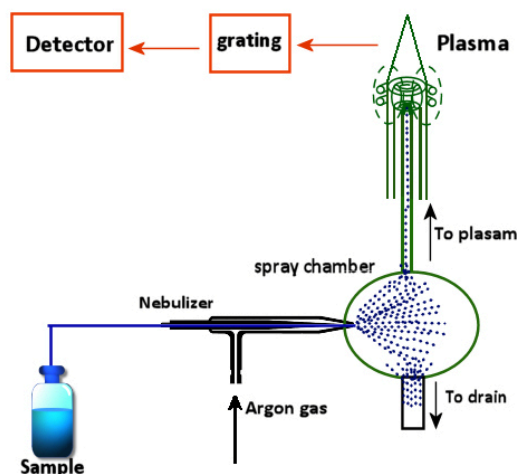


Fig. 2.4. Depiction of sample introduction to ICP-OES.

ICP-OES analysis was carried out on a Spectro Arcos instrument equipped with the Winlab software. Metals can be analyzed by either a radial or an axial plasma configuration. Standard solutions containing different elements were used for the calibration purpose. The catalysts (OMS-1 and OMS-2) were dissolved using con HCl

and the obtained solution were made up to 100ml and analyzed by using an ICP-OES instrument.

2.3.6. Infrared Spectroscopy (IR)

Infrared spectroscopy (IR) is considered as the first and the foremost of the modern spectroscopic techniques that found general acceptance in catalysis. The technique is used to identify phases that are present in a catalyst material or its precursor, the adsorbed species, adsorption sites and the way in which the adsorbed species are chemisorbed on the surface of the catalyst [13].

Infrared spectroscopy is the most common form of vibrational spectroscopy. It depends on the vibrations of molecules in a material or in solid lattices by the absorption of photons, which occurs if a dipole moment changes during the vibration. The intensity of the infrared band is proportional to the change in dipole moment. A variety of IR techniques have been used to get information on the surface chemistry of different solids. With respect to the characterization of metal oxide catalysts, two techniques largely predominate, namely, the transmission/absorption and the diffuse reflection techniques. In the first case, the sample consists typically of 10-100 mg of catalyst, pressed into a self-supporting disc of approximately 1 cm² and a few tenths of a millimeter thickness. In diffuse reflectance mode (DRIFT), samples can be measured by simply depositing on a sample holder, avoiding the tedious preparation of wafers. This technique is especially useful for strongly scattering or absorption by samples.

The infrared absorption spectrum is described by Kubelka Munk function [14]

$$F(R_{\infty}) = (1-R_{\infty})^2/2R_{\infty} = K/S \quad (2.8)$$

Where K is the absorption coefficient, which is a function of the frequency ν , S is the scattering coefficient and R_{∞} is the reflectivity of a sample of infinite thickness, measured as a function of ν .

The Fourier transform-infrared spectra of the catalysts reported here were recorded on Bruker Tensor 27 FT-IR spectrometer under ambient conditions. The

spectra were recorded using thin self-supporting discs made by pressing the mixture of the catalyst sample and KBr.

2.3.7. Thermal analysis

Thermo analytical techniques involve the measurements of the response of the solid under study (energy or mass released or consumed) as a function of temperature (or time) dynamically by application of a linear temperature program. Thermogravimetry is a technique which measures the mass change of a material as a function of temperature and time, in a controlled manner. This variation in mass can be either a loss of mass (vapor emission) or a gain of mass (gas fixation). It is ideally used to assess volatile content, thermal stability, degradation characteristics, aging/lifetime breakdown, sintering behavior and reaction kinetics. Differential thermal analysis is a technique which measures the temperature difference of the sample versus a reference, caused by thermal events in a material. It is ideally used to determine melting point, glass transition temperature, crystallinity, degree of curing, heat capacity, impurities present etc [15].

In the present work, thermogravimetry and differential thermal analysis measurements of the as synthesized samples were performed with a Mettler Toledo TGA/SDTA 851 apparatus equipped with a control and data acquisition system. The analyses were carried out in air (40 mL min^{-1}) at a heating rate of 10 K min^{-1} using about 10 mg samples in a Pt pan. Calcium oxalate was used to calibrate the instrument.

2.3.8. Cyclic Voltammetry Studies

Cyclic voltammetry (CV) is an electrochemical technique which measures the current that develops in an electrochemical cell under conditions where voltage is in excess of that predicted by the Nernst equation. CV is performed by cycling the potential of a working electrode and measuring the resulting current.

A cyclic voltammogram is obtained by measuring the current at the working electrode during the potential scans. Fig. 2.5 shows a cyclic voltammogram resulting from a single electron reduction and oxidation. Consider the following reversible reaction:

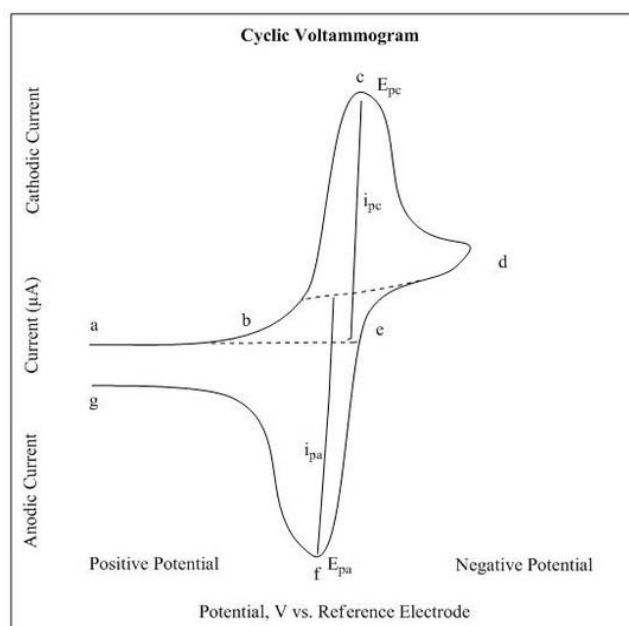
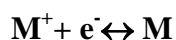


Fig. 2.5. Voltammogram of a single electron oxidation-reduction.

In Fig 2.5, the reduction process occurs from (a) the initial potential to (d) the switching potential. In this region the potential is scanned negatively to cause a reduction. The resulting current is called cathodic current (i_{pc}). The corresponding peak potential occurs at (c), and is called the cathodic peak potential (E_{pc}). The E_{pc} is reached when all of the substrate at the surface of the electrode has been reduced. After the switching potential has been reached (d), the potential scans positively from (d) to (g). This results in anodic current (I_{pa}) and oxidation to occur. The peak potential at (f) is called the anodic peak potential (E_{pa}), and is reached when all of the substrate at the surface of the electrode has been oxidized [16].

CV can also be used to determine the electron stoichiometry of a system, the diffusion coefficient of an analyte and the formal reduction potential, which can be used as an identification tool. In addition, as concentration is proportional to current in a reversible nernstian system, concentration of an unknown solution can be determined by generating a calibration curve of current vs. concentration. The main focus of the CV experiments in the present thesis is to determine the oxygen reduction reaction of the prepared catalysts.

Cyclic Voltammetry and linear sweep voltammetry (LSV) were carried out on an Autolab PGSTAT 30 instrument. The rotation rate of the electrode was controlled by a Pine made rotating disk electrode (RDE) system. A large area Pt foil was used as the counter electrode while and Hg/HgO was used as quasi reference electrode in basic medium (0.1MKOH), while Ag/AgCl as reference electrode in acidic medium (0.5M HClO₄).

2.4. References

- 1 R. DeGuzman, Y. Shen, E. Neth, S. Suib, C. O'Young, S. Levine, J. Newsam, *Chem. Mater.* **6** (1994) 815.
- 2 J. Luo, Q. Zhang, A. Huang, O. Giraldo, and Steven L. Suib, *Inorg. Chem.* **38** (1999) 6106.
- 3 J Gao, Y Zhou,* Z Li, S Yan, N Wang, Z Zou, *Nanoscale* **4** (2012) 3687.
- 4 J. W. Niemantsverdriet, *Spectroscopic methods in Heterogeneous catalysis*, VCH, Weinheim, 1993.
- 5 B. D. Cullity and S. R. Stock, *Elements of X-ray Diffraction*, Prentice Hall, 3rd ed. (2001).
- 6 N. F. M. Henry, J. Lipson and W. A. Wooster, *The interpretation of x-ray diffraction photographs*, Macmillan and Co Ltd., London, (1951).
- 7 S. Brunauer, P.H. Emmett, E. Teller, *J. Am. Chem. Soc.* **60** (1938) 309.
- 8 (a) A. V. Kiselev and Y. A. Eltekov , *World Congress on Surface Activity*, Vol. II, p. 228, Butterworths, London, 1957. (b) S. Lowell, J. Shields, G. Charalambous and J. Manzione, *J. Colloid Interface Sci.* **86** (1982) 191.
- 9 P. J. Goodhew, J. Humphreys, R. Beanland, *Electron Microscopy and Analysis*, 3rd edition, 2001.
- 10 (a) T. A. Carlson, *X-ray Photoelectron Spectroscopy*, Dowden, Hutchinson & Ross: Stroudsburg, PA, 1978. (b) D. Briggs and M. P. Seah, *Practical Surface Analysis, Vol. 1: Auger and X-ray Photoelectron Spectroscopy*, 2nd ed., Wiley, New York, 1990.
- 11 W. Egelhoff Jr., *Surf. Sci. Rep.* **6** (1987) 253.
- 12 C.B. Boss, K.J. Fredeen, *Concept, Instrumentation and Techniques in Inductively Coupled Plasma Optical Emission Spectrometry*, 2nd edition, Perkin-Elmer,

Norwalk, CT, 1997.

- 13 B. Stuart, *Infrared Spectroscopy: Fundamentals and Applications*, Wiley, 2004.
- 14 (a) P. Kubelka, F. Munk, *Z. Tech. Phys.* **12** (1931) 593. (b) P. Kortum, W. Braun, C. Harzog, *Angew. Chem. Int. Ed.* **2** (1963) 333.
- 15 M.B. Kluwer *Introduction to Thermal Analysis Techniques and applications second edition*, academic publishers, 2001.
- 16 (a) F. Scholz, *Electroanalytical methods: Guide to Experiments and applications*, second edition, Springer, 2010. (b) F. G. Thomas and G. Henze, *Introduction to voltammetric Analysis: Theory and practice*, 2001.

Chapter 3

**Selective oxidation of cyclohexane to adipic acid using
Co substituted K-OMS-2 catalysts**

3.1. Introduction

Selective oxidation of hydrocarbons is an important process in the chemical industry, as it helps to manufacture of many useful chemicals like alcohols, aldehydes and carboxylic acids [1]. Though there were many publications/patents that deal with this area, it still remains a very significant research challenge as many processes need green chemical routes and cost effective manufacturing. As a result, there is a vigorous drive to develop green and efficient processes for the oxyfunctionalization of hydrocarbons [2]. Usually; efficient activation of a hydrocarbon requires precious metal catalyst and strong oxidizing agents (H_2O_2 , TBHP and HNO_3). The impact on the environment would have been much greater, had it not been for continuous improvement of various green technologies applied for production of various chemicals [3].

Currently, partial oxidation processes are conducted either in the gas or liquid phase using homogeneous/ heterogeneous catalysts. Since molecular oxygen is cheap and omnipresent, it is the most practicable oxidant for partial oxidation processes. But, most of the heterogeneous catalyst based processes offer poor selectivity for the desired product when molecular oxygen is used as an oxidant. Large quantities of energy are needed to separate the desired product from unwanted side products. In addition, it leads to waste generation and inefficient use of starting materials [4]. Hence, achieving desired product selectivity remains an important task in the case of selective oxidation of hydrocarbons using heterogeneous catalyst processes.

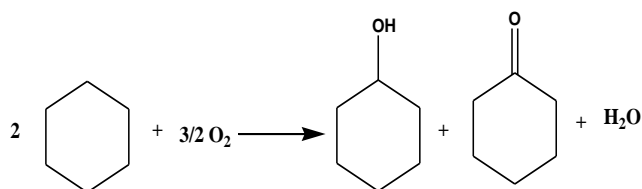
Adipic acid (AA) is an important selective oxidation product, which is obtained starting from cyclohexane. The projected consumption of AA is expected to be around 6 billion pounds by 2017 at a projected growth rate of 5-7 % [5]. Major part of AA produced is used as a precursor for the synthesis of nylon-6,6. In addition, AA is widely used for the production of polyesters, polyurethane resins, plasticizers in the production of polyvinyl chloride (PVC) and polyvinyl butyral (PVB) [6]. Current industrial production of AA involves multi steps as well as highly corrosive environmentally hazardous acids. Thus, developing novel, clean and green routes for AA production is an important research theme.

3.2. Current industrial processes for the production of AA

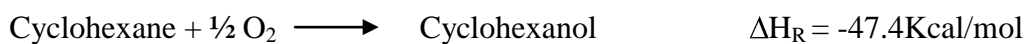
Adipic acid is produced in a two step elective oxidation process. The first one is (as in practice today) oxidation of cyclohexane with air to get a mixture of cyclohexanone/cyclohexanol (called KA oil); the second one is the oxidation of KA oil or cyclohexanol with nitric acid [7].

3.2.1. First step: Oxidation of cyclohexane with air

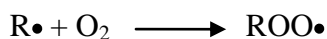
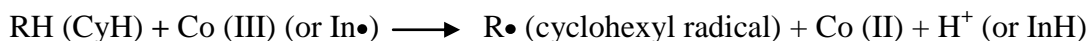
Cyclohexane (CyH) is produced either by the hydrogenation of benzene or separated from the naphtha fraction in small amounts. Selective oxidation of CyH was first demonstrated by Dupont in mid 20th century. The process was successfully conducted at 10-20 atm pressure, 423-453 K with Co and Mn organic salts as catalysts. The process constitutes two steps. The first step is a partial oxidation to get peroxide, which is carried out without catalyst. The second step is deperoxidation which must be done always in the presence of a catalyst. The rate limiting step of the process is the production of hydroperoxides, which is carried out in the absence of transition metal complexes in the passivated reactors in order to avoid the decomposition of hydroperoxides. The selectivity to KA oil is about 75-80%, the by-products are carboxylic acids. The unconverted cyclohexane is recycled [8].

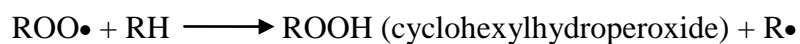


Scheme 3.1. Cyclohexane oxidation to cyclohexanol and cyclohexanone.



The chemistry of the reaction is a homolytic auto oxidation. Alcohol is formed from RO• radical (R = C₆H₁₁).





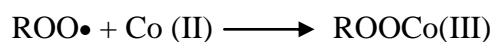
The vital role of Co is to accelerate the reaction by decomposition of the intermediate hydroperoxides, ROOH, leading to the formation of alkoxy or peroxy radicals (Haber-Weiss mechanism) [9].



Which corresponds to:

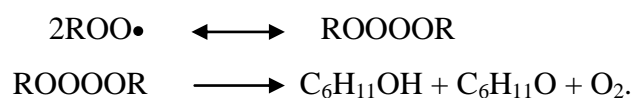


At high concentration of Co (II) it competes with cyclohexane for the alkylperoxy radical:

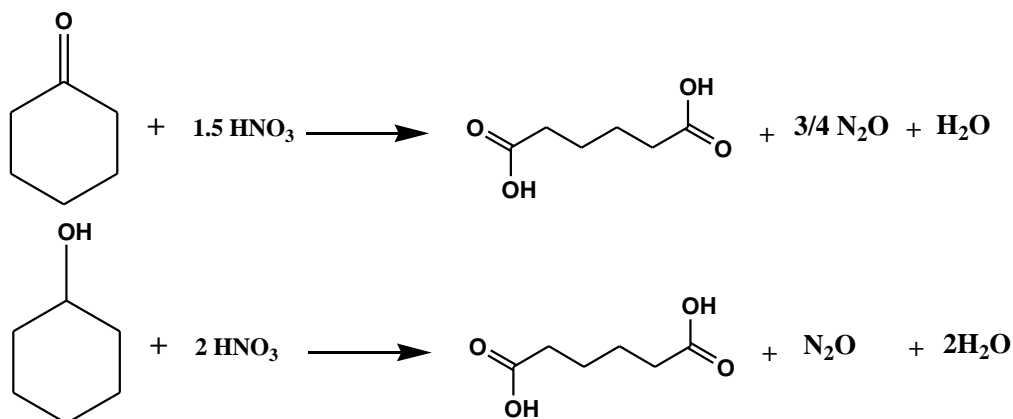


And therefore termination step would occur instead of propagation step. In that case catalyst would act as an inhibitor of the reaction.

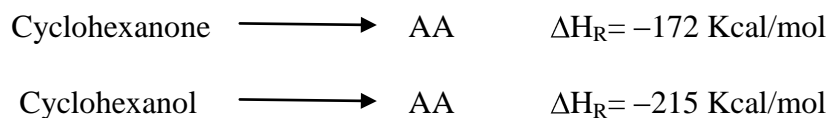
Russell mechanism of decomposition of secondary cyclohexylperoxy radicals is a prevailing reaction for the formation of alcohol and ketone. It consist in coupling of alkylperoxy radical, which then reacts by a non-radical, six-center 1,5H atom shift, which is also a terminating step of the radical chain reaction.



3.2.2. Second step: Oxidation of KA oil with nitric acid



The second step in the production of adipic acid is oxidation of KA oil in presence of large excess of 65% nitric acid (molar ratio of HNO₃/KA oil is at least 7/1), in the presence of Cu (II) ammonium metavanadate catalyst [10].

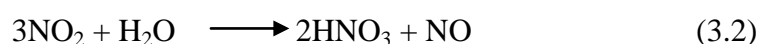


Scheme 3.2. Oxidation of cyclohexanol & cyclohexanone to adipic acid.

The reaction is carried out in two in-series reactors, first one operating at 333-353 K, the second one at 363-373 K at a pressure of 1-4 atm. The molar yield for total KA oil conversion is 95%, the by products are glutaric acid (selectivity 3%) and succinic acid (selectivity 2%).

3.2.3. Environmental impact of the second step

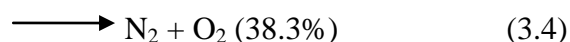
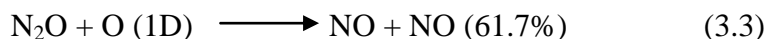
The intermediate of the nitric acid oxidation is HNO₂, which ultimately decomposes to NO and NO₂. These two gases can be simply recovered in water by absorption in a multistage column, yielding nitric acid solution, which can be reused in the oxidation process .



Because of the poor solubility of NO_x in water, the key factors for this process are the temperature and the pressure. However, it is possible to have a complete recovery of NO_x. Meanwhile the co-products of the nitric oxidation of KA oil, NO and NO₂ are easily recoverable, as shown above (eq. 3.1, 3.2), co-production of N₂O represents a big drawback of the second step of the synthesis of AA.

Nitrous oxide belongs to so called long lived greenhouse gases LLGHGS (other being CH₄, CO₂ and radioactively active constituents such as ozone and different types of aerosol), which contribute to the climatic changes [11]. The estimated atmospheric lifetime of N₂O is 150 years and the estimated impact of N₂O is a 6% increase in the ozone depletion layer. Although the absolute concentration of

N_2O is relatively low, 300 ppbv, it influences climatic changes as a result of one of its stratospheric removal reaction:



The equations show that the major part of N_2O is converted to NO, which is unambiguously implicated in catalytic ozone destruction [12].

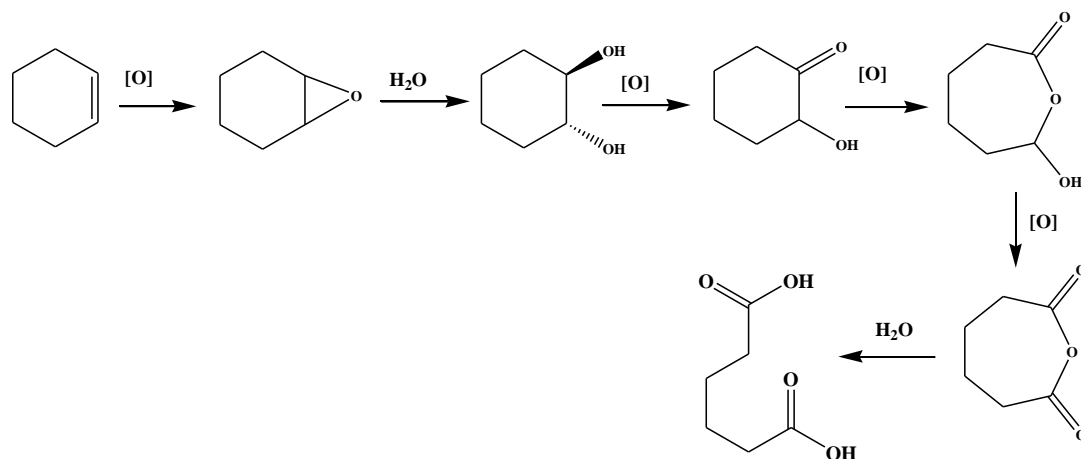
The emission factor of adipic acid is estimated to be about 300 kg of N_2O per ton of adipic acid, depending on the amount of catalyst used and KA oil composition. In 1990, adipic acid production was the largest source of industrial N_2O emissions. By 1999 all major adipic acid producers have implemented N_2O abatement technologies and, as a result, this source has been decreased substantially [13]. Consequently, currently the production of nitric acid is the largest industrial source of N_2O .

3.3. Alternate Pathways for AA production

In addition to the above discussed commercial process, there are alternative routes for the production of AA.

3.3.1. Oxidation of cyclohexene

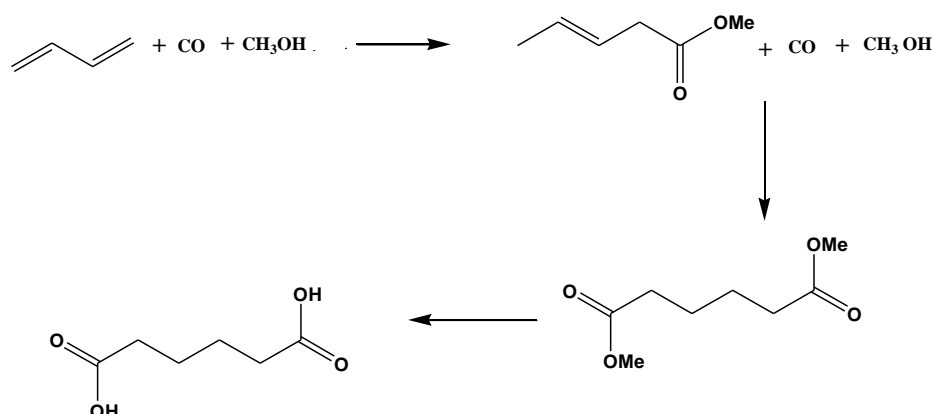
There were a plethora of reports in the literature for AA production from cyclohexene. The best result was reported by Noyori [14] with 30% hydrogen peroxide as oxidant and in the presence of small amounts of NaWO_4 and phase transfer catalyst (PTC) (in this case $\text{CH}_3(\text{n-C}_8\text{H}_{17})\text{NHSO}_4$) in the absence of solvent.



Scheme 3.3. Single step oxidation of cyclohexene to adipic acid with aqueous H_2O_2

3.3.2. Butadiene as a starting material

BASF has proposed a very innovative process, methoxycarbonylation of butadiene in the presence of the Co-based catalyst [15]. Although a good amount of AA yield (~ 72%) was obtained using this system, the process didn't lead to the implementation, possibly because of the extreme reaction conditions used. First step under 300 atm and the second step under the pressure of 150–200 atm) [16].



Scheme 3.4. Methoxycarbonylation of butadiene to adipic acid.

3.3.3. n-Hexane as a starting material

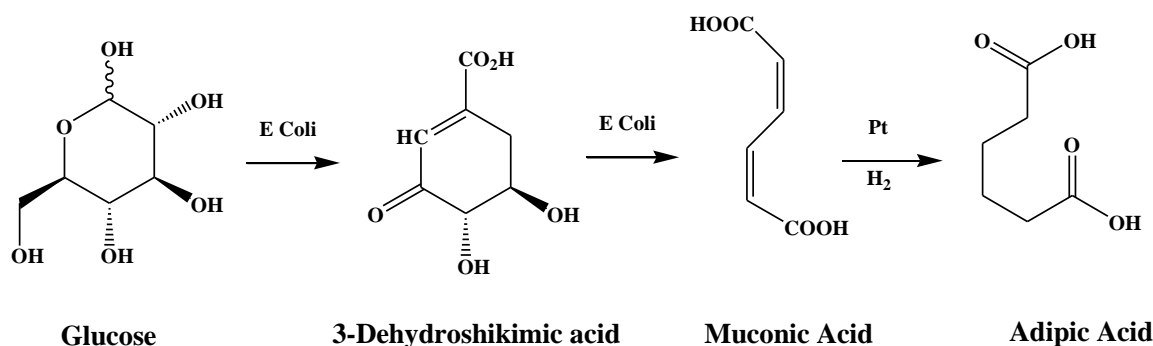
It is very well known that alkanes are difficult to oxidize. Performing oxyfunctionalization selectively at terminal positions is almost impossible. This reaction is catalyzed by enzymes with non-heme iron active center.

Robert Raja *et al.* reported production of AA from n-hexane using Co framework substituted aluminophosphate catalyst (Co-AlPO-18, Co-AlPO-5) in air. After 24 hours of reaction at 373 K under air pressure of 1.5 MPa, 9.5% of n-hexane was converted with 33.6% selectivity to AA. Among the other detected products were 2-hexanone and 2-hexanol [17].

3.3.4. D-Glucose as a starting material

Preparation of AA from renewable source like glucose has been proposed by Frost [18]. It consist of enzymatic transformation of D-glucose to cis,cis-muconic via 3-dehydroshikimic acid, protocatechuic acid and catechol. The key parameter of these steps is the presence of three enzymes not typically found in ESTERICHIA Coli. The

final step of the reaction is hydrogenation of the cis,cis-muconic, using supported Ru, Pt catalyst. Under the pressure of 3400 kPa of H₂ 97% of cis,cis-muconic acid into AA can be converted after 2.5 hours of the reaction at the ambient temperature, see scheme 3.5. Still the problems concerning scaling-up and process implementation have to be solved and these problems could make this process economically viable.



Scheme 3.5. Enzymatic transformation of D-glucose to adipic acid.

3.4. Literature overview of one step oxidation of cyclohexane

Single step production of AA from cyclohexane with air as an oxidant is a highly tempting idea, because of the abundance and cost of the green oxidant. Replacing the corrosive oxidizing agent with air also makes the investment cost low.

3.4.1. Homogeneous catalysts

Cyclohexane oxidation was carried out using Co and Mn containing catalyst. By changing reaction conditions, it is possible to synthesize AA using the same catalyst. In fact Asahi almost 70 years ago industrialized this process, using Co acetate as catalyst and acetic acid as solvent, under 30 atm of O₂ pressure and at temperature 363–373 K. Conversion of CyH 50-75% and 70% selectivity to AA was achieved (the main byproduct was glutaric acid) [19].

In order to attain maximum AA yield, many industries experimented with different catalyst compositions and reaction conditions. For example in the Gulf process the reaction is carried out at the same temperature as the original Asahi process, using the same solvent but with higher concentration of catalyst, the AA selectivity obtained was 70-75% with 80-85% conversion of CyH [20]. Amoco process achieved 98% conversion of CyH with 88% yield of AA under 70 atm of air

pressure at 368 K [21]. However, all these were homogeneous catalyst based processes.

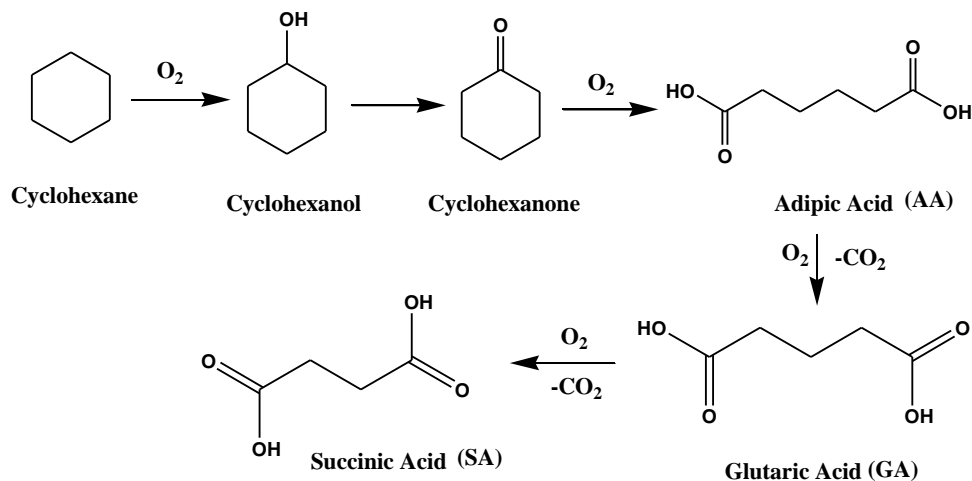
3.4.2. Heterogeneous catalysts

Schuchardt *et al.* thoroughly reviewed both homogeneous and heterogeneous catalytic systems, reported in the literature up to the year 2000 including those that use oxidants other than oxygen (e.g., H₂O₂ or TBHP) [22]. Recent review by Van de Vyver *et al.* discussed emerging catalytic processes for the production of AA [23]. Sankar *et al.* obtained a very high selectivity to cyclohexanol/cyclohexanone, at 9.6 % cyclohexane conversion (T=423 K) using Co-AlPO-36 as catalyst [24]. Good AA yield was achieved by J.M.Thomas group by using Fe-AlPO-31 [25]. Still improved yield was observed when they used a solid source of active oxygen (acetylperoxy borate) and H₂O₂ [26]. On CeO₂ supported on alumina, the oxidation of CyH was performed under 15 atm pressure of O₂ in the presence of cyclohexanone as a co-oxidant at 383 K. The conversion of cyclohexane was 36% with AA selectivity of 42%. The by-products of the reaction were lower dicarboxylic acid (glutaric, succinic), CO_x and caprolactone [27]. Using Ti-containing beta zeolite and hydrogen peroxide as oxidant and 2-butanone as a solvent, 47% conversion of cyclohexane with 54% selectivity to AA was obtained after 1 hour of reaction at 369 K [28].

Nano structured gold catalysts were also reported for the oxidation of CyH which include catalysts like Au/graphite, Au/Al₂O₃, Au/TiO₂, Au nano particles on Ti-doped SiO₂, Au/MCM-41, Au/SBA-15 and Au/C [29]. Recently, Alshammari *et al.* reported that by fine tuning Au particle size on TiO₂ supported catalysts, AA can be obtained to some extent with acetonitrile as solvent and TBHP as an initiator [30]. Low yield of AA was the major issue in addition to the recovery of catalysts for the scale up of above reported processes.

Ishii group had conducted the reaction using N-hydroxyphthalimide (NHPI, 10-20 mol %) as radical initiator and Mn and Co acetates as homogeneous catalysts and got maximum selectivity of 73 mol% along with CyH conversion of 73%, which was scaled up by Daicel chemical industry [31]. The major limitation in the Ishii process was that metal salts contaminate the products which require one more step for

purification. So, instead of metal salts a heterogeneous catalyst containing Co& Mn should be used which can be easily separated from the product. Therefore there is a need to get maximum selectivity and conversion with a heterogeneous catalysts using molecular O₂ as oxygen source.



Scheme 3.6. Oxidation of cyclohexane and their products.

3.5. Experimental procedures

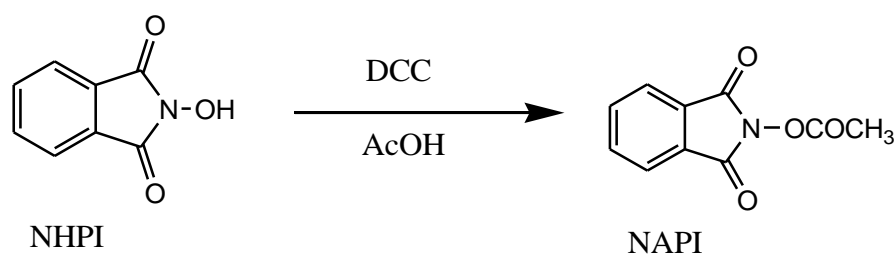
3.5.1. Materials

Potassium permanganate, manganese (II) sulphate and cobalt nitrate were used (Loba chemical Ltd.) for the preparation of K-OMS-2. acetic acid, methanol, NHPI (N-hydroxyphthalimide) and sodium hydroxide were purchased from Thomas Baker Pvt. Ltd. N-acetoxypthalimide (NAPI) was prepared in laboratory. All the chemicals were used without any further purification.

3.5.2. Initiator Preparation

N-Acetoxyphthalimide (NAPI)

N-Hydroxyphthalimide (0.7 g, 4.35 mmol), acetic acid (HOAc, 258μL, 4.35 mmol), and dicyclohexylcarbodiimide (DCC 0.85 g, 4.35 mmol) were added to dry ethyl acetate (EtOAc, 125mL) and the mixture was stirred for 3h at room temperature and then filtered. The filtrate was dried (Na₂SO₄), and the residue was crystallized from ethanol to give a white solid [32].



Scheme 3.7. Acylation of N-hydroxyphthalimide.

3.5.3. Experimental setup

Selective oxidation of CyH was performed in a 50 ml titanium lined Parr Reactor (4842) which was connected to an O₂ cylinder. In a typical run, reactor was charged with 8 mmol of CyH, 20 mol % of NAPI and 20 mL of acetic acid and 150 mg of catalyst. The whole mixture was stirred at 373 K at 500 rpm. After reaching to desired temperature, O₂ was filled into the reactor to reach the desired pressure. After completion of reaction, solid part was separated by simple filtration and liquid portion was analyzed by GC (Agilent 7890) equipped with HP-5 capillary column to arrive at conversion of cyclohexane, selectivity's of cyclohexanol and cyclohexanone. The product mixture with solvent (acetic acid) was subjected to rotavaporator so that the solvent can be evaporated; the remaining solid was dissolved in 10ml of millipore water and filtered to obtain soluble diacids in water, with initiator being insoluble. The soluble part was made up to 10 mL.

3.6. Analytical procedure

3.6.1. Esterification procedure of diacids

Part (2 mL) of the above solution was esterified using (4 mL) 4% BF₃ methanol solution for 12h at 353 K. To this mixture, 4 mL of millipore water and 4 mL dichloromethane was added, since the required esters dissolves in DCM. Aqueous and organic layers were separated by using separating funnel. The final DCM mixture was analyzed by GC for finding the selectivity of diacids.

3.7. Textural Characterization of Catalysts

3.7.1. Powder X-ray diffraction (PXRD)

The XRD patterns of K-OMS-2 and Co-K-OMS-2 are given in Fig. 3.1. XRD peaks of all catalysts match with the reported data of cryptomelane OMS-2 (JCPDS 05-0681). Peaks in Co-OMS catalysts are sharp and similar to the OMS-2, showing that the substituted cobalt OMS-2 materials also crystallized with cryptomelane structure. It also confirms that cryptomelane structure of OMS-2 material is retained even after substitution of cobalt. No additional peaks corresponding to cobalt oxides were observed, indicating the absence of any other cobalt containing oxides, which confirms the substitution of Co into OMS-2.

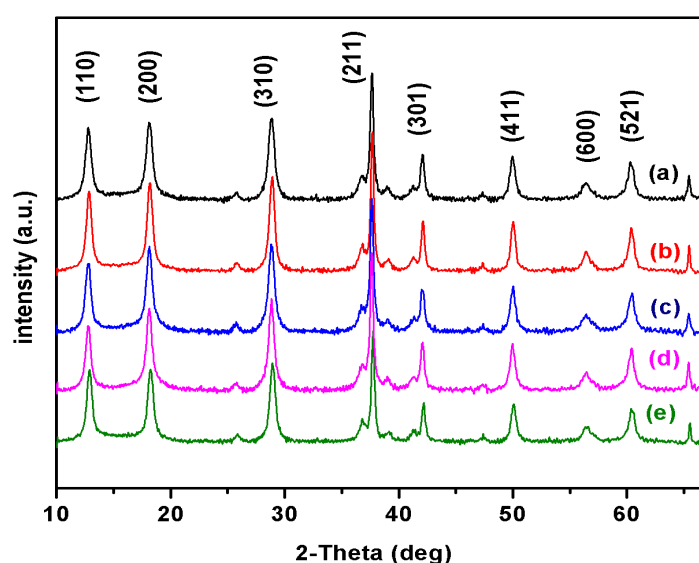


Fig 3.1. XRD pattern of (a) K-OMS-2, (b) Co-OMS-I (0.58 wt %), (c) Co-OMS-II (1.03 wt %), (d) Co-OMS-III (2.26 wt %) (e) Co-OMS-IV (2.98 wt %).

3.7.2. N₂ Physisorption

The N₂ adsorption/desorption isotherms of parent and Co doped samples are given in Fig. 3.2. (A). All the samples showed a characteristic Type II sorption and H₃-type hysteresis loop for P/P₀ > 0.6 that can be attributed to inter crystalline mesopores between particles with non uniform size or shapes. With increasing Co content in the sample, surface area, pore volume of the material dropped. This decrease may be attributed to partial blockage of pores by extra lattice cobalt oxide which is not detected by XRD due to its very low content. Micropore and total pore volume of the sample also decreased with Co doping but the H-K pore size of the

material is increased which was tabulated in Table 3.1. The H-K plot of parent and Co doped OMS-2 materials are illustrated in Fig. 3.2. (B).

Table 3.1. N₂ physisorption data of the prepared materials

Catalyst	Co content	BET Surface Area (m ² /g)	Pore Volume (cc/g) @p/p ₀ = 0.95	Micropore volume (cc/g) DR Method	Pore Size (Å) H-K Method
K-OMS-2	--	97.6	0.27	0.031	5.025
Co-OMS-I	0.58	81.5	0.17	0.026	5.075
Co-OMS-II	1.03	79.0	0.16	0.024	5.174
Co-OMS-III	2.26	74.8	0.14	0.023	5.175
Co-OMS-IV	2.98	60.4	0.11	0.021	5.525

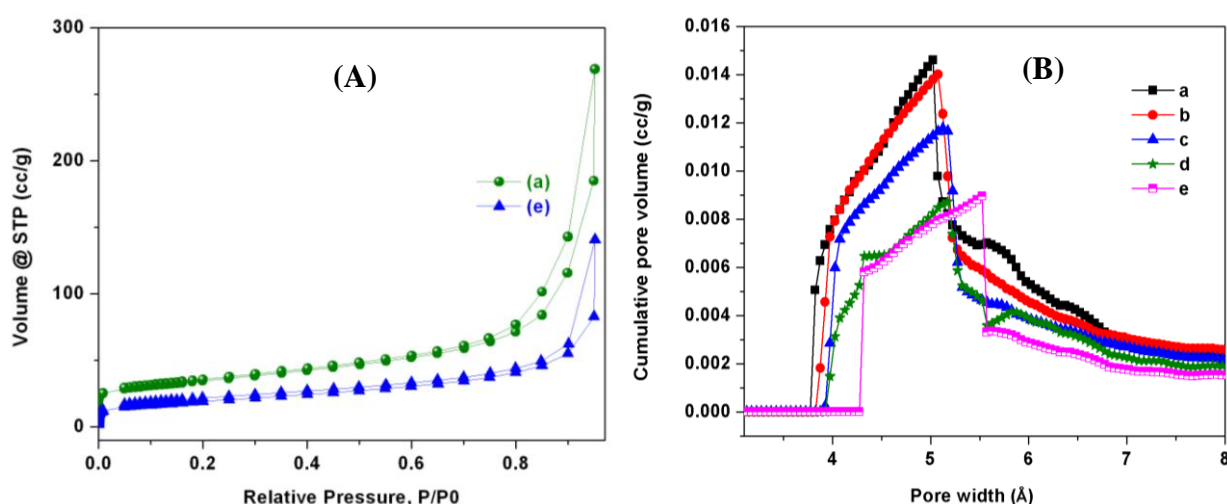


Fig. 3.2. (A) N₂ adsorption/ desorption isotherms; (B) H-K plots of (a) K-OMS-2, (b) Co-OMS-I (0.58 wt %), (c) Co-OMS-II (1.03 wt %), (d) Co-OMS-III (2.26 wt %) (e) Co-OMS-IV (2.98 wt %).

3.7.3. Raman spectroscopy

Raman spectroscopy was used to probe the effect of Co substitution and also look for the presence of segregated metal oxides. The regular OMS-2 (cryptomelane) belongs to the I4/m space group [33]. Using Factor group analysis, [34] the following irreducible representations (without tunnel cations contribution) can be attributed to the Mn-O lattice vibrations within the MnO₆ octahedral double chain:

$$\Gamma = 6A_g + 6B_g + 3E_g + 2A_u + 3B_u + 5E_u$$

Where the A_g , B_g and E_g (double-degenerated) modes are Raman active, the A_u and E_u (double-degenerated) modes are IR active and the B_u mode is silent. The Raman spectrum obtained for the regular OMS-2 material only shows six Raman peaks at around 750, 647, 582, 480, 392 and 187 cm^{-1} as opposed to fifteen peaks predicted from Factor group analysis (Fig. 3.3). This could be because of low polarizabilities of some of these modes and low resolution of other modes [34].

The two strong, sharp peaks at 647 and 582 cm^{-1} correspond to A_{1g} spectroscopic modes whereas the peaks at 480 cm^{-1} correspond to the F_{2g} spectroscopic species [35]. The two sharp peaks at 647 cm^{-1} and 582 cm^{-1} are associated with Mn-O vibrations that are orthogonal and along the direction of the MnO_6 octahedral double chains, respectively, which are indicative of a well-developed tetragonal structure with 2×2 tunnels [36].

There was no segregated undoped cobalt oxide peaks expected at 455 and 675 cm^{-1} [37]. The Raman spectra, with respect to the crystallinity are in good agreement with the structural data obtained by XRD for these materials.

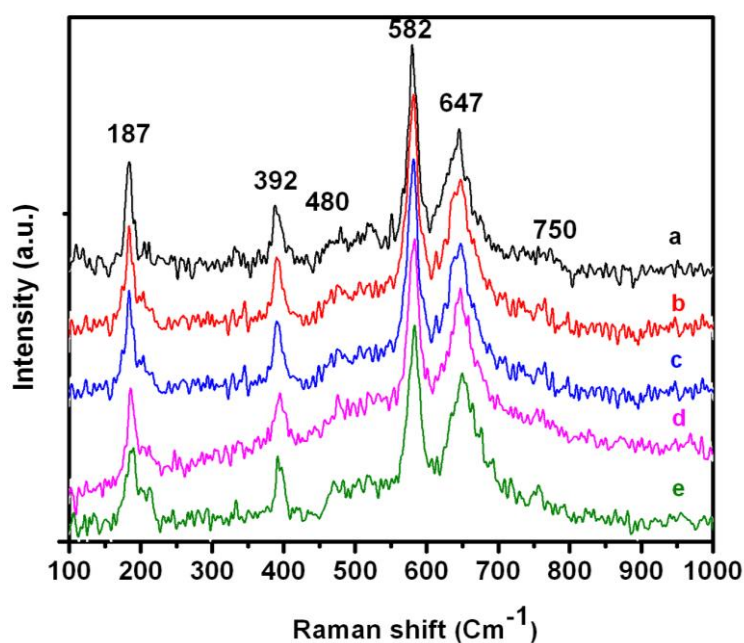


Fig. 3.3. Raman spectra of (a) K-OMS-2, (b) Co-OMS-I (0.58 wt %), (c) Co-OMS-II (1.03 wt %), (d) Co-OMS-III (2.26 wt %) and (e) Co-OMS-IV (2.98 wt %).

3.7.4. Fourier-Transform infrared spectroscopy

On substitution of Mn in the octahedral OMS-2 framework by other isomorphous metal ions, the local environment of oxygen coordination around the octahedral site changes along with the masses of the lattice vibrators hence, the bond length and force constant. Consequently, the lattice vibrations and spectral features of the bulk OMS-2 material changes. As a result, the peak positions will shift and/or the peak intensities will vary [38]. Because of the sensitivity of IR spectroscopy towards lattice vibrational changes, this technique was used to probe the effect of multiple substitution(s) on the spectral features of cryptomelane.

The results of the IR spectrum of the as-synthesized regular OMS-2 material shows features similar to those previously reported; namely, absorption bands at around 720, 590, 530, and 470 cm^{-1} [36]. These bands are ascribed to the regular Mn-O lattice vibrations of the MnO_6 octahedra framework (Fig. 3.4). Upon doping of Co into the OMS-2 structure, a dramatic fall in peak intensities was observed. This attenuation of peak intensity needs to be investigated further. The IR data depicted the absence of segregated metal oxide impurities and therefore corroborates the Raman and the XRD data, that showed no extra peaks attributed to segregated metal oxide.

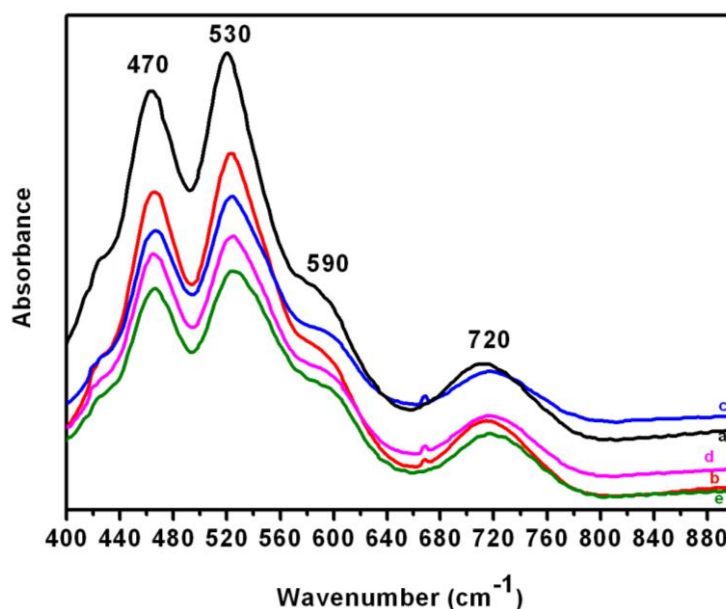


Fig. 3.4. FT-IR spectra of (a) K-OMS-2, (b) Co-OMS-I (0.58 wt %), (c) Co-OMS-II (1.03 wt %), (d) Co-OMS-III (2.26 wt %) and (e) Co-OMS-IV (2.98 wt %).

3.7.5. Thermo gravimetric analysis

Thermal stability of Co-OMS-2 materials was studied through thermo gravimetric analysis (TGA) in air flow in the temperature range 293-1273 K at a ramping rate of 10 K/min, which are depicted in Fig. 3.6.

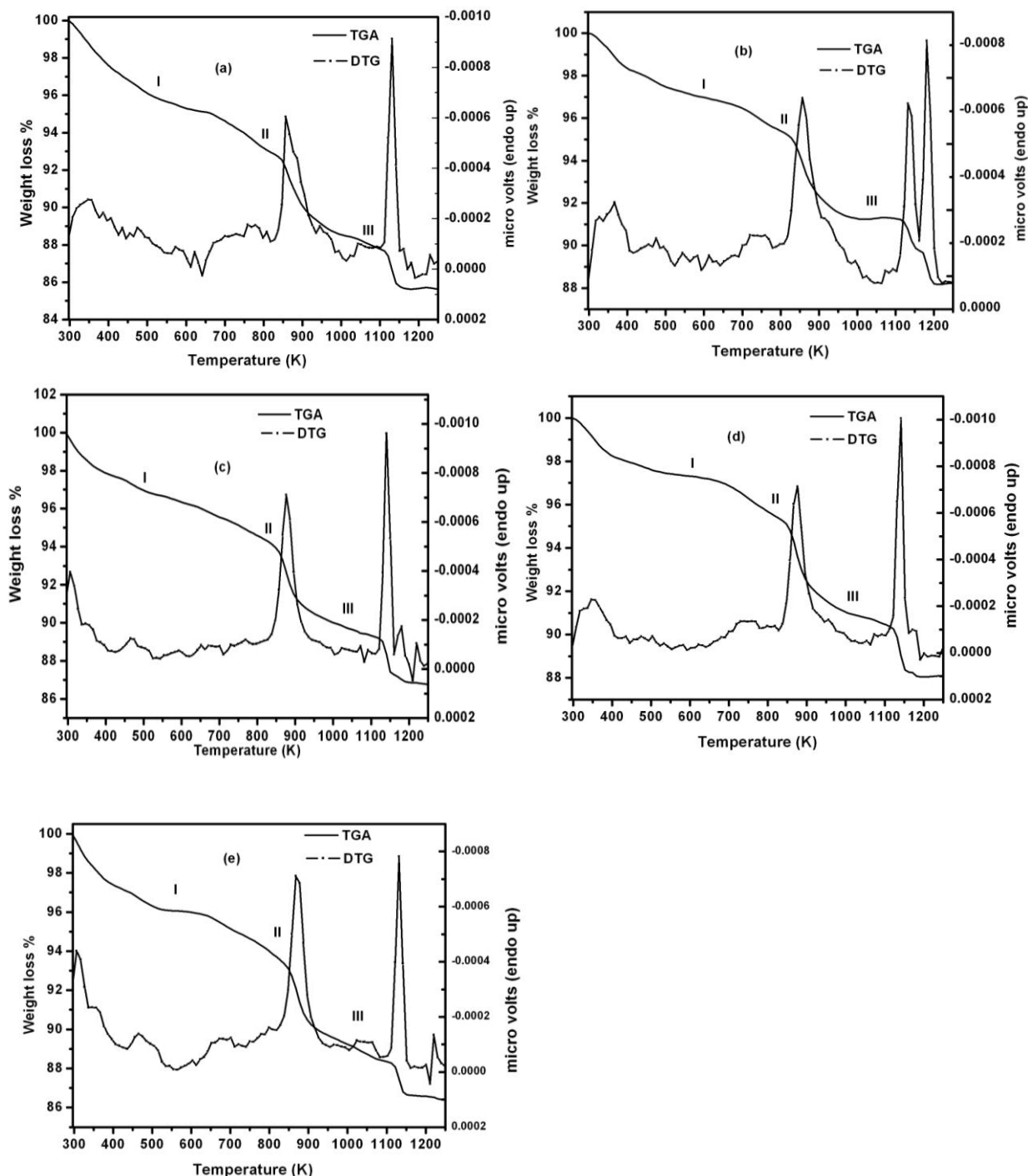


Fig. 3.5. TGA in air of (a) K-OMS-2, (b) Co-OMS-I (0.58 wt %), (c) Co-OMS-II (1.03 wt %), (d) Co-OMS-III (2.26 wt %) and (e) Co-OMS-IV (2.98 wt %).

Parent K-OMS-2 material synthesized by reflux method shows weight loss in the temperature range between 293-1273 K. The initial weight loss (2.5%) in the temperature range of 323-543 K is attributed to the loss of water in the sample. The second weight loss of about 6.4 % in the 543-973 K temperature zone is due to loss of lattice oxygen, as the manganese cations reduce to lower oxidation state forming manganese oxide such as bixbyite (Mn_2O_3) [41].

The third weight loss of about 2.7%, observed in the temperature zone of 973-1173 K is attributed to a further loss of oxygen from bixbyite leading to the formation of more stable spinel hausmanite (Mn_3O_4) [42]. The general trend remained similar for each temperature zone but the weight loss differed based on cobalt content in the OMS-2 structures. The weight losses attributed to water loss in the samples was 2.7% for Co-OMS-I, 3.3% for Co-OMS-II, 3.9% for Co-OMS-III, and 4.2% for Co-OMS-IV. The first weight loss increases with Co loading which suggest that water in the lattice increases with Co loading

The 2nd weight loss is due to change in phase of manganese from KMn_8O_{16} to Mn_2O_3 in the mid temperature zone of 543-973 K. The weight loss slightly increases with Co loading. The weight losses were 5.9, 6.4, 6.5 and 7.2 wt % for Co-OMS-I, Co-OMS-II, Co-OMS-III and Co-OMS-IV respectively. The 3rd weight loss, for phase transition from Mn_2O_3 to Mn_3O_4 , was almost similar as that of K-OMS-2 without any trend. The weight losses were 3.0, 3.1, 2.8, and 2.8 wt% for Co-OMS-I, Co-OMS-II, Co-OMS-III and Co-OMS-IV respectively. The DTG of materials found that the major weight loss occurred at 870 K and 1135K. Substituted OMS-2 materials show slightly lower thermal stability, which in turn may be attributed to the substitution of Co into OMS-2 lattice.

3.7.6. Scanning Electron Microscopy

The scanning electron micrographs show fibrous needle-like morphology of K-OMS-2 and Co-K-OMS-2 (Fig. 3.6). The morphology of K-OMS-2 is similar to that of Co-K-OMS-2 with 20 to 200 nm size fiber length. The length and breadth of the rods increased with Co doping. The result shows that the Co substitution affects

the rod dimensions and morphology. The fibrous morphology of the produced materials is indicative of an anisotropic growth behavior of OMS-2 [43].

During the crystallization process of the undoped synthetic OMS-2 material the crystal growth in the c-direction [44] leads to the formation of fibrous/nanorods with 1×1 and 2×2 tunnels running along the length of the nanofibers /nanorods. The increase in width and length of our Co doped materials was probably due to a slight distortion of the tetragonal crystal structure of cryptomelane to the monoclinic geometry. No particles as secondary phases were observed in the products, an indication of highly pure nanofibers as synthesized products.

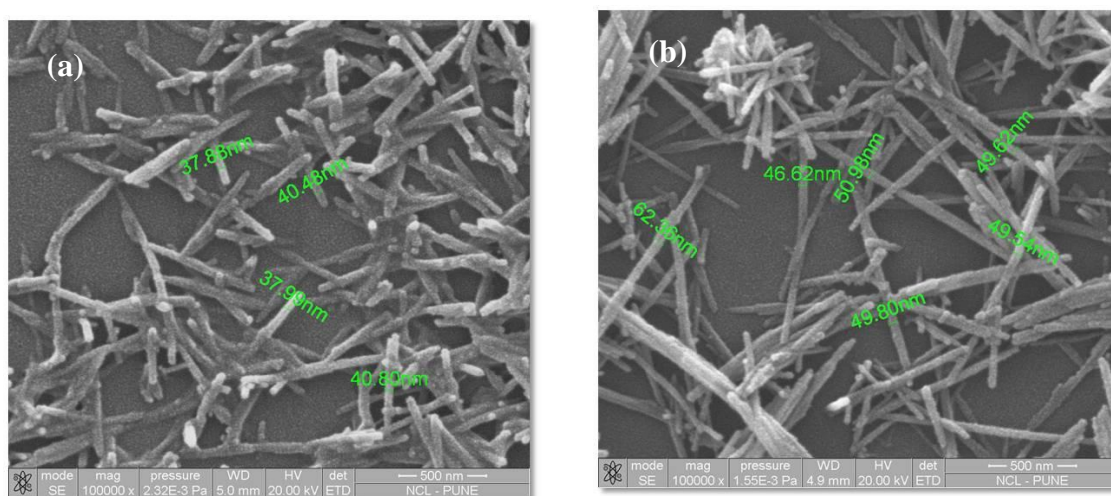


Fig. 3.6. SEM of (a) K-OMS-2 and (b) Co-OMS-IV (2.98 wt %).

3.7.7. Transmission electron microscopy (TEM)

High resolution TEM images of materials K-OMS-2 and Co-K-OMS-2 are given in Fig. 3.7. They show the nanoscale size of the fibers self-assembled into the complex hollow structures. The well-defined lattice planes observed in the high-resolution TEM (HRTEM) images of undoped, Co doped K-OMS-2 confirmed the excellent crystallinity of these nano materials. The lattice fringe spacing of 0.47 & 0.69 nm in the undoped K-OMS-2 can be attributed to the (2 0 0) and (1 1 0) planes respectively which corresponds to the planes of the cryptomelane structure [45]. In Co-OMS-I & Co-OMS-IV, the (2 0 0) plane was identified which is in agreement with parent K-OMS-2 structure.

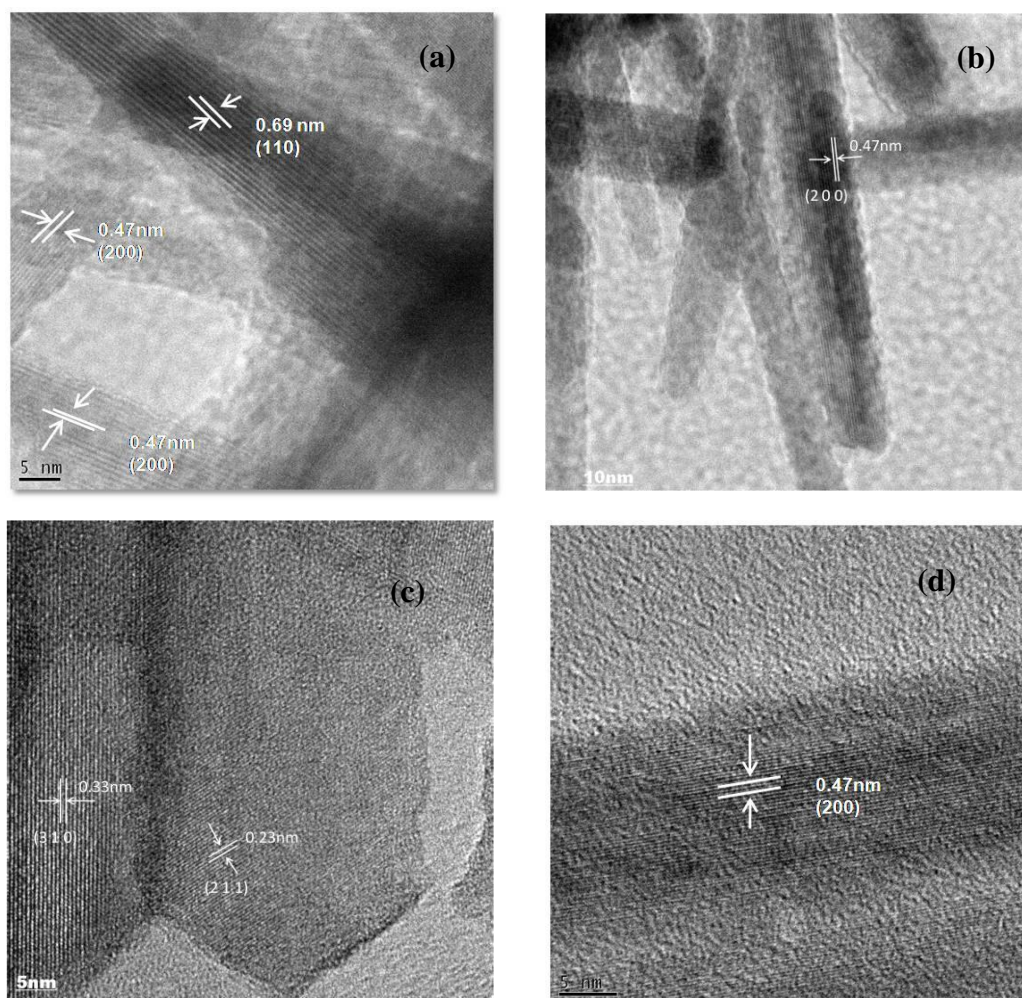


Fig. 3.7. TEM of (a) K-OMS-2, (b) Co-OMS-I (0.58 wt %), (c) Co-OMS-III (2.26 wt %), (d) Co-OMS-IV (2.98 wt %).

In case of Co-OMS-III, the 0.23 nm and 0.33 nm spacing's can be assigned to (2 1 1) and (3 1 0) planes of its crystal structure. Perfect surface structures were observed; hence, no obvious surface defect sites were formed in the typical structures of undoped, Co doped K-OMS-2 material.

3.7.8. H₂-Temperature programmed reduction

The H₂-TPR profiles of the synthesized materials are shown in Fig. 3.8. Four prominent peaks were observed in the TPR analysis. The assignment of each peaks is as follows: Peak I, relates to the consumption of structural oxygen close to the

surface, without decomposition of the material; Peak II, Peak III and Peak IV are related to the following reduction processes: $\text{MnO}_2 \rightarrow \text{Mn}_2\text{O}_3$ (Peak II), $\text{Mn}_2\text{O}_3 \rightarrow \text{Mn}_3\text{O}_4$ (Peak III) and $\text{Mn}_3\text{O}_4 \rightarrow \text{MnO}$ (Peak IV) [39]. It is evident that with increasing Co loading, there is a slight reduction in the temperature of I, II, and III reduction peaks. The data suggests that the oxygen available for reduction is strongly influenced by the presence of Co in the samples, which is related to oxygen mobility. The doping cation (Co in this case) substantially effects the change in reactivity and availability of oxygen due to heat of formation of corresponding oxides and their electro negativity properties [40]. Accordingly, the presence of Co in the material influences the reactivity of the oxygen in the Mn–O–Co bridges. Since Co (1.88) has higher electro negativity compared to Mn (1.55), there will be electron delocalization and consequently weaker Mn–O bond. The reduction temperature of the $\text{Mn}_3\text{O}_4 \rightarrow \text{MnO}$ (Peak IV) hardly changed, on modifying with doping cation, suggesting an important role of the structural and morphological properties of the material in the reactivity of lattice oxygen

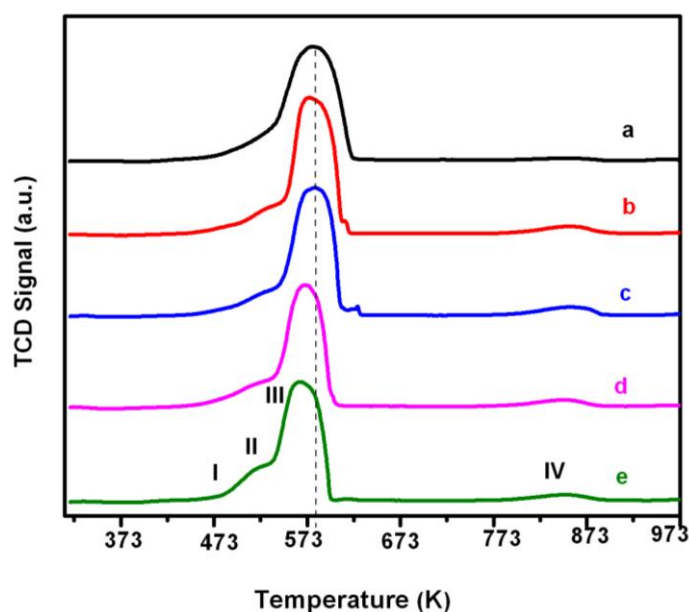


Fig. 3.8. H_2 -TPR of (a) K-OMS-2, (b) Co-OMS-I (0.58 wt %), (c) Co-OMS-II (1.03 wt %), (d) Co-OMS-III (2.26 wt %) and (e) Co-OMS-IV (2.98 wt %).

3.7.9. X-ray Photoelectron Spectroscopy

XPS measurements were carried out to investigate the oxidation state, surface composition and atomic environment of Mn, O and Co Species.

3.7.9.1. Mn 2p spectra

The Mn 2p_{3/2} spectra of the OMS-2 nanorod samples are given in Fig.3.9.

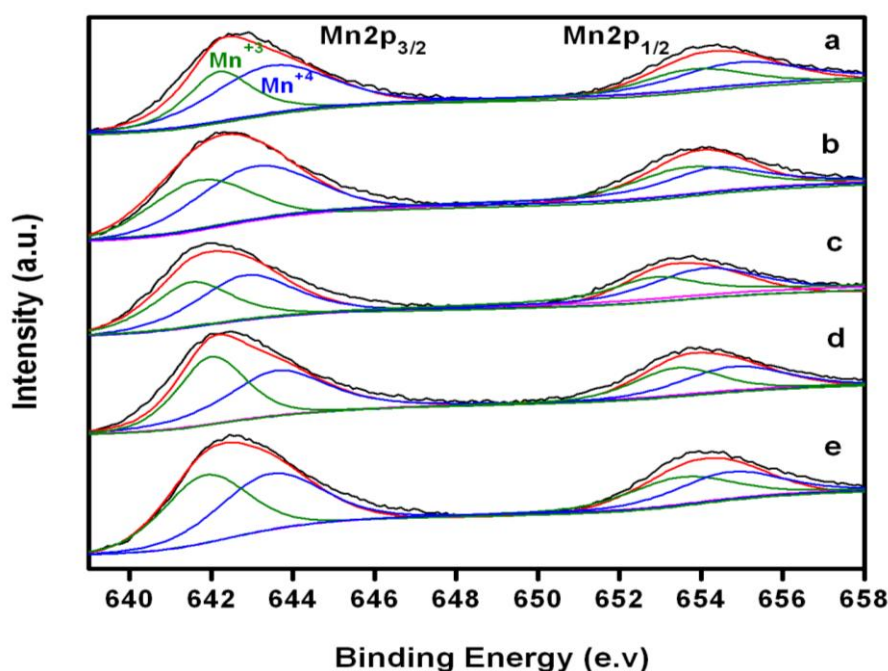


Fig. 3.9. Mn 2p spectra of (a) K-OMS-2, (b) Co-OMS-I (0.58 wt %), (c) Co-OMS-II (1.03 wt %), (d) Co-OMS-III (2.26 wt %) and (e) Co-OMS-IV (2.98 wt %).

These spectra were deconvoluted into two peaks around 642.1 and 643.4 eV (Fig. 3.9), which are attributed to the Mn⁺³ and Mn⁺⁴ species [46]. Considerable change in Mn⁺⁴/Mn⁺³ intensity ratios with Co loading was observed, which is tabulated in Table 3.2 (a). This change in the ratio is attributed to replacement of Mn⁺⁴ by Co⁺³ (0.685 Å) which has similar crystal radius like Mn⁺⁴ (0.67 Å). Hence, with increase in Co doping, Mn⁺⁴/Mn⁺³ ratios were found to decrease.

Table 3.2 (a) Variation of Mn⁺⁴/Mn⁺³ ratio with Co loading.

CATA	Mn ⁺⁴ /Mn ⁺³
K-OMS-2	1.30
Co-OMS-I	1.19
Co-OMS-II	1.15
Co-OMS-III	1.04
Co-OMS-IV	0.97

Table 3.2(b) Binding energies of Mn 2p in K-OMS-2

Mn 2p 3/2 (eV)		Mn 2p 1/2 (eV)	
Mn ⁺³	Mn ⁺⁴	Mn ⁺³	Mn ⁺⁴
642.18	643.46	653.77	654.9

3.7.9.2. Oxygen 1s spectra

Fig. 3.10. shows the Oxygen 1s spectra of the K-OMS-2 and Co substituted materials. Based on the peak positions, three types of oxygen species can be identified: the lower binding energy peak (O_I ~ 529.7 eV), which is attributed to lattice oxygen or oxygen ions bonded to metal cations in coordinatively saturated environment (O^{2-}), the medium value binding energy peak (O_{II} ~531.3 eV) assigned to surface adsorbed oxygen or oxygen ions bonded to metal ions in coordinatively unsaturated environment (O^{2-} or O^- , $-OH$ groups and oxygen vacancies) and finally the high binding energy peak (O_{III} ~533.1 eV), likely associated with adsorbed molecular water [47]. The peak positions and relative abundance of O_I , O_{II} and O_{III} species are listed in Table 3.3. The principal component corresponds to the lattice oxygen, followed by the peak O_{II} of adsorbed oxygen and O_{III} of adsorbed water. The relative abundances of O_I and O_{II} species are listed in the table below. The ratio of O_{II}/O_I increases with the increasing of cobalt content (from 20.1% to 27%), implies that more cobalt is incorporated into the framework of the OMS-2 results in higher surface metal cations in a low coordination environment, implying that there was gradual increase in oxygen vacancies with Co doping. The interaction of these point defects with molecular oxygen and/or water leads to generation of peroxides, superoxides and hydroxyl species [48]. Thus, insertion of Co in the oxide structure enhances the oxygen lability and reducibility of the material which is in agreement with earlier discussed TPR results.

Table 3.3 Variation of oxygen species with Co loading

CATA	O_I (%) (Lattice)	O_{II} (%) (Surface)	O_{III} (%) (H ₂ O)
K-OMS-2	71.3	23.5	5.0
Co-OMS-I	66.6	27.2	6.0
Co-OMS-II	63.9	31.5	4.4
Co-OMS-III	59.7	34.5	5.5
Co-OMS-IV	54.5	40.4	5.0

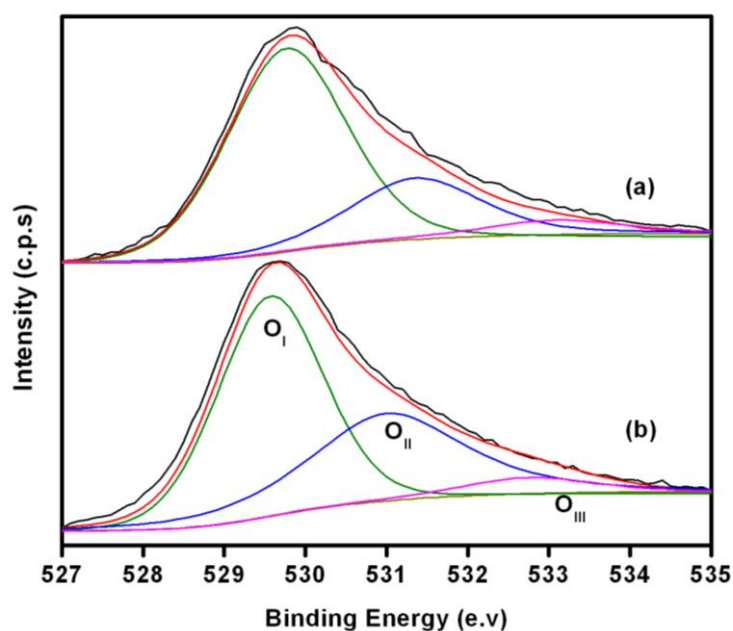


Fig. 3.10. O 1s spectra of a) K-OMS-2, (b) Co-OMS-IV (2.98 wt %).

3.7.9.3. Co 2p spectra

The Co 2p spectrum of cobalt doped OMS-2 is given in Fig. 3.11. All Co-containing samples consisted of two main peaks at about 777 and 795 eV, corresponding to Co 2p_{3/2} and Co 2p_{1/2}, respectively. A spectral feature that distinguishes between Co²⁺ and Co³⁺ is that the main Co²⁺ peaks present a satellite, arising from interaction of photoemitted electrons with core vacancy and valence electrons, whereas Co³⁺ peaks do not [49]. All Co doped samples exhibited a satellite (788.9 eV) at higher BE by about 6 eV compared to Co 2p_{3/2}, indicating the presence of Co²⁺. With increasing in Co loading, the intensity ratio of the 2p_{3/2} satellite to the relevant main peak decreased from $I_{\text{sat}}/I_{\text{main}} = 0.39$, close to the value reported for CoO [50], to $I_{\text{sat}}/I_{\text{main}} = 0.32$, indicating the presence of an increasing amount of Co³⁺. The spin-orbit separation between Co 2p_{3/2} and Co 2p_{1/2} is around 16.2 eV, thus confirming a parallel increase in Co³⁺.

Table 3.4 XPS parameters of Co-OMS-IV

CATA	Co ⁺³ /Co ⁺²	I _{sat} /I _{main}	Spinorbit Separation ($\Delta_{1/2-3/2}$)
Co-OMS-IV	2.57	0.39	16.2 eV

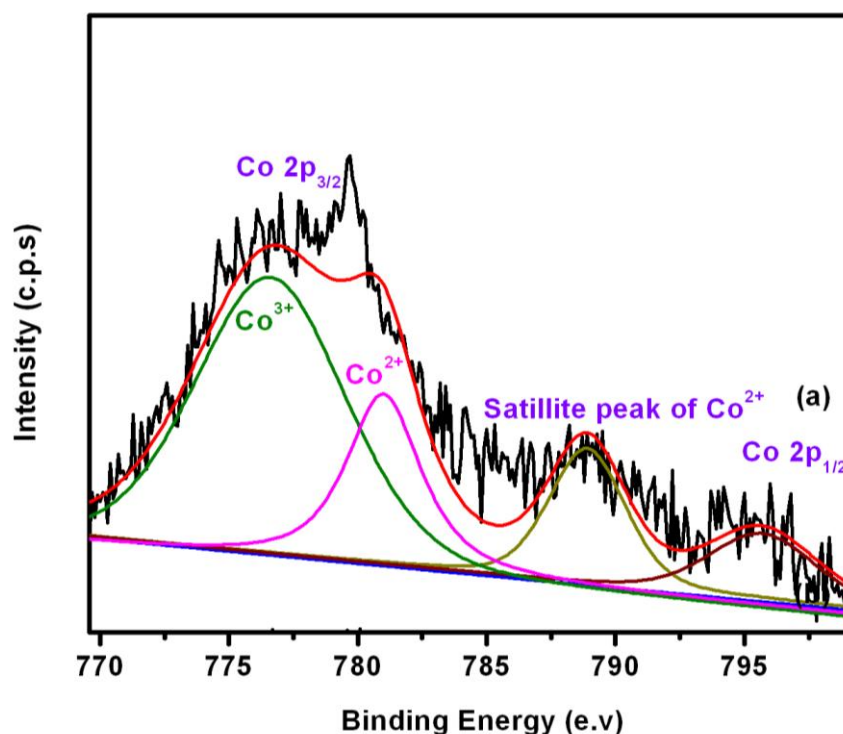


Fig. 3.11. Co 2p spectra (a) Co-OMS-IV (2.98 wt %).

3.8. Catalytic Activity-Single step selective oxidation of cyclohexane to adipic Acid

For the preparation of adipic acid from cyclohexane in a single step, a heterogeneous catalyst was chosen in such a way that it contains both Co & Mn, since both metals work synergistically in oxidation reactions. The heterogeneous catalyst should have metal (Mn or Co) with different oxidation states, as it is important for partial oxidation reactions that metal should have variable oxidation states. The catalyst should be non toxic and cheap for commercial use of the process. The above oxidation reaction should be possible to carry out with molecular oxygen. Following

these criteria, cobalt substituted manganese containing octahedral molecular sieves were chosen. Instead of NHPI (N-Hydroxyphthalimide) as radical initiator, which was used in the Ishii process, we have tested NAPI (N-Acetoxyphthalimide) which is an acetylated derivative of NHPI [21].

3.8.1. Effect of temperature on Adipic acid yield

The effect of the reaction temperature on the catalytic activity of Co-OMS-2 in the oxidation of CyH is given in Table 3.5. As one would expect, with increasing reaction temperature, the conversion of CyH increased significantly. At 353 K, CyH conversion was 52.8 % with 90.6 % selectivity for AA. By increasing the temperature further, the selectivity's of by-products succinic and glutaric acids increased. Tinker *et al.* have also observed similar effect. Increasing reaction temperature leads to enhanced decarboxylation rate of adipic acid [51]. Hence, in order to have high yield of AA, reaction was optimized at 363 K. With K-OMS as catalyst, the yield of AA was low due to the low conversion of CyH (entry 5). This shows that by substituting Mn with cobalt in OMS-2, the reaction rate is accelerated as a result of synergistic effect.

Table 3.5. Influence of reaction temperature on selective oxidation of cyclohexane

S. No	Temp (K)	Conversion of CyH (mol %)	Product Selectivity (mol %)					AA (Yield%)
			Cyclo hexanol	Cyclo hexanon	Succinic acid	Glutaric acid	Adipic acid	
1	353	52.8	2.9	0.2	0.5	5.7	90.6	47.9
2	363	96.9	0.0	0.9	3.8	9.5	84.2	81.7
3	373	95.6	0.4	0.7	2.8	11.7	83.2	79.6
4	383	98.7	0.0	1.2	6.6	13.7	78.3	77.3
5*	363	54.9	2.2	0.2	1.1	7.2	89.1	48.9

Conditions: Cyclohexane = 8 mmol, NAPI = 20 mol%, Acetic acid = 20 mL, Time = 3h, Co-OMS-I = 150 mg, 20 bar O₂, * Catalyst K-OMS-2 (150mg)

3.8.2. Effect of reaction time on AA yield

The effect of the reaction time on the catalytic activity and selectivity of different products in oxidation of CyH is given in Fig. 3.12. After one hour of

reaction, CyH conversion was 56.6% with AA selectivity at 89.8 %. With increase in reaction time to 2h, conversion has increased to 76.3 mol% with AA selectivity nearly same at 89.6 %. After 3 hours, conversion further increased to 95.8 %, but AA selectivity decreased to 84.1%. After 4 hours of reaction, conversion almost remained unchanged (96.2%), but AA selectivity decreased to 80.3%. With increasing reaction time, the yield of adipic acid increased as a result of increase in CyH conversion. However, on further increasing time, the rate of side reactions (degradation) gradually increased to form GA followed by SA.

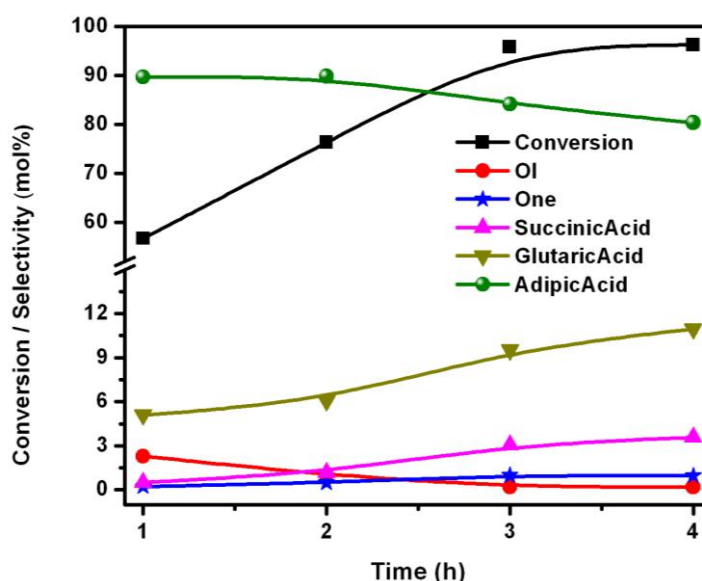


Fig. 3.12. Effect of reaction time on cyclohexane oxidation.

Conditions: Cyclohexane = 8 mmol, NAPI = 20 mol%, Acetic acid = 20 mL, Co-OMS-I = 150 mg, Temp = 363 K, 20 bar O₂.

Kollar *et al.* have also made similar observations in the selective oxidation of cyclohexane to AA [52]. Even though the AA selectivity decreased after 3h, we have optimized the reaction time to 3h, to get higher conversion of CyH that lead to higher AA yield.

3.8.3. Effect of Catalyst content on AA yield

The effect of the catalyst content on catalytic activity in the selective oxidation of CyH is illustrated in Fig. 3.13. With a catalyst content of 50mg, CyH conversion was 69.9% with AA selectivity at 90.2%. With increasing the amount of catalyst the CyH conversion also increased, which shows the promotional effect of increasing

catalytic sites on the reaction. With 100 mg of catalyst, 80.8% CyH conversion and 90.7% AA selectivity were obtained, whereas the selectivity for by products GA, SA increased slightly. However, when the amount of catalyst is further increased to 150 mg, the conversion reached to a maximum of 97%, while selectivity of AA decreased to 84.2% and there was two fold increase in GA and SA selectivity's. The overall yield of AA was maximum after 3h due to the increase in conversion. With time on stream, the selectivity's of the decarboxylated by products increased due to Co^{2+} catalyzed degradation of dicarboxylic acid. The rate of degradation of acid increased with temperature and cobalt catalyst concentration [51].

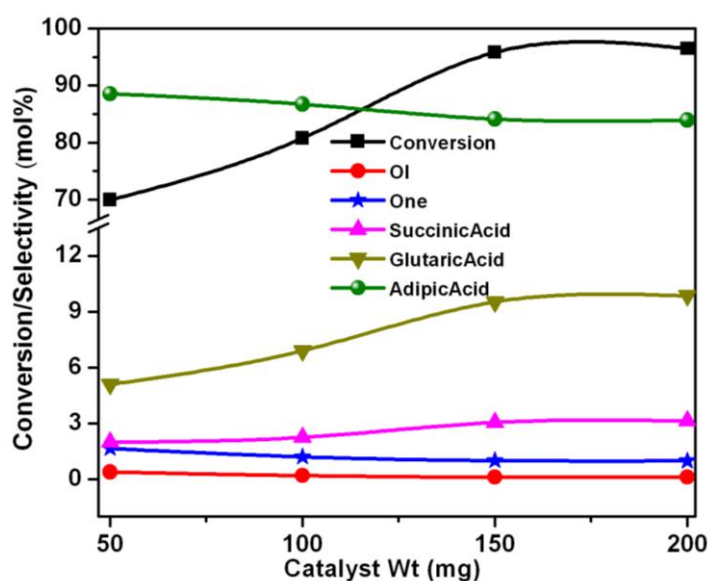


Fig. 3.13. Influence of catalyst content on cyclohexane oxidation.

Conditions: Cyclohexane = 8 mmol, NAPI = 20 mol%, Acetic acid = 20 mL, Temp = 363 K, Time = 3 h, Co-OMS-I, 20 bar O_2 .

3.8.4. Effect of initiator amount on the yield of AA

Figure 3.14 shows the effect of the initiator content on the catalytic activity in the selective oxidation of CyH. Initiator content plays a vital role in hydrocarbon oxidation. CyH conversion increased with increasing initiator content. Conversion of 64.2, 73.8, 84.6 and 95.8% were obtained for initiator contents a 5, 10, 15 and 20 mol%, respectively after 3h of reaction. Kerry *et al.* also reported similar effect of increase in conversion with initiator content [53]. The AA selectivity is independent of initiator content, which implies that the role of initiator is just to initiates the reaction by forming the radical producing species of substrate and has nothing to do

with the product selectivity's. At 20 mol% of the initiator, the rate of reaction was fast and yield of AA was high after 3h of reaction itself.

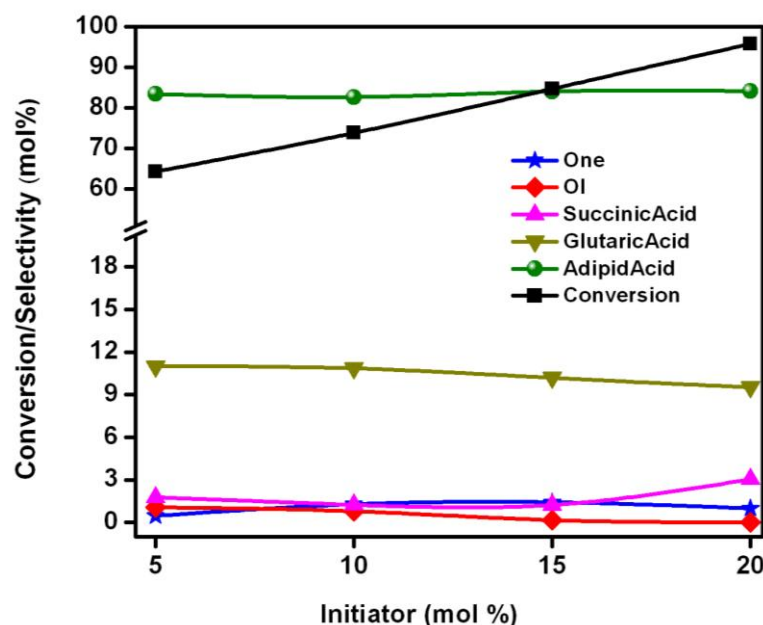


Fig. 3.14. Effect of initiator content on selective cyclohexane oxidation.

Conditions: Cyclohexane = 8 mmol, Acetic acid = 20 mL, Co-OMS-I = 150 mg, Temp = 363 K, Time = 3 h, 20 bar O₂.

3.8.5. Effect of Co content in the catalyst on the yield of AA

The influence of Co content in the catalyst on CyH selective oxidation was examined and the results are shown in Fig. 3.15. With increasing Co content, conversion of CyH increased, while the AA selectivity decreased. Selectivity of AA was found to be 82.2, 79.8, 77.5 and 73.1% for the catalyst Co-OMS-I, Co-OMS-II, Co-OMS-III and Co-OMS-IV respectively. The decrease in AA selectivity and simultaneous increase in by-product (SA and GA) selectivity's indicate degradation of AA in subsequent steps. With Co-OMS-IV catalyst, high amount of by-products were found. Hence, at higher temperatures and high Co concentrations, the rate of degradation of AA is higher. Belkhir *et al.* reported almost similar observations of Co concentration effect in AA selectivity in their investigations using Co molecular sieves [54]. These results substantiate our observations on catalyst content study.

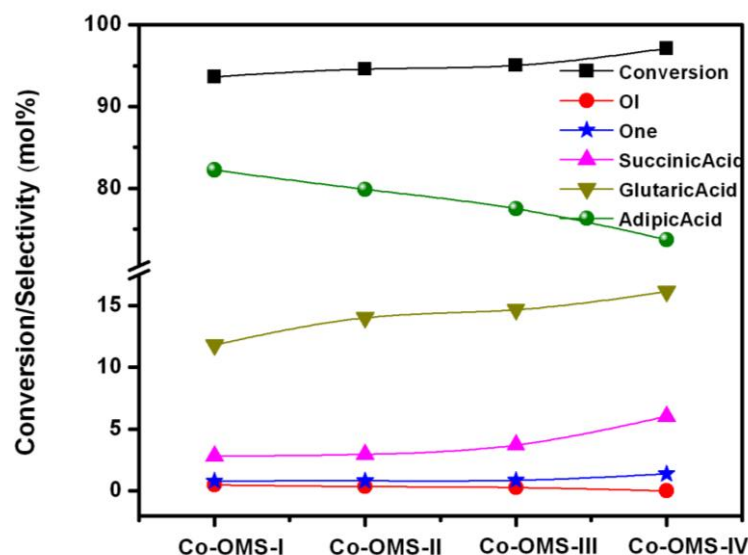


Fig. 3.15. Influence of Co content on cyclohexane oxidation

Conditions: Cyclohexane = 8 mmol, Acetic acid = 20 mL, NAPI = 20 mol%
Catalyst = 150 mg, Temp = 363 K, Time = 3 h, 20 bar O₂.

3.8.6. Recycle study of the catalyst

To study the recyclability of Co-K-OMS-2 catalyst in selective oxidation of CyH, catalyst was recovered after the completion of reaction by centrifugation, washed with methanol till it is free from organic substrate and dried at 373 K for 4h.

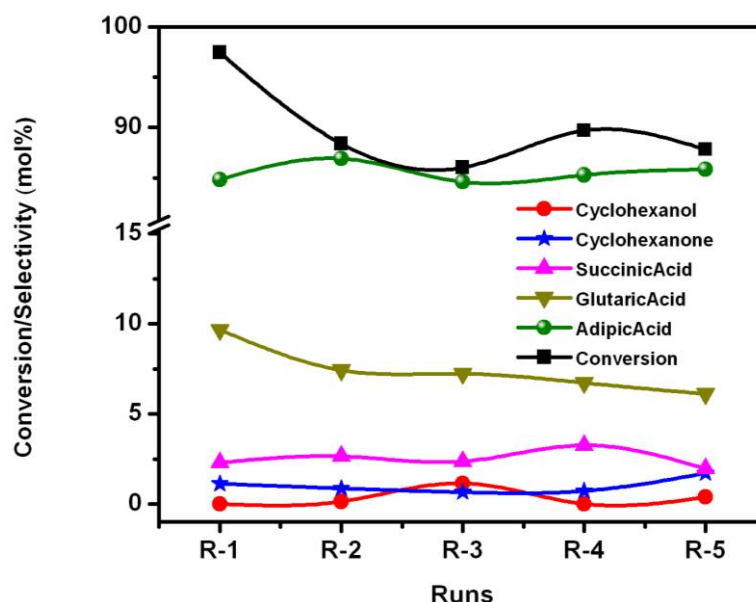


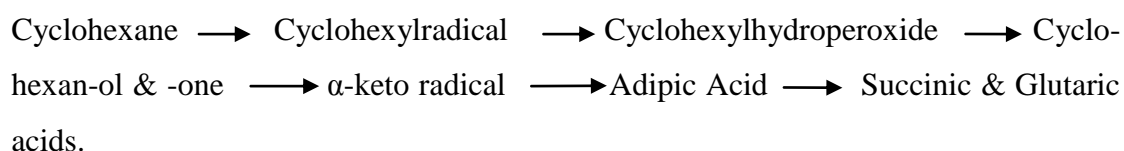
Fig. 3.16. Catalyst reusability study in cyclohexane oxidation

Conditions: Cyclohexane = 8 mmol, Acetic acid = 20 mL, NAPI = 20 mol%,
Co-OMS-I = 150 mg, Temp = 363 K, Time = 3h, 20 bar O₂.

This catalyst was re-used for the reaction with fresh reactant. The catalyst was found to be quite stable even after the 5 recycles. After the 1st recycle, there was some loss in conversion; however, no further loss in conversion was observed in subsequent runs. The AA selectivity was almost stable, though slight reduction in GA selectivity was observed. The spent catalyst (after the 5th recycle) was characterized by ICP-OES. No loss in Co or Mn content was detected in the used catalyst. The results are given in Fig. 3.16., which shows that catalyst was recycled at least five times with not much loss in activity.

3.9. Proposed reaction mechanism

From the experimental data and literature reports a tentative reaction scheme was proposed for the oxidation of CyH to adipic acid as follows:



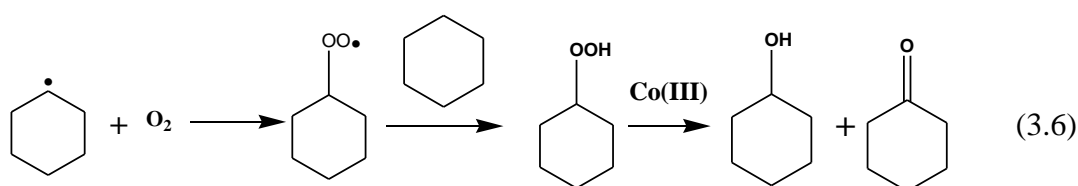
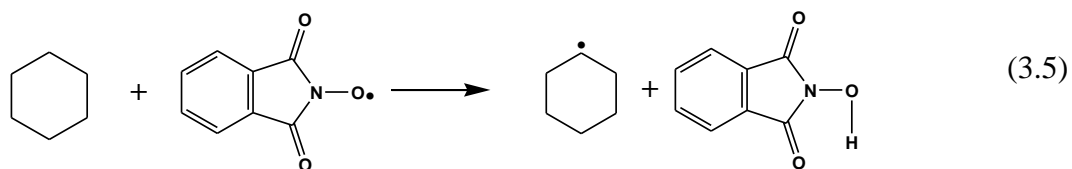
The conversion of CyH in the presence of Co & Mn catalysts with NAPI involves series of steps including inert C-H bond activation, enolization of ketone, electron transfer oxidation, redox decomposition of hydroperoxides.

The possible mechanism of Co-K-OMS-2 & NAPI catalyzed oxidation of cyclohexane is presented in Scheme 3.8. It proceeds in three steps. The first step involves the generation of phthalimido-N-oxyl radical (PINO) from NAPI. The generated radical abstracts hydrogen from the inert C-H bond of hydrocarbon to form cyclohexyl radical [55] (eq. 3.5). The produced highly reactive radical rapidly reacts with O₂ to form cyclohexyl hydroperoxide (CHHP) which in turn generates cyclohexanol and cyclohexanone by the decomposition assisted by Co (III) (eq. 3.6).

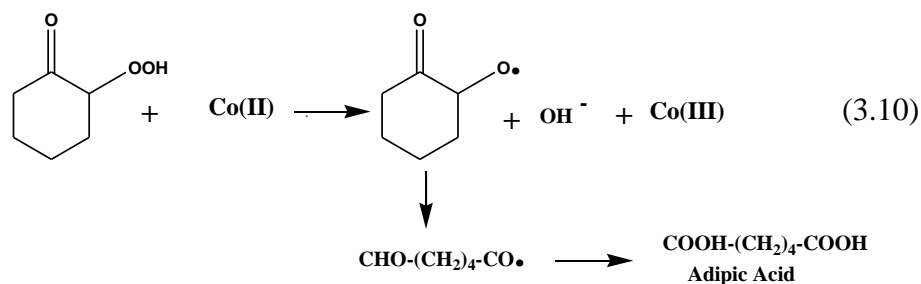
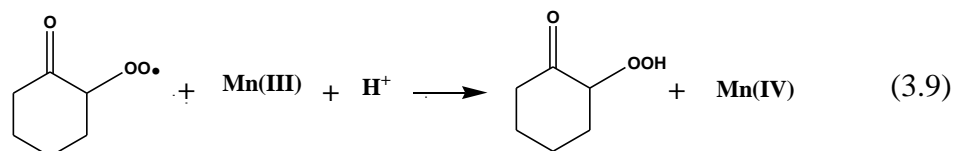
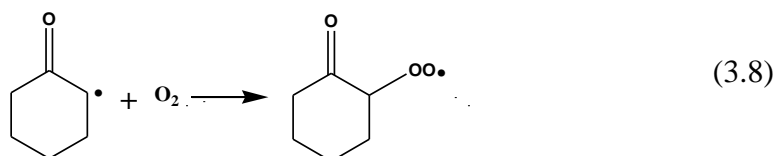
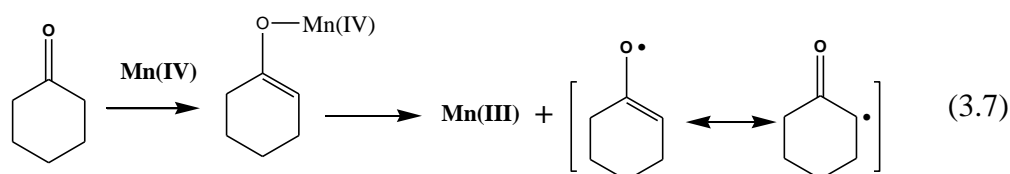
The second step involves the generation of α -keto radicals from cyclohexanone in the presence of bifunctional Mn (IV) ion (Lewis acid & redox). Mn(III), which forms Mn (IV) by oxidation with peroxyradicals via oxidation of the enol form of the ketone, is essential for the cleavage of the cyclohexanone, formed at first

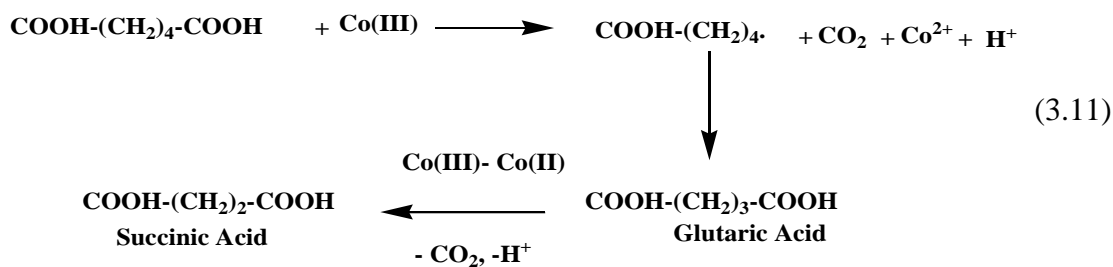
instance in the autoxidation [56]. This cleavage proceeds through the formation of the α -keto radicals via oxidation of the enol form of the ketone (eq 3.7). Once formed, the α -keto radicals are quickly trapped by oxygen, leading to the formation of adipic acid (eq. 3.8, 3.9 & 3.10) [57].

Step 1 (Oxidation of cyclohexane to ol and one)



Step 2: (Oxidation of cyclohexanone to Adipic acid)



Step – 3 (Decarboxylation of AA to GA and SA)**Scheme 3.8.** Plausible mechanism for the oxidation of cyclohexane.

The third step proceeds via the decarboxylation of product adipic acid into glutaric and succinic acids. The decarboxylation of AA proceeds via the generation of alkyl radical R^\bullet ($\text{COOH-(CH}_2\text{)}_4\bullet$) with CO_2 as by product in the presence of Co (III). The originated radical undergoes terminal oxidation to form glutaric acid which is the decarboxylated product of AA. The GA undergoes further decarboxylation to generate succinic acid [56] (eq 3.11).

The availability of Mn (IV) and Mn (III) in the catalyst play key role in electron transfer oxidation (eq 3.7), while the Co (III, II) is more effective in the redox decomposition of the hydroperoxides (eq 3.10).

3.10. Conclusions

In the present investigation, Co substituted octahedral molecular sieves (Co-K-OMS-2) were synthesized, characterized and used as selective oxidation catalysts for CyH conversion. Catalysts with different Co content were prepared through a simple reflux method. They were characterized by different physico-chemical techniques to understand their structural and textural characteristics. No perceptible changes were observed in the cryptomelane phase of KOMS-2 on substitution of cobalt. Similarly, no additional phases belonging to cobalt or cobalt oxide were observed through powder XRD investigations. The Co-OMS-2 catalysts show well resolved sharp XRD peaks. Compared to the KOMS-2, cobalt substituted Co-OMS-2 catalysts have relatively lower surface area and pore volume. Scanning electron microscopy confirmed formation of pure phases of cryptomelane with fibrous morphology for parent K-OMS-2, but the width and length of the rod

increased with Co loading. TEM images of both parent and doped samples were used for calculating lattice planes and d-spacings. Profiles of H₂-TPR confirm that Mn-O bond strength weakens on Co doping. Raman and IR spectroscopy demonstrated the absence of peaks that corresponds to the segregated cobalt oxide. Thermo gravimetric analysis of Co-OMS-2 materials indicate similarity in weight losses in different temperature regimes when compared to K-OMS-2 materials, but slightly lower thermal stabilities were seen as compared to the K-OMS-2. From XPS data it was found that, with increase in Co doping the Mn⁺⁴/Mn⁺³ ratio was found to decrease, surface oxygen content increased and Co⁺³ is present in higher content.

The Co-K-OMS-2 catalysts were investigated for selective oxidation of CyH to adipic acid. The catalysts showed their utility and versatility for the oxidation reaction. The catalysts were highly active for the above oxidation giving good conversion, AA selectivity at short reaction times. High conversion (95.6%) of CyH was obtained with 83.2% adipic acid selectivity. Temperature, time, catalyst content, initiator amount, Co content plays vital role and on AA yield depends on them. Further, the catalysts are stable under the reaction conditions and retain good activity and selectivity for at least upto five successive runs. The catalysts reported here are easy to prepare, the initiator and the process are a step forward in the direction for potential commercial exploitation of these materials for selective heterogeneously catalyzed oxidations.

3.11. References

- 1 D. D. Davis in *Ullman's Encyclopedia of Industrial Chemistry*, Vol. A1(Eds.: W. Gerhartz), Wiley-VCH, Weinheim, 1985, pp. 269 – 276.
- 2 A. E. Shilov, G. B. Shul'pin, *Activation and Catalytic Reactions of Saturated Hydrocarbons in the Presence of Metal Complexes*, Kluwer Academic Publishers, Dordrecht, 2000.
- 3 K. Hodnett, *Heterogeneous Catalytic Oxidation*, Wiley-VCH, Weinheim, 2000
- 4 (a) H. Frei, *Science* **313** (2006) 309. (b) G. Centi, M. Misono, *Catal. Today* **41** (1998) 287.
- 5 Adipic Acid: A Global Strategic Business Report, 2012, Global Industry Analysts, Inc., USA. Available electronically at http://www.strategyr.com/adipic_acid_market_report.asp
- 6 (a) K. Weissermel, H. Harpe, *Industrial Organic Chemistry*, 4th ed., WileyVCH, Weinheim, 2003. (b) A. Castellan, J. C. J. Bart, S. Cavallaro, *Catal. Today* **9** (1991) 237.
- 7 V. Hessel, I. Vural Gu'rsel, Q. Wang, T. Noe'l and J. Lang, *Chem. Eng. Technol.* **35** (2012) 1184.
- 8 U. Schuchardt, D. Cardos, *Appl. Catalysis A* **211** (2000) 1
- 9 R.A. Sheldon, J.K. Kochi, *Adv. Catalysis* **25** (1976) 272
- 10 (a) Trettenhahn, M. Nagl, *Angew. Chemie, Int. Ed.* **45** (2006) 2794. (b) A. Castellan, J.C.J. Bart, *Catal. Today* **9** (199) 255.
- 11 IPCC Fourth Assessment Report: Climate Change 2007, 7th chapter
- 12 M.H. Thiemens, W. C. Trogler, *Science* **251** (1991) 93
- 13 (a) F Cavani, J H Teles, *ChemSusChem* **2** (2009) 508. (b) IPCC, Good Practice Guidance and Uncertainty Management in National Greenhouse Gas Inventories.
- 14 (a) K. Sato, M. Aoki, R. Noyori, *Science* **281** (1998) 1646. (b) R. Noyori, M. Aoki *Chem. Commun.* (2003) 1977.
- 15 M. Roper, *Stud. Surf. Sci. Catal.* **64** (1991) 381
- 16 http://www.chemweek.com/sections/business_finance/europe_mideast/6951.html
- 17 R. Raja, G. Sankar, *Angew. Chem. Int. Ed.* **39** (2000) 2313

- 18 K.M. Draths, J.H. Frost, *J. Am. Chem. Soc.* **116** (1) (1994) 399.
- 19 (a) K. Tanaka, *CHEMTECH* (1974) 555. (b) K. Tanaka, *Hydrocarbon Process* **53** (1974) 114, (c) K. Tanaka, A. Shimizu, JP 20011253845 (assigned to Asahi Chem Co)
- 20 (a) A. Onopchenko, J.G.D. Schulz, *US Patent* 1977, 4,032,569, (assigned to Gulf R&D) (b) J.G.D. Schulz, A. Onopchenko, *US Patent* 1981, US 4,263,453 (assigned to Gulf R&D)
- 21 C.M. Park, N. Goroff, *US Patent* 1993, 5,221,800 (assigned to Amoco Corp)
- 22 U. Schuchardt, D. Cardoso, R. Sercheli, R. Pereira, R. S. da Cruz, M. C Guerreiro, D. Mandelli, E. V. Spinace, E. L. Pires, *Appl. Catal. A* **1** (2001) 211.
- 23 S Van de Vyver and Y Roma'n-Leshkov *Catal. Sci. Technol.* **3** (2013) 1465.
- 24 G. Sankar, R.Raja and J.M.Thomas *Catalysis letters* **55** (1998) 15.
- 25 M. Dugal, G.Sankar, R. Raja, J. M. Thomas, *Angew. Chem. Int. Ed* **112** (2000) 2399.
- 26 R. Raja, J. M. Thomas, M. Xu, K. D. M. Harris, M. Greenhill-Hooper, K. Quill, *Chem. Commun.* (2006) 448.
- 27 C.S. Yao, H.S. Weng, *Ind. Eng. Chem. Res.* **37** (1998) 2647.
- 28 D. Huybrechts, 1998, US patent 5,739,076.(assigned to Exxon chemical patents)
- 29 (a) Y.J. Xu, P. Landon, D. Enache, A.F. Carley, M.W. Roberts and G.J. Hutchings, *Catal. Lett.* **101** (2005) 175. (b) B.P.C. Hereijgers and B.M. Weckhuysen, *J. Catal.* **270** (2010) 16. (c) L.X. Xu, C.H. He, M.Q. Zhu, K.J. Wu and Y.L. Lai, *Catal. Lett.***118** (2007) 248. (d) G. Lu, R. Zhao, G. Qian, Y. Qi, X. Wang and J. Suo, *Catal. Lett.* **97** (2004) 115. (e) L. Li, C. Jin, X. Wang, W. Ji, Y. Pan, T. van der Knaap, R. van der Stoel and C. Au, *Catal. Lett.***129** (2009) 303. (f) G. Hutchings, S. Carrettin, P. Landon, J. Edwards, D. Enache, D. Knight, Y.-J. Xu and A. Carley, *Top. Catal.* **38** (2006) 223.
- 30 A. Alshammari, A. Koeckritz, V. N. Kalevaru, A. Bagabas and A. Martin, *ChemCatChem* **4** (2012) 1330.
- 31 (a) T. Iwahama, K. Syojyo, S. Sakaguchi, Y. Ishii, *Org. Process Res. Dev.* **2** (1998) 255. (b) Y. Ishii, T. Iwahama, S. Sakaguchi, K. Nakayama, Y. Nishiyama, *J. Org. Chem.* **61** (1996) 4520.
- 32 M. Saljoughian, H. Morimoto, P. G. Williams, C. Than, and S. J. Seligman *J. Org. Chem.* **61** (1996) 9625.

- 33 C. Calvert, R. Joesten, K. Ngala, J. Villegas, A. Morey, X. Shen, S. L. Suib, *Chem. Mater.* **20** (2008) 6382.
- 34 T. Gao, M. Glerup, F. Krumeich, R. Nesper, H. Fjellvåg, P. Norby, *J. Phys. Chem. C.* **112** (2008) 13134
- 35 E. K. Nyutu, C.-H. Chen, S. Sithambaram, V. M. B. Crisostomo, S. L. Suib, *J. Phys. Chem. C.* **112** (2008) 6786
- 36 (a) C. K. King'onde, N. Opembe, Chun-hu Chen, K. Ngala, Hui Huang, A. Iyer, H. F. Garcés and Steven L. Suib *Adv. Funct. Mater.* **21** (2011) 312. (b) R. M. Potter, G. R. Rossman, *Am. Mineral.* **64** (1979) 1199.
- 37 C. Tang, T. Leu, W.Y. Yu, Chen-Bin Wang and Shu-Hua Chien *Thermochimica Acta*, **473** (2003) 68.
- 38 J. Cai, J. Liu, W. S. Willis, S. L. Suib, *Chem. Mater.* **13** (2001) 2413.
- 40 R. Wang, Junhua Li, *Catal Lett.* **139** (2009) 500.
- 41 P. R. Ettireddy, N. Ettireddy, S. Mamedov, P. Boolchand, P.G. Smirniotis *Applied Catalysis B: Environmental* **76** (2007) 123.
- 42 R. Jothiramalingam, B. Viswanathan, T. Varadarajan, *J. Mol. Catal. A: Chem.* **252** (2006) 49.
- 43 A. Nohman, H. Ismail, G. Hussein, *J. Anal. Appl. Pyrol.* **34** (1995) 265.
- 44 Y.G. Yin, W.Q. Xu, Y.F. Shen, S.L. Suib, *Chem. Mater.* **6** (1994) 1803.
- 45 H. M. Galindo, Y. Carvajal, E. Njagi, Roger A. Ristau, and Steven L. Suib *Langmuir* **26** (16) (2010) 13677.
- 46 T. Zhang, X. Zhang, J. Ng, H. Yang, J. Liu and D. D.Sun *Chem. Commun.* **47** (2011) 1890.
- 47 (a) V.P. Santos, M.F.R. Pereira, J.J.M. Órfão, J.L. Figueired *Applied Catalysis B: Environmental* **99** (2010) 353. (b) W.Y. Hernández, M.A. C.S. Ivanova, Pierre Eloy, E. Odriozola *Applied Catalysis B: Environmental* **27** (2012) 124.
- 48 (a) M.I. Domínguez, F. Romero-Sarria, M.A. Centeno, J.A. Odriozola, *Applied Catalysis B* **87** (2009) 245, (b) R. Schaub, P. Thostrup, N. Lopez, E. Lagsgaard, I. Stensgaard, J.K. Nørskov, F. Besenbacher, *Physical Review Letters* **87** (2001) 2661041.
- 49 D. Gazzoli, M. Occhiuzzi, A. Cimino, D. Cordischi, G. Minelli, F. Pinzari, *J. Chem. Soc., Faraday Trans.* **92** (1996) 4567.
- 50 (a) T.J. Chuang, C.R. Brundle, D.W. Rice, *Surf. Sci.* **59** (1976) 413.

- 51 H.B.Tinker, *Journal of catalysis* **19** (1970) 237.
- 52 J. Kollar *US patent US 5321157 A*
- 53 K.M. Kerry, R. Hummeida, A. Abutaki and Shik Chi Tsang, *Cata. Lett.* **111** (2006) 51.
- 54 I. Belkhir, A. Germain, F. Fajula and Eric Fache, *J. Chem. Soc. Faraday Trans.* **94** (1998) 1761.
- 55 I. Hermans, P.A. Jacobs, J. Peeters, *Phys. Chem. Chem. Phys.* **9** (2007) 686.
- 56 A. Shimizu, K. Tanaka, H. Ogawa, Y. Matsuoka, M. Fujimori, Y. Nagamori, H. Hamachi, K. Rimura, *Bull. Chem. Soc. Jpn.* **76** (2003) 1993.
- 57 J. D. Druliner and E. Wasserman, *J. Am. Chem. Soc.* **110** (1988) 5270.

Chapter 4

**Metal free carbon nitride nano tubes as catalysts for
hydrocarbon oxidations**

4.1. Introduction

Hydrocarbons from petroleum and natural gas are most abundant and low cost feedstocks. Many petrochemical technologies have emerged to convert these hydrocarbon feedstocks to energy, fuels and chemicals. Functionalised hydrocarbons are of great interest as feedstocks in the chemical industry [1]. Alcohols are very important chemicals in the world market and are the most versatile feedstocks [2]. Therefore; transformation of these saturated alkanes to more valuable products, such as alcohols, ketones, acids and peroxides is important in the field of catalysis chemistry. There are plethora of methods available to convert these hydrocarbons through oxidation, hydrogenation, dehydrogenation, dehydroxylation into value added products [3].

Selective oxyfunctionalization of hydrocarbons, especially hydrocarbons like inert alkanes, to valuable oxygenates is an extremely important area of contemporary industrial chemistry [4]. Currently, selective oxidation processes are conducted either in gas phase or liquid phase using homogeneous/ heterogeneous catalysts. Since molecular oxygen is cheap and omnipresent, it is the most practical oxidant for selective oxidation processes [5]. But due to triplet ground state structure of oxygen, it is difficult to activate it, especially to react with stable C-H bonds of hydrocarbons [6]. With dioxygen as oxidant, attaining desired product selectively among all possible oxidize products is also important. In view of environmental and economical concerns, there is a strong move to develop sustainable catalytic oxidation process which use dioxygen as oxidant, while being corrosive solvent free. The catalyst should also be recyclable with good conversion and selectivity leading to high yield of desired products [7].

4.1.1. Elemental Sustainability

Elemental sustainability is a concept whereby the sustainability of each element in the periodic table is assured. In order to make the element sustainable, its use by this current generation should not impair or restrict future generations from utilising that element.

All elements within the earth’s crust are available in finite and limited quantities, though some, like aluminium, iron and silicon, are available in many orders of magnitude higher in abundance than compared to Pt, Ru, Rh and selenium [8]. Each element in the periodic table also has varying levels use and demand. This demand undergoes change as new technological advances come on-stream, while others become antique.

As shown in Fig. 1.1, large number of elements fall into the range where they will be exhausted within 50 years if the current rates of extraction are maintained. Because of the very low abundance, some of these elements are at high risk and these include the precious metals where only 200 tonnes is produced annually[9].

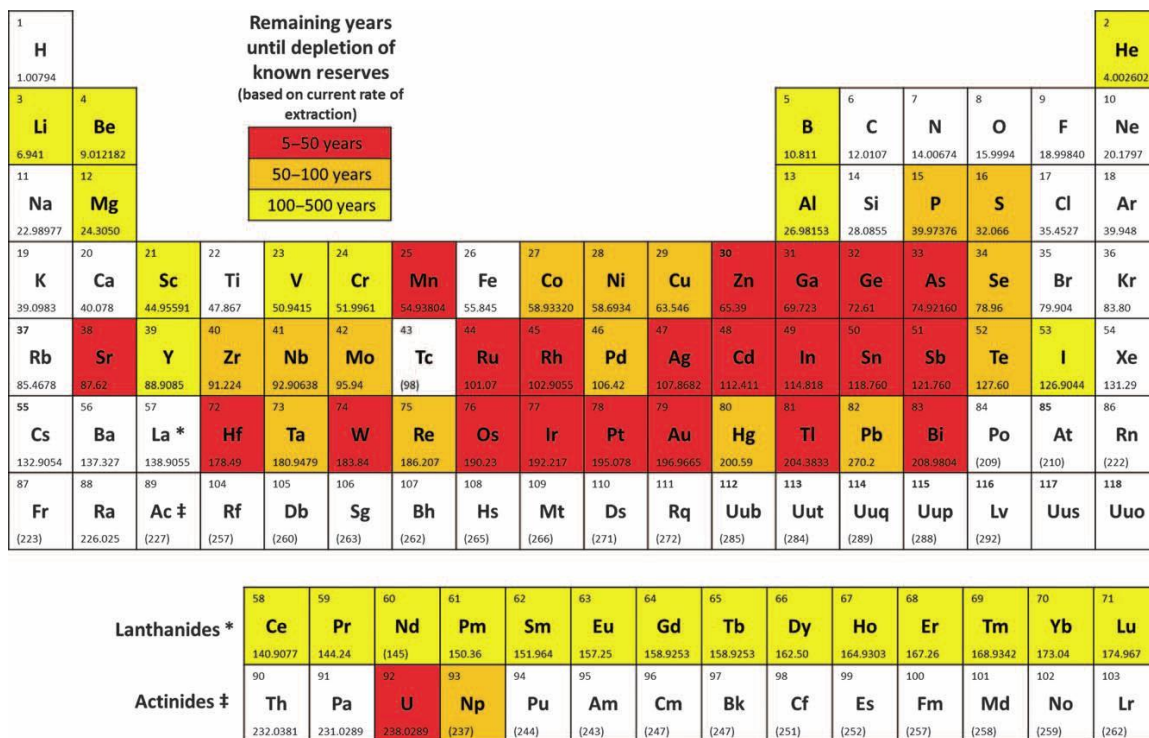


Fig. 4.1. Number of years remaining of rare and precious metal reserves if consumption continues at present rate [10]

All the major industrial reactions are catalyzed by metals. Because of the elemental unsustainability, these processes will be defunct in the future. So, designing a metal-free catalyst for the industrially significant process will be a great demand in the future.

Recently, researchers are focussing their attention towards nitrogen containing carbon materials as metal free heterogeneous catalysts for hydrocarbon oxidations. The efficient use of carbon nitride as catalyst for hydrocarbon oxidation was first studied by Wang *et al.* [11] tested oxidation of cyclohexane with B and N doped mesoporous carbon nitride polymers. The reactions were carried out at 150 °C using H₂O₂ as oxidant. The catalysts showed remarkably high selectivity towards the formation of cyclohexanone (99% selectivity). Catalysts were highly stable and could be recycled several times.

In 2011, Li *et al.* proposed metal free activation of molecular oxygen for oxidation of hydrocarbons. They have found out that graphene/carbon nitride composite material can successfully oxidize saturated hydrocarbons [12]. The authors have reported that the graphene and carbon nitride nanocomposites exhibit high-performance to activate molecular oxygen for selective oxidation of secondary C-H bonds of saturated alkanes with good conversion and high selectivity to the corresponding ketone.

Yu *et al.* conceptualized the use of metal-free catalysts for selective oxidation of hydrocarbons. Authors demonstrated that carbon materials can be used as a metal-free catalyst for the aerobic oxidation of hydrocarbons. Excellent performance was achieved by using multiwalled carbon nanotubes produced by chemical vapor deposition. However, high cost of the catalysts and requirement of solvent are the drawbacks of this process [13].

A very recent communication by Gao *et al.* showed the possibility of a variety of hydrocarbon oxidations with a metal free carbon catalyst. Nitrogen-doped sp²-hybridized carbon provided quantitative yield of oxidized products from aryl alkanes exhibiting superior performance for the oxidation [14]. The authors demonstrated that the incorporated nitrogen (mostly graphitic-type sites) in layered carbon catalysts is pivotal for the C-H bond activation reaction. The nitrogen dopant did not participate in the activation of reactant, but instead changed the electronic structure of the adjacent carbon atoms and promoted/stimulated their chemical reactivity.

Nitrogen doped carbons were reported to have diverse applications in catalysis, particularly as electrocatalysts [15], photocatalysts [16] and as heterogeneous catalysts [17]. From the literature, it was found that N- doping enhances the activity of the catalyst, hence N content is directly proportional to the rate of reaction. Among different types of nitrogen, graphitic nitrogen is found to be effective active centre for the oxidation reaction. Recently chen *et al.* reported that pyridinic nitrogen can also promote the oxygen reduction [18]. Compared to sp^3 , sp^2 carbon has been found to be more active in selective oxidations [19]. So, it is recommended to choose a nitrogen doped carbon that consists of sp^2 carbon and high nitrogen content with more of pyridinic and graphitic nitrogen.

Carbon nitride nano tubes (CNNT) exhibit semiconductor properties, high chemical stability and high sunlight harvesting capability. They were found to be excellent visible light photocatalysts [20]. Their nanostructures (tubes, wires, rods, sheets, spheres, etc.) were found to be more efficient than their bulk counterparts. When used in supercapacitors and as photocatalysts their performance has been found to be better due to their larger specific surface areas and more suitable bandgaps [21].

The selective oxidation of CyH is extremely important in the modern chemical industry, as its products, KA oil, is starting-material for the synthesis of adipic acid and caprolactam, intermediates of nylon-66 and nylon-6 polymers [22]. Single step oxidation of cyclohexane to adipic acid using molecular oxygen and heterogeneous catalyst is one of the most challenging reactions. Adipic acid is an important industrial chemical and typically ranks top 10 in terms of the volume used annually by the chemical industry. Present day processes for AA involve multiple steps; also use highly corrosive and environmentally harmful acids [23]. Thus, developing novel, clean and green routes for AA production is an important research theme

Through our present investigations, we demonstrate that CNNTs containing nitrogen atoms can act as a new class of metal-free catalyst that can afford excellent activity in the aerobic oxidation of cyclohexane. CNNT's were proven to promote the

cyclohexane conversion with high selectivity towards AA. These catalysts were also tested for other important hydrocarbon oxidations.

4.2. Experimental procedures

4.2.1 Materials

Melamine, ethylene glycol and nitric acid were used (Thomas Baker Pvt Ltd.) for the preparation of carbon nitride nano tubes. All the laboratory grade chemicals were used without any further purification

4.2.2 Experimental set up for selective oxidation

Selective oxidation reactions were performed in a 50 ml Parr autoclave. Reactant along with the catalyst was transferred in to the Parr reactor and purged with oxygen. After heating the reaction mixture to the desired temperature, reactor was pressurized with oxygen. Conversion of reactant and product selectivity's were monitored using GC and HPLC analysis respectively. Product mixture was analyzed using Agilent HPLC, equipped with RI detector and Rezex ROA-Organic Acid H⁺ column (300 mm × 7.8 mm) with 5mM H₂SO₄ as the mobile phase at a flow rate of 0.6 mL.min⁻¹.

4.3. Textural and morphological characterization of the catalysts

The above synthesized catalysts were characterized with the help of a variety of physic-chemical and spectroscopic techniques.

4.3.1 Powder XRD

The structural aspects of the catalysts were investigated by powder X-ray diffraction. Figure 4.3 (a) shows two peaks. The most intense peak at around 27.2° corresponds to interlayer distance $d=0.336$ nm, close to the characteristic peak of the (002) plane in the g-C₃N₄ structure ($d =0.336$ nm) which is reported for graphite-like carbon nitride ($d = 0.321$, or 0.328 nm) [24]. The Peak characteristic to in-plane structural packing motif of the nanotube appears at 17.8° ($d=0.49$ nm), close to the theoretical $d=0.47$ nm [25]. Experimental distances of the s-triazine based structure of carbon nitride

anotube is different from that of tri-s-triazine-based $g\text{-C}_3\text{N}_4$ ($2\theta=13^\circ$, $d=0.681$ nm) [26]. So it is evident from XRD that the present nanotube acquires a s-triazine based structure rather than the reported commonly known tri-s-triazine unit (Fig. 4.2 b) [27]. Hence, Fig. 4.3 (b) depicts the clear transformation of melamine to carbon nitride nano tubes.

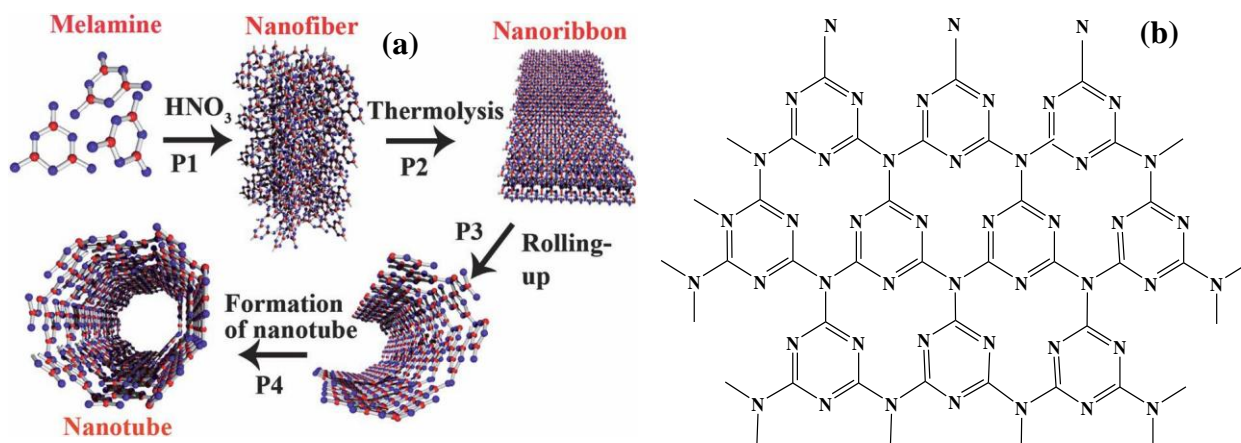


Fig 4.2. (a) Schematic illustration of the formation of the carbon nitride nanotubes. (b) Molecular structure of carbon nitride nano tubes.

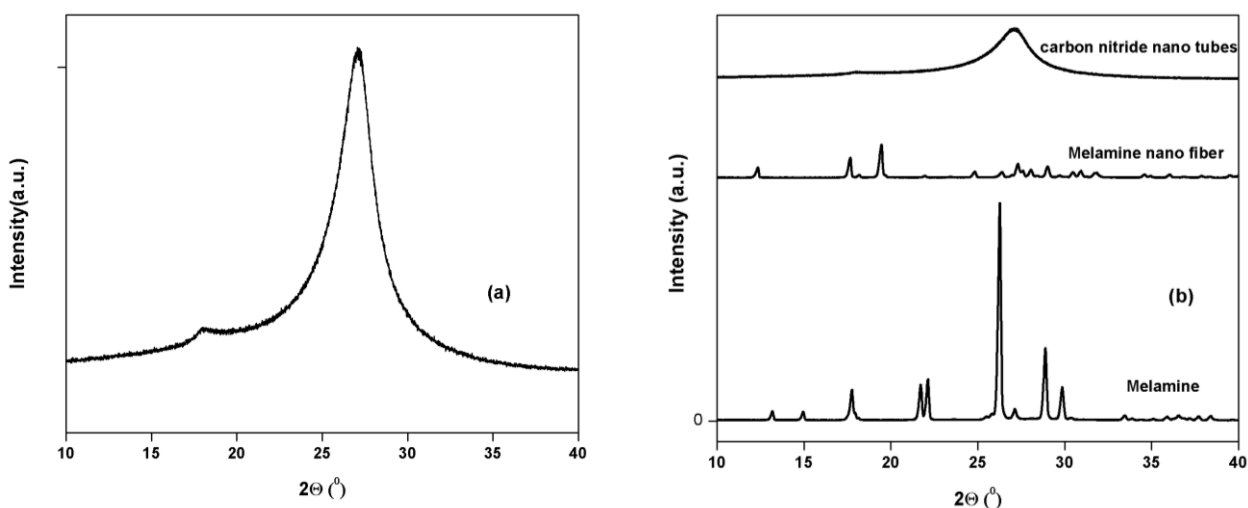


Fig. 4.3. (a) XRD of carbon nitride nano tubes, (b) At different stages of preparation

Upon addition of nitric acid to melamine, the amino group of the melamine gets protonated and it is conceived that the obtained white precipitate is formed by nitrate ions and melamine with a protonated amino group. The self-assembly of NH_3^+ and NO_3^- into

fibrous structures is believed to be a solvent mediated process by the combined effect of two factors. One is that the NH_2 group of the melamine gets easily protonated with the addition of HNO_3 because of its high basicity. This protonation decreases the solubility of melamine in ethylene glycol. The other is increase in polarity of the ethylene glycol solution because of the high polarity of nitrate ion and water. Hence, the decrease in solubility of the melamine leads to its precipitation. The existence of both H^+ and NO_3^- are essential for the self assembly fibrous material.

The nano tubular transformation from fibrous structures was thus conjectured to involve two steps. In the first step, on thermal treatment, protonated amine gets polymerized along the fibrous longitude to form the s-triazine ring based molecular ribbons. These ribbons get stabilized and stacked on each other because of the Π - Π electron interaction. The second step is that the formed stacking layers after reaching a certain thickness, tends to curl into nanotubes. Minimization of the surface free energy is the sole reason for this curling process. Schematic representation of CNNT is shown in Fig. 4.2 (a).

4.3.2 IR spectra of as synthesized materials

The IR spectra of melamine, nanofibers and nano tubes are illustrated in Fig. 4.4. The strong absorption peaks in the $3330\text{-}3550\text{ cm}^{-1}$ range are attributed to the stretching vibrations of NH_2 and NH groups. The above modes were absent in the nanotubes, suggesting that deamination occurs during calcination of nanofibers, which destroys most of the N-H bonds. The similarity of all the spectra is clearly evidenced by the sharp semicircle ring stretch at around 800 cm^{-1} , which indicates that all the samples are built up from heptazine or triazine units. A peak at 1550 cm^{-1} show that nanofibers were formed by the protonation of amine which eventually forms NH_3^+ [28]. Thus, it may be believed that the fibrous crystal is a class of salt composed of protonated melamine and nitric ions probably maintained hydrogen bonding, electrostatic attraction and Π - Π stacking interactions. Nitrate ions in the white precipitate may also decompose into nitrous oxide and oxygen because of its low stability over 443 K [29].

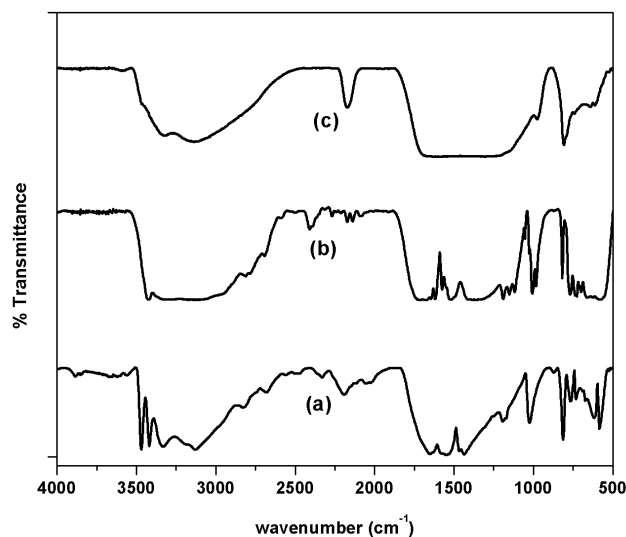


Fig. 4.4. FT-IR of (a) Melamine, (b) Melamine nanofibers, (c) CNNT

4.3.3. UV-visible spectra of carbon nitride nanotubes

UV-Vis provides information about the ability of samples to absorb light in the visible and near-UV range of the electromagnetic spectrum. Hence, CNNT catalyst was investigated using UV-vis spectroscopy. Figure 4.5 illustrates the UV-vis spectra of carbon nitride. It shows the absorption edge at 440 nm centered around 300 nm, originating from π - π^* electronic transition in the aromatic 1, 3, 5-triazine compound [30]. Band gap of the material was found to be 2.8 eV.

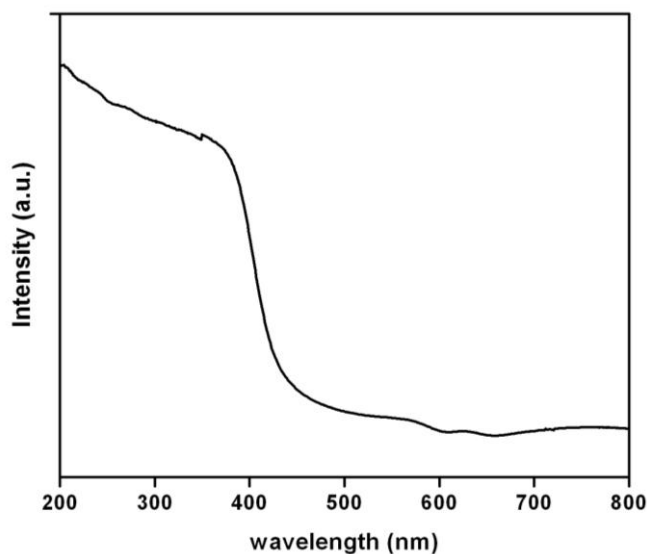


Fig. 4.5. UV visible spectra of CNNT.

4.3.4. Scanning electron microscopy

Scanning electron microscopy was used to investigate the morphology of CNNT.

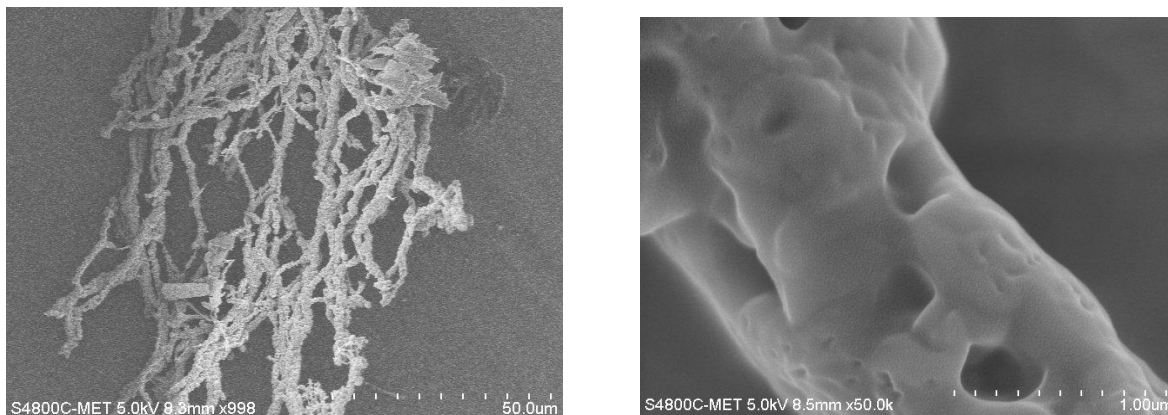


Fig. 4.6. SEM images of CNNT

The SEM micrographs (Fig. 4.6) show nanotube like morphology of carbon nitride. The FE-SEM images reveal high yield of elegant, flexible and ultra-long nanotubes. The nanotube is of a general average outer diameter of 1.5μ with lengths up to several millimetres. The resulting aspect ratio of the length to diameter is higher than 10 000. As reported, very little particle- and sheet-like morphology was observed [31].

4.3.5. Transmission electron microscopy

To further confirm tubular morphology, investigations were carried out using TEM.

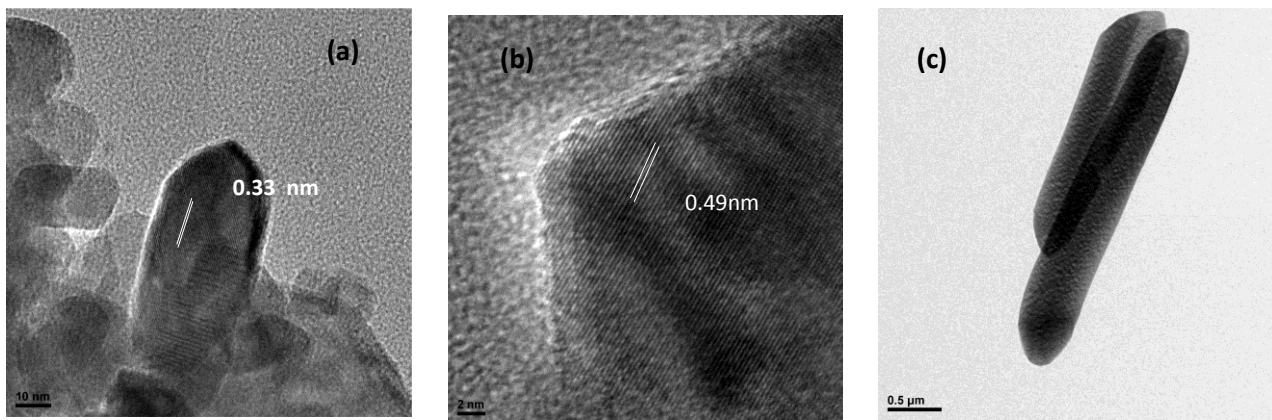


Fig. 4.7. (a,b) TEM images of CNNT, (c) TEM image of melamine nano fiber.

The TEM images given in Fig.4.7 show nanorods with clear lattice fringes. The magnified TEM images reveal that carbon nitride nanotube wall consists of several layers analogous to multiwall carbon nanotubes. The d-spacings (0.36 nm & 0.49 nm) obtained from TEM images are in agreement with the XRD results. Figure 4.7c shows fibre like shape of the nanofibres.

4.3.6. X-ray Photo electron spectroscopy

The elemental composition and nature of the chemical states of the elements present studied by X-ray photoelectron spectroscopy. The XPS of C 1s spectrum of CNNT is given in Fig. 4.8(b). The peak at 287.4 eV corresponds to sp^2 carbon bonded with nitrogen and the peak around 284.5 eV is assigned to surface adventitious carbon [32]. Similarly N 1s spectrum (Fig. 4.8(a)) has three peaks at around 398.5, 399.95 and 401.0 eV which correspond to pyridinic, pyrrolic and graphitic respectively. The first two peaks may be attributed to sp^3 C–N bonds while the third one is due to a N– sp^2 C bond, which proves that there is bonding between the nitrogen and carbon atoms [33].

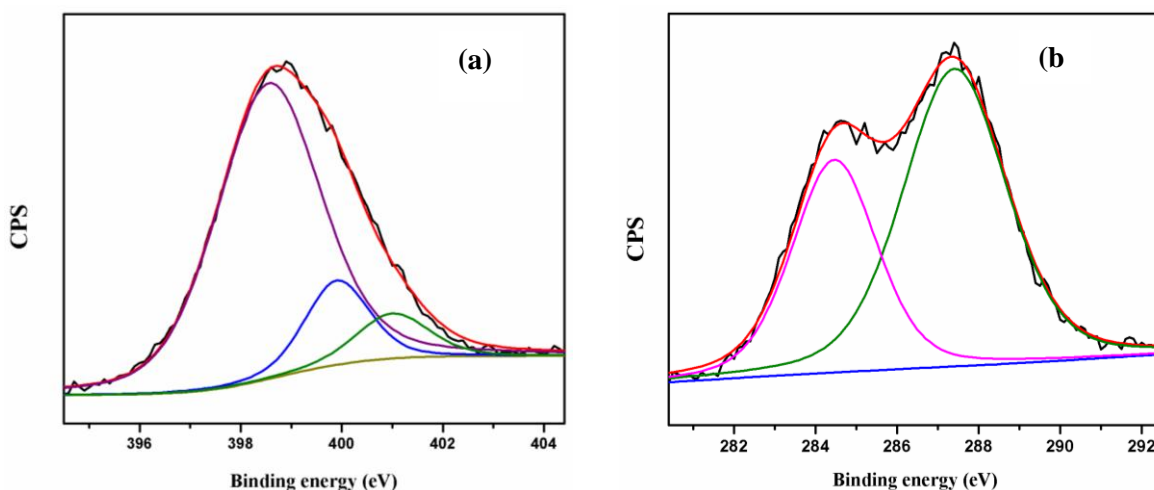


Fig. 4.8. X-ray phototelectron spectroscopy of (a) N 1s, (b) C1s.

4.3.7. Cyclic voltammetry

The electro catalytic activity of the synthesized CNNT's was examined using cyclic voltammetry (CV) and rotating disc electrode (RDE) voltammetry. The CV

profiles of the materials in an oxygen-saturated 0.1M solution of KOH and 0.5M solution of HClO₄, cycled between 1.2 and -0.8 V versus NHE at different voltammograms are shown in Fig. 4.9 a & b respectively. In the basic medium, oxygen was getting reduced in a potential range between -0.3 to -0.5 V and subsequently getting oxidized in the potential range of -0.2 and 0.1. The RDE voltammograms of the catalysts in 0.1M KOH throws better information on the ORR activity of this system (Fig 4.9. c). The study

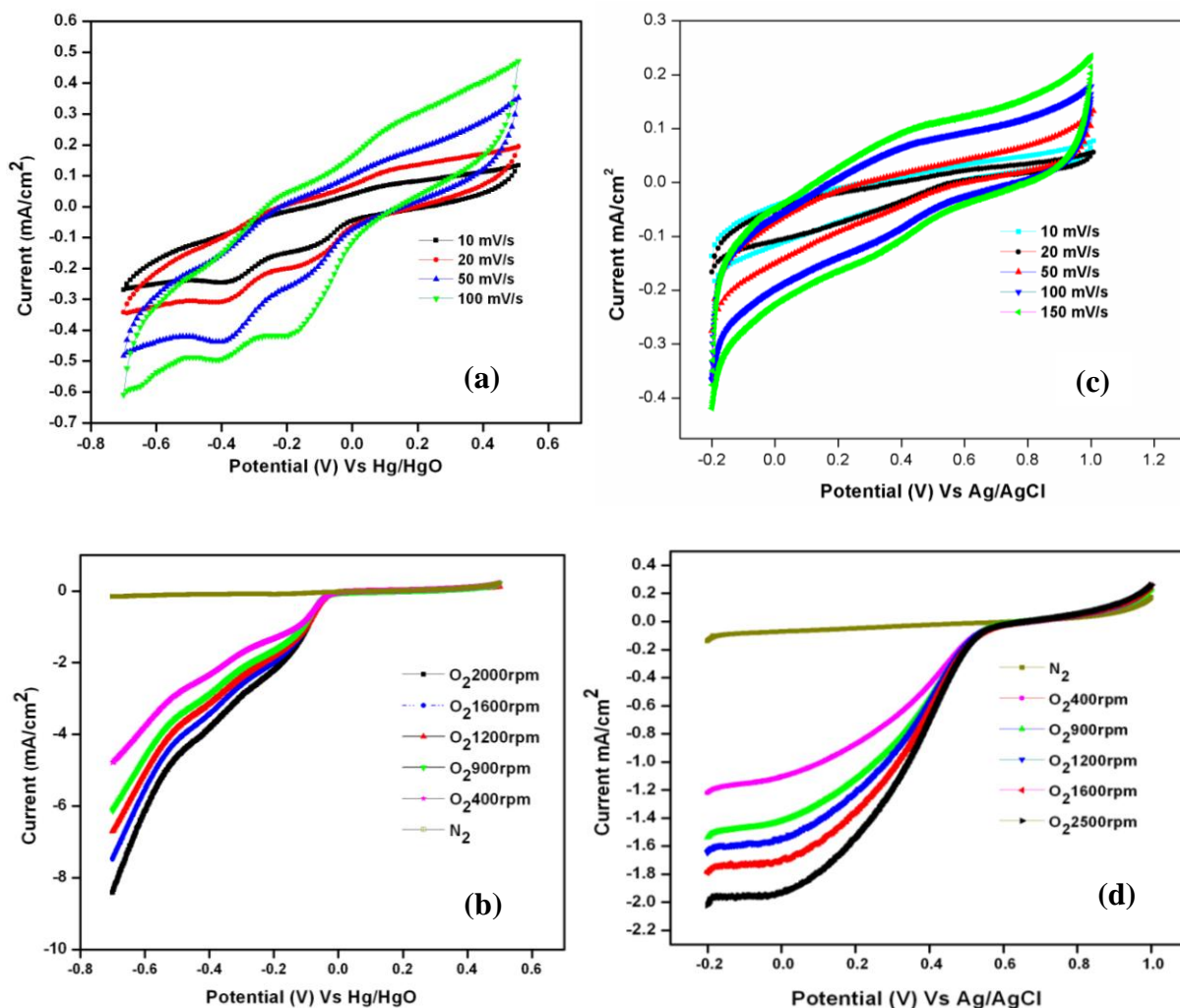


Fig. 4.9. Cyclic Voltammetry of CNNT catalysts in (a) 0.1M KOH, (c) 0.5M HClO₄. Linear sweep cyclic voltammetry in (b) 0.1M KOH, (d) 0.5M HClO₄.

confirms significant ORR activity of carbon nitride nanotubes, as shown from the linear sweep voltammograms (LSVs) at different RPM. The onset potential of the material is around -0.01V. In the acidic medium, oxygen was getting reduced at potentials 0.5 - 0.1

V and subsequently getting oxidized in the potential range of 0.0 - 0.4 V. The RDE voltammograms of the catalysts in 0.5M HClO₄ confirms significant ORR activity of carbon nitride nano tubes, as shown from the linear sweep voltammograms (LSVs) at different RPM (Fig. 4.9 d). The onset potential of the material was found to be around 0.6V. The above described CV measurements show that the material has redox sites that can reduce O₂ even in the absence of any metal.

4.4 Selective oxidation of cyclohexane to adipic acid in single step

Selective oxidation of cyclohexane (CyH) to adipic acid was carried out using CNNT catalysts. Optimization of various experimental parameters was carried out to get high adipic acid yields.

4.4.1 Effect of temperature

The effect of temperature on selective oxidation of CyH is shown in Fig. 4.10. It may be seen that CyH conversion as well as AA selectivity increased initially with temperature, but the AA yield drops after reaching a maximum. On the other hand, CyH conversion increased continuously with temperature with about 24% at 398 K to reach 86 mol% at 413 K. Cyclohexanol and cyclohexanone were also seen in the product mixture,

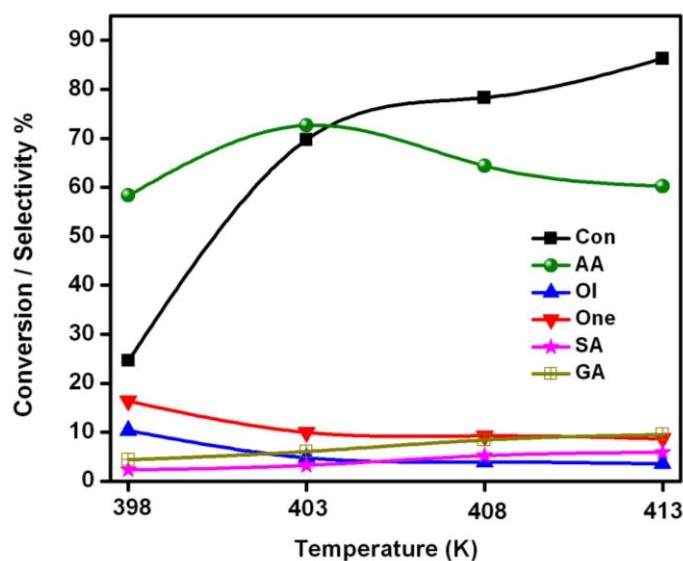


Fig. 4.10. Effect of temperature on adipic acid yield during selective CyH oxidation

Conditions: Cyclohexane-12.6g, Acetonitrile-6.1g, catalyst -50mg, 4h, 20 bar O₂.

particularly at low reaction temperatures, implying that the K-A oil is formed as primary product, which is further oxidized to AA in a subsequent step.

When the temperature was raised, the rate of consecutive oxidation increased, accelerating the conversion of cyclohexanol to cyclohexanone and then to AA. Hence, the AA selectivity increased with increasing temperature up to 403 K. However, further rise in temperature led to the formation of undesired products, mainly the glutaric and succinic acids. These results guide us to a optimum temperature of 403 K, where we can get reasonably high conversion along with high selectivity to AA. Hence, this temperature was chosen for further investigations. Similar observations that increase in selectivity of AA with increase in temperature were also reported by Alshammari *et al.* [34]

4.4.2. Effect of reaction time

Effect of reaction time on conversion of cyclohexane and AA selectivity is shown in Fig 4.11. The AA selectivity increased with time, reaching a maximum after 4 hours. The cyclohexanol (OI) and cyclohexanone (One) selectivity's decreased with increasing time. Between 2-4 h, the selectivity of AA increased at the expense of K-A oil.

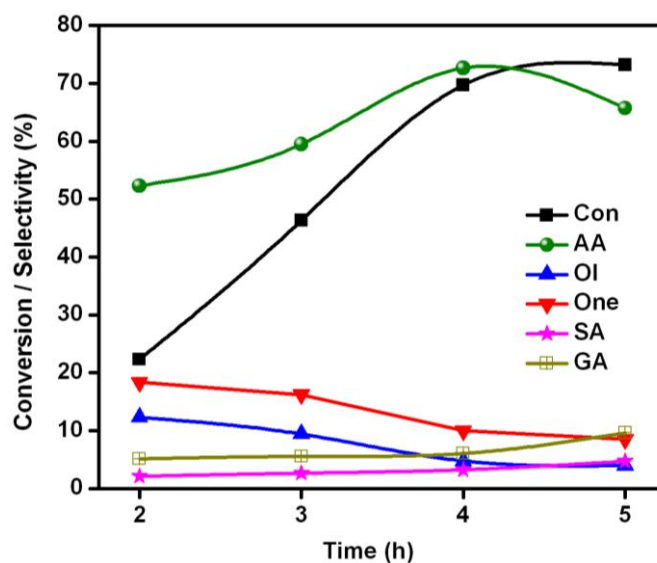


Fig. 4.11. Effect of reaction time on adipic acid yield during selective CyH oxidation
Conditions: Cyclohexane-12.6g, Acetonitrile-6.1g, 403 K, Catalyst-50mg, 20 bar O₂.

After 4th hour, the AA selectivity decreased due to its degradation to glutaric acid (GA) and succinic acid (SA). This data shows that the KA concentration was high in the initial stages (induction period) of the reaction, which subsequently converts to AA with increasing TOS. Hao *et al.* also reported similar observation that initially OL and ONE are the major products which eventually converts to AA with time [13].

4.4.3. Effect of catalyst content

Influence of catalyst content on the progress of reaction and product concentration in the reaction mixture is shown in Fig. 4.12. The same substrate quantity was maintained for all runs. With increasing catalyst content, conversion of cyclohexane has increased, which reached a maximum at around 50mg for 12.6g of substrate (CyH). Conversion gets further increase with increasing the catalyst content from 50 -100mg. So clearly catalyst has the promotional effect in the cyclohexane conversion. At lower catalysts content, selectivity of least oxidized products like ‘Ol’ and ‘One’ are prominent, but at higher catalyst amounts, selectivity of over oxidized products increased. Alshammari *et al.* reported similar effects with catalyst content [34]. So it is important to find the best catalyst content which can give maximum yield of AA. On optimization, we have found that 50mg is best for good yield of AA.

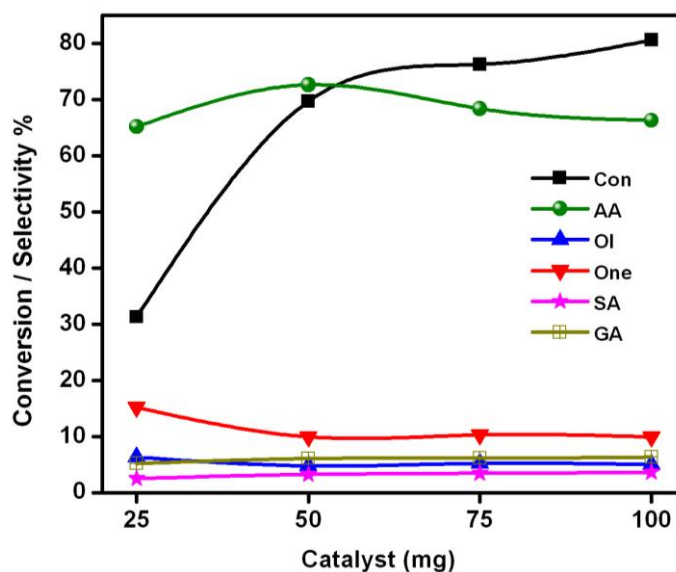


Fig. 4.12. Effect of catalyst content on AA yield during selective CyH oxidation

Conditions: Cyclohexane-12.6g, Acetonitrile-6.1g, 403 K, 4h, 20 bar O₂.

4.4.4 Effect of oxygen pressure

Figure 4.13 demonstrates the influence of oxygen pressure on reaction and product pattern. It is evident that with increase in oxygen pressure from 5- 20bar, conversion of cyclohexane has increased significantly from 10 to 70 mol%. At lower O₂ partial pressure, mostly K-A oil has formed. Further increase in O₂ pressure led to the higher AA formation. But, over-oxidation also led to the formation of byproduct dicarboxylic acids (GA and SA). The results clearly show that oxygen pressure plays vital role in AA yield. Yuan et. al observed similar observation that with increase in O₂ pressure leads to the enhanced formation of dicarboxylic acids [35].

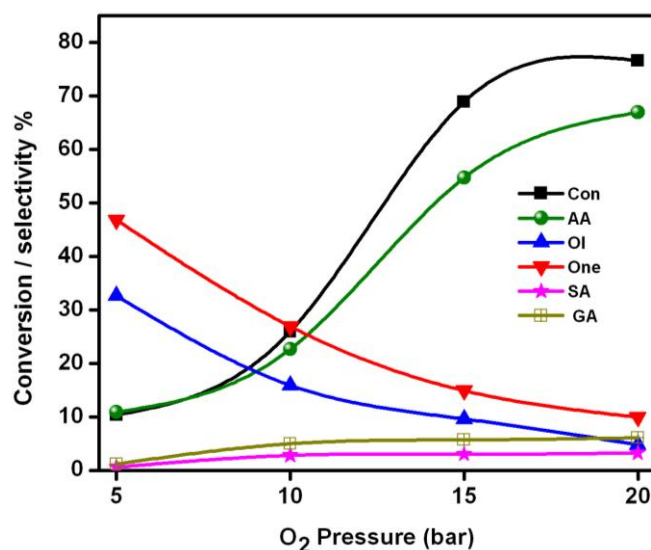


Fig. 4.13. Effect of O₂ pressure on AA yield

Conditions: Cyclohexane-12.6g, Acetonitrile-6.1g, Catalyst-50mg, 403 K, 4h.

4.4.5. Recyclability of the catalyst

To check the reusability and stability of the catalyst, recycling tests were carried out, after washing the catalyst with acetonitrile prior to its re-use. The catalyst was used for five such cycles. There was no significant change either in catalytic activity or AA selectivity even after 5th recycle as can be seen from Fig. 4.14.

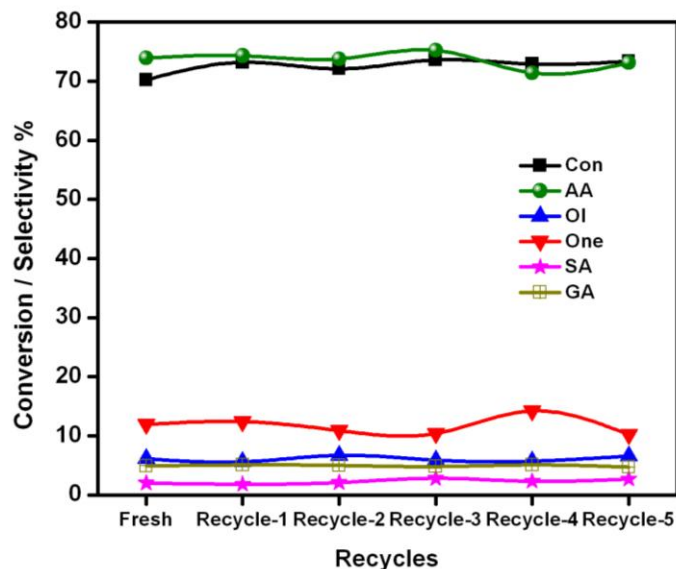


Fig. 4.14. Recyclability study of the catalyst during CyH oxidation

Conditions: Cyclohexane, Acetonitrile, catalyst = 50mg, 403 K, 4h, 20 bar O₂.

4.5.0 Solvent free oxidation of cyclohexane

For a selective oxidation process to be called ‘green’, in addition to use of environmental friendly oxygen source such as O₂, no solvent should be used for carrying out the reaction. When no solvent is used, it leads to saving of energy, as there is no need to separate the solvent from products and un-reacted substrates. Hence, we have conducted selective oxidation of cyclohexane in solvent free conditions. Effect of various parameters has been investigated; results of these experiments are illustrated below.

4.5.1. Effect of temperature

Effect of temperature on the yield of AA in solvent free conditions is shown in Fig. 4.15. It can be clearly seen, CyH conversion increased with temperature up to 71 mol% at 413 K, as was the case when solvent was used for the reaction. The AA selectivity also increased, but it reached a maximum at 403 K and thereafter it decreased with increasing temperature. Cyclohexanol and cyclohexanone were present in significant quantities at lower reaction temperature, as they are the primary products of the reaction. Since, at higher temperatures, subsequent oxidation is favoured, it leads to the formation of AA

from cyclohexanol and cyclohexanone. As a result, the AA selectivity increased with increasing temperature up to 403 K.

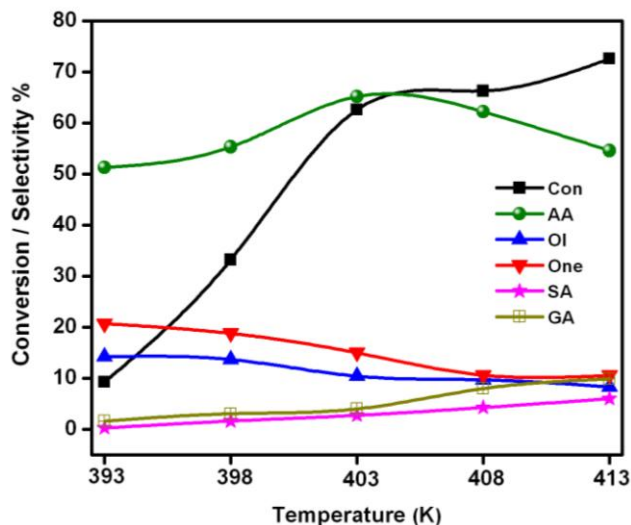


Fig. 4.15. Effect of reaction temperature on CyH conversion and AA yield
Conditions: Cyclohexane-15.58g, 4 h, Catalyst-50mg, 20 bar O₂.

Further increase in temperature to 408-413 K led to the formation of undesirable GA and SA by-products. These results show that even in the absence of solvent, reaction temperature of 403 K seems to be optimum for achieving high CyH conversion and AA selectivity. However, both these values are on lower side as compared to the conversion and yields achieved in the presence of solvent.

4.5.2 Effect of time

The effect of reaction time on CyH conversion and AA yield in solvent free conditions is shown in Fig. 4.16. With TOS, conversion of cyclohexane has increased monotonously, but the AA selectivity increased to a maximum after 4th hour and dropped further on stream. The selectivity's of 'One' and 'Ol' also decreased with increasing time on stream. Between 1-4 h, the AA selectivity increased at the expense of KA oil. These results indicate that the AA formation is favoured with increasing reaction time. But, after 4th hour, the AA selectivity decreased due to its degradation to by products such as GA and SA.

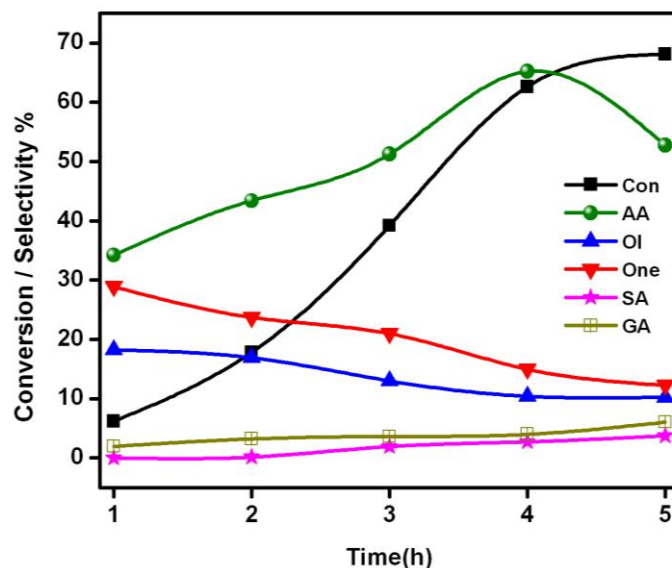


Fig. 4.16. Effect of reaction time on CyH conversion and AA yield
 Conditions: Cyclohexane=15.58g, 403 K, Catalyst=50mg, 20 bar O₂.

4.6. Comparison of various catalysts in the selective oxidation of cyclohexane

Table 4.1: Performance of various catalysts in selective oxidation of cyclohexane

S.No	Catalyst	Cyclohexane : Acetonitrile	Conv. mol%	Selectivity (mole %)				
				ol	one	Glutaric acid	Succinic acid	Adipic acid
1	Melamine carbon nano fibers(after HNO ₃ treatment)	1 : 1 (12.6 : 6.1 g)	10.2	7.3	21.0	8.78	3.2	61.2
2	Carbon nitride nano tubes ^{\$}	1: 1 (12.6 : 8.7 g)	89.5	10.2	18.2	13.4	5.9	45.3
3	Carbon nitride nano tubes [@]	1 : 1 (12.6: 6.1g)	69.7	4.7	9.9	6.0	3.5	72.4
4	Carbon nitride nano tubes [*]	1 : 1 (12.6: 6.1g)	0.6	--	--	--	--	--
5	Carbon nitride nano tubes [#]	15.6g	62.6	10.4	14.9	3.9	2.7	65.2

Conditions: 403 K, 4h, 20bar O₂, 50 mg catalyst
 \$- Acetone as solvent, @ -Acetonitrile as solvent
 *- butylated hydroxytoluene (10mol %)
 #- in the absence of solvent

Under blank reaction conditions, without any catalyst the conversion of cyclohexane was negligible. The CyH conversion was high, as reaction rate has increased with acetone as solvent, but AA selectivity was low. Melamine carbon nano fibers, obtained on HNO_3 treatment of melamine, but before the calcinations at $350\text{ }^\circ\text{C}$, did not offer good result. Use of radical scavenger BHT terminates the oxidation process by capturing the superoxide radical which shows that the reaction is initiated by superoxide radical.

4.7. Proposed reaction mechanism

After the completion of the reaction, IR spectra were recorded for the liquid reaction product mixture. Peak at 1750 cm^{-1} corresponds to $\text{C}=\text{O}$ stretching frequency of cyclohexanone. Peaks at 1452 , 1413 and 1361 cm^{-1} corresponds to the CH_2 bending modes of cyclohexyl hydroperoxides (CHHP). The presence of CHHP suggests that the reaction is going through the formation of CHHP intermediate.

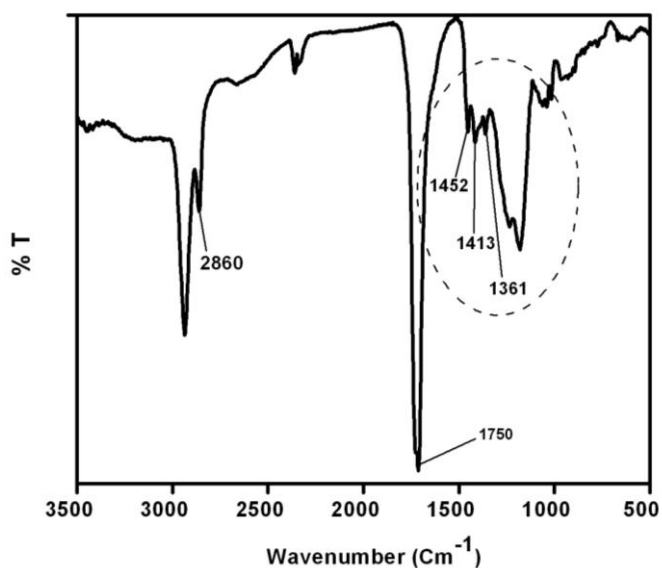
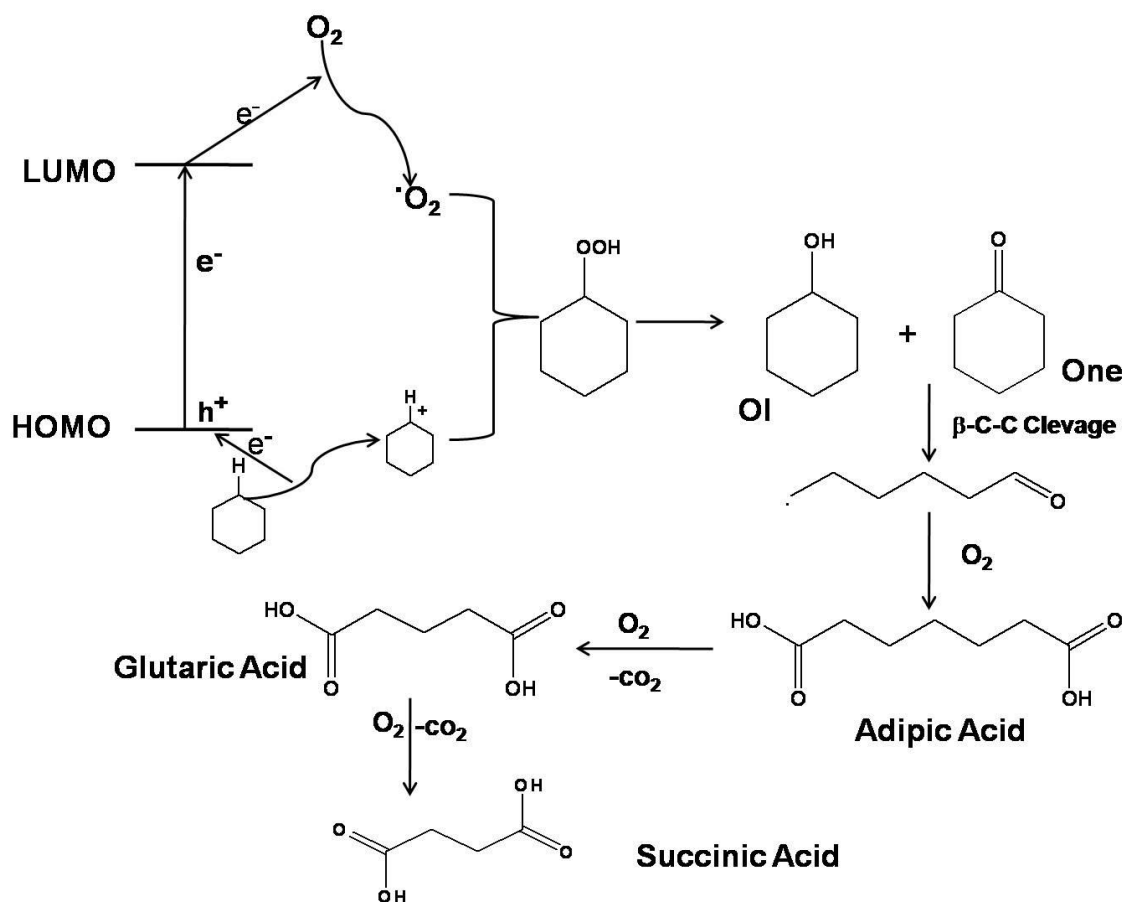


Fig. 4.17. IR spectrum of cyclohexane reaction mixture after completion of reaction.

Since the catalyst is a semiconductor (band gap of 2.8 eV), with thermal energy the electrons from conduction band (LUMO) gets excited to reach valence band (HOMO). The excited electrons reduce the molecular oxygen to form $\cdot\text{O}_2^-$, which stays surface

bound to the catalyst to compensate the positive charge of the hole. At the same time, the substrates are oxidized by the HOMO (positive hole) of catalyst and then react with the surface-bound $\cdot\text{O}_2^-$, to generate cyclohexyl hydroperoxide. The CHHP formed is subsequently dissociated to cyclohexanol and cyclohexanone. On β -C-C scission to form ω -formyl radicals, which in turn undergoes terminal oxidation to yield adipic acid. The formed AA can undergo decarboxylation to form lower dicarboxylic acids like glutaric acid and succinic acids.



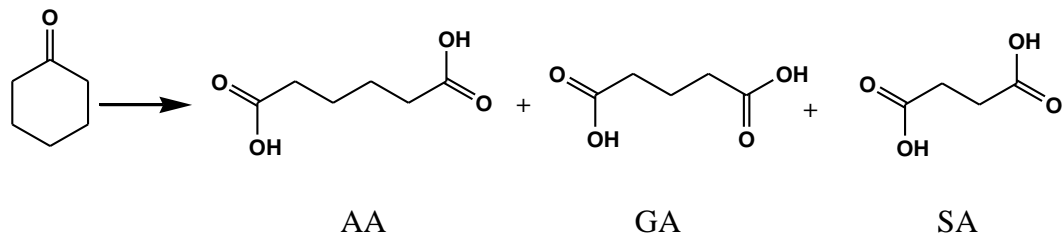
Scheme 4.1. Plausible mechanism for cyclohexane oxidation with CNNT.

4.8. Carbon nitride nanotube as catalyst for other selective oxidation processes

Carbon nitride nanotube catalysts were also investigated for selective oxidation of other hydrocarbons.

4.8.1. Oxidation of cyclohexanone to Adipic Acid

Since the cyclohexane to AA reaction goes through cyclohexanone as intermediate, we have tested CNNT catalyst for selective oxidation of cyclohexanone to adipic acid.



Scheme 4.2 Selective oxidation of cyclohexanone.

4.8.1.1 Effect of temperature

The effect of the reaction temperature on catalytic activity in the selective oxidation of cyclohexanone to AA is shown in Fig. 4.18. Increasing the reaction temperature has promoted the conversion of cyclohexanone. Selectivity of AA reached maximum at 393 K, but decreased beyond this temperature. The decrease in AA selectivity is attributed to the decarboxylation at higher reaction temperatures leading to the formation of C₅, C₄ dicarboxylic acids. Edwin *et al.* reported similar results on variation of temperature [36]

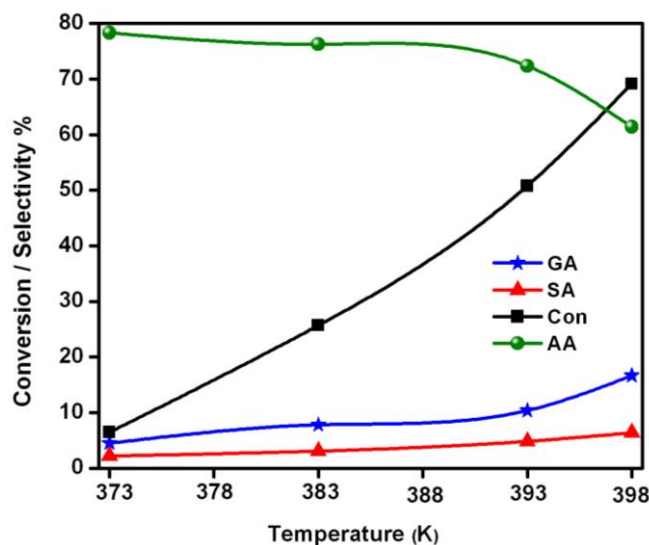


Fig. 4.18. Effect of temperature on cyclohexanone oxidation

Conditions: Cyclohexanone- 9 g, Acetonitrile-7 g, H₂O- 2 g, 4h, catalyst 50mg, 20bar O₂.

4.8.1.2 Effect of reaction time

Effect of reaction time on catalytic activity of CNNT in the selective oxidation of cyclohexanone is given in Fig. 4.19. Conversion has increased with increasing time on stream, while AA yield was found to decrease with time as a result of increased decarboxylation of AA. So in order to achieve higher amount of AA, choosing optimum reaction time is important for this reaction. Cavani et.al also observed similar trend in cyclohexanone oxidation with heteropolyacids as catalysts [37].

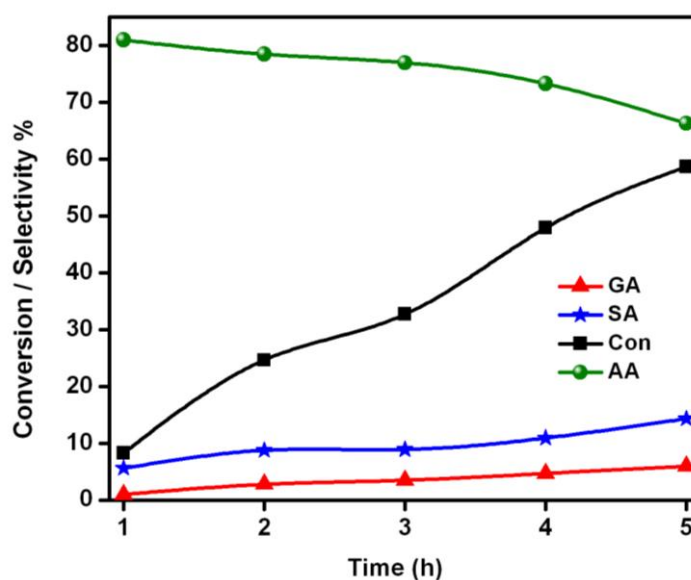


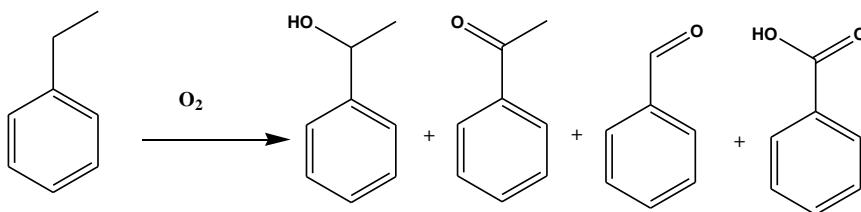
Fig. 4.19. Effect of time on selective oxidation of cyclohexanone

Conditions: 9g cyclohexanone, Acetonitrile 7g, 393 K, CNNT 50mg, 20bar O₂.

4.8.2. Selective oxidation ethyl benzene to acetophenone

Selective oxidation of ethyl benzene (EB) to value added products such as acetophenone (AcPO) has received increasing attention because of its commercial applications as an intermediate for the manufacture of perfumes, pharmaceuticals, resins, alcohols, esters and aldehydes. Production of this ketone is traditionally carried out through Friedel–Crafts acylation of benzene by an acyl halide or acid anhydride in the presence of stoichiometric quantities of homogeneous Lewis acids (e.g., AlCl₃, BF₃, FeCl₃, ZnCl₂, SnCl₄, TiCl₄) or strong protic acids (e.g., H₂SO₄, HF). Unfortunately, these

reagents are not only expensive but also produce large quantities of noxious and corrosive waste [38]. To make this process green, we have investigated the utility of carbon nitride nanotube catalysts for this reaction.



Scheme 4.3. Ethyl benzene oxidation to various possible products.

4.8.2.1. Effect of reaction temperature

Effect of reaction temperature on the catalytic activity of carbon nitride nanotube in the selective oxidation of EB is shown in Fig. 4.20. As expected, when the reaction temperature is increased, conversion of EB also has increased. At 393 K, EB conversion was 34.1 % with 49.0 % selectivity for acetophenone (AcPO) and 27.4 % for 1-phenylethyl alcohol (PEA). When the reaction temperature was increased in the range of 398-403 K, EB conversion and selectivity to AcPO also increased. On the other hand,

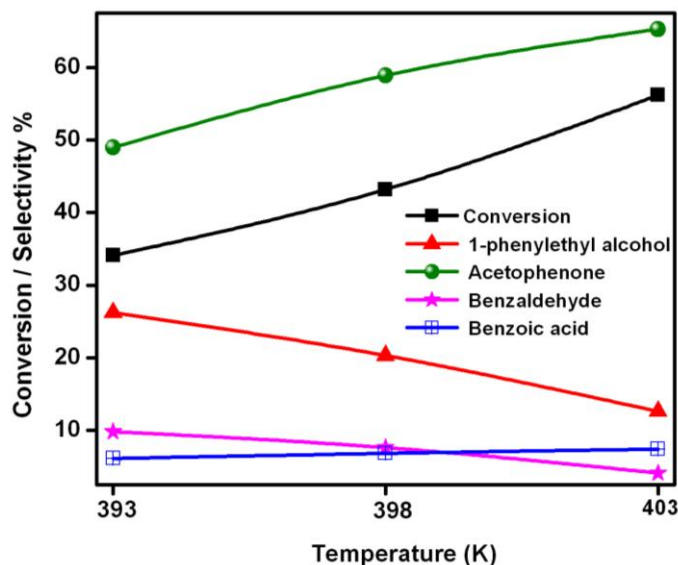


Fig. 4.20. Effect of temperature on EB conversion acetophenone selectivity.

Conditions: 6.0g EB, 12.7mL Acetonitrile, 100mg CNNT, 8h, 20bar O₂.

the PEA and benzaldehyde selectivity decreased with increasing temperature. However, benzoic acid (BzA) formation was favoured, as its concentration increased at higher temperatures. It appears that β -C-C cleavage of the 1-phenylethyl oxy radical is favoured to form benzaldehyde (BA) [39]. These results show that the reaction temperature is a key factor for the oxidation of EB to AcPO. Jin *et al.* also observed similar trend in the distribution of products [40]

4.9.2.2. Effect of reaction time

Figure 4.21 shows the effect of reaction time on the catalytic activity of CNNT in the selective oxidation of EB. Conversion of EB and AcPO selectivity increased sharply with reaction time upto 6 h, after which conversion reached a plateau. But the AcPO selectivity drops after this, which indicates that the side reactions gradually increased as the reaction progressed, thus leading to a lower selectivity for AcPO. On the other hand, the selectivity's for both PEA and BA decreased with increasing reaction time. The results manifest that PEA was the initial product which was efficiently converted to oxidized products by catalyst, such as AcPO. After 8 h of reaction time, 56.2 % conversion of EB and 65.9 % selectivity for AcPO were obtained.

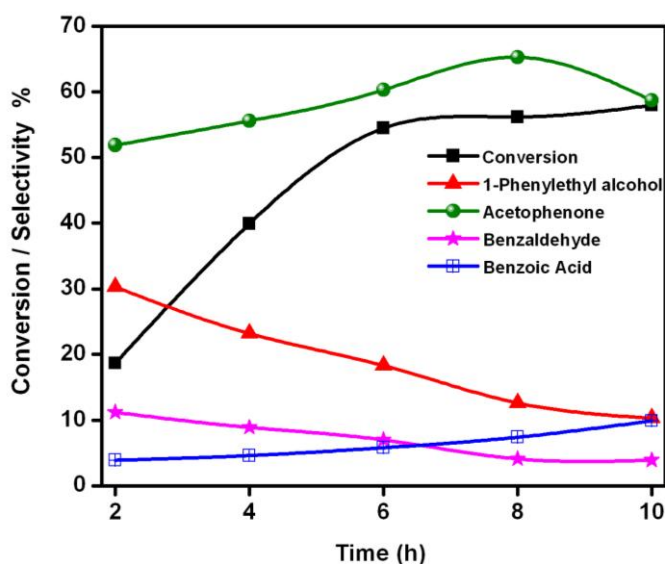


Fig.4.21. Effect of reaction time on EB conversion and acetophenone selectivity.
Conditions: 6.0g EB, 12.7mL Acetonitrile, 100mg CNNT, 403 K, 20bar O₂.

However with further increase of reaction time, the conversion did not change significantly anymore and the selectivity for AcPO slightly decreased because of the formation of more byproducts (BzA). These results reveal that 8 h reaction period is adequate. Increase in selectivity of AcPO with time is also reported by Song *et al.* [41]

4.8.2.3. Effect of catalyst content

The effect of catalyst content on the catalytic activity in the oxidation of EB is given in Figure 4.22. Results show that with CNNT content of 50 mg, EB conversion was 33.6 % with AcPO selectivity of 67.6 %. With increasing CNNT catalyst content to 100mg, conversion of EB has increased, while there was slight drop in AcPO selectivity. The reason for this reduction in selectivity is attributed to a small increase in BzA and BA selectivity. However, when the amount of CNNT is increased further to 150 mg, there was no noticeable change in EB conversion. Jin *et al.* also observed that with increase in catalyst content, conversion of EB has improved.[40]

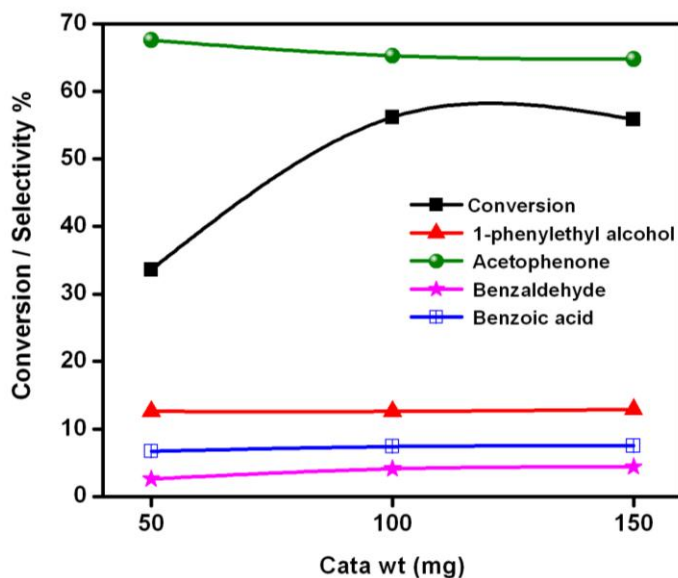


Fig. 4.22. Effect of catalyst content on EB conversion and product selectivity.

Conditions: 6.0g EB, 12.7 mL Acetonitrile, 8 h, 403 K, 20 bar O₂.

4.8.3 Baeyer-Villiger oxidation of cyclohexanone to Caprolactone

Baeyer-Villiger reaction is an important oxidation process because of its wide applicability in the preparation of pharmaceutical intermediates and fine chemicals [36]. This reaction provides single step pathway for the conversion of ketones to lactones with organic peracids and peroxides as oxidants [37].

ϵ -caprolactone is a vital chemical used in the preparation of polyesters. The current production in industry is carried out by oxidation of cyclohexanone with *m*-chlorobenzoic acid as oxidant [38]. A variety of metal based catalysts were tested for the Baeyer villiger oxidation, such as Fe-MCM-41 [39], Sn-MCM-41 [40], Fe_2O_3 [41] and Al_2O_3 [42]. However, there are drawbacks in the use of metal based catalysts: low selectivity, high cost and detrimental environmental effects caused by catalyst residues and unwanted side products. Hence, it is advisable to search for effective catalysts that are metal free. The CNNT catalysts were also tested for Bayer-Villiger oxidation of cyclohexanone to caprolactone.

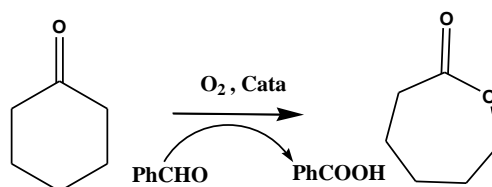
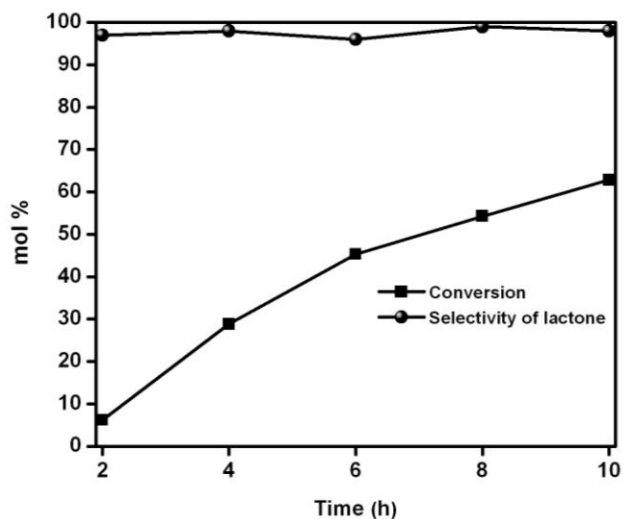


Figure 4.23 shows the effect of reaction time on Bayer-Villiger oxidation of cyclohexanone to caprolactone. With increase in reaction time, the conversion of cyclohexanone has increased. Similar observations were also made by Yue-Fang *et al.* that both cyclohexanone conversion and caprolactone selectivity improved with time [43]

Scheme 4.4 Bayer villager oxidation of cyclohexanone to caprolactone.**Fig. 4.23** Effect of time on the yield of caprolactone.

Conditions: 10mmol 'One', 20mmol benzaldehyde, 50mg Catalyst, 323 K 10bar O₂.

4.10. Conclusions

Carbon nitride nano tube catalyst was prepared and investigated for single step oxidation of cyclohexane to adipic acid and selective oxidation of other hydrocarbons. The detailed characterization of carbon nitride nano tube catalysts helped to understand these materials. Powder XRD of the CNNT suggests that the material is constructed through repetition of triazine rings. The IR spectrum of CNNT confirms the absence of free amine groups which are condensed during the polymerization process. Scanning and transmission electron microscopic technique substantiates the tube structure and the d-spacing obtained with this technique is in line with that obtained using XRD. Presence of pyridinic and graphitic nitrogen in the material is confirmed by XPS. Their respective ratios were determined with this technique. The oxygen reducing capacity of material is studied with cyclic voltammetry in both alkaline and acidic environment. The CV measurements show that the material has redox sites that can reduce O₂ even in the absence of any metal.

The catalytic activity of CNNT catalysts was investigated for the selective oxidation of CyH as well as other hydrocarbons. Cyclohexane oxidation was conducted both in presence and absence of solvent. The parameters like temperature, time, catalyst content, oxygen pressure etc play important role in selectivity of AA and CyH conversion. Very good conversion of (~70%) cyclohexane and AA selectivity (~70%) were found on CNNT catalysts. Such high (~49%) yield of AA in single step is being reported for the first time. However, this catalyst system needs intensive investigations to for further improving the AA yield and to suppress glutaric acid (GA) and succinic acid yields. It is also important to investigate the respective role of pyridinic and glutaric acid during cyclohexane conversion to AA. Oxidation of cyclohexanone, ethyl benzene and Bayer-Villiger oxidation of cyclohexanone were also studied with metal free carbon nitride catalysts and the CNNT catalysts were found to be good for even these selective oxidations. However, more investigations are required for fine tuning of process conditions.

4.11. References

- 1 T. Blasco, J. M. Lopez Nieto, *Applied Catalysis A* **157** (1997) 117.
- 2 G. Centi, F. Cavani, F. Trifiro, *Selective Oxidation by Heterogeneous Catalysis*, Kluwer Academic/Plenum Publishers, New York, 2001
- 3 (a) M. M. Bhasin, J. H. McCain, B. V. Vora, T. Imai, P. R. Pujado, *Applied Catalysis A* **221** (2001) 397. (b) E. A. Mamedov, V. Cortes-Corberan, *Applied Catalysis A* **127** (1995) 1.
- 4 (a) P. Zhang, Y. Gong, H. Li, Z. Chen, Y. Wang, *Nature Communications* **4** (2013) 1593. b) A. E. Shilov, G. B. Shulpin, *Chem. Rev.* **97** (1997) 2879.
- 5 A. Bielanski, J. Haber, *Oxygen in catalysis*, Marcel Dekker, 1991
- 6 N. Mizuno, *Modern heterogeneous oxidation catalysis*, Wiley, 2009.
- 7 (a) S. Das, C. D. Incarvito, R. H. Crabtree, G. W. Brudvig, *Science* **312** (2006) 1941. (b) J. Meeuwissen, J. N. H. Reek, *Nat. Chem.* **2** (2010) 615. (c) S. J. Lee, S. H. Cho, K. L. Mulfort, D. M. Tiede, J. T. Hupp, S. T. Nguyen, *J. Am. Chem. Soc.* **130** (2008) 16828.
- 8 D. R. Lide, *Handbook of Chemistry and Physics*, CRC Press, Boca Raton, Florida, 85th edn, 2005. Section 14, *Geophysics, Astronomy, and Acoustics; Abundance of Elements in the Earth's Crust and in the Sea*.
- 9 (a) K. Salazar, Mineral Commodity Summaries 2013: *US Geological Survey* (USGS), 2013. (b) T. J. Brown, R. A. Shaw, T. Bide, E. Petavratzi, E. R. Raycraft and A. S. Walters, *World Mineral Production 2007–11*, *British Geological Survey*, 2013.
- 10 Andrew Hunt, James Clarke *Element Recovery and Sustainability* RSc Green Chemistry series 2013.
- 11 Y. Wang, J. Zhang, X. Wang, Markus Antonietti, and Haoran Li *Angew. Chem. Int. Ed.* **49** (2010) 3356.
- 12 X. Li, S. Chen, X. Wang, J. Sun, and Markus Antonietti, *J. Am. Chem. Soc.* **133** (2011) 8074.
- 13 H. Yu, F. Peng, J. Tan, X. Hu, H. Wang, J. Yang, W. Zheng, *Angew. Chem. Int. Ed.* **50** (2011) 3978.
- 14 Y. Gao, G. Hu, J. Zhong, Z. Shi, Y. Zhu, D. S. Su, J. Wang, X. Bao, and Ding Ma,

- Angew. Chem. Int. Ed.* **52** (2013) 2109.
- 15 Gong KP, Du F, Xia ZH, Durstock M, Dai LM. *Science* **323** (2009) 760.
- 16 Wang Y, Wang XC, Antonietti M. *Angew Chem Int Ed.* **51** (2012) 68.
- 17 (a) Thomas A, Fischer A, Goettmann F, Antonietti M, Muller JO, Schloßgl R *J Mater Chem* **18(41)** (2008) 4893 (b) Y Wang, J Zhang, X Wang, Markus Antonietti, and Haoran Li *Angew. Chem. Int. Ed.* **49** (2010) 3356.
- 18 J. Chen, X. Wang, X. Cui, G. Yang and W. Zheng, *Chem. Commun.* **50** (2014) 557.
- 19 Y. Cao, X. Luo, Hao Yu, F. Peng, H. Wang, G. Ning *Catal. Sci. Technol* **3** (2013) 2654.
- 20 J. Gao, Y. Zhou, Z. Li, S. Yan, N. Wang and Z. Zou, *Nanoscale* **4** (2012) 3687.
- 21 (a) X. S. Zhou, F. Peng, H. J. Wang, H. Yu and Y. P. Fang, *Chem. Commun.* **47** (2011) 10323. (b) P. Ragupathy, D. H. Park, G. Campet, H. N. Vasana, S.-J. Hwang, J.-H. Choy and N. Munichandraiah, *J. Phys. Chem. C*, **113** (2009) 6303.
- 22 RA Sheldon, JK Kochi. *Metal-catalyzed oxidations of organic compounds*. New York: Academic Press; 1981.
- 23 Cavani et al., *Sustainable Industrial Processes*, Wiley-VCH, 1st edition (2009).
- 24 (a) M. Groenewolt and M. Antonietti, *Adv. Mater.* **17** (2005) 1789. (b) Q. X. Guo, Q. Yang, C. Q. Yi, L. Zhu and Y. Xie, *Carbon* **43** (2005) 1386.
- 25 D. M. Teter and R. J. Hemley, *Science*, **271** (1996) 53.
- 26 X. C. Wang, K. Maeda, A. Thomas, K. Takanabe, G. Xin, J. M. Carlsson, K. Domen and M. Antonietti, *Nat. Mater.* **8** (2008) 76.
- 27 B. V. Lotsch, M. Doeblinger, J. Sehnert, L. Seyfarth, J. Senker, O. Oeckler and W. Schnick, *Chem. Eur. J.* **13** (2007) 4969.
- 28 S. K. Srinivasan and S. Ganguly, *Catal. Lett.* **10** (1991) 279.
- 29 T. L. Davis and A. J. J. Abrams, *J. Am. Chem. Soc.* **47** (1925) 1043.
- 30 V. N. Khabashesku, J. L. Zimmerman and J. L. Margrave, *Chem. Mater.* **12** (2000) 3264.
- 31 M. Tahir, C. Cao, F. K. Butt, F. Idrees, N. Mahmood, Z. Ali, I. Aslam, M. Tanveer, M. Rizwana and Tariq Mahmood *J. Mater. Chem. A* **1** (2013) 1394.
- 32 X. Bai, C. Cao, X. Xu and Q. Yu, *Solid State Commun.* **150** (2010) 2148.

- 33 (a) X. Bai, J. Li and C. Cao, *Appl. Surf. Sci.* **256** (2010) 2327. (b) A. Thomas, A. Fischer, F. Goettmann, M. Antonietti, J. O. Muller, R. Schlogl and J. M. Carlsson *J. Mater. Chem.*, **18** (2008) 4893.
- 34 A. Alshammari, A. Koeckritz, V. N. Kalevaru, A. Bagabas and A. Martin, *ChemCatChem* **4** (2012) 1330.
- 35 H.-X. Yuan, Q.-H. Xia, H.-J. Zhan, X.-H. Lu and K.-X. Su, *Appl. Catal., A*, **304** (2006) 178.
- 36 E. Crezee, A. Barendregt, F. Kapteijn, J. Moulijn *Catalysis Today* **69** (2001) 283.
- 37 F. Cavani, L. Ferronia, A. Frattini, C. Lucarelli, A. Mazzinia, K. Raabova, S. Alini, P. Accorinti, P. Babini *Appl Catal A Gen* **391** (2011) 118.
- 38 G. A. Olah, Friedel – Crafts and related reactions, Vol. 2, Interscience Publishers, 1963
- 39 S. Evans, J. R. L. Smith, *J. Chem. Soc. Perkin Trans. 2* (2000) 1541.
- 40 L. Jin, Feng peng, H. Yu, H. Wang and W. Zheng *ChemcatChem* **5** (2013) 1578
- 41 S. Shi, C. Chen, M. Wang, J. Ma, J. Gao and Jie Xu *Catal. Sci. Technol* (2014)
- 42 (a) G. Strukul, *Angew. Chem.* **110** (1998) 1256. (b) R. A. Michelin, P. Sgarbossa, A. Scarso, G. Strukul, *Coord. Chem. Rev.* **254** (2010) 646.
- 43 Hudlicky, M. *Oxidations in Organic Chemistry*; ACS Monograph **186**; American Chemical Society: Washington, D.C., 1990
- 44 S.D. Burke, R.L. Danheiser (Eds.), *Handbook of Reagents for Organic Synthesis*, John Wiley and Sons, New York, 1999.
- 45 T. Kawabata, Y. Ohishi, S. Itsuki, N. Fujisaki, T. Shishido, K. Takaki, *J Mol Catal A: Chem* **236** (2005) 99.
- 46 Corma, A.; Navarro, M. T.; Nemeth, L. T.; Renz, M. *Chem. Commun.* **21** (2001), 2190.
- 47 S. Murahashi, O. Naota, *Tetrahedron Lett* **33(49)** (1992) 7557.
- 48 R. Steffen, S. Teixeira, J. Sepulveda, R. Rinaldi, U. Schuchardt *Journal of Molecular Catalysis A: Chemical* **287** (2008) 41.
- 49 Y. Li, M. Guo, S. Yin, L. Chen, Y. Zhou, R. Qiu, C. Au *Carbon* **55** (2013) 269

Chapter 5

**Base free process for the oxidation of biomass derived
feedstocks to corresponding acids**

5.1. Introduction

Effective utilization of biomass for the sustainable production of chemicals and fuels is important to minimize dependence on fossil fuels, which helps to contain net CO₂ emissions to the atmosphere [1]. Towards this goal, researchers have been focusing on technologies that can facilitate the conversion of renewable biomass into fuels and chemicals [2]. Moreover, in future, economic and industrial growth of a nation will depend upon its ability to utilize locally available sustainable feedstock (biomass) for fuel and chemical production [3]. In addition, shift away from traditional petroleum and coal based feedstocks will help to preserve ecology thus benefiting the humanity [4].

Lignocelluloses biomass is a major source of carbon. Designing process technologies for its selective hydrolysis with efficient separation techniques to get lignin, cellulose and hemicelluloses is one of the most challenging tasks in future [5]. Major fraction of lignocellulose is cellulose (~ 40%), a polymer of glucose. The efficient utilization of the cellulose via chemical transformations into potential platform chemicals is expected to play a crucial role in the transition to bio-refinery schemes [6].

Bearing in mind the utilization of biomass, several sustainable feedstocks have been suggested. Hexoses are abundant monosaccharides existing in nature. Among them D- glucose and fructose are economical and most suitable to be used as the chemical feedstocks [7]. Selective hydrolysis of hexoses gives a potential platform chemical called 5-hydroxymethylfurfural (HMF). It is a biomass derived component, obtained without fermentation, qualifying it as a potential "carbon-neutral" feedstock for fuels and chemicals. HMF on selective oxidation gives 2,5-furandicarboxylic acid (FDCA), which has many applications [8].

5.2. HMF – A precursor for commercial chemicals

As described above, carbohydrates are one of the most important types of biomass feedstock. Sugars, in the form of mono- and disaccharides are readily available from

various biomass sources, e.g. enzymatic hydrolysis and form part of useful feedstock for the production of versatile chemicals (Fig. 5.1). Presently, most research on saccharides conversion into HMF comprises dehydration of fructose, glucose or cellulose in water, high-boiling organic solvents or ionic liquids [9].

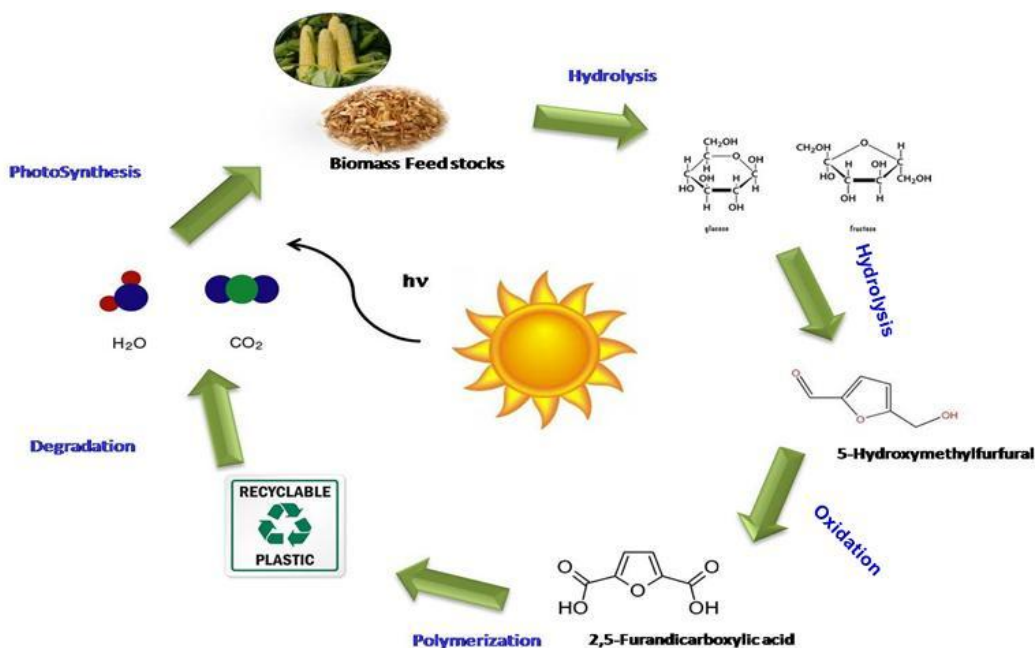


Fig. 5.1. Lifecycle of biomass as a renewable feedstock for plastics and polymers.

HMF is listed as one of the top twelve most important chemicals from biomass by the U.S. Department of Energy [10]. Because of its diversity, it is also considered a "platform chemical". HMF is used in many applications in different industries. It has been extensively covered in several reviews [11] and is primarily considered to be a starting material for the production of other chemicals with important applications, such as monomers for plastics, solvents and fuels (Fig. 5.2.).

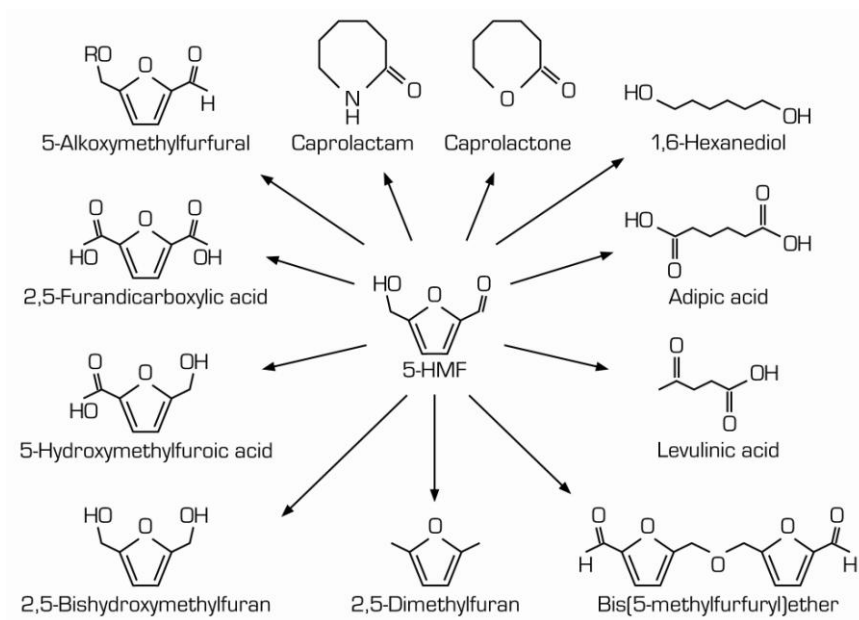
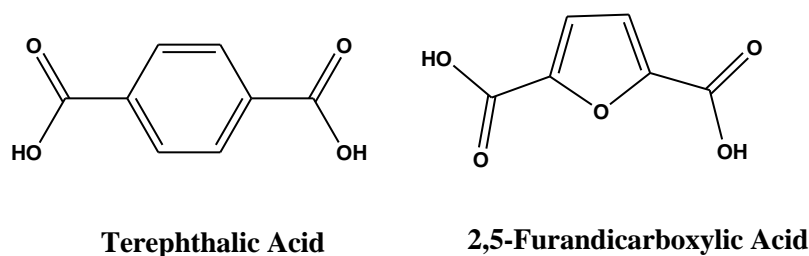


Fig. 5.2. Transformation of HMF in to variety of chemicals.

5.3. FDCA- a polymer building block

In 2004, the US Department of Energy (DOE) sought to enlist the molecules with the greatest potential for use as value-added chemicals from biomass [12]. One of these molecules is 2,5-furandicarboxylic acid (FDCA). This molecule is of great interest as it has potential to replace terephthalic acid, a monomer used in the production of polyethylene terephthalate (PET plastics) and polybutylene terephthalate (PBT plastics). FDCA can be used as a monomer in the production of biomass-derived polymers. Terephthalic acid and the structural similarity between FDCA and terephthalic acid is highlighted in Scheme 5.1.



Scheme 5.1. Structural similarity between TPA and 2,5-FDCA.

The physical and chemical properties of plastics made from FDCA polymers (Polyethylene furanoate, PEF) have been shown to be similar to PET plastics [13]. Avantium (renewable chemicals company) has recently announced a multi million Euro project in the development of a commercial facility for the large scale production of PEF and other FDCA based polymers [14]. Very recently, the synthesis of poly (butylene 2,5-furandicarboxylate, PBF) was reported, as a potential renewable alternative to petroleum-derived thermoplastic PBT [15]. But FDCA is more applications and can be applied as chemical building block in a wide variety of industrial applications. Fig.5.3. shows enormous market potential FDCA.

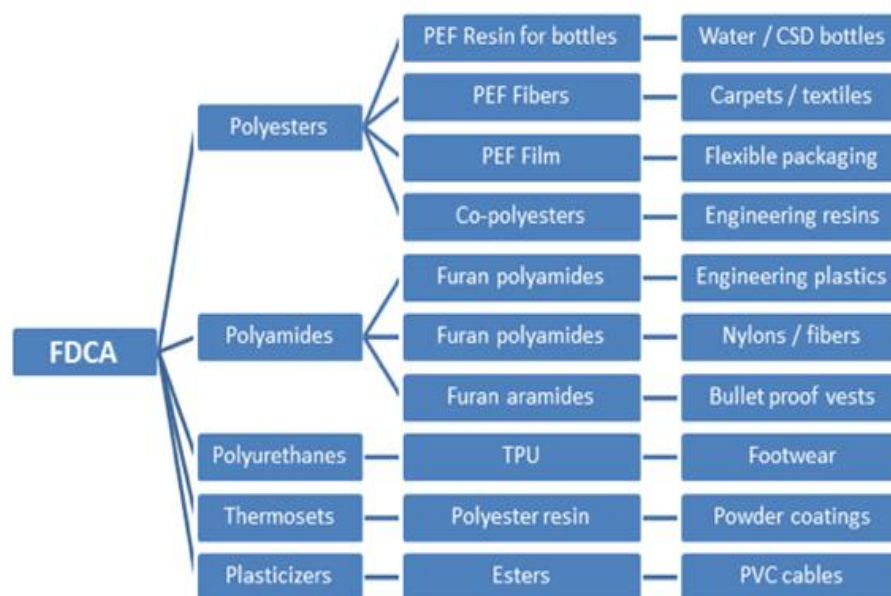
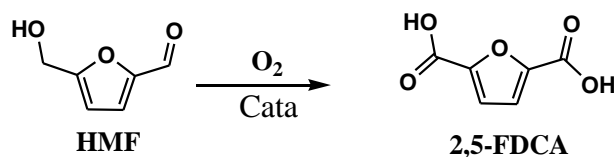


Fig. 5.3. Derivates of 2,5-FDCA.

5.4. Literature overview on selective oxidation of HMF to 2,5-FDCA.

HMF can be readily oxidized into FDCA through various reaction routes. Several reviews cover the topic of FDCA production from HMF [16]. For instance, Lewkowski reports a vast variety of chemical methods for HMF oxidation to FDCA, including, the use of barium and potassium permanganates, nitric acid and chromium trioxide and also via electrochemical oxidation. The present chapter focuses on some of the reported catalytic routes for the oxidation of HMF into FDCA (scheme 5.2), including recent ones.



Scheme 5.2. Selective oxidation of 5-HMF to 2,5-FDCA.

Partenheimer and Grushin [17] carried out the HMF oxidation using metal bromide catalysts (Co/Mn/Zr/Br). The reactions were carried out in acetic acid at 1-70 bar of air pressure; to get FDCA yield of over 60%. Bifunctional cobalt acetylacetonate encapsulated silica (acidic and redox) was used as a catalyst by Ribeiro and Schuchardt [18]. Selectivity to FDCA was 99% at 72% conversion of fructose. Kröger proposed an in situ oxidation of HMF to FDCA starting from fructose described a way of producing FDCA via acid-catalyzed formation and subsequent oxidation of HMF in MIBK/water mixture using solid acids for fructose transformation and PtBi-catalyst encapsulated in silicone and swollen in MIBK [19, 20]. The reaction was carried out in a reactor divided with a PTFE-membrane in order to prevent the oxidation of fructose. Though in principle the integration of the process is demonstrated, FDCA yields remain quite low at 25% of fructose.

Noble metals were used in the oxidation of HMF to FDCA by Vinke *et al.* [21]. They used Ru, Pt and Pd supported on catalysts for the aerobic oxidation. Though all of them showed good catalytic activity, only Pt supported on Al₂O₃ remained active and stable, to give quantitative yields of FDCA. The reactions were carried out in aqueous medium at pH 9 at a temperature of 333 K and oxygen partial pressure of 0.2Mpa. Lilga *et al.* have proposed an industrially viable method to oxidize HMF to FDCA to get an yield of 98 % under 1MPa oxygen pressure at 373 K using a Pt/ZrO₂ catalyst [22]. Later, the same group reported the oxidation of HMF in a fixed-bed continuous flow reactor [23]. Basic, neutral and acidic feeds of HMF were oxidized using Pt catalysts supported on carbon and ZrO₂. With neutral and acidic supports they have observed that most of product is an intermediated oxidized product diformyl Furan (DFF).

Supported gold nano particle catalysts have drawn wider attention for oxidation reactions. Corma *et al.* [24] performed the aerobic oxidation of HMF in aqueous solutions with external base using gold nanoparticles supported on iron oxide, titania, ceria and carbon at different concentrations of NaOH. Quantitative yields of FDCA were obtained in the temperature range of 298-403 K at different oxygen pressures. Au/TiO₂ and Au/CeO₂ catalysts proved to be most effective for HMF oxidation to FDCA. Under the optimized conditions of 403 K, 1000 KPa O₂ and 4:1 ratio NaOH: HMF, >99 % yield of FDCA was obtained after 8 h of reaction over Au/CeO₂. Hutchings *et al.* [25] performed HMF oxidation using Au-Cu nanoparticles supported on titania. Oxidation of HMF was conducted at 373 K, 10bar oxygen pressure using 4 equivalents of base. High yield of FDCA (95%) was achieved without much loss in recycle activity. Xu *et al.* obtained FDCA from HMF using gold nanoclusters confined in a super cage of Y Zeolite as a catalyst. The reactions were carried out in water, 0.3Mpa O₂ and at 333 K; that gave FDCA yield of over 99 % in the presence of base [26].

Davis *et al.*[27] conducted a comparative study of Pt, Pd and Au catalysts for the aerobic oxidation of HMF at high pH. It was found that the rate of oxidation of HMF on Au catalysts was an order of magnitude higher under the standard conditions of 295 K, 690 kPa O₂, 0.15 M HMF and 0.3M NaOH. However, the rapid conversion of HMF over the Au catalysts resulted in the formation of intermediate product 5-(hydroxymethyl) furan carboxylic acid (HMFCFA) as a result of partial oxidation of the aldehyde group in HMF. Under identical conditions, Pt and Pd were shown to provide high yields of FDCA, indicating that Pt and Pd can activate the alcohol side chain of HMFCFA while Au cannot do the same. Thus, gold catalysts required high pressures of O₂ and high concentrations of base to efficiently oxidize HMF to FDA.

Another approach to the oxidation of HMF, which leads to the formation of furan-2,5-dimethylcarboxylate (FDMC) was first reported by Taarning group [28]. The authors oxidized HMF in methanol solutions to form furan-2,5-methyldicarboxylate (FDMC) with Au/TiO₂ catalyst under 4 bar of O₂ at 403 K to get 60% isolated yield of FDMC.

Oxidative esterification of HMF in various alcohols over catalysts comprising gold nanoparticles supported on carbon and iron, cerium, titanium oxides was reported by Corma *et al.* [29]. Among all the supports, CeO₂ catalyst was shown to be an efficient catalyst for the oxidation of HMF to FDMC without added base at different oxidant pressures and temperatures. Under optimized conditions, 100 % yields of FDMC were obtained. Also, the effect of adding water to the reaction was found to be negative for the oxidation towards FDMC.

The addition of external homogeneous base, however has an environmental impact, as high pH of the medium is corrosive and the product salts need to be neutralized. Hence, there has been a recent push to find alternatives to the use of homogeneous bases.

Though the above reported process produces high yield of FDCA, use of homogeneous base (1–20 equiv. NaOH) and high O₂ pressure (10–20 bar) makes them difficult to scale up. In order to make the process free of corrosive base, researchers have conducted the above reaction without base. Recent communication by Ebitani *et al.* showed possibility of carrying out HMF oxidation with no added homogeneous external base [30]. Gold nanoparticles supported on hydrotalcite gave quantitative yield of FDCA in the aerobic oxidation of HMF in water at 368 K under an ambient oxygen pressure. Recyclability of the above catalyst is an issue due to the leaching of OH⁻ and HCO₃⁻ groups after reaction from the support. Riisager and his co workers have worked over spinel supported Ru catalyst, but the yield of FDCA was not good [31]. Hence, there is a need to design a base free process and catalyst which can produce high yield of FDCA.

In view of the above reported work, metal catalysts employed for the synthesis of FDCA impose technical constrains like lack of recyclability as a result of leaching of metal, lower reaction time, poor yield of the FDCA and requirement of external base. To overcome these shortcomings we have developed alternative, cost-effective and recyclable catalyst comprising metal and alkaline earth exchanged octahedral molecular

sieve; having both redox and basic sites. The basic site is part of the structure and does not leach out during the reaction giving very good yields of FDCA within short span of reaction time. Further the said catalyst is highly active for selective oxidation of HMF to give high yield of FDCA in short reaction time.

5.5. Experimental procedures

5.5.1. Materials

Potassium permanganate, manganese acetate, sodium hydroxide, magnesium chloride and magnesium acetate were used (Thomas Baker Chemical Ltd.) for the preparation of Mg-OMS-1. Ruthenium chloride, HMF, 2,5-FDCA (for standard) were procured from Sigma-Aldrich. All the chemicals were used without any further purification.

5.5.2. Standard procedure for HMF selective oxidation

HMF (99%) oxidation was performed in a 50 mL Titanium lined Parr Reactor (4842) which was connected to a O₂ Cylinder. In a typical run, reactor was charged with reactant, 20 mL of water and catalyst. The mixture was stirred at 500 rpm and oxygen was introduced after attaining the desired temperature. At the end of reaction, 1mL of 1.0 M NaOH was added to the reaction mixture to make sure that FDCA is completely soluble. The aqueous samples were filtered using 0.22 μm nylon filter and the filtrate was analyzed using HPLC, equipped with RI detector and Resex ROA-Organic Acid H⁺ column (300 mm × 7.8 mm). Mobile phase, 5mM H₂SO₄, was pumped at a flow rate of 0.6 mL.min⁻¹. HMF conversion and FDCA yield were quantified by HPLC through standard calibration method.

5.6. Textural characterization of catalysts

5.6.1. Powder X-ray diffraction (PXRD)

Figure 5.4. shows the PXRD profiles of the catalyst at different stages of preparation. It was observed that the two peaks at $2\theta = 12.6^\circ$ and 25.2° in half stabilized

Na-Buserite increased in intensity after second stabilization corresponding to birnessite phase. The peak at 19.5° has considerably narrowed compared to other peaks which is due to feitknechtite, also known as β -MnOOH, a brownish solid which is formed from the oxidation of $\text{Mn}(\text{OH})_2$ with the coproduction of hausmanite [32] (γ - Mn_3O_4 , JCPDS card 24-0734). A broad peak at $2\theta = 37^\circ$ is quite likely due to oxidized hausmanite [33]. However; many other manganese oxides with MnO_6 units may have some XRD reflections in this region.

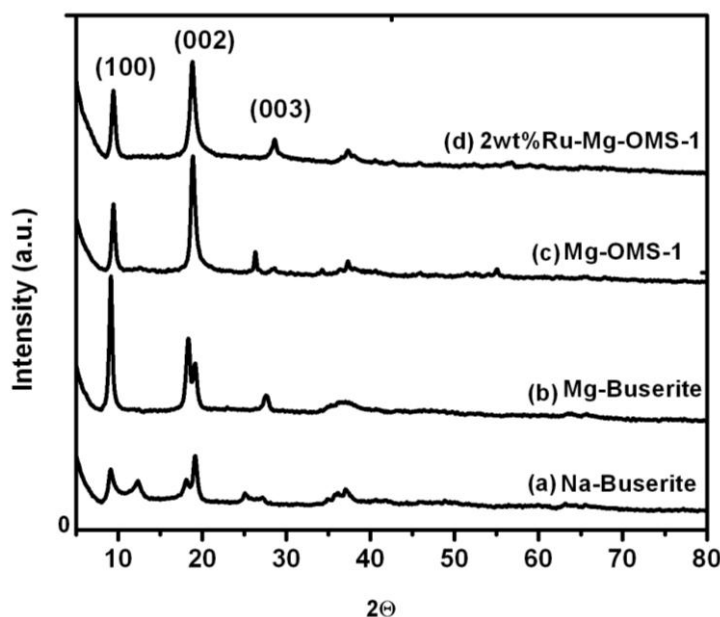


Fig. 5.4. XRD patterns of as synthesized materials.

XRD pattern of Mg-OMS-1 clearly show that all peaks are well resolved and assigned to parent Mg-OMS-1. The major peaks (1 0 0), (0 0 2), (0 0 3) that correspond to d-spacings of 9.8, 4.9 and 3.3 Å respectively match with the reported data of Todorokite Mg-OMS-1 (JCPDS 13-164). The change in the relative intensities of XRD reflections at 4.9 and 9.8 Å suggest a gradual transformation from buserite to todorokite (OMS-1). It is clearly observed in Fig. 5.4. that (a) to (d) is the clear translation of disordered to ordered structure. Ruthenium exchange into Mg-OMS-1 doesn't lead to any noticeable change in powder XRD spectra, suggesting no structural changes on Ru exchange.

5.6.2. N₂ physisorption

The BET specific surface area values for Mg-OMS-1 and 2% Ru-Mg-OMS-1 is given in Table 5.1 herein below. The support Mg-OMS-1 has surface area of 98.7 m²g⁻¹ which has increased to 119.8 m²g⁻¹ after exchanging with Ru. The Ru exchanged sample has higher external surface area compared to the parent as determined by t-method (Table 5.1). The increase in surface area after Ru exchanged is attributed to the high surface area of exchanged metal compared to the support. Whereas, the internal surface area, total pore volume, H-K method pore diameter after Ru exchange material has declined due to the replacement of magnesium by heavier Ru leading to the partial blockage of pores.

Table 5.1. N₂ adsorption results of the materials

Catalyst	Surface Area (m ² g ⁻¹)	H-K method Pore size (Å)	Pore volume (cc/g)	T-method surface area	
				Ext	Int
Mg-OMS-1	98.2	7.7	0.61	97.0	1.25
Ru-Mg-OMS-1	118.6	7.3	0.40	118.6	0

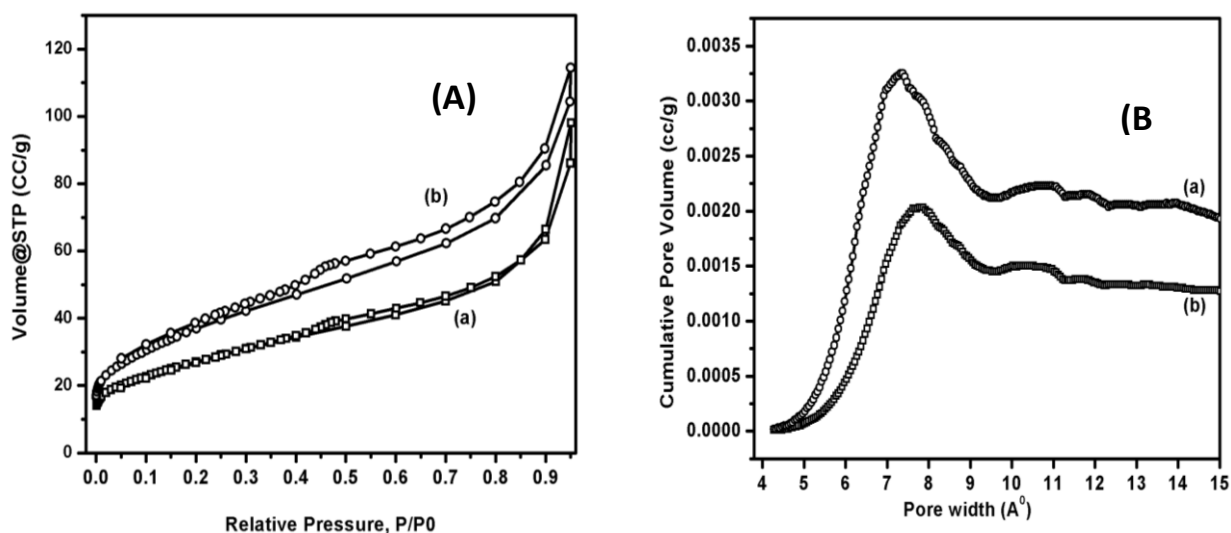


Fig. 5.5. (a) Mg-OMS-1, (b) 2wt% Ru-Mg-OMS-1. (A) N₂ adsorption & desorption isotherm. (B) H-K plot for the pore size

5.6.3. H₂ Chemisorption of 2wt% Ru-Mg-OMS-1 catalyst

Hydrogen chemisorption results are given in Table 5.2. These clearly demonstrate that Ru is finely dispersed in the catalyst. The size of the crystallites was found to be 1.62 nm.

Table 5.2. H₂ Chemisorption of 2wt% Ru-Mg-OMS-1

Analysis gas	Monolayer uptake ($\mu\text{mol/g}$)	Active metal surface area (m^2/g)	Average crystallite size (\AA)	Metal Dispersion %
Hydrogen	159.8	5.9	16.2	82.9

5.6.4. Chemical analysis of the prepared materials

Chemical analysis of various catalysts used was carried out using ICP-OES. It was observed that on Ru exchange, Mg content was found to decrease in OMS-1 catalyst. This observation suggests that Ru was exchanged in place of magnesium due to their similar ionic radii.

Table 5.3: ICP-OES Analysis of the catalyst for chemical composition

Catalyst	Metal wt %			
	Ru	Mn	Mg	K
Mg-OMS-1	--	44.45	3.34	--
Ru-Mg-OMS-1	1.98	44.13	2.51	--
K-OMS-2	--	51.33	--	3.16
Mg-K-OMS-2	--	51.29	0.73	2.01
Ru-Mg-OMS-2	1.79	51.32	0.76	2.48

5.6.5. Thermo gravimetric analysis

Thermo gravimetric analysis results of the materials were carried out in air flow in the temperature range of 295-1250 K, while heating the sample at a rate of 10 K/ min. The TGA curves of Mg-OMS-1 and Ru-Mg-OMS-1 showed that it loses weight in three steps at temperatures 323-523 K, 523-673 K and 673-873 K respectively

(Fig. 5.6a and b). Weight loss upto 523 K may probably be due to the loss of physically adsorbed water on the internal surface. The second weight loss is attributed to the water bound to the tunnels (confirmed by heating the sample at 573 K and found that the

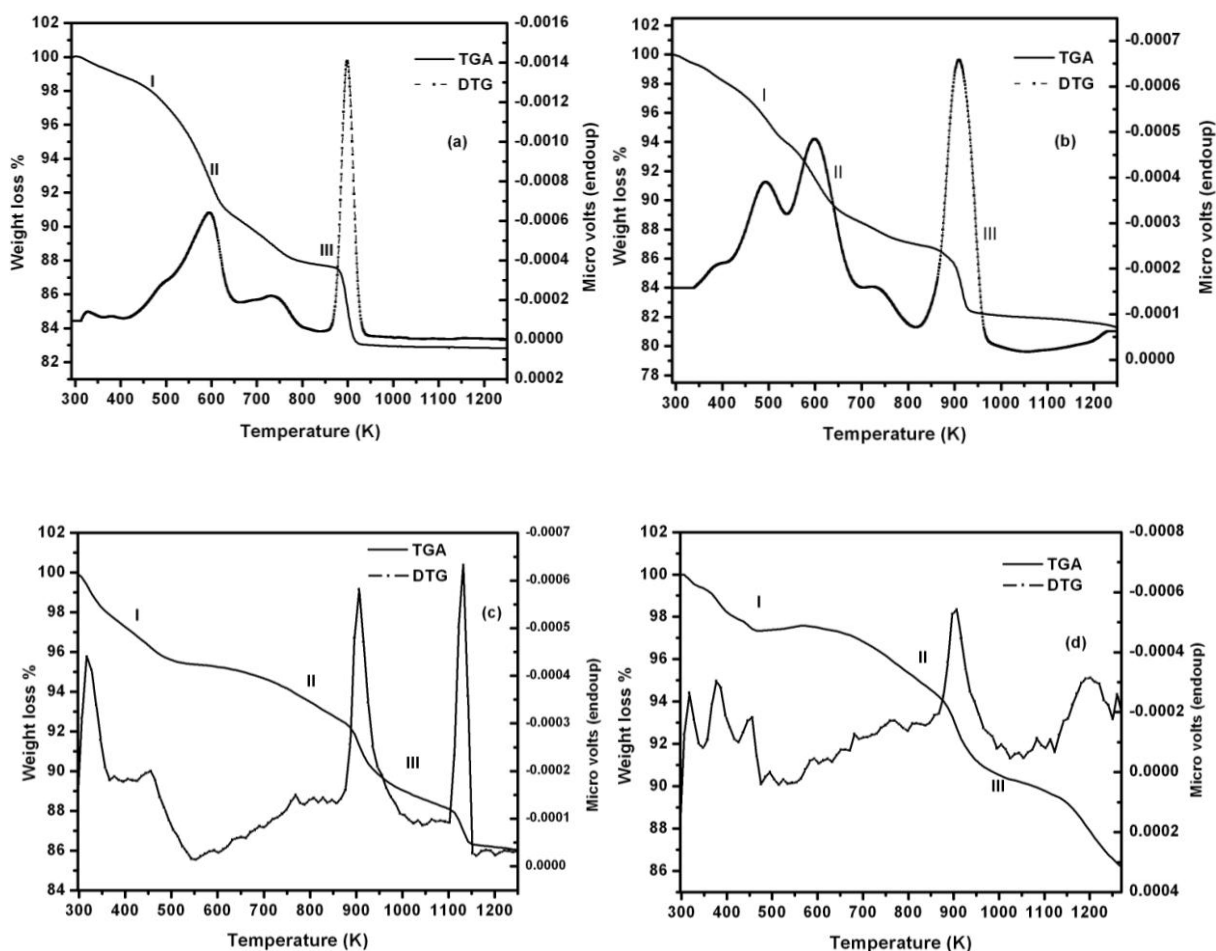


Fig. 5.6. TGA and DTG of (a) Mg-OMS-1, (b) 2wt% Ru-Mg-OMS-1, (c) Mg-OMS-2, (d) 2wt% Ru-Mg-OMS-2 in air flow

structure is intact (by XRD). As the temperature increased, Mn gets reduced releasing oxygen which led to the break down of octahedral framework. The last step of weight loss could be attributed to the destruction and collapse of tunnel structure, which corresponds to the formation of MgMn_2O_4 [34]. TGA curve shows that the OMS-1 can stay thermally stable up to 673 K, which is similar to the thermal stability of OMS-1

prepared by other methods [35]. DTG analysis of the materials shows a major weight loss around 595K and 900K which corresponds to loss of water in tunnel and loss of lattice oxygen respectively.

The TGA curves obtained for Mg-OMS-2 and Ru-Mg-OMS-2 were similar to that of K-OMS-2, which were discussed in chapter 3. Major weight loss occurred in the temperature regions 543-973K and 973-1173K as a result of loss of lattice oxygen that led to the formation of bixbyite (Mn_2O_3) and hausmanite (Mn_3O_4) from K-OMS-2 respectively.

5.6.6. Scanning electron microscopy

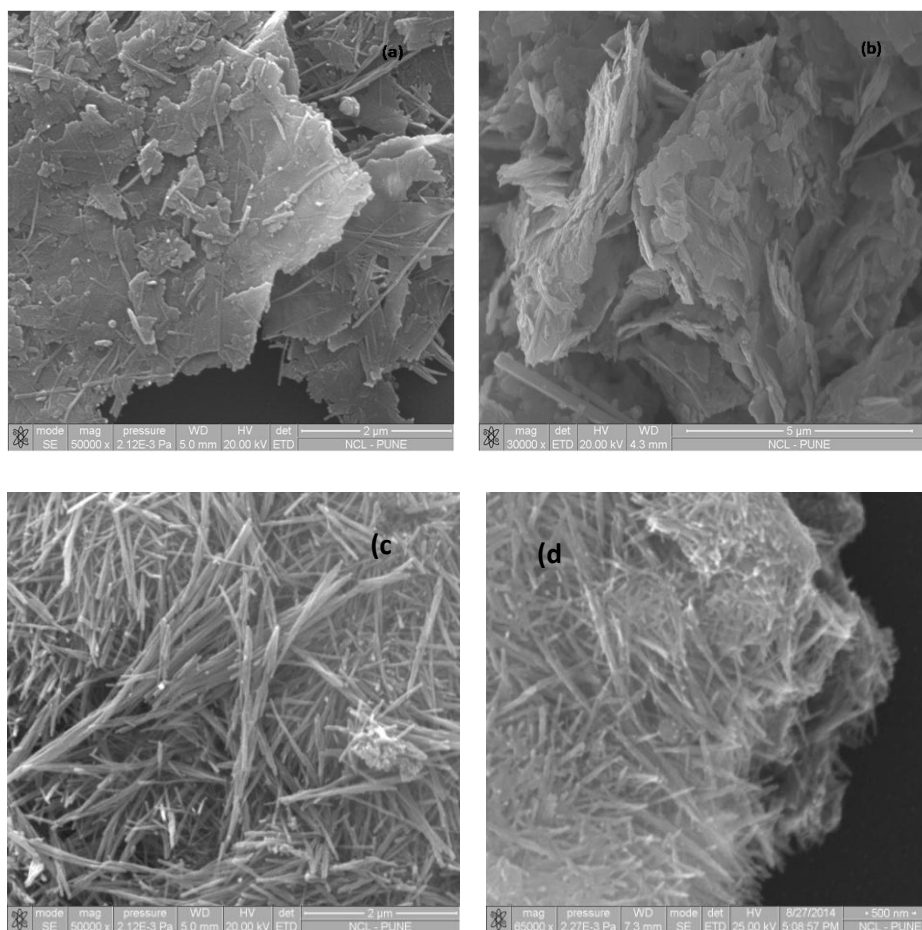


Fig. 5.7. SEM images of (a) Mg-OMS-1, (b) 2wt% Ru-Mg-OMS-1, (c) Mg-OMS-2 and (d) 2wt% Ru-Mg-OMS-2.

The scanning electron micrographs of Mg-OMS-1 and Ru-Mg-OMS-1 show fibrous needle and platelet like morphology (Fig. 5.7). The morphology of Mg-OMS-1 is similar to that of Ru-Mg-OMS-1. The results show that the Ru exchange has no effect on the morphology. Both parent and Ru loaded Mg-OMS-2 show characteristic rod like morphology. So in case of OMS-2 also Ru substitution has no affect on its morphology.

5.6.7. Transmission electron microscopy

TEM images of Mg-OMS-1 and Ru-Mg-OMS-1 show (Fig. 5.8) fibrous nanorods with clear lattice fringes. The length of the fiber is mostly in the range of 20 to 200 nm. Similar images were obtained for Ru exchanged material. This indicates that no changes occurred in Todorokite structure upon exchange. Existence of Ru nano particle on catalyst surface was confirmed by conducting EDAX by both SEM and TEM.

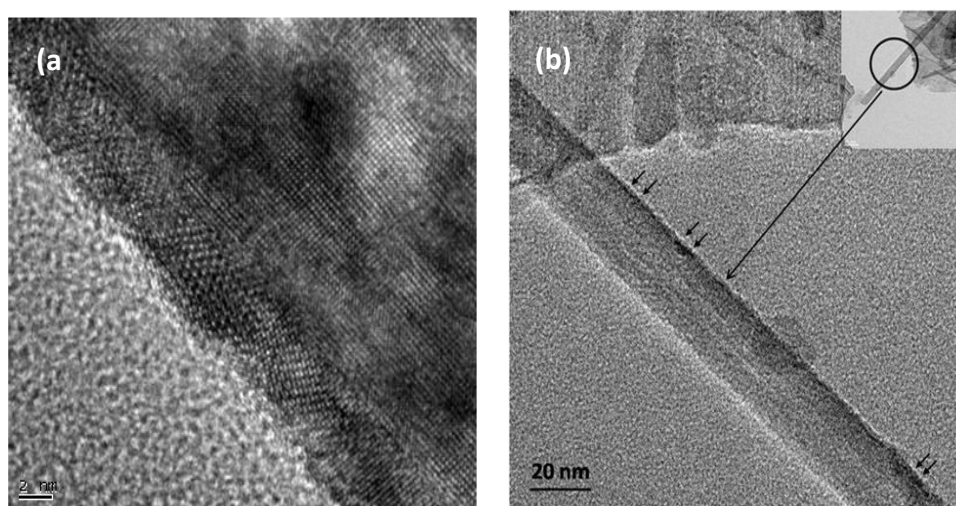


Fig. 5.8. TEM images of (a) Mg-OMS-1, (b) 2wt% Ru-Mg-OMS-1.

5.6.8. Temperature programmed desorption of CO₂

The CO₂-TPD profile of Mg-OMS-1 is given in Figure 5.9. It shows two desorption peaks. The first peak begins at 373 K with center at 443 K. The second prominent peak starts at 573 K and centered at 648 K. The later was found to be sharp and symmetric.

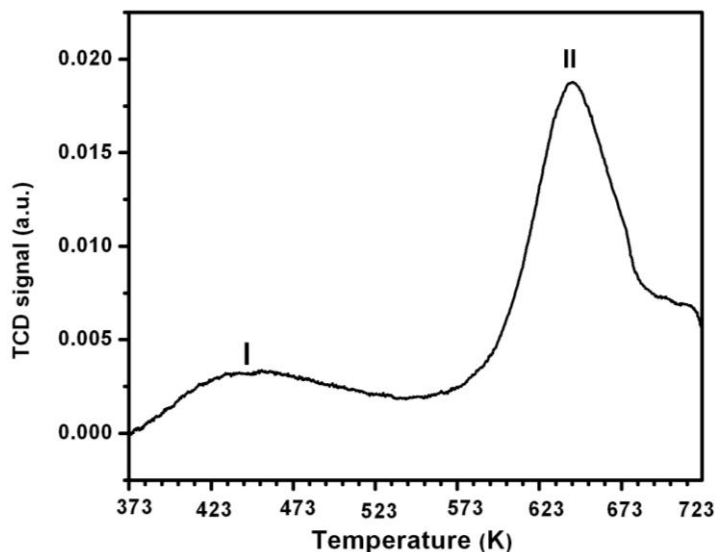


Fig. 5.9. CO₂ TPD of Mg-OMS-1

The first peak may arise from the desorption of CO₂ from the undoped, weak Mg ions on the surface of the catalyst. The Mg ions which were present in octahedral positions and tunnels give rise to the second CO₂ desorption peak. The above result substantiates the fact that the majority of magnesium is in octahedral position.

5.6.9. X-ray photoelectron microscopy (XPS)

In order to understand the nature of chemical states of the elements, XPS of catalysts were studied. After background subtraction, the curves were deconvoluted to their components using Gaussian–Lorentzian (G–L) functions. Photoelectron spectra of Ru 3d, Mn 2p, O1s are shown in Fig. 5.10.

The Ru 3d spectrum in Fig. 5.10 (a) it can be resolved into two groups of doublets and a single peak. Pure metallic ruthenium (Ru⁰) constitutes the spin–orbit doublet peaks at 280.7eV and 285.8 eV corresponding to Ru⁰ 3d_{5/2} and Ru⁰ 3d_{3/2}, respectively [36]. The doublet peaks at 281.8 and 287.3 eV originate from ruthenium oxide (RuO₂) due to Ru⁺⁴ 3d_{5/2} and Ru⁺⁴ 3d_{3/2} respectively [37]. The prominent single peak at 284.5 eV is related to C 1s due to carbon contamination. Figure 5.10(a) clearly illustrates that Ru mostly exists in (+4) oxidation state. The reduced Ru is prone to oxidize on exposure to air [38].

The O1s spectrum clearly shows three components which were illustrated in Figure 5.10 (b). According to the peak positions, three types of oxygen species can be identified: the low binding energy peak (530.32 eV), O^I, which is associated to lattice oxygen (O²⁻), the medium binding energy peak (531.93 eV), O^{II}, attributed to surface oxygen (O²⁻ or O⁻), OH⁻ groups and oxygen vacancies; finally the high binding energy peak (533.1 eV), O^{III}, assigned to the adsorbed molecular water [39]. The principal component

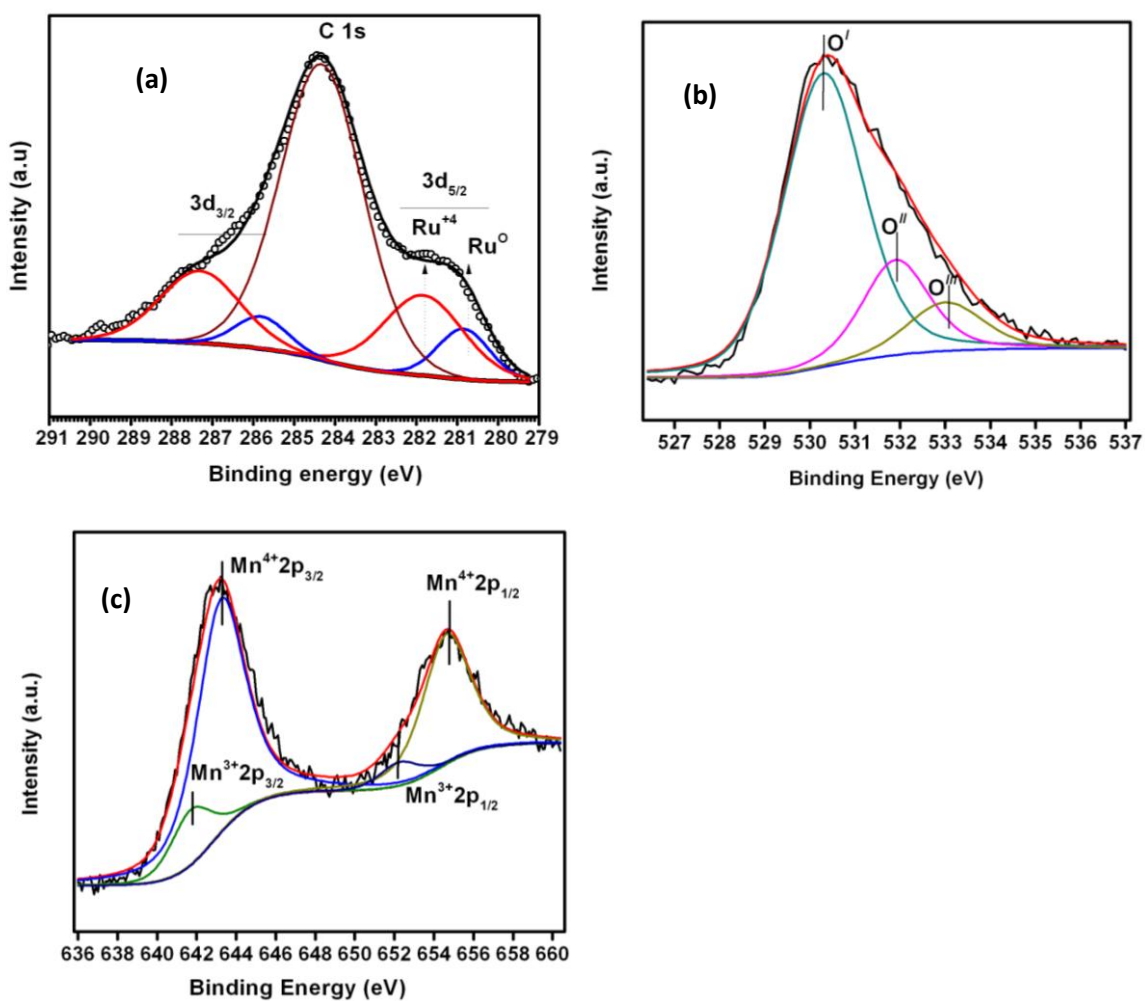


Fig. 5.10. XPS of (a) Ru 3d, (b) O 1S, (c) Mn 2p.

corresponds to the lattice oxygen, followed by the peak O^{II} of adsorbed oxygen and O^{III} of adsorbed water. The nature of the O^{II} species in these materials may be related to the presence of oxygen vacancies that creates defects. The interaction of

these point defects with molecular oxygen and/or water generates peroxides, super oxides and hydroxyl species [40].

Fig. 5.10 (c) shows the XPS spectra of Mn 2p in OMS catalyst. The prominent peaks at 643.2 and 654.7 eV correspond to Mn 2p_{3/2} and Mn 2p_{1/2} respectively for +4 oxidation state. The peaks at 641.7 and 652.3 eV corresponds to Mn 2p_{3/2} and Mn 2p_{1/2} respectively for +3 oxidation state. Binding energy of each species is tabulated in Table 5.4.

Table 5.4. Percent abundance of different elemental species derived from XPS

Element	Species	B.E (eV)	% of Abundance
Oxygen	O ^I	530.32	67.4
	O ^{II}	531.93	21.5
	O ^{III}	533.06	10.9
Mn(+4)	Mn 2p _{3/2}	643.37	51.76
	Mn 2p _{1/2}	654.7	30.92
Mn(+3)	Mn 2p _{3/2}	641.7	12.31
	Mn 2p _{3/2}	652.1	5.00
Ru (0)	Ru 3d _{5/2}	280.7	21.6
	Ru 3d _{3/2}	285.8	34.7
Ru (+4)	Ru 3d _{5/2}	281.8	13.2
	Ru 3d _{3/2}	287.3	30.33

5.7. Base free oxidation of 5-HMF to 2,5-FDCA with 2Wt% Ru-Mg-OMS-1

Selective oxidation of HMF to get 2,5-FDCA was studied in the absence of homogeneous base. Various process parameters such as temperature, O₂ pressure, reaction time, HMF/Ru mole ratio, variation of precious metal and the influence of OMS structure were investigated. At the end, recyclability of the catalyst was also investigated.

5.7.1. Effect of temperature and reaction time on the yield

The effect of reaction temperature and reaction time on HMF selective oxidation to FDCA was examined and results are shown in Fig. 5.11. Complete conversion of HMF was achieved at all temperatures within 2h. Increasing the temperature from 363-383 K has a positive influence on the yield of FDCA. At 363 K, yield of FDCA increased continuously with time and reached maximum after 8 h. However, at higher reaction temperatures (373-393 K), the yield increased with reaction time initially, but after reaching maximum, it decreased with time. This fall in yield may be attributed to the condensation of acid (FDCA) and alcohol (HMFCFA), catalyzed by acidic Mn^{4+} ion. Initially, HMFCFA (5-hydroxymethyl-2-furancarboxylic acid) is formed on oxidation of HMF, which subsequently converted to FDCA, a more stable product. It has to be pointed out that hardly any FDCA is formed before all HMF was converted into HMFCFA, indicating the lower reactivity of HMFCFA compared with HMF. The time taken to convert HMF to HMFCFA is much lower compared to the time needed to convert HMFCFA to FDCA. The above observation was also reported by Casanova *et al.* [29] Therefore, oxidative conversion of HMFCFA to FDCA was found to be the rate determining step for the reaction.

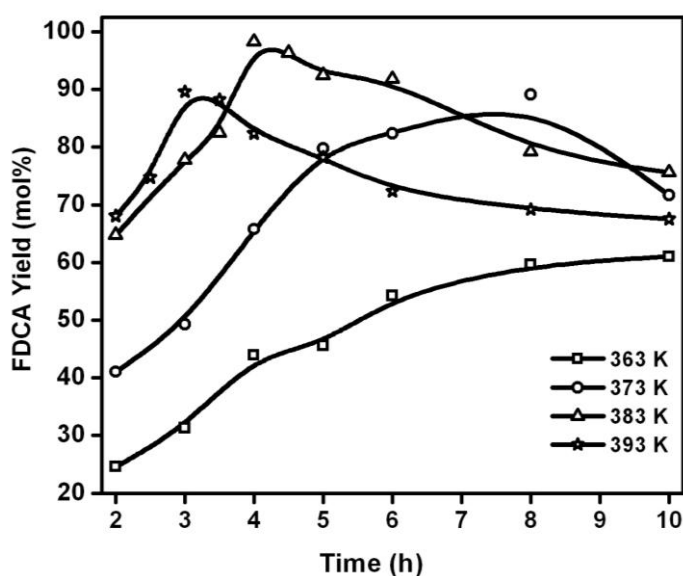


Fig. 5.11. Influence of temperature on the yield of FDCA with TOS.

Conditions: 1.3 mmol HMF, 20 mL water, HMF/Ru mole ratio = 100, 2 bar O_2 .

5.7.2. Effect of HMF/Ru mole ratio on the yield

The effect of substrate to metal ratio on HMF oxidation was investigated and results are shown in Fig. 5.12. Since we got highest yield at 373 K, effect of substrate to metal ratio with TOS was studied at this temperature. Maximum yield was achieved after 8 h (53.7%) for 200 ratio, while yield was 90.2% after 8h at 100 ratio. For HMF/Ru mole ratio 50, yield was 97.8% after 6 h. On the other hand, at 383 K, 96.6 % yield was achieved in 4 h, but fell with further increase of time. With decreasing HMF/Ru ratio, the time taken to achieve maximum yield was reduced as more active sites are available to drive the reaction for an early completion. This dependence of FDCA yield with substrate mole ratio was also observed by Gupta *et al.*[30] From the temp study we had found that increasing temperature leads to improved yield of FDCA, so instead of HMF/Ru ratio 50 simply increasing the reaction temperature by 10 K helped to achieve maximum yield of FDCA at 383 K, with HMF/Ru mole ratio of 100.

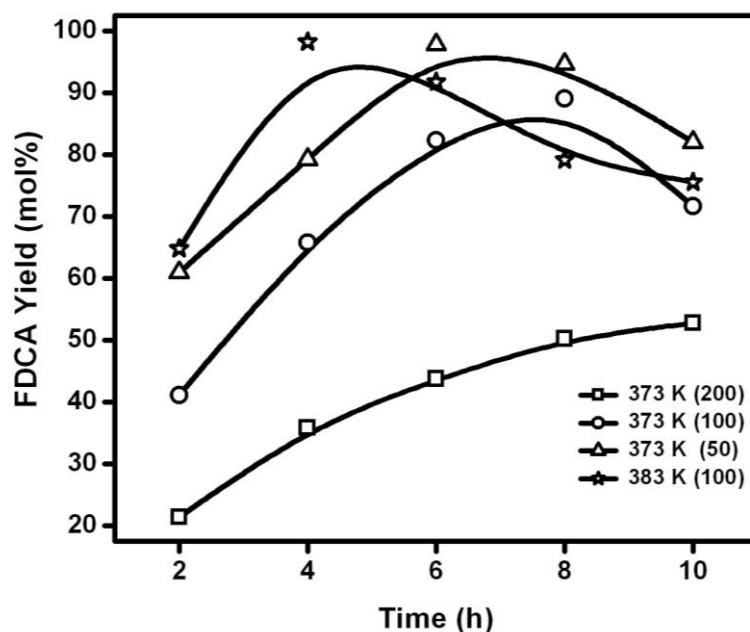


Fig. 5.12. Influence of HMF/Ru molar ratio on the yield of FDCA.

Conditions: 1.3 mmol HMF, 20 mL water, 2 bar O₂. Values in the parenthesis indicate the HMF/Ru ratio (mole/mole).

5.7.3. Effect of oxygen pressure on FDCA yield

The effect of oxygen pressure on HMF oxidation was investigated and results are shown in Fig. 5.13. Oxygen pressure has a marked effect on the yield of FDCA. When oxygen pressure was varied from 2 to 20 bar. Conversion of HMF was nearly 100% at all oxygen pressures. However, as seen from Fig. 5.13., FDCA formation was higher (93% at the end of 8 h) when the pressure was 1 bar than when it was 10 or 20bar (85%). This shows that higher oxygen pressure leads to adverse effect on the FDCA yield. An optimum pressure of 2 bar was sufficient to oxidize the intermediates especially the primary alcohol substituent of the furan derivatives.

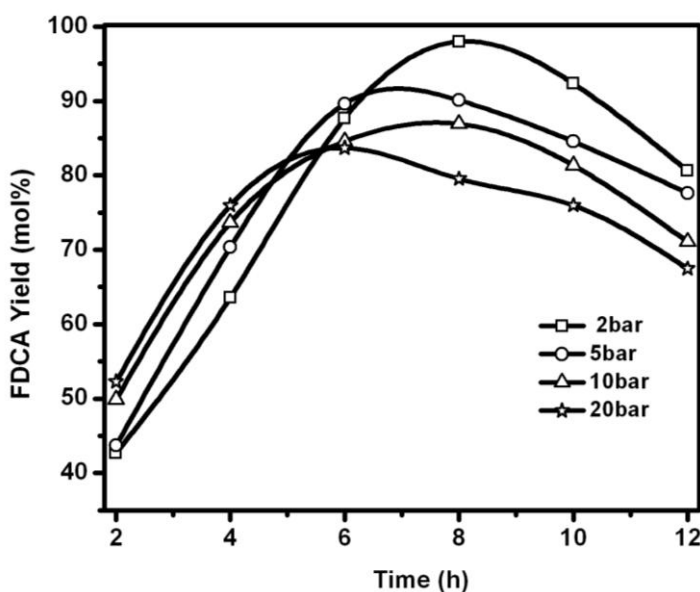


Fig. 5.13. Influence of oxygen pressure on the yield of FDCA with TOS.
Conditions: 1.3 mmol HMF, 20 mL water, HMF/Ru mole ratio = 100, 373 K.

5.7.4. Effect of OMS structure on FDCA yield

The effect OMS structure, its pore size and the basic metal of the support was investigated on HMF selective oxidation. These results are shown in the Fig. 5.14. So far investigated OMS-1 has pore size of 6.9 Å, which is bigger than the OMS-2 which has pore size of 4.6 Å, though both belong to same family. In order to find out the role of pore size effect, reaction was conducted with Ru-Mg-OMS-2 catalyst.

The results given in Fig. 5.14. show that the yield of FDCA was much lower compared to the OMS-1 support under the same conditions. The lower yield may be attributed to the fact that substrate is not able to enter in to the tunnels of the OMS-2 structure. Hence, it is not able to access Mg and Ru, which are present in the tunnels.

Figure 5.14 also demonstrates the effect of basic metal (Mg and K) on the yield. Nearly 1.1 wt % of Mg was exchanged in the Mg-OMS-2 lattice for Ru incorporation. With Mg exchange, K content was found to be decrease (from ICP) .Compared to the potassium, magnesium exchanged support showed better yield.

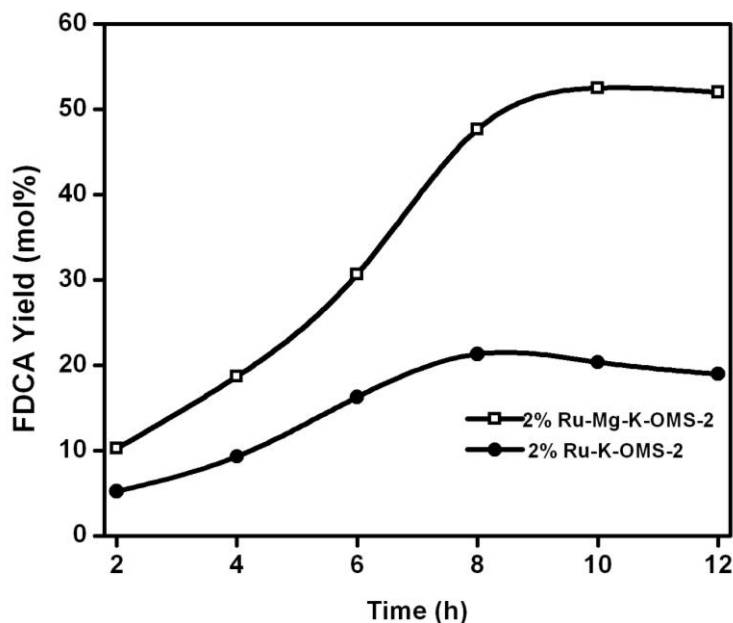


Fig.5.14. Influence of OMS structure on the yield of FDCA yield.

Conditions: 1.3 mmol HMF, 20 mL H₂O, HMF/Ru mole ratio 100, 373 K, 2 bar O₂.

In order to study the effect of support; parent Mg-OMS-1 was also used as the catalyst. Complete conversion of HMF was obtained but instead of FDCA, formation of HMFCA was observed. In the catalyst the major percentage of Mn was in +4 oxidation state. Since support has Mn⁴⁺/Mn³⁺ redox couple [41], it drove the oxidation of more reactive aldehyde group to acid to form HMFCA. While the above redox couple potential was not sufficient to oxidize the much less reactive alcohol group of HMF.

5.7.5. Effect of noble metal on the yield of FDCA

The effect of noble metal on HMF oxidation was investigated and the results are shown in Table 5.5. Catalysts were prepared by exchanging Au, Pt and Pd into Mg-OMS-1 structure

Table 5.5: Effect of different Nobel metals on FDCA yield

S.No	Catalyst	FDCA Yield (mol %)
1	2wt % Ru-Mg-OMS-1	89.1
2	2wt% Au-Mg-OMS-1	68.25
3	2wt% Pt-Mg-OMS-1	52.36
4	2wt% Pd-Mg-OMS-1	44.22

Conditions: 1 mmol HMF, 20 mL water, 8h, HMF/metal mole ratio=100, 373 K, 2 bar O₂

The selective oxidation reaction was conducted with different precious metals on the same support. From the table 5.5, one can see that the yield of FDCA follows the following trend Ru > Au > Pt > Pd.

5.7.6. Recyclability of Catalyst

Most of the reports suggest that when heterogeneous catalysts are used for biomass related reactions, they tend to deactivate rapidly or cannot be recycled. Hence, Ru-Mg-OMS-1 was recycled many times to check the catalytic activity. The optimized condition for the recycle study were temperature at 383 K, 2bar O₂, HMF/Ru molar ratio 100. The products were monitored after 4 hours. After the completion of reaction, required amount of base was added to make sure that FDCA is completely dissolved. Catalyst was recovered on centrifugation, washed with double distilled water and dried. The obtained catalyst was again reduced by NaBH₄ and tested for next run.

Figure 5.15. Shows the recycle study which were conducted for 3 runs. Catalyst was successfully recycled. From Run 1 to 3, only a slight decrease in the yield of FDCA was observed. From ICP analysis, we observed that some Mg (0.2 wt %) was found to leach after 3 rd recycle. This decrease in yield of FDCA was because of incomplete conversion of intermediate product at that particular span of time. This minimal leaching of Mg may lead to incomplete conversion of intermediate into FDCA

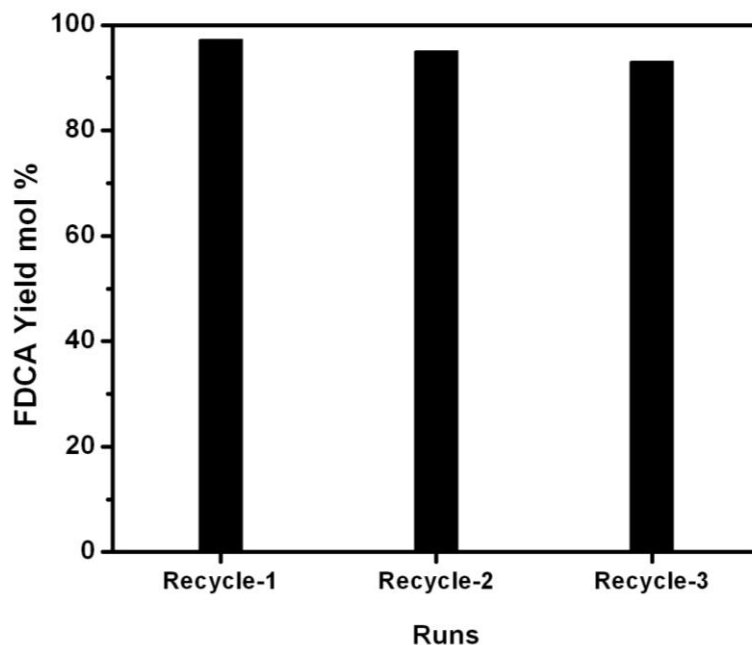


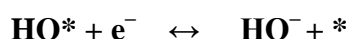
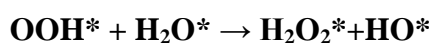
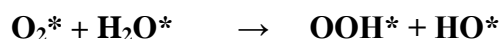
Fig. 5.15. Recyclability of 2wt% Ru-Mg-OMS-1 catalyst.

Conditions: 1.3mmol HMF, 20mL water, HMF/Ru mole ratio = 100, 383 K, 2 bar O₂, 4h.

5.7.7. Possible Mechanism of HMF selective oxidation to FDCA

The results so far discussed show that without adding base to the reaction mixture, it is possible to get good yields of FDCA from HMF. This was possible by the use of solid base as support for precious metal catalysts where the electron donating capacity of the redox metal (Ru) to oxygen enhanced with the aid of basic metal in the support. Thus, oxygen is reduced to generate hydroxide. To implement the above idea, we have selected Ru exchanged Mg and Mn containing octahedral molecular sieve as basic support for the base free process. Magnesium in the OMS-1 catalyst imparts basic character to the

catalyst which in turn provides optimum pH for the reaction. In addition, Mg can donate electrons to Ru to keep the metal in reduced state that facilitates the redox cycle. Electron donating atoms like Mg provide electrons to catalyst surface which in combination with redox metal (Ru) will promote the dissociation of H₂O with oxygen to hydroxide through hydroperoxides intermediate.

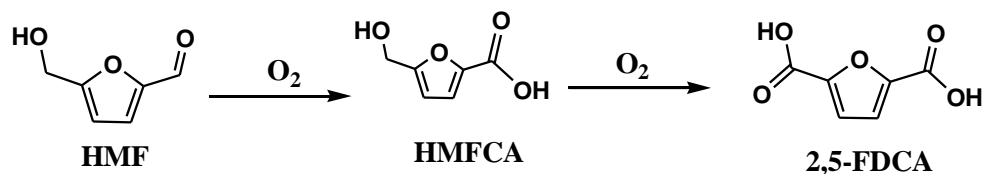


Where * represents a metallic site on the catalyst.

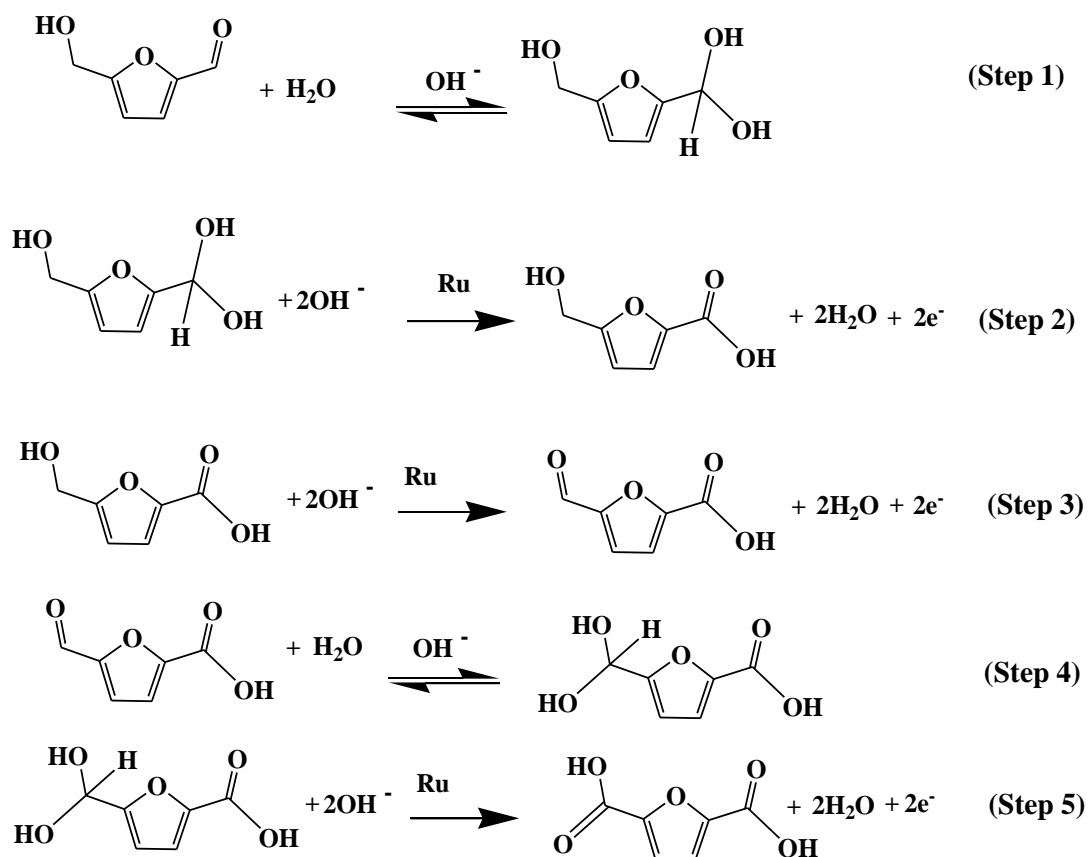
Activation of O₂ occurs through formation of peroxide intermediates. In the next step, the peroxide intermediate most likely undergoes further reduction to form hydroxide. Thus, O₂ is suggested to undergo reduction by removing the electrons deposited into the metal particles during the adsorption and reaction of hydroxide ions, thereby completing the catalytic redox cycle

We propose that the oxidation of HMF in base-free solution proceeds rapid reversible hydration to a geminal diol via nucleophilic addition of a hydroxide ion to the carbonyl and subsequent proton transfer from water to the alkoxy ion intermediate (Scheme 5.4, step 1). Oxidation of the geminal diol to carboxylic acid is likely to occur on the catalyst surface, via dehydrogenation of the geminal diol intermediate, facilitated by the hydroxide ions adsorbed on the metal surface (Scheme 5.4, step 2). The base is believed to deprotonate the alcohol side-chain to form an alkoxy intermediate, a step that may occur primarily in the solution [42]. Hydroxide ions on the catalyst surface then facilitate the activation of the C–H bond in the alcohol side-chain to form the aldehyde intermediate, 5-formyl-2-furancarboxylic acid (FCA) (Scheme 5.4, step 3). The next two steps (Scheme 5.4, steps 4 and 5) oxidize the aldehyde side-chain of FCA to form FDCA by depositing a two more electrons on the metal surface. These two steps are expected to proceed analogously to steps 1 and 2 for oxidation of HMF to HFCA.

It is also proposed that the role of dioxygen in HMF oxidation in base-free solution is to scavenge electrons from the metal surface, being reduced to peroxide and other species, thus closing the catalytic cycle in the process.



Scheme 5.3. HMF oxidation to FDCA via HMFA



Scheme 5.4. Proposed mechanism of HMF oxidation to 2,5-FDCA.

Part II base free Oxidation of Furfural

5.8. Introduction to base free Oxidation of Furfural to 2-Furoic acid.

2-Furoic Acid (FA) is an important intermediate, which is mainly obtained by selective oxidation of furfural. Commercial production of FA can be carried out using microbial biocatalytic organism called '*Nocardia coralline*' [43].

5.8.1 Applications and literature overview of 2-furoic Acid

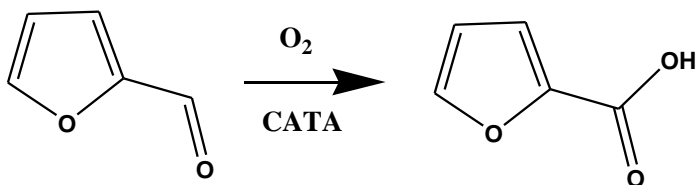
2-Furoic acid is used as preservative because of its bactericide and fungicide properties. It is also considered as an acceptable flavoring agent and is generally recognized as safe (GRAS) in 1995. 2-Furoic acid has an important role in the field of optic technology. Studies concerning the preparation of 2-furoic acid crystals have shown indication of several favorable properties of non linear optical materials (NLO) [44]. It is often used as a starting material for the production of furoate esters. Its derivatives also aid in the production of nylons which are often used in biomedical research. It helps to sterilize and pasteurize many foods [45].

Oxidation of furfural to FA was carried by researchers with different homogeneous catalysts such as MnO_2 [46], $KMnO_4$ [47] and $NaOCl$ [48]. The excess usage of the above reagents is more than the stoichiometric quantity, leads to highly polluted effluents. Heterogeneous catalysts like Ag_2O [49], mixture of metallic oxides such as Cu, Fe and noble metals like Pt were also used. [50] Verdeguer *et al.* reported Pb/ Pt on charcoal as catalyst for the furfural to FA reaction [51].

But, so far, all the processes reported for the selective oxidation of furfural to FA were conducted with the aid of external base. Therefore to make the process environmentally benign, we have conducted the above reaction in the absence of an external base. The, above discussed Ru exchanged Mg-OMS-1 catalyst was investigated for furfural oxidation, as it can generate hydroxides on dissociation of water and oxygen.

5.9. Standard operating procedure for furfural selective oxidation reaction

The selective oxidation of furfural was performed in a 50 ml Titanium lined Parr reactor (4842) which was connected to O₂ cylinder. In a typical run, reactor was charged with 1mmol of reactant, 25mL of water and 100 mg of catalyst. The mixture was stirred at 600 rpm speed while maintaining the temperature at 373 K. After reaching the desired temperature, pure oxygen was introduced into the reactor and maintained at the desired O₂ pressure. At the end of the reaction, the aqueous samples were filtered using 0.22 μm nylon filter and the filtrate was analyzed using HPLC, equipped with RI detector and Resex ROA-Organic Acid H⁺ column (300 mm × 7.8 mm) with 5mM H₂SO₄ as the mobile phase (flow rate of 0.6 mL.min⁻¹). The column temperature was kept at 60 °C. Furfural conversion and furoic Acid yield were quantified by HPLC through standard calibration curves.



Scheme 5.5. Oxidation of 2-furfural to 2-furoic acid.

5.10. Catalytic activity of 2wt% Ru-Mg-OMS-1 for selective oxidation of furfural

The catalysts that were used for HMF to FDCA reaction were also investigated for selective oxidation of furfural.

5.10.1. Effect of temperature and time

Reaction temperature and time are important parameters that play important role in attaining desired product selectivity in any oxidation reactions. The effect of temperature and time on furfural oxidation was investigated and results are shown in Fig. 5.16. Increasing the temperature from 363 to 383 K led to enhancement of 2-furfural conversion. At 363 K, the FA yield increased continuously with reaction time. Increasing

reaction temperature to 373 K helped to reach maximum yields rapidly, but further increase in temperature to 383 K has led to a drop in FA selectivity. This decrease in FA selectivity beyond 373 K may be attributed to the degradation of furfural through secondary reactions. Hence, maintaining optimum temperature is very important.

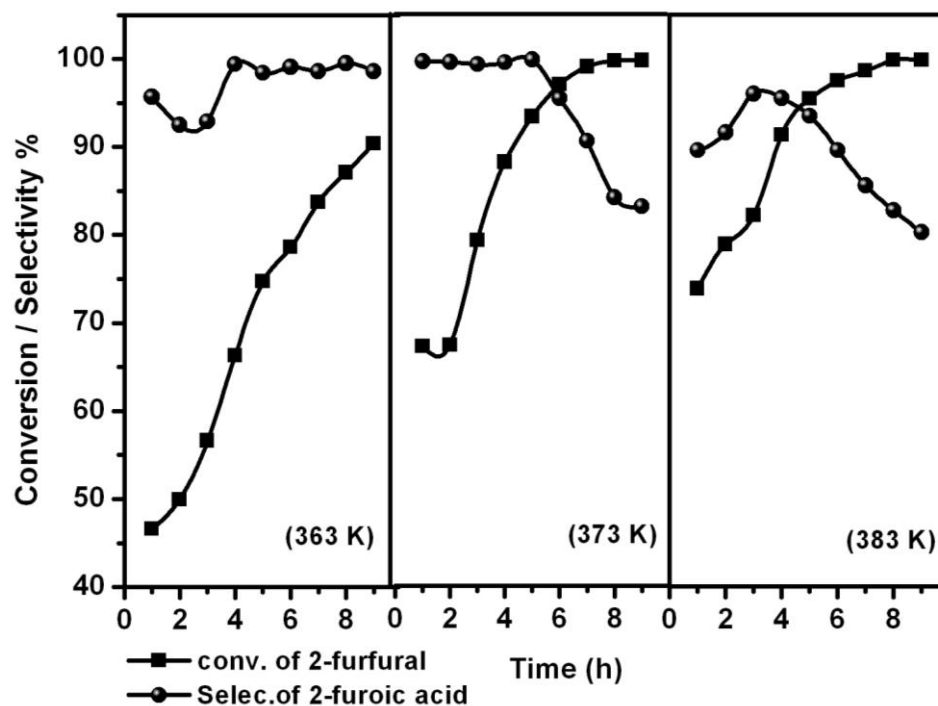


Fig. 5.16. Effect of Temperature on 2-furfural oxidation to 2-furoic acid. *Conditions:* 1.3 mmol 2-furfural, 20 mL water, HMF/Ru mole ratio = 70, 2 bar O₂.

5.10.2. Effect of substrate to metal mole ratio

The influence of the substrate to metal ratio on FA oxidation was studied and found to be extremely important. Rate of conversion of FA increased from higher to lower substrate to metal mole ratio. Conversion was found to increase with reaction time irrespective of the ratio. But, comparatively steep rise in conversion was observed at lower substrate to metal ratios. Formation of FA from furfural is higher at lower substrate to metal ratio as more catalytic sites are available. Major issue for this reaction is at higher TOS, as the FA formed tends to degrade into secondary products with prolonged

contact time. So, in order to achieve maximum yield of FA, it is recommended that the reaction must be stopped before the degradation of FA begins. The Fig. 5.17. clearly shows the role of substrate to metal ratio.

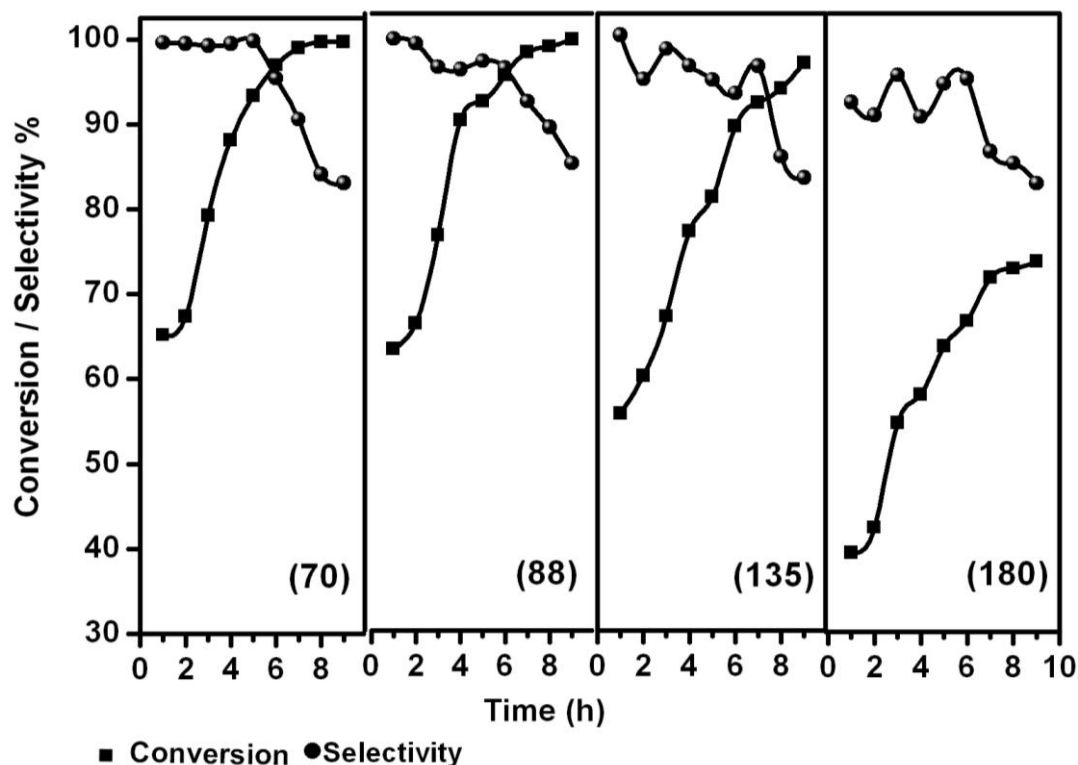


Fig. 5.17 Effect of substrate to Ru molar ratio on selective oxidation of 2-furfural
Conditions: 1.3 mmol 2-furfural, 20 mL water, 373 K, 2 bar O₂.
 HMF /Ru molar ratio (a) 70, (b) 88, (c) 135, (d) 180.

5.10.3. Variation of precious metals on selective oxidation of 2-furfural

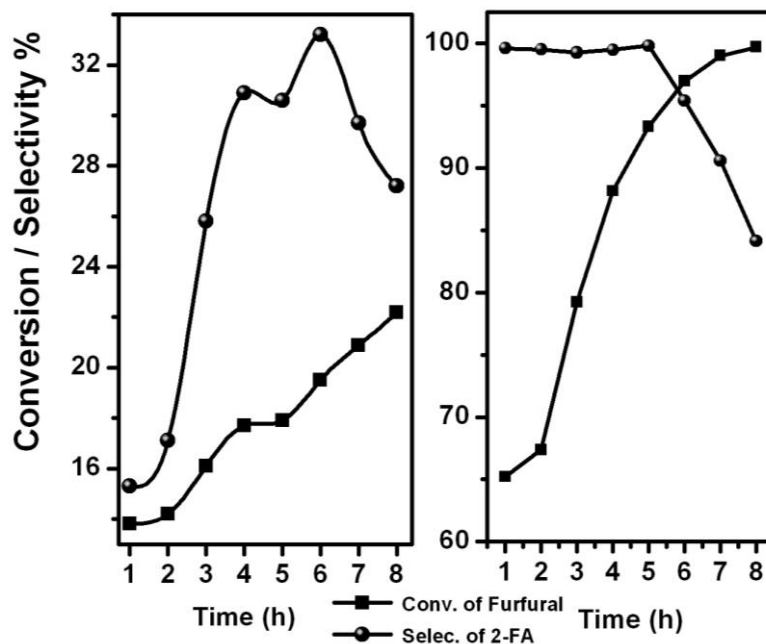
Effect of various metals on the yield of FA was studied and tabulated in Table 5.6. It was observed that the Ru metal was the most active among all other precious metals. Bimetallic supported OMS-1 catalyst was found to be more selective to FA even though the rate of conversion is low. The increasing order of activity with the precious metals is as follows Ru > Au-Pt > Pt > Au.

Table 5.6. Variartion of precious metals on the yield of 2-furoic acid.

S.No	Catalyst	Time	Conversion of furfural (mol%)	Selectivity of 2-furoic acid (mol%)
1	2Wt%Ru-Mg-OMS-1	6	95.2	96.0
		12	99.6	82.6
1	2Wt%Au-Mg-OMS-1	6	17.3	74.5
		12	22.1	68.4
2	2Wt%Pt-Mg-OMS-1	6	49.3	60.2
		12	61.7	63.7
3	Au-Pt(1:1wt%)Mg-OMS-1	6	21.7	88.0
		12	58.1	92.9

Conditions: 1.3 mmol furfural, 25 mL water, Substrate: metal ratio= 88, 373 K, 2bar O₂

5.10.4. Role of support on selective oxidation of 2-furfural

**Fig. 5.18.** Role of support on the yield of FA

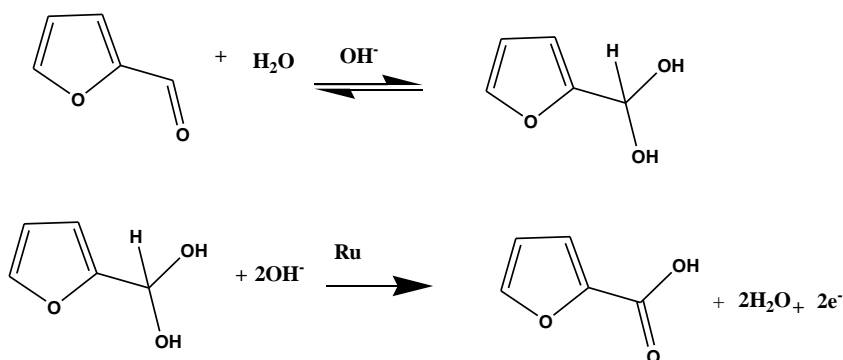
(a) Mg-OMS-1, (b) 2wt% Ru-Mg-OMS-1

Conditions: 1.3 mmol furfural, 20 mL water, Mg-OMS-1= 100 mg, 373 K, 2 bar O₂

In order to investigate the role of support, the selective oxidation of furfural was conducted with Mg-OMS-1 catalyst and compared with 2%Ru-Mg-OMS-1. The results are shown in the Fig 5.18. It was observed that conversion increases with TOS monotonously. But, the selectivity of FA was found to be low. The decrease in both conversion and selectivity were because of the absence of redox metal. Furfural degrades with TOS and secondary reactions become predominant. So, it is inferred that redox metal is essential for the selective oxidation of furfural to FA.

5.11. Possible Mechanism for the oxidation of 2-furfural to 2-furoic acid

As described for HMF to FDCA reaction, the catalyst reduces H_2O to generate OH^- initially. The aldehyde side chain is believed to undergo rapid reversible hydration to a geminal diol via nucleophilic addition of a hydroxide ion to the carbonyl and subsequent proton transfer from water to the alkoxy ion intermediate. The second step is the dehydrogenation of the geminal diol intermediate, facilitated by the hydroxide ions adsorbed on the metal surface, to produce the carboxylic acid. Hence, Ru-Mg-OMS-1 catalyst can be used as stable catalyst for the base free process of oxidation of furfural to furoic acid.



Scheme 5.6 Proposed mechanism for furfural oxidation to furoic acid

The present process not only gave a high yield of furoic acid but it is also environmentally benign in the absence of external base. Results show that we are

successful in developing base free oxidation of furfural. The present process is benign compared to any other process reported so far.

5.12. Conclusions

Ruthenium loaded Mg-OMS-1 catalyst was synthesized and characterized with different physico-chemical techniques. Powder XRD demonstrated the formation of pure Mg-OMS-1 phase. The change in the relative intensities of XRD reflections at 4.9 and 9.8 Å suggested gradual transformation of busenite to todorokite (OMS-1) structure. Chemical analysis suggests that Ru exchanged into magnesium positions due to their similar ionic radii. Hydrogen chemisorption results clearly demonstrate that Ru is finely dispersed in the catalyst, with a crystallite size of 1.62 nm. Photoelectron spectroscopy studies show that Ru is present in +4 as well as zero valent states.

The prepared catalysts were investigated for selective base free oxidation of HMF and furfural. The catalysts were highly active to give close to 100% HMF conversion and very high selectivity at short contact time. Reaction conditions used for oxidation reactions were very moderate. The yields of FDCA & FA were highly dependent on reaction time, temperature and pressure. Compared to other precious metals, Ru was found to be more active. Further, the catalysts were stable under the reaction conditions and retained high activity and selectivity for at least upto three successive cycles. The catalysts reported here are easy to prepare, and the present process is a step forward for the development of an alternative base free process for selective oxidation of biomass derivatives and their commercial exploitation as renewable feed stocks.

5.13. References

- 1 A. Fukuoka, P. L. Dhepe, *Angew. Chem. Int. Ed.* **45** (2006) 5161.
- 2 A. J. Ragauskas, C. K. Williams, B. H. Davison, G. Britovsek, J. Cairney, C. Eckert, W. Frederick Jr., J. Hallett, D. Leak, C. Liotta, J. Mielenz, R. Murphy, R. Templer, T Tschaplinski, *Science*, **311** (2006) 484.
- 3 B. Kamm, M. Kamm, *Adv. Biochem. Eng./Biotechnology* **105** (2007) 175.
- 4 C. H. Christensen, J. Rass-Hansen, C. C. Marsden, E. Taarning, K. Egeblad, *ChemSusChem* **1** (2008) 283.
- 5 H.Zhao, J.E.Holladay, H.Brown, Z.C.Zhang, *Science* **316** (2007) 597.
- 6 A. M. Ruppert, K. Weinberg, R. Palkovits, *Angew. Chem. Int. Ed.* **51** (2012) 2564.
- 7 (a) B.M.F. Kuster, *Starch/Stärke* **42** (1990) 314. (b) G.W. Huber, J.N. Chheda, C.J. Barrett, J.A. Dumesic, *Science* **308** (2005) 1446.
- 8 J. Lewkowski, *Arkivoc* **1** (2001) 17.
- 9 (a) T. Ståhlberg, W. Fu, J. M. Woodley, A. Riisager, *ChemSusChem* **4** (2011) 451. (b) T. S. Hansen, J. M. Woodley, A. Riisager, *Carbohydr. Res.* **344** (2009) 2568. (c) T. Ståhlberg, M. G. Sørensen, A. Riisager, *Green Chem.* **12** (2010) 321. (d) K. D. O. Vigier, F. Jerome, *Top. Curr. Chem.* **295** (2010) 63. (e) T. S. Hansen, J. Mielby, A. Riisager, *Green Chem.* **13** (2011) 109. (f) M. Tan, L. Zhao, Y. Zhang, *Biomass Bioenergy* **35** (2011) 1367. (g) F. Yang, Q. Liu, X. Bai, Y. Du, *Bioresour. Technol.* **102** (2011) 3424. (h) F. K. Kazi, A. D. Patel, J. C. Serrano-Ruiz, J. A. Dumesic, R. P. Anex, *Chem. Eng. J.* **169** (2011) 329.
- 10 T. Werpy, G. Petersen, U.S. DOE, 2004, No. DOE/GO-102004- 1992; available online at: <http://www.nrel.gov/docs/fy04osti/35523.pdf>.
- 11 (a) F. K. Kazi, A. D. Patel, J. C. Serrano-Ruiz, J. A. Dumesic, R. P. Anex, *Chem. Eng. J.* **169** (2011) 329. (b) M. E. Zakrzewska, E. Bogel-Lukasik, R. Bogel-Lukasik, *Chem. Rev.* **111** (2011) 397.
- 12 J. J. Bozell and G. R. Petersen. *Green Chem.* **12** (2010) 539.
- 13 A. Gandini, A. J. D. Silvestre, C. Pascoal Neto, A. F. Sousa and M. Gomes *J. Polym. Sci., Part A: Polym. Chem.* **47** (2008) 295.
- 14 <http://avantium.com/yxy/markets-partnerships/commercialization.html>. Accessed

9/14/14 Sept 2012.

- 15 J. Ma, X. Yu and Y. Pang, *Polymer* **53** (2012) 4145.
- 16 M. E. Zakrzewska, E. Bogel-Lukasik, R. Bogel-Lukasik, *Chem. Rev.* **111** (2011) 397.
- 17 W. Partenheimer, V. V. Grushin, *Adv. Synth. Catal.* **343** (2000) 102.
- 18 M. L. Ribeiro, U. Schuchardt, *Catal. Commun.* **4** (2003) 83.
- 19 M. Kröger, U. Prüße, K.-D. Vorlop, *Top. Catal.* **13** (2000) 237.
- 20 F. Koopman, N. Wierckx, J. H. de Winde, H. J. Ruijsenaars, *Bioresour. Technol.* **101** (2010) 6291.
- 21 Vinke, W. van der Poel, H. van Bekkum, *Stud. Surf. Sci. Catal.* **59** (1991) 385.
- 22 M. A. Lilga, R. T. Hallen, J. Hu, J. F. White, M. J. Gray, U.S. Patent 20080103318, 2008.
- 23 M. A. Lilga, R. T. Hallen, M. Gray, *Top. Catal.* **53** (2010) 1264.
- 24 O. Casanova, S. Iborra, A. Corma, *ChemSusChem* **2** (2009) 1138.
- 25 T Pasini, M Piccinini, M Blosi, R Bonelli, S Albonetti, N Dimitratos, J A. Lopez-Sanchez, M Sankar, Qian He, C J. Kiely, G. J. Hutchings and Fabrizio Cavani , *Green Chem*, **13** (2011) 2091.
- 26 J. Cai, H. Ma, J. Zhang, Qi Song, Z. Du, Y. Huang, and Jie Xu, *Chem. Eur. J.* **19** (2013) 14215.
- 27 S. E. Davis, L. R. Houk, E. C. Tamargo, A. K. Datye, R. J. Davis, *Catal Today.* **160** (2011) 55.
- 28 E. Taarning, I. S. Nielsen, K. Egeblad, R. Madsen, C. H. Christensen, *ChemSusChem* **1** (2008) 1.
- 29 G. C. Bond, P. A. Sermon, G. Webb, D. A. Buchanan, P. B. Wells, *J. Chem. Soc., Chem. Commun.* (1973) 444.
- 30 N. K. Gupta, S. Nishimura, A. Takagaki, K. Ebitani, *Green Chem.* **13** (2011) 824.
- 31 (a) Y. Y. Gorbanev, S Kegnaes, Anders Riisager, *Topics in catalysis* **54** (2011) 1318. (b) Y. Y. Gorbanev, S Kegnaes, Anders Riisager, *Catal Lett.* **142** (2011) 1752.
- 32 W. Feitknecht, W. Marti, *Heiv. Chim. Acta* **28** (1945) 12.
- 33 A Luo A. Huang, S. H. Park, Steven L. Suib, and Chi-Lin O'Young *Chem. Mater.* **10** (1998) 1561.

- 34 Y.F. Shen, S.L. Suib, C.L. Young *J. Am. Chem. Soc.* **116** (1994) 11020.
- 35 H. Feng, W. F. Tan, F. Liu, J. B. Wang and H. D. Ruan, *Chem.Mater.***16** (2004) 4330.
- 36 Chakroune N, Viau G, Ammar S, Poul L, Veautier D, Chehimi M M, Mangeney C, Villain F and Fievet F, *Langmuir* **21** (2005) 6788.
- 37 Rochefort D, Dabo P, Guay D and Sherwood P M A *Electrochim. Acta*, **48** (2003) 4245.
- 38 M. Zhang, W. Chen, Shi-Jin Ding, Z. Liu, Y. Huang, Z.-W. Liao and David Wei Zhang, *J. Phys. D: Appl. Phys.*, **41** (2008) 032007.
- 39 (a) V.P. Santos, M.F.R. Pereira, J.J.M. Órfão, J.L. Figueiredo, *Applied Catalysis B* **99** (2010) 353. (b) X. Yang, J. Han, Z. Du, H. Yuan, F. Jin, Y. Wu, *Catalysis Communications* **11** (2010) 643.
- 40 (a) Romero-Sarria, A. Penkova, L.M. Martinez, T.M.A. Centeno, K. Hadjiivanov, J.A. Odriozola, *Applied Catalysis B* **84** (2008) 119. (b) H.T. Chen, J.G. Chang, H.L. Chen, S.P. Ju, *Journal of Computational Chemistry* **30** (2009) 2433.
- 41 Alexey Serov, Chan Kwak, *Appl. Catal. B.Environmental* **90** (2009) 313.
- 42 B. N. Zope, D. D. Hibbitts, M. Neurock and R. J. Davis, *Science* **330** (2010) 74.
- 43 Pérez, Herminia. *African Journal of Biotechnology* **8** (2009) 10.
- 44 B. Uma, S. Jerome Das, S. Krishnan, B. Milton Boaz, *Physica B: Condensed Matter*, **406** (2011) 2834.
- 45 B. Hucker, P. Varelis, *Food Chemistry*, **126** (2011) 1512.
- 46 H. Baba, Kagaku Kenkyusto, *H6koku*, **33** (1957) 168.
- 47 F.P. Franckland and F.W. Aston, *J. Chem. Soc.* **13** (1936) 265.
- 48 Y.M. Shapiro, O.A. Pustovarova, E. Baum, V.G. Kul'nevich, *Khim. Geterotsikl Soedin*, **11** (1982) 1463.
- 49 L.L. Isenhour, US Patent (1936) 2 041 184.
- 50 A.P. Dunlop, US Patent (1946) 2 407 866.
- 51 Philippe Verdeguer, Nadine Merat, Antoine Gase *Applied Catalysis A: General* **112** (1994) 1.

Chapter 6

Summary and Conclusions

6.1 Summary & Conclusions

The present thesis has covered different approaches on oxidation of hydrocarbons and biomass derived feedstocks using porous metal oxides and metal free carbon nitride nanotube catalysts. The characterization of the catalysts was carried out using X-ray diffraction (XRD), Raman spectroscopy, temperature programmed desorption (TPD) and reduction (TPR), elemental analysis, X-ray photoelectron spectroscopy (XPS), thermo gravimetric analysis (TGA), Infrared spectroscopy (IR), cyclic voltammetry (CV) and N₂ sorption for BET surface area and micropore analysis by BJH and t-plot method. The materials synthesized, Co substituted OMS-2 were used for selective oxidation of cyclohexane to AA in presence of an initiator NAPI. To avoid addition of initiator, a novel carbon nitride nanotube catalyst was prepared and used for selective oxidation of cyclohexane to AA, in single step, with O₂ as the oxidant. Similarly, Mg-OMS-1 was prepared and exchanged with Ru to apply it for base free oxidation of HMF to 2,5-FDCA. When compared to Ru exchanged Mg-OMS-2, the Mg-OMS-1 exchanged with Ru was found to be a superior catalyst. Based on these investigations, the thesis is divided into 6 chapters which includes a chapter for summarization of the work carried out for this dissertation.

Chapter 1 provides a brief introduction to heterogeneous catalysis. It gives an outlook about green chemistry and reactivity of oxygen. This chapter also presents an introduction to selective oxidation of hydrocarbon and biomass derived HMF. It underlines the significance of these industrially important organic transformations. Basic principles of biomass valorization and composition of the biomass is also discussed. It discusses the brief development history of carbon nitride and its various structures. It also gives literature background about variety of manganese oxide mineral structures. This chapter enumerates all the conclusions drawn upon the investigations conducted with regard to various catalysts in the selective oxidation of hydrocarbons as well as biomass components.

Chapter 2 describes the methods of catalyst synthesis and important experimental techniques employed for their characterization. The catalysts synthesized were Co

substituted K-OMS-2, Ru exchanged Mg-OMS-1 and carbon nitride nano tubes (CNNT). It also described various experimental techniques deployed for their characterization. The characterization of these materials was carried out using powder XRD, by N₂ sorption (for BET surface area), SEM, TEM, UV-Vis, IR and XPS to correlate the results with their catalyst properties. A detailed description of these techniques, their theory and experimental procedures have been outlined in this chapter.

Chapter 3 begins with an extensive introduction to selective oxidation of cyclohexane to adipic acid. Thereafter, it describes the results of investigations pertaining to selective oxidation of CyH on Co-K-OMS-2 in presence of an initiator. This chapter is divided into two parts, viz., Part A and Part B. Part A deals with detailed studies on structural, spectroscopic and electronic structure of Co substituted Manganese containing octahedral molecular sieves. XRD of the Co doped material shows similar peaks that of parent K-OMS-2. Absence of any extraneous peaks belonging to Co impurities in the XRD confirms the substitution of Co into OMS-2 lattice. The IR and Raman data also demonstrated the absence of segregated metal oxide impurities which corroborate the XRD data, with regard to impurity phases of metal oxides. Transmission electron microscopy and SEM confirm the fibrous needle like morphology of Co doped samples. Photoelectron spectroscopy (XPS) results of the Co in Co-OMS-2 loading reveals that Co⁺³ is substituted in place of Mn⁺⁴ and the surface oxygen is found to increase with Co loading. In addition, the results of TGA investigations and N₂ sorption etc were discussed in detail.

Part-B deals with the applications of Co-OMS-2 catalysts in the selective oxidation of hydrocarbons. These catalysts show high activity towards single step oxidation of cyclohexane to adipic acid. Cyclohexane was converted to adipic acid with high selectivity at 97% conversion using N-Acetoxyphthalimide as free radical initiator and molecular oxygen as the oxidant. Temperature, time and Co content have marked effect on the catalytic activity. The catalysts were found to be recyclable without any loss in activity. Conclusions drawn from the catalytic cyclohexane oxidation reaction studies

and their correlation with the characterization results, is described at the end of this section.

Chapter 4 starts with the introduction to elemental sustainability and description of metal free carbon nitride catalysts. This chapter is divided in to two parts. Part-A provides the detail studies on characterization of carbon nitride nano tube catalysts. Powder XRD of the CNNT catalyst suggests that the material is constructed through repetition of triazine rings. The IR spectrum of CNNT confirms the absence of free amine groups which are condensed during the polymerization process. Scanning and transmission electron microscopic techniques substantiate the tube structure and correlates the d-spacings that are obtained with XRD. Presence of pyridinc and graphitic nitrogen in the material is confirmed by XPS. Their respective ratios were determined with this technique. The oxygen reducing capacity of material has been studied with cyclic voltammetry in both alkaline and acidic environment.

Part-B presents the catalytic activity of CNNT catalysts in the selective oxidation of CyH and also other hydrocarbons. Cyclohexane oxidation was conducted both in presence and absence of solvent. The parameters like temperature, time, catalyst content, oxygen pressure etc play important role in selectivity of AA and CyH conversion. Oxidation of cyclohexanone, ethyl benzene and Bayer-Villiger oxidation of cyclohexanone were also studied with metal free carbon nitride catalysts. At the end of the chapter, conclusions were drawn and catalytic activity was correlated with characterization results.

Chapter 5 at the stat provides introduction to biomass utilization, especially oxidative transformations of biomass derived compounds. This chapter is also divided into two parts. Part-A describes the detailed results of characterization of Ru exchanged OMS-1catalysts. XRD of the prepared materials clearly showed the transformation of amorphous material to crystalline structure. Hydrogen chemisorption results provide the information about size of Ru nano particles. Scanning and transmission electron microscopic analysis suggest rod or flake like morphology and also d-spacing of the material respectively. Photoelectron spectra of the material shows that Ru existed mostly

in (+4) and (0) oxidation states. The zero valent Ru is outside framework. Thermal stability of the material was studied by TGA analysis.

Part- B describes the catalytic activity of the metal exchanged OMS-1 material in the selective oxidation of 5-HMF and 2-furfural. Temperature, metal to substrate mole ratio, oxygen pressure and OMS structure were found to be key factors in order to attain maximum selectivity towards acids. Catalyst recyclability was also successfully demonstrated. In the present study, oxidation of biomass derived compounds was carried out in the absence of external base which is an important breakthrough for the biomass utilization. The mechanism for the above oxidations has been proposed and possible reasons for the high catalytic activity of these catalysts was also examined.

It is mandatory at the end of all chapters in a dissertation to summarize the research work undertaken for the advantage of the reader. Hence, this chapter summarizes the conclusions reached based on the experimental results during these investigations. Initially it describes the content of each chapter in detail with glimpses of results at the end. This section also offers suggestions for further research work in given areas and scope of their applications.

6.2. Suggestions for future research

The aim of the present investigation was to develop processes which are environmentally benign for the selective oxidation of hydrocarbons and biomass derived compounds. Hence, this thesis dealt with the preparation and characterization of heterogeneous catalysts that are useful for green oxidation reactions. In order to commercialize any hydrocarbon oxidation process, achieving maximum yield of the desired product is an important criterion. It should also be accomplished in an environmentally benign way. Cobalt substituted K-OMS-2 catalyst gave good yield of AA from cyclohexane oxidation in presence of an initiator. The developed catalysts were easy to prepare, inexpensive and the key metals required to prepare these catalysts are abundant. Therefore, there is a great opportunity to test different kinds of hydrocarbon

oxidations with these catalysts. It is also important to convert these process into a commercially viable one by scaling up to the desirable levels.

Currently, chemical industry is keen to practice green processes that have no environmental impact, with renewable raw materials. At the same time, the process should be low cost and inexpensive to establish a new plant or to convert the existing plant. In the commercial heterogeneous catalyst based processes, leaching of metal from the catalyst is a major drawback for the longevity of the catalyst life. Also, one should keep in mind about the elemental sustainability. Present industrial process for the oxidation of hydrocarbons (cyclohexane) utilizes homogeneous metal catalyst, which are corrosive and prone to leaching. Moreover, most processes constitute multi steps. The industrially practiced process for AA from cyclohexane, utilizes corrosive oxidants (HNO_3), which in turn releases toxic NO_x gases. These gases damage the ozone layer and have significant negative impact on global climate, ocean currents and on the overall environment. Because of the high industrial growth, majority of elements of the periodic table, which act a catalysts are depleting. Hence, it is highly desirable to design a metal free catalyst for various catalytic applications. For the present thesis, a metal free carbon nitride nano tube catalyst (CNNT) was prepared and applied for selective oxidation of hydrocarbons. These CNNT catalysts were proved to be excellent for cyclohexane oxidation to give adipic acid. The advantages of these catalysts is that they do not contain any metal, hence no problem of leaching during reaction. These catalysts are sustainable, recyclable and inexpensive. These CNNT catalysts can successfully overcome the disadvantages of present industrial process because there is no usage of metals, corrosive solvents, oxidants and single step process. Because of the above advantages, the CNNT catalysts can replace the present existing industrial catalysts. The catalysts reported here are easy to prepare, renewable and the process will be a huge step forward in the direction of commercially exploiting these materials for selective heterogeneously catalyzed oxidation reactions.

Researchers are focusing on technologies that can facilitate the conversion of renewable biomass into fuels and chemicals, as a result of its easy availability and

distribution. Utilization of biomass to chemicals can be regarded as best alternative for producing chemicals in a sustainable manner. Oxidative transformation of biomass to chemicals (corresponding acids) is a major pathway in producing renewable chemicals. However a major drawback in the reported biomass oxidations is the use of high equivalents of external base, which makes the process not so environmentally benign. Hence it is highly recommended to design a process which doesn't require addition of a base. Ruthenium exchanged Mg-OMS-1 bifunctional catalyst was designed and base free oxidations of 5-HMF, 2-furfural were conducted. The experiments demonstrated high yield of corresponding acids even in the absence of base as it contains Mg in the form of base. The catalysts were found to be recyclable. We believe metal exchanged Mg-OMS-1 catalyst could be tested for variety of biomass oxidations like glucose, glycerol and other hexoses. This work is progressing well presently in the group.

By and large, this study advances the knowledge on the oxidative conversion of hydrocarbons and biomass to value added chemicals. It describes an eco-friendly, sustainable and green methodology by means of using heterogeneous catalysts and greener oxidants (oxygen) for the conversion of hydrocarbons and biomass. Although, more research and process optimization is still needed, this study on designing green process is a huge step forward towards achievable success. The processes involving these catalysts, i am sure will find industrial application in the very foreseeable future.

List of Patents

1. Novel oxidation catalyst, the process for the preparation there of and green process for Selective aerobic oxidation of biomass compounds.
Narasimharao Kanna, Ganesh K, Lakshmi Prasad, C.V.V. Satyanarayana
US Patent Appl. no 14/283663 (NCL No.2013-NCL-0076, CSIR No.2013-NF-0192)
2. Selective aerobic oxidation of hydrocarbons using metal free catalysts.
Narasimharao Kanna, LakshmiPrasad, C.V.V. Satyanarayana
India and PCT (NCL No.2013-NCL-0099, Appln. No. 3490/DEL/2013. CSIR No 2013-NF-0253)
3. Method for rapid and selective production of dicarboxylic acids from petroleum based hydrocarbons.
Narasimharao Kanna, Ganesh K, C.V.V. Satyanarayana (Patent disclosure filed)

List of Publications

1. Novel Catalysts for valorization of biomass to value added chemicals and fuels.
Nishita Lucas, **Narasimharao Kanna**, Atul Nagpure, Ganesh Kokate and Satyanarayana Chilukuri, Journal of Chemical Sciences 126 (2014) 403-413.
2. Base free selective oxidation of 5-hydroxymethylfurfural to 2,5furandicarboxylic acid over Ru exchanged Manganese containing octahedral molecular sieves
NarasimharaoKanna, LakshmiPrasad, C.V.V. Satyanarayana (communicated)
3. Metal free catalysts for selective oxidation of cyclohexane to yield adipic acid in a single step.
Narasimharao Kanna, LakshmiPrasad, C.V.V. Satyanarayana (communicated)
4. Rapid and selective oxidation of hydrocarbons to dicarboxylic acids with Co substituted octahedral molecular sieves.
Narasimharao Kanna, Ganesh Kokate, C.V.V. Satyanarayana (Manuscript under preparation)